STUDY OF SPATIOTEMPORAL ORIENTATIONS AND CROSS BRIDGE KINETICS IN VENTRICULAR AND SKELETAL MUSCLES

DISSERTATION

Presented to the Graduate Council of the

Graduate School of Biomedical Science

University of North Texas

Health Science Center at Fort Worth

in Partial Fulfillment of the Requirements

For the Degree of

Doctor of Philosophy

By

Janhavi Nagwekar

Fort Worth, Texas

March 2016

ACKNOWLEDGEMENTS

Although only my name appears on the cover of this Dissertation, many people have contributed to the production of this thesis. I would like to reflect my gratitude to the all those people who have made this dissertation possible and sincerely thank them for their love, help and support.

My deepest gratitude is to my advisor, Dr. Julian Borejdo for his guidance and supervision at every step of this research. I consider myself to be extremely fortunate to have an advisor like Julian. He has supported me throughout my PhD study. His admirable patience, ingenious knowledge on the subject and caring quality as a person has made my graduate experience very memorable, one that I will cherish forever. I couldn't have wished for a supervisor better than him. In the future if I could meet any individual even half as good as Julian, I will consider myself lucky.

Besides my advisor, I gratefully thank the members of my committee: Dr. Lisa Hodge, Dr. Kristine Kamm, Dr. Ignacy Gryczynski, Dr. Andras Lacko and my University member Dr. Joseph Yuan for their insightful comments, advice and suggestions that incented me to widen my research outlook. I would also like to thank the CFTN group for their encouragement and all the beautiful and unforgettable memories I hence will carry with me. I would like to thank Sebastian Requena, Dr. Ryan Rich and Dr. Sangram Raut for helping me with my experimental setup.

I am greatly indebted to my family especially my Mum, for her constant love, patience, support and encouragement without whom none of this would have been possible. I cannot express in words of how deeply I appreciate my loving husband, Kshitij, whose support and care helped me overcome very difficult moments and let me stay sane throughout the difficult years of my life. I would like to express my heart-felt gratitude to him for his friendship, love and his belief in me.

I have been blessed with good friends and I would like to take this moment to appreciate their role in bringing this thesis to fruition. I appreciate the efforts of Sarika Chaudhari and Kiran Bhandarkar for their invaluable help for the entirety of this thesis.

TABLE OF CONTENTS

LIST OF ILLUSTRATIONS

Chapter II

Chapter IV

Chapter V

Chapter VI

Chapter VII

Chapter IX

Chapter X

Chapter XI

LIST OF TABLES

Chapter VII

Chapter IX

Chapter X

Chapter XI

Conclusion

LIST OF ABBREVIATIONS

ACF - AutoCorrelation Function

ADP- Adenosine diphosphate

AP - Alexa 633 Phalloidin

APD - Avalanche PhotoDiode

ATP - Adenosine triphosphate

DTT - Dithiothreitol

DV - Detection Volume

EDC - 1-ethyl-3-(3’-dimethylaminopropyl) carbodiimide

EDTA - Ethylene-diamine-tetra-acetic acid

EGTA - Ethylene glycol-bis(β-aminoethyl) ether

FCS - Fluorescence Correlation Spectroscopy

FWHM - Full width at half maximum

ELC - Essential light chain

FHC - Familial hypertrophic cardiomyopathy

HM - Hypertrophic cardiomyopathy

LC1 - Light chain 1

LMM - Light Meromyosin

LV - Left Ventricle

MF - Myofibrils

MHC - Myosin heavy chain

MLC - Myosin light chain

MLCK - Myosin light chain kinase

MUT - Mutant

MyHC - Myosin heavy chain

PF - Polarization of fluorescence

RLC - Regulatory light chain

RP - Rhodamine phalloidin

RV - Right Ventricle

S1 - Myosin subfragment-1

SD - Standard Deviation

SeTau – SeTau 647 mono maleimide

Tg - Transgenic Human RLC

TMRIA – tetramethylrhodamine 5 iodoacetamide dihydroiodide (5-TMRIA) (single isomer)

TnC - Troponin C

TnI - Troponin I

TnT - Troponin T

Tbx5 – T box 5

UP - Unlabeled Phalloidin

WT - Wild Type

XB - Cross bridge

CHAPTER I

BACKGROUND

This research thesis is focused on understanding the basic contractile mechanism in striated muscle at varying stratifications that encompass a study ranging from normal healthy function surpassed into ailments, to deleterious effect of mutations that overturn this normal behavior to precipitate into disease forms. The thesis investigates the muscle function at their basic contractile motors by focusing on the order of orientations and kinetics of these molecules.

The goal of my doctoral thesis is to determine the differences in the molecular mechanism of actins and myosins in cardiac muscle contraction and regulation, and elucidate the mechanisms underlying their related diseases. Despite various efforts, not much is known about the molecular differences in the contractile functions in the LV and RV of the heart. I focused on understanding the functional differences in the fundamental actomyosin molecules of muscle architecture and their involvement in the process of contraction in healthy ventricles of the hearts of mice and rabbits. After gaining more knowledge, I extended the research to understand the contractile mechanisms in healthy human ventricles and their associated abnormalities during heart failures. I hypothesized that the ventricles of healthy human hearts differed at their very basic contractile function and thus their associated heart failures will need ventricular specific and distinct treatment modalities than the ones currently administered.

The second goal of the thesis was to comprehend the underlying molecular mechanisms that cause the physiological and phenotypical changes associated with familial hypertrophic cardiomyopathy (FHC). Since many factors may contribute to an ailing heart, I aimed to elaborate the research by investigating the molecular mechanisms involved in FHC by studying the role of myosin mutations (A13T and K104E) and troponin mutation (R21C) in causing hypertrophy of the ventricular walls that may lead to heart failure. I hypothesized that mutations can significantly alter the function and structure in the sarcomeric proteins and subsequently lead to abnormality in muscle contraction.

It is quite established that regulatory light chain (RLC) phosphorylation via myosin light chain kinase (MLCK)-calmodulin is involved in modulating the cardiac function induced through changes in calcium sensitivity. skMLCK is known to phosphorylate skeletal, cardiac and smooth muscles with similar catalytic activities. Thus in addition to the knowledge on cardiovascular health and their related maladies, the thesis has also touched base to explore the role of phosphorylation in skeletal muscles.

CHAPTER II

INTRODUCTION

History of Muscle Biology

Movement has been looked upon as the index of life and survival. The organ that renders this movement is a muscle. Muscles are biomechanical tissues shaped by bones and forces of gravitation. Speculations about its locomotive characteristics have a long history that date back to the BC era and since, many theories on muscle contraction have appeared over the ages. Like the theory of motility attributed by muscles put forth by Erasistratus in third century BC to the alluring, elaborative depictions of muscle anatomy by Leonardo Da Vinci exemplifying the ideas of muscle contraction and many other[1]. However, the muscle research probably began by 1674 with the microscopic observation of cross-striations on myofibrils in muscle fibers by Leeuwenhoek who identified and defined the filament structures[2]. A few years later, Croone, an English physician, suggested that the sarcomeres delineated by cross-striations may serve as units of contraction and that the process was induced by nerve impulses received from the brain to conduct the stimulus[3]. This marked the modern era of muscle research. Muscle is a contractile tissue that is made up of thousands of parallel, cylindrical fibers that run the length of the tissue. The fibers constitute of smaller protein filaments called myofibrils that contain ever smaller protein myofilaments called actin and myosin. Myosin – a viscous protein was extracted from muscles with concentrated salt solution by Kühne in the year 1864 and considered it responsible for the occurrence of rigor mortis in dead bodies[4]. Years passed and in the year 1929, a brilliant student named A.V. Hill from Trinity and Kings Colleges, England, attracted the world's attention upon the mechanical efficiency of muscle and its energy processes during muscle recovery in the Sartorius muscles of frog. This Nobel Prize winner demonstrated that the muscle tension decreased as its shortening velocity increased which could be attributed to two main causes, first, loss in tension of the cross bridges in the contractile element and second, loss of fluid viscosity in both, the contractile element and the connective tissue of the muscles[5].

Around 1930, Muralt and Edsall reported the birefringent property of muscles that indicated the myosin particles were of similar shape and size[6]. Couple of years later in 1939, Engelhardt and Ljubimova demonstrated another fascinating phenomenon of myosin exhibiting ATPase activity i.e. the ability of myosin molecule to act as enzyme in itself and with the probable notion of having this precise process being the source of energy for contraction[4,7]. In the year 1942 with combined efforts of Bruno Straub and Szent-Györgyi led to the discovery of yet another muscle protein called actin whose presence with myosin was responsible for high viscosity and contractility. The newly discovered protein existed in two forms: globular actin (G actin) that was stable in the absence of salt, and polymerized to form fibrous actin (F actin) in the presence of divalent ions[8,9]. Thus it was established that it is the interaction of these two proteins, namely, actins and myosins, with ATP molecules that constitute the contractile system. This system of contraction was later studied by A F Huxley and H E Huxley in 1954 who proposed the now widely accepted muscle contraction model renownedly called the 'Sliding Filament Theory' that elaborates the working of contraction through myosin molecules sliding over actin molecules to produce force and thus contraction[10]. The sliding filament theory contributed to two predictions: 1) Tension was produced only in the overlap section and that there should be a predictable link between sarcomeric length and the overlap of actin and myosin. 2) The shortening caused by load should be independent of the overlap[11,12]. Testing the relationship between tension and overlap required sophisticated equipment that could accurately measure the lengths of

thick and thin filaments and elemental measurements of the tension in muscles. In furtherance to being able to measure muscle tension as a function of sarcomere length, it was fundamental to work on single muscle fibers cleaned of most connective tissues to visualize the sarcomeres clearly. This technique that uses electron micrographs was pioneered by Ramsey and Street in the year 1940[13]. By 1961, Huxley and Peachey demonstrated that the sarcomeres in single fibers were non-uniform and that they were shorter at the ends of the fiber as compared to the middle of the sarcomeres[14]. This finding and its further research on skeletal muscle provided powerful support to the sliding filament theory as tension dependent geometrical studies on sliding filaments could be studied profoundly[14,15].

Myosin

Myosin (hexameric) protein **(Fig.1)** is a classic self-enzyme that hydrolyses ATP to ADP and Pi through conformational changes to bring about muscle contractions. Approximately 400 myosin molecules assemble to form a filament, which interact with actin filament containing about the same number of actin monomers[10,16]. Myosin is made of many domains. The most important functional domain is S1 which interacts with actin and possess ATPase activity. S1 is made of globular catalytic domain at its N terminal (upper domain-left in Fig1) and an α-helical regulatory domain at its C terminal (lower domain-right in Fig1)[17], an α-helical tail made of Light Meromyosin (LMM) and Heavy Meromyosin (HMM)[18,19]. Myosin protein is made of heavy chain (200,000 M.wt) and four light chains, two each of ELC (LC3 16,000 M.wt, LC1 25,000 M.wt) and RLC (LC2 18,000 M.wt)[20]. One pair of light chains bind to each S1. The coiled coil region, termed as the myosin rod, interacts with pseudo-repeats of opposite charged amino acids to form filaments that have regular intervals at ~14.3 nm[21]. With this faltering arrangement, the two S1 head regions project outward at regular intervals. A feature of S1 head is a narrow cleft that runs from below the ATP binding site to the end of the head dividing the head into two clefts, upper and lower 50kDa domains[17]. The upper 50kDa domain has an ATP binding site (P-loop) and lower 50kDa domain primarily has an actin binding site in lysine rich loop-2 (weak residues Gly 627– Phe 646)[20] which are the probable electrostatic interaction sites while presumed contact interaction sites are strong residues 324-334[22]. The space between the upper domain and the N terminus (25kD) forms the nucleotide binding region[17,23]. The two myosin domains make a cleft (7 β-strands and α-helices) which are responsible for gauging the conformational changes induced by actin and ATP binding sites[24]. When actin binds in the region of myosin actin binding site, conformational change in the β-strand pushes the inorganic phosphate (Pi) out and helps actin to bind. In this state, actin bound in the cleft leads the relay helix and converter domain to converge at the base of the lever arm that changes the conformation of nucleotide binding pocket. This also sets it in close proximity to the myosin-actin region. It has been known that rotation of the regulatory domain around gly-699 is responsible for muscle to contract[25]. During contraction, the upper and lower domain of the myosin head undergoes 45^o conformational angular shift resulting in 70^o

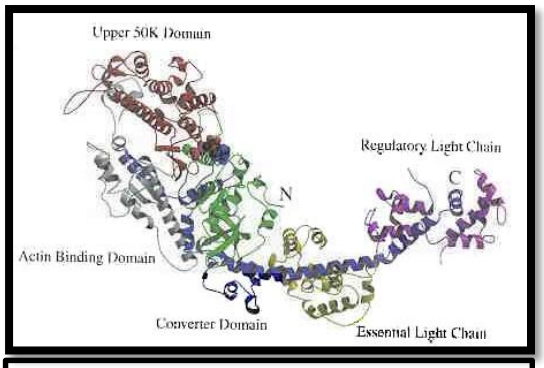

Fig 1: Structure of Myosin

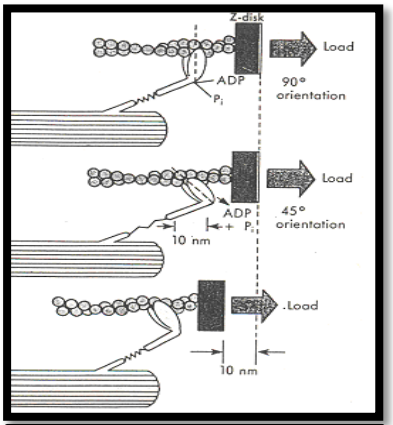

Fig 2: Conformational changes in myosin cross-bridge cycle

angular shift in the lever arm consisting of ELC and RLC as shown in **Fig.2**[26]. With the neck region serving as an important element of XB, RLC is responsible for maintaining the stiffness of the neck of the myosin head lever arm to attach actin and undergo power stroke[27]. Since the conformational changes are conferred mainly in the lever arm, the actin myosin contraction model is modified to lever arm model. Several studies were performed to correlate kinetics and biomechanics of the lever arm. Total internal reflection techniques were used to study the conformational changes in the myosin V while other paramagnetic probes were used to study the actomyosin conformational changes[28,29]. Previous studies performed on ***isolated myosin and actin*** or synthetically derived actin and myosin failed to indicate the physiological working of actomyosin and original characteristics of muscle functioning. Hence, study of actin and myosin in live working myofibrils is of the essence.

Actin

Vertebrates express three main isoforms of actin, three α-isoforms of skeletal, cardiac, and smooth muscles and the β- and γ-isoforms expressed in non-muscle and muscle cells. Mammals have at least six distinct genes of actin, four expressed in different muscle cells and two expressed in non-muscle cells[30]. Actins belong to the structural superfamily with sugar kinases and hexokinases[31]. It is a globular multifunctional protein that reversibly polymerizes to form thin, flexible fibers of 7nm in diameter and several micrometers in length. Actin is made of two clefts, upper cleft that binds nucleotides and lower cleft that is predominantly hydrophobic. Individual actin molecules are globular proteins (G-actins) consisting of 375 amino acids (43kd) that fold into two major α/β-domains (namely outer and inner domain) that have tight binding sites to mediate head-to-tail interactions with two other actin monomers to form filamentous actin (F-actin)[32,33]. G-actin is not an effective ATPase, whereas F-actin is[34]. Actin comprises of four subdomains that are known to surround the binding pocket for a divalent ion (Mg^{2+} or Ca^{2+}). Subdomains 1 and 2 are located at the periphery of the filament and subdomain 1 in particular contains both NH2 and COOH termini and is the one that interacts with myosin. Each actin makes contact with four other actins, the following and preceding actin on the same helix and two on each side of the filament across. Each actin uses ten surface loops and 2 α-helices to make these interactions[35,36]. In physiological state, each monomer is rotated at 166.15^0, therefore gives the filament double helical (right handed) appearance that has a total rise of $27.3A^0$ [37,38]. An actin filament is flexible, has a helical repeat every 37 nm, ranges from 5-9 nm in diameter, and has 13 actin subunits repeating every six turns between each cross-over of two long actin helices[39,40]. Since all actin monomers are oriented in the same direction and have similar polarity, their polymerizing plus and minus ends are distinguishably visible. Although ATP is not required for actin polymerization, the ones with bound ATP readily undergo the process of polymerization than the ones with ADP[41]. The polarity of actins is absolutely essential both in their assembly and in determining the direction of myosin with respect to actin during contraction in a muscle[42]

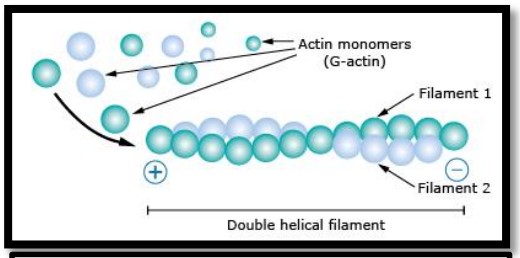

Fig 3: Structure of Actin

Sliding Filament Theory

A striated muscle is an organized intermittent molecular structure of actin and myosin in sarcomeres with repeating units of ~2–3-µm long. 1.6-µm long thick filaments located in the A-band are the myosin while 1-µm long thin filaments stretching from the Z-band to the H-zone are the actin molecules[43]. **Fig.4** shows the shortening of the sarcomere. As the sarcomere shortens, myosin molecules interact with actin and pivot the actin molecules into the center of the sarcomere. It was observed that A-band containing myosin thick filaments remain central and constant in length during contraction while the I-band, richer in thin filaments of actin, change its length along with the sarcomere[44]. It is quite interesting to know that, since muscles have near-constant volume, the distance between thick and thin filament changes from 9nm at short lengths and 4nm at long lengths. However, in cardiac muscles, it has been proposed that the change in the distance over which the cross-bridges function is partly dependent on Ca^{2+} sensitivity which is a major contributor of length dependence and tension in heart[45].

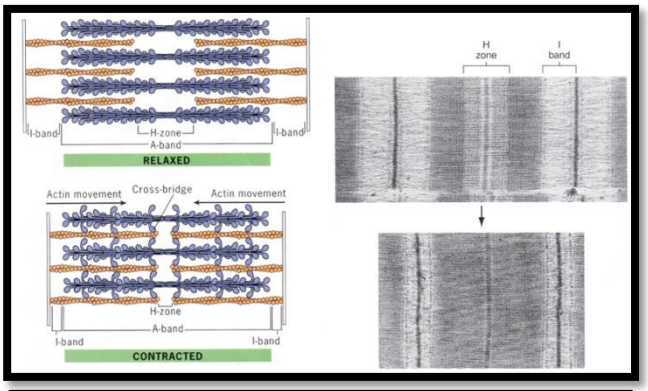

Fig 4: Depiction of a contracted and relaxed sarcomere

The Cross-bridge Cycle

Contraction is driven by cross-bridge activity. The cross-bridge cycle was proposed by Lymn-Taylor in 1971 and clearly visualized by Huxley on electron microscope using ultrathin sections, however, the direct evidence of change in shape of cross-bridges during the process of contraction was obtained by Reedy in 1965[46]. Kinetic analysis of S1 revealed that along with the existence of several ATP and ADP states, the bound ATP is in equilibrium with ADP and Pi with an equilibrium constant of ~7 [47]. This equilibrium establishes the reversibility between the molecules of ATP, ADP and Pi and therefore, does not allow the energy of ATP to dissipate while bound to myosin. The Lymn-Taylor model has four basic steps as shown in **Fig 5**: 1) Myosin with ADP and Pi binds to actin (Pre-Power stroke). 2) The release of inorganic phosphate renders a conformational change in the myosin that pivots actin molecules to the center of the sarcomere and delivers the power stroke for contraction. Release of ADP enables the rebinding of ATP. 3) The affinity of actin and myosin is greatly diminished with the attachment of ATP to myosin causing myosin to detach from actin and return back to its cocked position. 4) ATP hydrolyses into ADP and Pi[4]. A myofibril consists of millions of actin and myosin molecules interacting asynchronously to generate contraction. However, studying fewer actin myosin interactions as opposed to millions helps to avoid averaging numbers and thus reflect the actual spatiotemporal conformations of myosin is a concept used in this current study.

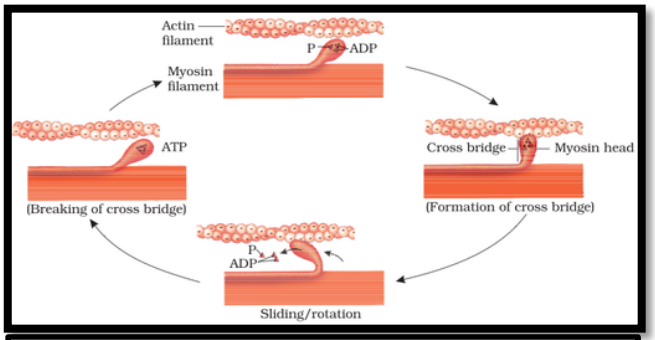

Fig 5: Cross-bridge cycle in a muscle

Regulation of Contraction in Striated muscle

Regulation of contraction in striated muscles is mainly exerted by Ca^{2+} through its effects on actomyosins via tropomyosin (Tm) and the three subunits of troponin (Tn), TnC, TnI discovered by John Gergely and TnT[21,48]. Biochemical studies have revealed that the positions of troponin and tropomyosin on thin filaments regulate their binding mechanisms with myosins by revealing the myosin binding sites on actin. These myosin binding sites on actin can be classified as 'blocked' (unable to bind cross-bridges), 'closed' (weakly able to bind cross-bridges) and 'open' (strongly bind cross-bridges with release of ATP hydrolysis products)[49]. The position of tropomyosin (Tm) on the actin filaments regulated by N-terminal Ca^{2+} binding sites on troponin C, conformational changes resulting from calcium in troponin T and troponin I, S1 myosin, in addition to 7 actin:1 tropomyosin:1 troponin (A_7TnTm) regulatory unit is essential to regulate contraction. Known regulatory positions so far include: 1) Ca^{2+} binding troponin complex undergoes 25^0conformational change[50,51] that renders tropomyosin to expose myosin binding sites on actin upon strong binding of cross-bridges (Geeves Model), 2) Neighboring units of actin can get activated with attachment of few cross-bridges to the regulatory unit (7actin:1tropomyosin :1troponin) with 1 μm-long actin filament of two sets of ~26 A_7TnTm structural units aligned end-to-end , 3) Following Ca^{2+} activation, actin myosin affinity is affected with structural changes in actin by allosteric actions, 4) Distance of myosin heads from actin binding sites depends on the inter-filament spacing with sarcomere length[21]. It has been suggested that myosin first binds actin with weak non-specific electrostatic contact (positively charged Lysine of S1 myosin with negatively charged amino acid of actin)[52], then second contact involves hydrophobic interactions and later upon strong binding (arginine 405 of myosin with actin) the cleft between upper and lower 50kD domains undergoes a change in conformation and thus releases the nucleotide to initiate a power stroke[53]. Up to four S1 myosin heads can potentially interact with each A_7TnTm regulatory unit. Many structural studies performed suggest that the angles at which myosin binds actin influences the position of tropomyosin on thin filaments that regulates the contraction in a muscle[50,51].

These functional mechanisms will be studied in greater depth in striated Heart and Skeletal muscles.

1. SKELETAL MUSCLES

Structure and function of skeletal muscles

Skeletal muscles are primarily made of contractile proteins. Skeletal muscle is a form of striated muscle tissue that is under the voluntary control of somatic nervous system. Most skeletal muscles are attached to the bones by bundles of collagen fibers called tendons. It is through this connective tissue the force generated in the muscles is transferred to the bones and thus movement occurs[54]. A dense layer of tissue called epimysium along with tendon surrounds each muscle. A muscle is made of number of muscle fibers called fascicles separated by the connective tissue called perimysium. Each muscle fiber is separated by endomysium. Each multinucleated myofiber is surrounded by a

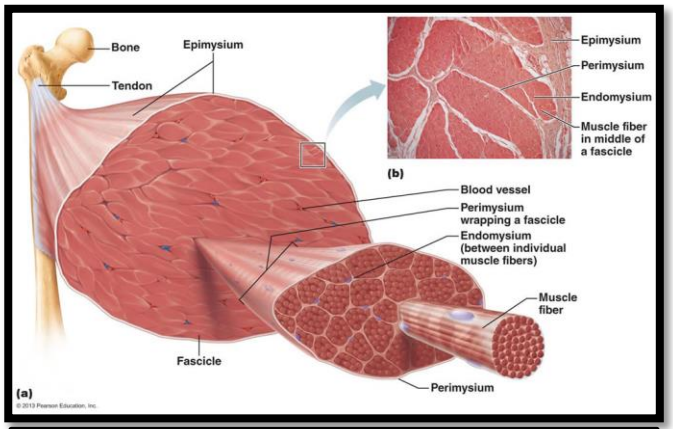

Fig 6: Gross anatomy to skeletal muscles

membrane called sarcolemma which is formed as a fusion of myoblasts during the process of myogenesis. Mature skeletal muscle cells are slender and range from 10-60 micrometers in diameter. The cytoplasm of each myofiber is termed sarcoplasm which is composed of myofibrils. The myofibrils are composed of sarcomeres that form the basic contractile unit of the muscle[55]. The muscle cell has additional protein molecules like glycogen, mitochondria, lipids etc. The transverse tubules (T-tubules) are invaginations in the muscle fibers that run perpendicular to the longitudinal axis of muscle fibers[56]. Skeletal muscles have regular striations which are alternating light and dark bands on the myofibrils. The thick filaments that form dark bands are composed of myosin while the thin filaments constitute actin, troponin and tropomyosin. A narrow band in the central region of the I-band is the Z line. The area between two adjacent Z-lines is termed a sarcomere which is about 2.5 micrometers long in a resting muscle. In the center of each sarcomere is a thin dark band termed the M band, flanked by thin pale H zones, where the thick and thin filaments that do not overlap[57].

Contraction of Skeletal Muscle

The contraction cycle begins in the neuromuscular junction. It is the site where neuro axonal terminal of the motor neuron meets the muscle plasma membrane through synaptic cleft. Upon stimulation, action potentials run down the neuron axonal terminal to depolarize the synaptic terminal and releases Ca^{2+} through calcium gated open channels[58]. Influx of Ca^{2+} ions leads to conformational changes in the synaptic terminal to release the neurotransmitter acetylcholine (ACh) through exocytosis. The neurotransmitter binds its nicotinic receptors on the plasma membrane and induces conformational changes in the membrane to open Na^{+} gated channels. The action potential travels to other muscle cells through T-tubules. The influx of sodium ions depolarizes the membrane and opens Ca^{2+} voltage gated channels in the sarcoplasmic reticulum as also on the membrane. The influx of Ca^{2+} inside the cells bring about the contraction by binding troponin

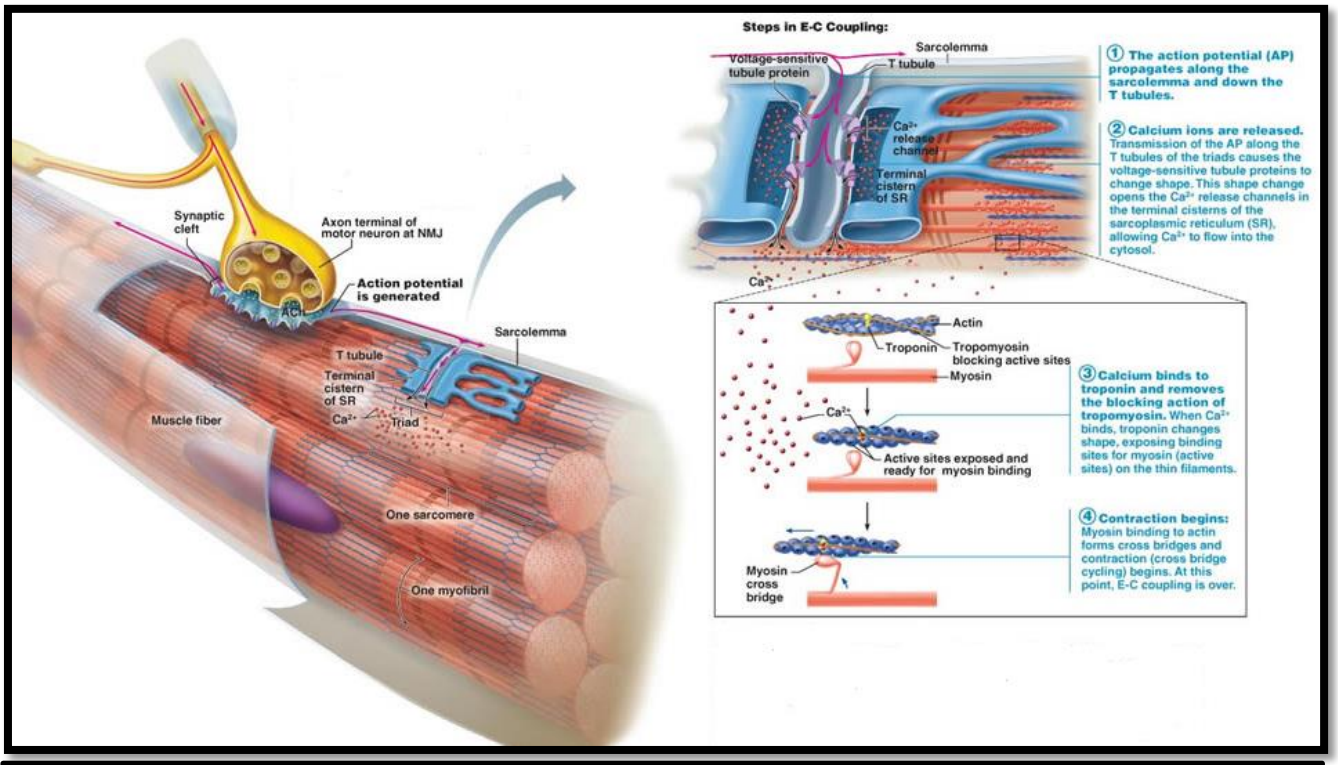

Fig 7: Contraction cycle in skeletal muscles

C and modulating tropomyosin to undergo conformational change to expose myosin binding sites on actin for myosin to bind[59-61]. In addition to Ca^{2+} ions, phosphorylation of RLC plays an important role in regulating skeletal muscles. In skeletal muscles, phosphorylatable light chain (P-LC) of myosin is known to regulate, however, not required for contraction[62]. Skeletal muscle myosin light chain kinase (skMLCK) is a Ca^{2+}/calmodulin-dependent serine-threonine protein kinase which is known to phosphorylate the regulatory light chain (RLC) of myosin molecule. It is expressed from *MYLK2* gene and found to be abundant in fast contracting muscles. Contraction begins when Ca^{2+} binds calmodulin to form $(Ca^{2+})_4$•calmodulin complex and displaces the regulatory segment of skeletal MLCK catalytic site to expose the N-terminal sequence of RLC with Ser15 phosphorylation site [63]to render actomyosin interactions in the force generating phase[62,63]. The lever arm of myosin then amplifies these small conformational changes into larger displacement of actins and thus actuating force in the process[64].

2. THE HEART

Functioning of the heart is an exquisite process. The organ of four chambers, which is the first organ formed, is the driving thrust to provide nutrients and oxygen in the embryo, and blood supply to the rest of the body throughout one's lifetime [65-68]. The heart is a muscular, autonomous, fist sized, blood pumping organ of four chambers - two superior atria and two inferior ventricles separated by interatrial and interventricular septum, is located in the medial cavity of the thorax (mediastinum) and extends from 2nd rib to 5th intercostal space[69-71]. The ventricular heart walls comprise of outer epicardium, middle myocardium and inner endocardium[70]. The cardiac muscle is an involuntary striated muscle with actin and myosin molecules as the running drivers to contract and generate force. The heart primarily made of myocardial fibers (covered with connective tissue endomysium) constitute of actomyosins, the muscle regulators that bring upon the process of contraction through sliding movement and utilization of ATP in the process[72-75]. The LV and RV of the heart are connected to each other in a series of processes that render them on an average to have similar stroke volume[67,73]. Previously, left and right ventricles of the heart were thought to function in complimentary to each other. However, recent identification of disparities in their physiology and proteins has modified the classical outlook of their similarity and their respective cause for cardiovascular diseases[76-78]. Additionally, different states of muscular contractions namely force induced studies, ATP hydrolysis etc. have been studied quite extensively in the past through x-ray diffraction[79,80], biochemical and physiological methods[46,53]. However, our knowledge on spatial and temporal conformational changes of individual myosin cross-bridges in live muscle remains superficial. The purpose of a part of the research is to elucidate (three) aspects of the project namely comprehending the characteristics, differences in spatial distribution and molecular kinetics of muscle contraction-relaxation cycles in the two ventricles of the heart. The answer that I aspire to determine is, if differences in the basic structures of left and right ventricles in healthy hearts exist, their influence on heart failures and the role of point mutations in the impaired functioning of the heart.

Structure and Function of Cardiac Muscle

Cardiac muscle is a type of involuntary striated muscle found only in the walls of the heart. This is a specialized muscle that, while similar in some ways to the skeletal and smooth muscles, has a unique structure and function. Cardiac muscles like skeletal muscles can contract strongly and like smooth muscles contract independent of external stimulation like hormones or nerves. Additionally, these muscles are capable of carrying action potentials like the neurons. Cardiac muscle cells are short (about 0.1 mm long

and 0.02 mm wide) and uninucleate. Anatomically, the myocytes are typically branched and arranged in regular parallel bundles and connected through intercalated discs that give them an appearance of synctium. The junctions between the cells are partly tight junctions for strong adherence, and partly gap junctions to allow free flow to small molecules and electrical currents. There are additional set of junctional complex called desmosomes that are specialized for cell-cell adhesion. The muscular tissue of the heart is called the myocardium that is composed of bundles of muscle cells known as myocytes[69]. The myocyte or the muscle fiber is essentially the single cell of the muscle. These muscle fibers contain many myofibrils, the contractile units of the muscle that run end to end with alternating actins and myosins[69,81] These filaments are organized into repeated subunits called the sarcomere that give these muscles their striated look. The cardiac thin filaments comprise of actins, tropomyosin that wraps around actins and complex of three troponins namely: Troponin I (cTnI) that holds tropomyosin-troponin complex intact, Troponin C (cTnC) that acts as calcium sensors and Troponin T (cTnT) that binds TnI. Cardiac myosin is conventionally a class II myosin composed of two heavy chains (MyHC) and two pair of light chains (MLCs). The heavy chains are further classified into two isoforms α and β isoforms. It is these heavy chains that determine the properties of the heart muscle with respect to its ATPase activity and rate of shortening. In mammalian cardiac muscle, three different isoforms of myosin have been identified: V_1 is a homodimer of α chains and has high ATPase activity, V_2 is a heterodimer of of α and β chains, V_3 is a homodimer of β chains and has low ATPase activity[82,83].

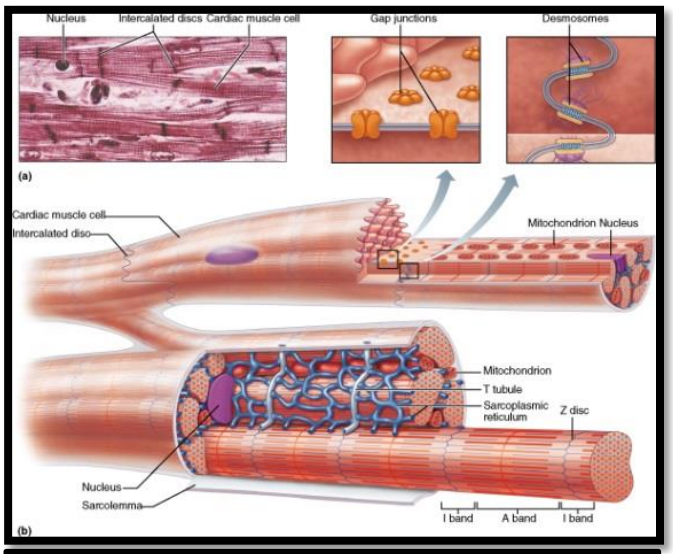

Fig 8: Cardiac muscle: a) Cardiac muscle tissue. b) Cardiac muscle cell

Cardiac Muscle Contraction

1. <u>*Electrical impulse of cardiac cells*</u>: Cardiac muscle being adapted to be highly resistant to fatigue is rich in mitochondria (enables aerobic respiration), myoglobins (oxygen storing pigment) and a good blood supply that provides necessary nutrients[84]. The mechanism of contraction is similar to skeletal muscle but the excitation contraction coupling differs slightly. Cardiac contraction is initiated in the excitable cell (pacemaker cells) of the sinoatrial node (SAN) by both, spontaneous depolarization (pacemaker potential) and sympathetic activity. These action potentials are propagated through gap junctions to non-pacemaker cells and from pacemaker cells to contractile cells to allow succinct coordinated contraction of the heart. The SA node excites the right atrium (RA) to travel through *Bachmann's bundle* to excite left atrium (LA) and further travel through the internodal pathways to atrioventricular node (AVN). The T-tubule is a deep invagination of the sarcolemma that allows depolarization to spread quickly through the cardiac cell. The excitation contraction coupling (ECC) in cardiac muscles is activated by the entry of Ca^{2+} ions through the L-type voltage calcium

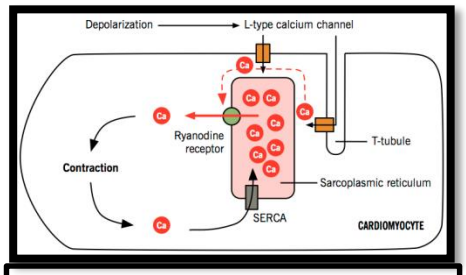

Fig 9: Initiation of contraction in cardiomyocyte

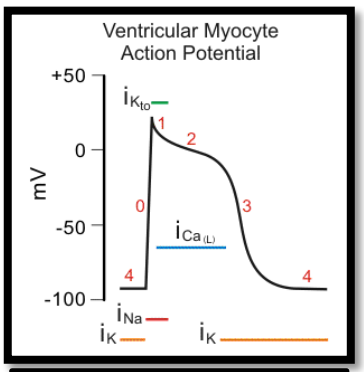

Fig 10: Action potential in a cardiomyocyte

channels (dihyropyridine receptors) in the terminal cisternae which then trigger calcium – induced – calcium release (CICR)[85,86] from the sarcoplasmic reticulum that further triggers the release of Ca^{2+} ions (calcium release channels – ryanodine receptors RyR2) into the cytoplasm. More recently, a second, quite separate sarcoplasmic reticulum Ca^{2+} release to enhance CICR has been seen[87-89]. These calcium ions cause the pacemaker cells to produce action potentials (AP). Typically, these APs travel to contractile cells which rapidly depolarize (phase 0) with the influx of Na^+ ions. Rapid inactivation of Na^+ channels mark phase 1. The cells begin to restore their ion concentrations through influx of Ca^{2+} balanced with efflux of K^+ leading to a plateau phase (phase 2) which renders the cells to have large concentrations of Ca^{2+} [90-92]. Similar to skeletal muscles, cardiac contraction begins when calcium ions bind to cardiac troponin- C, which allosterically modulates tropomyosin[93] and induces a conformational change in the regulatory complex Troponin – I to expose the site on the actin molecule that is able to bind to myosin ATPase located in myosin head[94]. Additionally, myosin binding protein C, binds myosin, and when phosphorylated, induces contraction. Phase 3 is marked with closure of L-type Ca^{2+} channels and opens rectifier K^+ channels to repolarize the cell when the intracellular Ca^{2+} is pumped out and taken up by the endoplasmic reticulum ATPase pump and Na^+/Ca^{2+} exchange pump. The cardiac cells return back to their resting membrane potential (phase 4) for another cycle to begin[90,92,95].

2. <u>Regulation by Autonomic Nervous System</u>: The depolarization and action potentials in the heart are affected, but not controlled by the autonomic nervous system. Parasympathetic activity releases acetylcholine (ACh) which binds to the muscarinic receptors (βγ subunit of G protein), induces potassium efflux and hyperpolarizes (resting potential is more negative) the cell to prolong the initiation of action potential of the pacemaker cells. Parasympathetic activity results in the decrease of heart rate. On the contrary, sympathetic nervous system induces depolarization through β1 receptors of G protein to open sodium and calcium channels, thereby results in an increase in heart rate[96,97].

Left and Right Ventricles of the Heart

The ventricles of the heart connected so intimately to each other in driving the function of the whole heart were therefore thought to have very similar function. Moreover, the proteins of LV and RV originate from the same genes (*MYL6* for ELC, *MYH6* and *MYH7* for HC, *MYL2* for RLC, *MYL3* for LC). Only, recent advances shed light on their dissimilarities at varying levels of genetics, proteomics[76], force studies, etc[24,98,99]. Much of the differences in the LV and RV are explicable from their different embryological origins[100,101]. Previously, the myocardium was thought to originate from a single source of myocardial progenitor cells, however, recent study's recognition of two different sets of cells contributing towards formation of the ventricles have changed our perspective on the formation of the heart[102,103]. The formation of heart progresses with primary heart tube development that eventually transcends to crescent formation in 19-20 days of embryological processes, undergo several convolutions and looping to finally bifurcate into two lineages, first of which form the anterior field to create right ventricle and the atria in the future while the second lineage of posterior dorsal progenitor cells develop the left ventricle of the heart[104,105]. Since LV pumps blood throughout the body, it generates more pressure (therefore is thicker than RV) and requires more energy as compared to RV that pumps blood at a shorter distance to the lungs. Morphologically,

owing to the known differences in the ventricular shapes, the left being ellipsoidal and right being triangular, crescent shaped wrap around left ventricle, the two ventricles were also at odds with their myofibrillar architecture. It was noted that the left ventricular myofibrils were lengthier and thinner than their right ventricular counterparts. Structurally, RVs are well known to have irregular surfaces with unrefined trabeculae and lack of fibrous continuity in the inflow and outflow tracts of the valves compared to the LVs[106].

At the molecular levels, the transcription factors expressed during the development like the *heart and neural crest derivatives (hand)* are dissimilar in the ventricles with hand1 restricted in LV and hand2 confined to the RV[107,108]. Tbx5 was restricted to LV during early development of the heart which was then seen to be uniformly distributed during the later stages of heart development[109]. Investigations performed at the gene level delineate differences in the mRNA and miRNA protein gene expressions between the two ventricles, with higher levels of expression concentrated in LV[110]. Other reports suggest differences at the protein levels of the two ventricles wherein higher amounts of energy using proteins like ATP synthase and others like Heat Shock Protein (HSP), Myosin Binding Protein C (MBPC) and Myosin Light Chain 2 (MLC2) were noted in Left compared to the Right ventricles in healthy mice hearts[76,98,99].

The dichotomy of LV and RV is also expressed at their physiological levels. The LV and RV although, linked intimately, also show differences at their basic fiber structures. The RV consists of transverse fibers in its free wall with shared oblique fibers in its interventricular septum while the LV is encircled by oblique and circumferential fibers[111]. It is known that the oblique septal fibers and circumferential LV fibers are more mechanically efficient than the transverse fibers of RV in an event of an afterload[112,113]. Thus mechanically, rotating and twisting motion of the left ventricular fibers is sufficient to expel blood from its ventricle while the right ventricular fibers undergo shortening of longitudinal fibers to eject blood from its ventricle. Some research performed on hearts using mechanical studies and computational modeling have revealed that the fibers in the LVs gradually change their geometry from right-handed in subendocardium to left-handed in subepicardium that render directional force to eject blood[113]. Although, differences have been noted at many levels, differences at the functional levels remain unexplored. Part of my project aims at studying the varying contractile properties at the elementary molecular levels in left and right ventricular tissues of hearts of healthy patients and their uncontrolled arrangements in the ventricular tissues of those who underwent failure and/or cardiomyopathy mutated ailment.

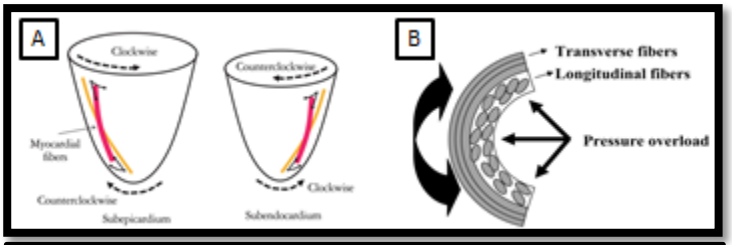

Fig 11: Basic fiber orientation in the ventricular walls. A) Orientation of fibers in left ventricular wall. B) Orientation of fibers Right Ventricular wall.

Cardiovascular Diseases and Heart Failure

Cardiovascular disease (CVD) is the leading global cause of death, accounting for 17.3 million deaths per year, a number that is expected to grow to more than 23.6 million by 2030[114]. Over the last two decades, major advances have been made in our understanding of the CVD. Cardiovascular disorders span all aspects of the disease that affect the structure and function of the heart. A part of my thesis work involves studying

the molecular mechanism in cardiomyopathy induced by single point mutations and in noting the differences in the LV and RV of hearts during non-ischemic heart failure.

1. Heart Failure (HF): Heart failure is the leading cause of hospitalization in the USA with common symptoms of angina pectoris, peripheral edema, dyspnea, etc[115,116]. Despite many improvements in the treatments of various cardiac disorders, Heart Failure (HF) is an exception, as the numbers on chart are on an ever rise with limited prolongation in survival, particularly when the functional changes are asymptomatic[117,118]. Since the process of silent alterations in the heart function take place over a long period of one's lifetime and while many medications offer promises to defer these heart failure related adversities, rarely do patients recuperate completely regardless of sophisticated treatments and are thus pushed over the edge to undergo transplants[119].

The prevailing ignored subtle differences, in part or combination, may lead towards developing the two different forms of heart failures these ventricles undergo. While 5.1 million people in the USA have been diagnosed with heart failure so far, heart failure contributed to 1 in 9 deaths in the year 2013, among which about half of the people diagnosed died in 5 years and it costs the nation approximately $32 billion each year[114]. Many conditions (Coronary Artery Disease--CAD, atrial fibrillation, kidney diseases etc.) contribute toward a failing heart[115]. However, determining differences in the function of the ventricular tissues remain the basic focus of this study. The outlet chambers of the heart, although responsible of filling blood from the atria and pumping it out to aorta and pulmonary veins, have quite varying pressures and afterloads. RV is low pressure chamber with low vasculature and oxygen consumption while, paradoxically, the LV is high pressure chamber, hence has higher vasculature and oxygen consumption[120,121]. The afterload exerted on LV compared to RV is uniquely different and so are their respective functions in response to these alterations. The sudden increases in the afterloads are not well tolerated in the RV as it is done in the LV rendering the RV more sensitive to afterload changes[110]. When LV undergoes heart failure upon LV systolic dysfunction, pulmonary artery pressure increases transcending to increased RV pressure resulting in reduced RV contractility. As the LV metamorphose to become progressively more spherical, the septal fibers lose their ability to remain oblique reducing their mechanical influence, further maim the RV function and result in RV failure[122]. By far known surgeries and many other preceding methods used to salvage HF have proven to be a major clinical challenge in maintaining the patient survival, particularly in right ventricular failures. The myofibrillar apparatus is important as these effector proteins themselves undergo marked changes to establish cardiac diseases in the process. Hence, it is imperative to understand the subtle differences between LV and RV of the heart prior to actuating treatments based on obscure knowledge.

1.a. Diagnosis: Heart failure is diagnosed based on medical/family history and tests like electrocardiogram (EKG), levels of brain natriuretic peptide (BNP) and creatinine in blood, radionuclide ventriculography, stress test etc. It has been postulated that heart failure develops once the number of viable myocytes drop below the required sustainable amounts to maintain cardiac compensation[123]. Acceleration in the death of myocytes appears in the presence of ventricular hypertrophy secondary to hypertension, smoking[124]. Despite biological and technological successes, it gradually became recognized that the war against cardiovascular diseases was far from over.

2. <u>Familial Hypertrophic Cardiomyopathy (FHC) or Hypertrophic Cardiomyopathy (HCM)</u>: FHC is the most commonly inherited (autosomal dominant trait caused by single missense point mutations in the genes encoding sarcomeric proteins) cardiovascular disease associated with high risks of heart failure, diverse age of onset and is characterized by increased ventricular wall thickness, myocardial disarray and fibrosis[125,126].

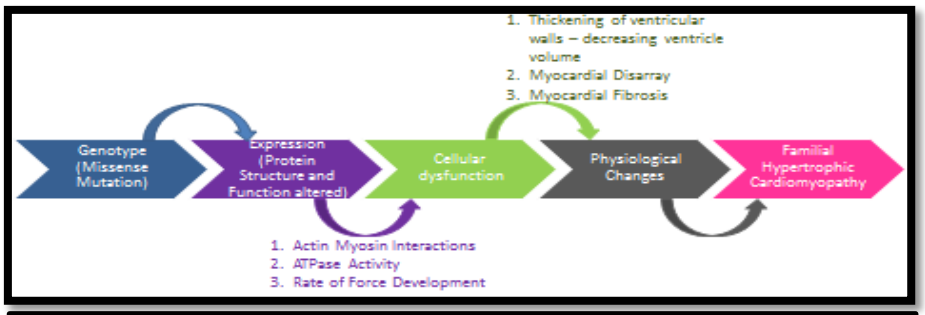

Fig 12: Schematic representation of the FHC disease progression with single point mutations.

FHC affects approximately 0.5% of the general population[127]. Heart failures that are commonly seen in the patients affected with FHC make FHC a leading cause of death, especially in young adults under the age of thirty[126]. In many individuals, the pathophysiology of the disease is featured by the thickening of the left ventricular wall and interventricular septum that impedes the flow of oxygen-rich blood from the heart during systole. Common symptoms, although not necessary to attribute to the disease as many may go asymptomatic are angina, dyspnea, syncope and arrhythmia. While many individuals with FHC are asymptomatic, this condition can have severe consequences viz. develop life threatening abnormal heart rhythms, more than often sudden cardiac deaths (SCD) in few extenuating mutations or worst heart failures that may require heart transplants. More than 1000 mutations in the sarcomeric proteins linked to FHC have been identified. Different FHC mutations in the sarcomeric proteins have been listed below[128].

Gene	Protein	Chromosome	Frequency
TTN	Titin	2	<1%
MYH7	β-myosin heavy chain	14	15-25%
MYH6	α-myosin heavy chain	14	<1%
MYL2	Myosin regulatory light chain	12	<2%
MYL3	Myosin essential light chain	3	<1%
MYBPC3	Myosin binding protein C	11	15-25%
TNNT2	Troponin T	1	<5%
TNNI3	Troponin I	19	<5%
TPM1	α-tropomyosin	15	<5%
ACTC	Alpha actin cardiac	15	<1%
TNNC1	Troponin C	3	<1%

Table 1: Myofilament genes implicated in hypertrophic cardiomyopathy and their frequencies in HCM

The interference of the mutations which impede the synchronized actin myosin contractile unit may alter protein function and eventually lead to malignant outcomes. Patients with FHC express wide heterogeneity in their clinical outcomes and the course of the disease progression which makes it equally difficult to establish a genotype-phenotype correlation for the manifestation of the disease. Several other non-genetic factors like age and lifestyle may also affect the manifestation of the disease. Despite medical advances, one of the greatest challenges is to discern the mechanisms of mutated gene related clinical outcome to cause the disease.

2.a. Genetic Testing: The diagnosis of FHC is most often established with non-invasive cardiac imaging like electrocardiography and cardiac magnetic resonance imaging (cardiac MRI). However, the clinical assessment of the disease is difficult, especially in the young, since ECG and electrocardiography readings may not be diagnostic and the severity of disease may vary[129]. By far, the most accurate FHC diagnostic technique is DNA analysis, it is however, laborious, because of the large number of FHC related genes, polymorphism in several amino acids and allelic heterogeneity in the disease loci[129-132]. Current medical help of diuretics, gold standard diagnostic approach of cardiac catheterization or catheter ablation, drugs targeting neurohormonal receptors like beta-blockers, L-type channel blockers, disopyramide or to suppress arrhythmias were accompanied with side effects and thus proved unhelpful[133]. Despite the feasibility of these approaches, benefits were trivial and alleviating the disease never a guarantee. The intriguing clinical variability of the disease, including onset (symptoms and hypertrophy) and prognosis has made it difficult to be diagnosed and warrants further research into developing methods for its early detection. Expanding research to elucidate the molecular mechanisms by which subtle genetic variation in contractile proteins overturn the normal functioning of the human heart, one with considerable promise to develop new strategies to limit or even prevent pathogenesis of FHC is the area of focus in this study. I hypothesize that the degree of cross-bridge disarray in the transgenic mutant myocardium will reflect the altered contractile properties of the muscle. This study will further give a deeper understanding into the molecular mechanistic disharmony the cross-bridges undergo during contraction, relaxation and rigor, owing to the degree of mutations. We look at a gene myosin regulatory light chain 2 (*MYL2*) and troponin I in particular with their mutations in causing FHC.

2.a.1. Regulatory Light Chain (RLC): The ventricular isoform of human cardiac myosin regulatory light chain (RLC) has been seen as one of the sarcomeric proteins associated with FHC. The RLC (171 amino acid long) wraps around myosin 35 amino acid IQ motif (Ile-Gln-x-x-x-Arg-Gly-x-x-x-Arg) in the neck domain. RLC along with other light chain protein called essential light chain (ELC) support the lever arm stiffness that help elaborate smaller conformational changes into larger movements to produce force[17,134]. As an EF-hand Ca^{2+} binding protein, the RLC contains Ca^{2+}-Mg^{2+} binding site (residues 37-48) that is known to act as a buffer to aid delayed release of Ca^{2+} from the sarcoplasmic reticulum during diastole[126,135]. The N-terminal divalent cation binding site is known to be occupied with Mg^{2+} when the muscles are in relaxed states and may become partially saturated with Ca^{2+} upon contraction[136]. Additionally, RLC contains highly preserved phosphorylation site Ser^{15} that along with Ca^{2+}-calmodulin (CaM) activated myosin light chain kinase (MLCK) is known to play an important role in regulating myosin during contraction[137]. Attenuation of RLC phosphorylation is usually associated with ventricular hypertrophy resulting in decreased cardiac performance. This may ultimately result in heart failure.

2.a.1.1. *Mutation in MYL2 (A13T):* The mutation A13T is replacement of an uncharged and nonpolar amino acid with an uncharged but polar amino acid threonine. The mutation was first noted in Danish population with severe hypertrophic cardiomyopathy[138]. Members of the family were heterozygous for the mutation and showed pronounced septal and ventricular hypertrophy. The mutation was identified yet again in 2005 in another Danish population[139]. The mutation represents patients with septal hypertrophy, mid left ventricular obstruction and enlarged left ventricular wall. Attenuation of the RLC phosphorylation has been shown to induce ventricular hypertrophy[140]. At the protein levels, RLC phosphorylation at Ser^{15} was shown to alter the secondary structure (α-helical content) and Ca^{2+} binding affinity of human ventricular RLC proteins[125] whereas at the level of myofilaments, phosphorylation demonstrated decreased distance between myosin head and actin filaments to help bring them close to each other[141]. Given the important role of RLC in regulating myosin-actin activity during contraction, one can hypothesize that the FHC mutations in RLC could affect the normal functioning of the cardiac muscle. In this part of the study, we look at the effect of mutation A13T near the phosphorylation site Ser^{15} in myosin RLC. We study the mutation in heterozygous mouse model with very low expression. The muscle contains 90% WT and only 10% mutated myofibrils. We hypothesize that the mutation alters the acto-myosin cross-bridges and affect the ATP cross bridge cycle in the process. This hypothesis is specifically addressed in Chapter VII.

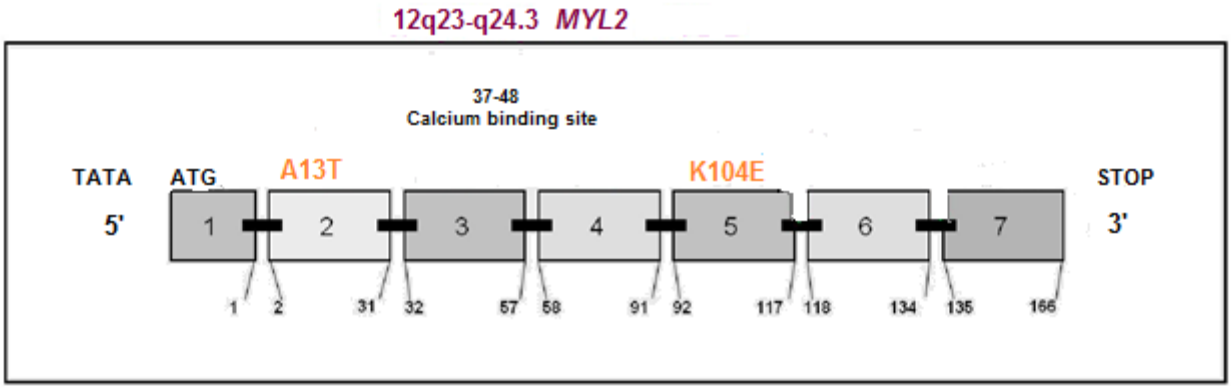

Fig 13: MYL2 (Regulatory Light Chain) gene mutations of A13T (Alanine to Threonine) and K104E (Lysine to Glutamate)

2.a.1.2. Mutation in MYL2 (K104E): K104E mutation results with replacement of positively charged lysine with negatively charged glutamate. The mutation was first observed in Danish population with their son displaying septal hypertrophy that progressed to diastolic filling abnormalities while the parents were completely asymptomatic with normal ECG. Quite alike the mutation A13T, K104E mutation is seen in the RLC. The replacement of lysine with glutamate is known to induce conformational changes in the structure of RLC which further affects its interactions with the heavy chains and ultimately alter the structure of the lever arm[142,143]. Not much research has been performed on the mutation but a few studies suggest that diastolic filling abnormalities have been reported in the patients with this mutation[144]. Diastolic dysfunction is often associated with changes in the muscle stiffness during relaxation that leads to the disease[145,146].

2.a.2. Mutation in Cardiac Troponin I (R21C): R21C mutation is a TnI mutation in the N terminus of TnI in *TNNI3* gene. Within the thin filaments of actin, troponin C (TnC), troponin T (TnT) and troponin I (TnI) constitute the troponin complex, which causes contraction in the myofilaments by propagating the calcium induced signals[147]. TnC binds Ca^{2+}, TnI binds actin and inhibits actomyosin interactions and TnT links Tn

complex and tropomyosin. Cardiac TnI (cTnI) is different from other TnI as it has additional ~ 30 amino acids in its N-terminal[148,149]. Troponin undergoes conformational change and allosterically modulates tropomyosin upon calcium binding, inducing release of TnI inhibition on actin to expose myosin binding sites and produce contraction[149]. There are several isoforms of the protein, all of which possess the plasticity to render these protein molecules to adapt to any conformations with TnT, TnC and tropomyosin that comes along with calcium binding[148,149]. The N-terminal of TnI responds to the high and low call of adrenergic responses. Troponin I consists of two serine sites at positions 23 and 24 (including the initial methionine) that upon β-adrenergic stimulation of the heart induces PKA-dependent phosphorylation[150]. At least basic residues at −2 and −3 positions are needed to cause phosphorylation of serine at position 0 by PKA[151]. R21C precisely has these requirements fulfilled with residues Ser^{23}/Ser^{24} in it of which Arg21 recognizes phosphorylatedserine cluster[152]. It has been shown that phosphorylation of cTnI increases rate of relaxation and decreases Ca^{2+} affinity of cTnC[153,154]. Approximately 35 mutations in cTnI have been reported to cause hypertrophy and dilated cardiomyopathy[155]. By far known, R21C is the only mutation identified in the N-terminal region of cTnI to be associated with Hypertrophic Cardiomyopathy (HCM)[156]. The mutation is located in the PKA substrate consensus sequence (RRRSS)[157]. It is known that the R21C mutation reduces PKA-dependent phosphorylation of Ser^{23}/Ser^{24} of TnI and curtails the decrease in Ca^{2+} sensitivity during contraction[154,158]. The mechanisms through which R21C may contribute in the reduction of phosphorylation are: i) R21C may disrupt the PKA consensus sequence and, ii) the mutant supersedes the WT cTnI that can be phosphorylated[159]. The aim of the study is to understand the detrimental effect of R21C on the degree of order and kinetics of myosin cross-bridges in LV and RV of mouse hearts.

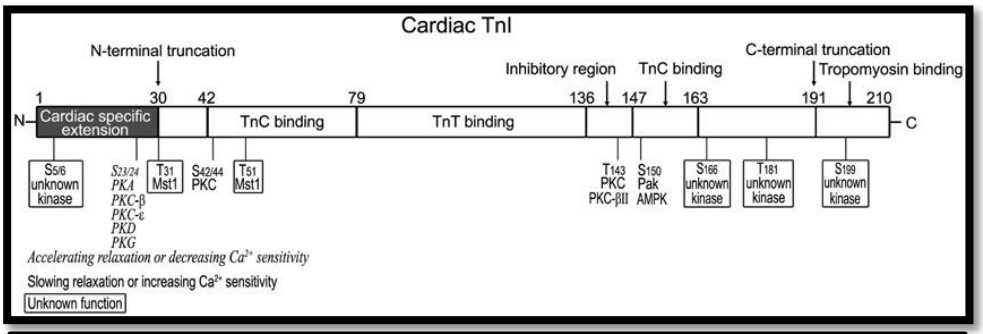

Fig 14: Ser $^{23/24}$ phosphorylation sites of cardiac TnI

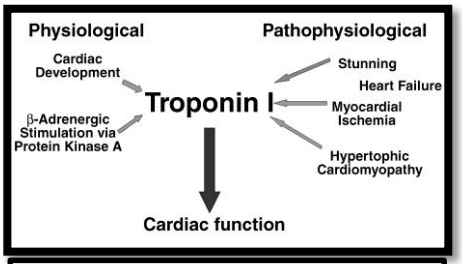

Fig 15: Clinical manifestation of mutation in TnI

Rationale: Molecular Influence of Proteins

Proteins are the most abundant class of molecules that contribute to over 60% of the dry weight of the cells. Although, all proteins are made of the same 20 amino acid conformations, their role and function in a cell is quite diverse and dependent on the given physiological and environmental conditions[160]. The current study focuses on two such driving protein molecules of heart muscles: Actins and Myosins. Besides proteins, cells also constitute of other macromolecules like lipids, nucleic acids etc. Because no single species of macromolecules may be present at higher concentrations, all species taken together occupy a significant volume which is called molecular crowding[161]. Hence in any intact cell, proteins constitute to mere μmolar concentrations. However, their size, ionization properties, hydrophobicity/ hydrophilicity is influenced by solubility, stability and structural organizations that exist essentially in an aqueous or membrane environment[162]. Since molecules are mutually impenetrable, their activity and function relies

upon their surroundings. Since the entry of small water molecules remain unrestrained, it renders protein molecules to be over hydrated as in any physiological state[163,164]. Therefore, it is imperative to study protein molecules in as close to physiological state as possible. The study performed on live myofibrils in current research is a step closer in understanding the role and function of actin and myosin in physiological states.

Changes endured in a muscle

All the muscles in the body, both voluntary and involuntary are affected. A muscle and thus its myofibrillar and sarcomeric proteins undergo change in shapes in order for the muscle to perform its activity. *Contraction:* A muscle contracts upon stimulation it receives (skeletal muscle) or has in itself (cardiac muscles) to initiate action potentials. The influx of Ca^{2+} ions during these action potentials trigger contractions and initiate the cross-bridge cycle in a myocyte. In addition to Ca^{2+} ions, ATP molecules are equally vital when they bind myosin of the actomyosin complex that helps detachment of myosin molecules from actin for another cycle to begin. Thus the presence of ATP weakens the actin-myosin interaction enough to let them slide past each other while Ca^{2+} ions initiate myosin ATPase and muscle shortening. The cross-bridges are formed between actin and myosin and released upon ATP binding. *Relaxation:* When contraction is no longer required, Ca^{2+} is resequestered by sarcoplasmic reticulum and muscles undergo relaxation. When ATP weakens the actin-myosin interactions, in the absence of Ca^{2+}, myosin ATPase activity is low as no force is required and thus no shortening in the muscle occurs. The cross-bridges are necessarily perpendicular to the actin filaments in the sarcomere. *Rigor:* Physiologically, this state can be achieved when the cells die. It is termed rigor mortis. When cells run out of ATP, during the cross bridge cycle, attachment of ATP to myosin helping detachment of myosin and actin is curtailed. Hence, myosin stays locked onto actin so rigidly that they cannot slide past each other and muscles cannot shorten. The cross-bridges change angle to the actin filaments[165,166]. The orientation of cross-bridges can thus help understand the different states of muscle contraction-relaxation states and give information on their possible alterations during FHC or heart failure.

Fluorescence Polarization

The technique was first theoretically described by Jean Perrin in the year 1926 and applied six decades ago by Gregorio Weber. When a linear light is used to excite a fluorophore, the fluorescent light emitted has both vertical and horizontal components. The ratiometric differences in the intensities to the sum of the intensities of polarized lights measured through emission polarizer is polarization of fluorescence. $PF = I\parallel - I\perp / I\parallel + I\perp$. The value of PF is determined by the fluorophore and is subject to rotational relaxation as given by Perrin's equation, $r_0/r = 1+(\tau/\theta)=1+6D\tau$ where τ is the fluorescence lifetime time, θ is the rotational correlation time, D is rotational diffusion coefficient, r_0 is the anisotropy at t=0. Fluorescence anisotropy measures depolarization of the fluorescence emission. The alignment of MT200 fluorescence spectrometer and polarization used in my study is schematically represented in the **Fig.16**. When the electric dipole moment of the fluorophore and incident light are aligned parallel to each other, maximum light is absorbed by the fluorophore. Therefore, when polarized light strikes a fluorophore immobilized on actin/myosin, the absorption and fluorescence measured reflects the conformation of cross-bridges. Polarized light from the laser (blue) is emitted from the laser to image the isolated myofibril. Only the fluorescent light emitted by the myofibril (green highlighted with orange) passes through the dichroic mirror which is condensed to pass through 50μm pinhole to omit the out of plane fluorescence light. The fluorescent light is then split into two by 50-50 beam splitter and is passed through two polarizers, one oriented parallel and other perpendicular to

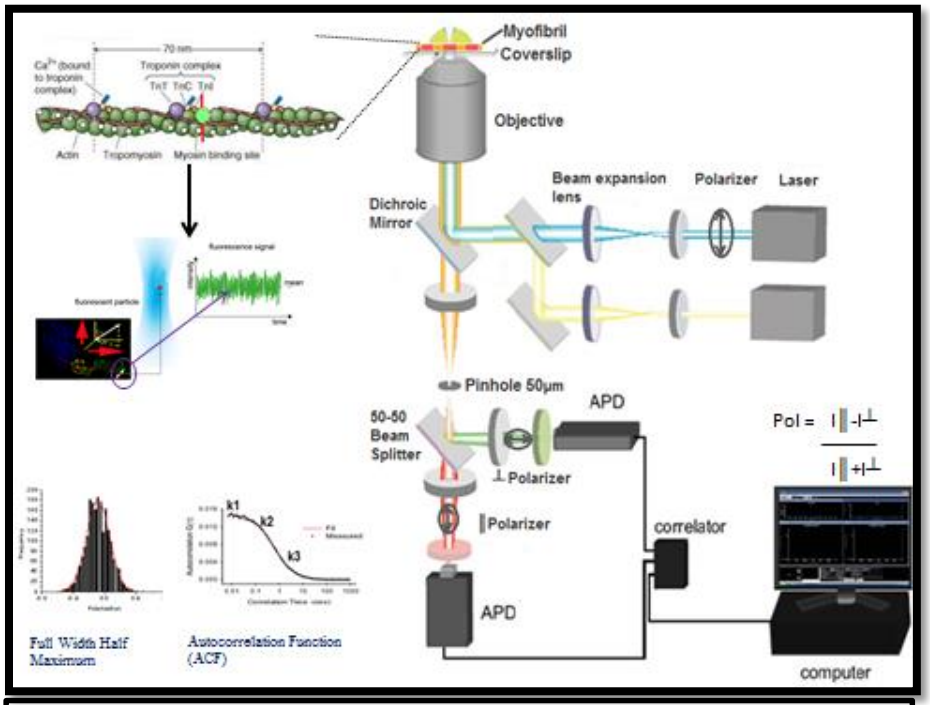

Fig 16: Schematic representation of MT200 with labeled actin molecule.

the axis of the myofibril. The polarized light is then finally collected by the avalanche photodiodes with single molecule detection capability. Polarized fluctuation intensities are plotted on histogram to study the cross-bridge orientation. Autocorrelation function of polarized fluctuation intensity is plotted to study the kinetic rate constants of cross-bridge contraction cycle. This remains the working hypothesis of the techniques in my project.

Method of Measuring Kinetics

The **Fig.17** shows the signal from the orientation of a single cross-bridge during contraction. In a three-state model, to begin on the left, the anisotropy is seen as 0 with unbound cross-bridge. When myosin attaches to actin (k1) at time t_1, anisotropy increases since the cross-bridge is immobilized. The release of ADP and Pi claims firm attachment of actin to myosin to produce force i.e. power stroke (k_2), thus increasing the anisotropy further. The cycle ends upon ATP attachment, and detachment of actin from myosin (k_3). In a typical two state model **Fig.18**, Time t_{PRE} represents the time that the XB is in the actomyosin attached adenosine di phosphate (ADP) state (i.e. attached to thin filaments either weakly or stronglybefore the power stroke), and the time t_{POST} represents the time the XBs remain in the rigor like state of actin attached myosin before binding to a fresh molecule of ATP that dissociates mysoin from thin filaments followed by a long period when it is not attached to thin filament.

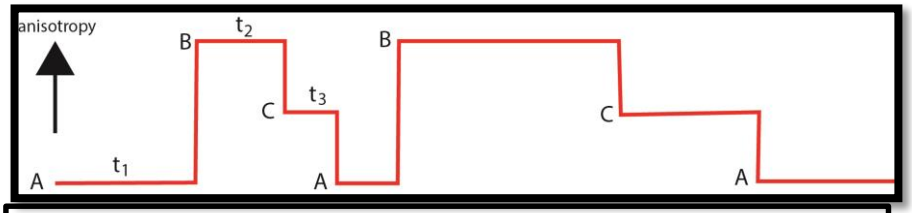

Fig 17: Change in anisotropy: three state model of myosin crossbridge

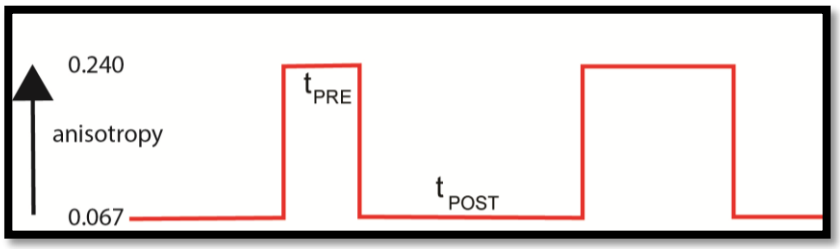

Fig 18: Change in anisotropy: two state Pre and Post power stroke crossbridge model

The series of fluctuations received from polarization fluorescence (PF) that indicate the changes in the kinetics of cross-bridges at a given time in contracting state is plotted as an Autocorrelation function (ACF). The rate of decay of ACF from maximum to zero depicts the time frame that average fluctuations take to undergo contraction. The decay determines the kinetics and time taken by actomyosin complexes during a cross-bridge cycle.

Method of measuring order of orientation

Orientation of XBs is an important parameter in muscular actomyosin interactions. Full Width Half Maximum (FWHM) is the distribution of fluorescence polarization of the transition dipole of the dye plotted as a histogram - a plot of number of events of a given polarization value occurring during a 20s experiment and fitted with Gaussian curves. Generally in a myofibril not all myosins attach actin (except rigor). Also myosins attach actins at a stipulated angle. This myosin bound actin undergoes angular changes before a power stroke takes place. The graph shows the average positions of myosin bound actin and the respective angular changes during contraction, relaxation and rigor in a muscle.

Significance

Fluorescence polarization (FP) at single molecule detection level will give an insight in the molecular spatiotemporal alignment and mechanism of actin - myosin interaction in working live myofibrils of skeletal and cardiac muscles in different conditions. FP is a very sensitive indicator of the orientation of the transition dipole of the fluorophore that gives information on the conformational changes of actomyosin interactions during contraction and relaxation states of the striated muscles. We investigate the areas of striated muscles with a mesoscopic approach (study of few molecules) for this study. The research on mesoscopic approach is quite naïve as only few researchers have opted this approach for their study[167,168]. Firstly, the thesis aims to discern the molecular basis of actomyosin cross-bridge functional differences between the two ventricles of the heart that were always thought to be similar all along with possible differences in their respective heart failures, thus setting the two ventricular functions and their ailments distinctively apart. Current therapeutics aimed to treat LVF offer less to no help for patients with RVF that are unknowingly treated with beta blockers, nitroglycerine etc. resulting in unprecedented deaths[117,122,169]. Hence, a wide range of research is now focused on elucidating the basic molecular distinction that involves studying the molecular function in disease models like cardiomyopathy, functional differences between the ventricles of healthy hearts and their deranged abnormalities culpable for the disease as opposed to treating the two heart failures squarely equal. There is a research gap in understanding these very basic molecular differences that my project aims to fathom through novel fluorescence based single molecule techniques. Secondly, the thesis will also venture into studying the mutation related cardiovascular ailments to help understand the overall working of the heart. Additionally, we will also investigate the mechanism of acto-mysoin phosphorylation in skeletal muscles. My study will help understand the provenance of disparities in the two ventricles of healthy and failed hearts in addition to shedding light over the pathophysiological influence of mutations in cardiomyopathy.

Innovation

1. *Mesoscopic Scale*: Conformational changes endured by myosin heads during contraction represent the physiological state of muscles. Previous traditional techniques of wide field microscopies and NMR performed to study actomyosin cross-bridges ended up averaging trillions of molecules. While these studies provided reliable data in the rigor state (identical conformation of myosin attached to actin filaments), it is challenging to study the conformational changes in live contracting myofibrils. In a single myofibril composed of trillions of actin-myosin molecules, the kinetics and spatiotemporal conformational changes are lost during averaging. When one measures signals from 10^{12} cross-bridges arranged randomly along the axis of a muscle fiber, the error associated with the orientation is only 10^{-4}% of the average value. The error is mainly contributed by the detector and carries no information about the error in the cross-bridge orientational changes that have important information about the muscle function. Thus the best way to avoid averaging of the signal is by studying a few molecules. For example, in **Fig.19**, anisotropic measurements of the top panel of left and right ventricles depicts averages of many molecules and thus delivers a flat line in each of the cases. Whereas, when single molecule (cross-bridge) is studied, distinct differences in the two ventricles are displayed. Fluorescence is the only technique that gives strong enough signal to be used in the current study. The innovation in the project is to limit the number of molecules under study through sparsely fluorescently labeled actin molecules in a mesoscopic arrangement (when the number of observed molecules is small). In mesoscopic arrangement, averaging of the data is minimal and study could be performed during any of the three states of the muscular events in great details: contraction, relaxation and rigor.

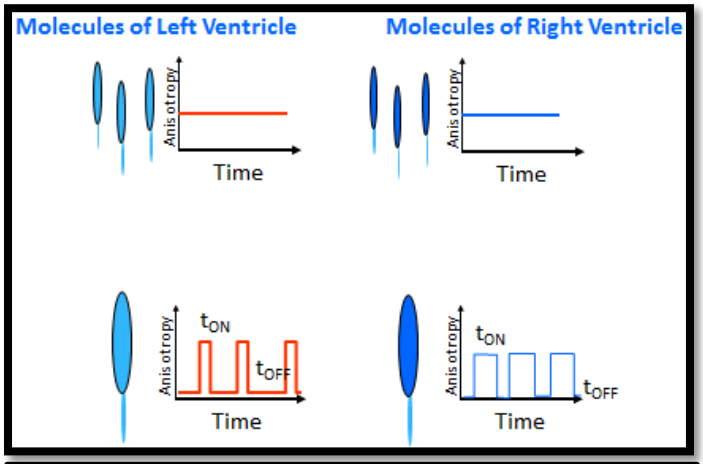

Fig.19: Mesoscopic approach: Schematic representation of the small number of molecules as opposed to many in contributing to the signal.

2. *Detection Volume (DV)*: In order to achieve higher and time resolution, we opted to limit the detection volume and reduce the number of fluorophores. The best way to minimize the DV was to use single myofibril as a sample in the detection volume of a confocal with depth of 0.5µm. This ensures that only a few molecules of fluorophores are observed. In my experiments, actins/myosins were labeled. A small volume of myofibril (half sarcomere) is observed in the confocal volume. The excited light beam is focused on the A-band of the sarcomere. Since the actins/myosins are deliberately sparsely labeled, only 16-50 cross-bridges are observed. The number of cross-bridges is determined by fluorescence correlation spectroscopy (FCS) from the number of fluctuations of the fluorescent dye. The number of molecules (N) contributing to the autocorrelation function of these fluctuations is equal to the inverse of the value of the autocorrelation function (ACF) at delay time 0 [G(0)], N=1/G(0).

Various studies have been performed on the heart muscles at their physiological, protein and biochemical levels. This thesis, however, ventures into deciphering the functional aspects of actin - myosin cross-bridges that have never been studied extensively before. The thesis accounts for studying cross-bridge kinetics and spatial and temporal conformational changes in single labeled cross-bridges of live working myofibrils through sensitive time resolved fluorescence polarization based assay. Previous research performed on hearts presumed both the ventricles to be very much alike with respect to their characteristics and functions. The question I aimed to answer is that the two ventricles thought to work and behave so similar to each other, in fact differ at their very basic cross-bridge activities. The first part of my thesis was aimed at elucidating the differences in the cross-bridge function of two ventricles of the heart, the left and the right, in small rodent - mice models. Having an appropriate animal model is needed to accurately investigate ventricular differences in hearts, results of which could later help study and translate into human research. Hence, the second part of my thesis was focused on extending the finding to another mammalian species – the rabbit that is phylogenetically similar to humans as compared to mice models. The third part of my thesis revolves around comprehending the differences in the basic mechanism of cross-bridge function in healthy human heart ventricles and their disconcerted arrangement during cardiovascular disease like heart failure. One of the biggest challenges in cardiovascular diseases is to be able to diagnose and direct treatment modalities according to specific ventricular ailment, should it boil down to a particular ventricular disease form. In addition to the differences in the very basic contractile units in the two ventricles, the conditions could be exacerbated upon introduction of mutations in any of the sarcomeric proteins. The fourth project of my thesis concentrates on one such regulatory light chain (RLC) protein mutation of A13T (Alanine to Threonine) and aims to understand the effect of the mutation that is only 10% expressed in the protein, in the normal functioning of the heart as a whole. My projects include studying the function of cardiac muscles through kinetics and spatiotemporal studies that illustrate the typical function of cardiac myofibrillar cross-bridges in both the ventricles and the ephemeral yet influential effect of the mutations, inconsistent cross-bridge arrangement during diseases like heart failure and thus their contribution towards the atypical behavior of cross-bridges in understanding the mechanism of the whole heart.

Project 1: The spatial distribution of actin and mechanical cycle of myosin are different in right and left ventricles of healthy mouse hearts.

Project 2: Differences in the kinetics and spatial distribution of actin in the left and right ventricles of rabbit hearts.

Project 3: Differences in the kinetics and spatial distribution of actin in the left and right ventricles of human hearts.

Project 4: A Novel Method of Determining the Functional Effects of a Minor Genetic Modification of a Protein.

In addition to the above projects, I have also worked on a few other projects that extend our knowledge into understanding the cardiovascular health and its anomalous behavior quite profoundly by studying the aspects of cross-bridges - effect of other lethal mutations in the sarcomeric protein of Troponin I (Arginine to Cysteine mutation - R21C) and regulatory light chain (RLC) (Lysine to Glutamate mutation K104E). Muscle movement is brought about by the process of contraction – relaxation that involves other elementary processes like phosphorylation of protein molecule RLC that play a crucial role in muscle activity.

Project 5: Phosphorylation of myosin regulatory light chain has minimal effect on kinetics and distribution of orientations of cross-bridges on rabbit skeletal muscle

Project 6: Effect of a myosin regulatory light chain mutation K104E on actin-myosin interactions

Project 7: Differences in the Degree of Order of Myosin Cross-bridges of Left and Right Ventricles in Knocked-In R21CTroponin I Mice

CHAPTER III

METHODS

The chemical and methods for each project is well described in their respective chapters.

CHAPTER IV

THE SPATIAL DISTRIBUTION OF ACTIN AND MECHANICAL CYCLE OF MYOSIN ARE DIFFERENT IN RIGHT AND LEFT VENTRICLES OF HEALTHY MOUSE HEARTS

J. Nagwekar[1], D. Duggal[1], R. Rich[1], S. Raut[1], R. Fudala[1], I. Gryczynski[1], Z. Gryczynski[2], and J. Borejdo[1]*

1. Department of Cell Biology and Center for Fluorescence Technology and Nanomedicine, University of North Texas Health Science Center, 3500 Camp Bowie Boulevard, Fort Worth, Texas 76107, United States

2. Department of Physics and Astronomy, Texas Christian University, 2800 South University Drive, Fort Worth, Texas 76129, United States

* Corresponding Authors: Julian Borejdo, Department of Cell Biology, University of North Texas Health Science Center, 3500 Camp Bowie Blvd, Fort Worth, TX 76107, USA, Tel.: (817) 735-2106, Fax: (817) 735-2118; E-mail: Julian.Borejdo@unthsc.edu

1. ABSTRACT

The contraction of the right ventricle (RV) expels blood into the pulmonary circulation, and the contraction of the left ventricle (LV) pumps blood into the systemic circulation through the aorta. The respective afterloads imposed on the LV and RV by aortic and pulmonary artery pressures create very different mechanical requirements for the two ventricles. Indeed, differences have been observed in the contractile performance between left and right ventricular myocytes in dilated cardiomyopathy, in congestive heart failure, and in energy usage and speed of contraction at light loads in healthy hearts. In spite of these functional differences, it is commonly believed that the right and left ventricular muscles are identical because there were no differences in stress development, twitch duration, work performance, or power among the RV and LV in dogs. This report shows that on a mesoscopic scale [when only a few molecules are studied (here three to six molecules of actin) in ex vivo ventricular myofibrils], the two ventricles in rigor differ in the degree of orientational disorder of actin within in filaments and during contraction in the kinetics of the cross-bridge cycle.

KEYWORDS: Actin orientation, heart ventricles, fluorescence polarization

2. INTRODUCTION

Muscle contraction[1−3] causes a left ventricle of a heart muscle to squeeze blood into an aorta and a right ventricle to squeeze blood into a pulmonary artery. The afterloads imposed by aorta and artery are different, implying that mechanical requirements of the two ventricles should be different. In fact, differences have been observed in the contractile performance between left and right ventricular myocytes in dilated cardiomyopathy[4] and congestive heart failure.[5] Differences were observed in energy usage of healthy LVs and RVs.[6,7] Samarel showed an increased level of fractional synthesis and degradation of myosin heavy chain and light chains, but not actin, in the left compared to the right ventricular free wall.[8] Sordahl[9] observed that mitochondria isolated from the right ventricles had rates of phosphorylation of respiration lower than those of left ventricular mitochondria. The proteomic differences between LVs and RVs have recently been observed.[10] However, Wikman-Coffelt and her collaborators[11] found no differences in stress development, twitch duration, work performance, or power among LVs and RVs in dogs.

The two ventricular muscles are morphologically identical. To the best of our knowledge, the issue of mechanical differences between LV and RV muscles has not been resolved. This report shows that on a mesoscopic scale (when only a few molecules are studied) the two ventricular muscles are different. Specifically, the probability distribution of spatial orientations of actin in the thin filaments, as well as the crossbridge cycle, is different in LVs and RVs. We were motivated to study a few molecules by the fact that the mean values of a sufficiently large number of independent random measurements, each with a well-defined expected value and well-defined variance, will be approximately normally distributed.[12] Therefore, when whole ventricles are studied, containing at least 10^{18} molecules of actin or myosin (the left ventricle of a B6 mouse typically weighs 30 mg), there is no hope of observing differences between distributions of molecules within ventricles. With regard to kinetics, an argument that a small number of molecules must be studied can also be made. Force-generating molecules are unsynchronized, and macroscopic measurements generate only the average values. The process of averaging large assemblies removes individual contributions, and information about the kinetics is lost.[13,14] In contrast, when only a few molecules are studied, the value of a variable is affected by fluctuations around the average.[15] Fluctuations are caused by chemical reaction,[16] and when the number of observed molecules is small, fluctuations can be very large. The relative size of fluctuations depends on the number of molecules under observation N as $\sqrt{N}/N$. In our experiments, there were typically three to six molecules, and the corresponding fluctuations were ∼5−41%. In contrast, if we are dealing with an N on the order of 10^{18} molecules of actin or myosin, the relative fluctuation of a signal is only 0.0000001%, much too small to be detected. Actin molecules in thin filaments were significantly less well ordered in rigor LVs than RVs. Kinetic analysis revealed that cross-bridges from RVs as compared to LVs displayed a 2-fold decrease in the rate of execution of a power stroke and a 36% decrease in the rate of dissociation from thin filaments. The fact that an increase in macroscopic tension has not been observed earlier suggests that two effects cancel each other. We speculate that the differences between ventricles arise because of the variation of external load between LVs and RVs.

3. MATERIALS AND METHODS

3.1. Chemicals and Solutions

All chemicals were from Sigma-Aldrich (St. Louis, MO). Alexa633-labeled phalloidin (AP) and unlabeled phalloidin (UP) were from Molecular Probes (Eugene, OR). The chemical skinning solution contained 50% glycerol, 1% Triton X-100, 10^{-8} M Ca^{2+}, 3.5 mM free Mg^{2+}, 7 mM EGTA, 2.5 mM Mg-ATP^{2-}, 20 mM Tris (pH 7.0), 15 mM creatine phosphate, and 15 units/mL phosphocreatine kinase. The contracting solution contained 50 mM KCl, 10 mM Tris-HCl (pH 7.5), 5 mM $MgCl_2$, 0.1 mM $CaCl_2$, 5 mM ATP, 20 mM creatine phosphate, and 10 units of 1 mg/mL creatine kinase/mL. The relaxing solution was the same as the contracting solution, but Ca^{2+} was replaced with 2 mM EGTA. The Ca rigor solution contained 50 mM KCl, 10 mM Tris-HCl (pH 7.5), 2 mM $MgCl_2$, and 0.1 mM $CaCl_2$.

3.2. Preparation of Ventricles

Whole hearts of healthy 6-month-old female C57BL/6 mice were stored for a few weeks at −80 °C [gift of N. Sumien, Department of Pharmacology, University of North Texas Health Science Center (UNTHSC); fresh hearts were provided by R. Berg, Department of Cell Biology and Immunology, UNTHSC]. Hearts were washed with a cold dissecting solution (50 mM KCl, 5 mM MgEGTA, and 15% glycerol) to wash out ATP without causing contraction. Right and left ventricles were dissected in the dissecting solution in the cold room. They were then chemically skinned by being placed in a skinning solution [15% glycerol, 3.5 mM $MgCl_2$, 20 mM Tris (pH 7.0), 1% Triton X-100, 7 mM EGTA, 2.5 mM ATP, 15 mM creatine phosphate, and 15 units/mL phosphocreatine kinase] for 24 h at 4 °C. After Triton had been washed out, they were either used immediately or stored for up to 3 weeks at −80 °C.

3.3. Preparation of Myofibrils

Ventricles were washed three times for 0.5 h with an ice-cold EDTA rigor solution [50 mM KCl, 10 mM Tris-HCl (pH 7.5), and 5 mM EDTA] for 30 min to wash out ATP present in the skinning solution without causing contraction. They were then washed thoroughly with the Ca rigor solution and homogenized in the Cole-Palmer LabGen 125 homogenizer for 10 s followed by homogenization for a further 10 s after a cooling period of 30 s.

3.4. Cross-Linking

To inhibit shortening, 1 mg/mL myofibrils were incubated for 20 min at room temperature with 20 mM water-soluble cross-linker 1-ethyl-3-[3-(dimethylamino)propyl]carbodiimide (EDC).[17−20] The reaction was stopped by adding 20 mM DTT. The pH of the solution remained unchanged at 7.5 throughout the time course of reaction. The absence of shortening was verified by observing myofibrils irrigated with the contraction solution in a Nomarski microscope.

3.5. Labeling of Thin Filaments

AP (10 nM) was mixed with 10 μM UP and the mixture added to 1 mg/mL myofibrils for 10 min at room temperature. Figure 1S of the Supporting Information shows a typical image of a ventricular myofibril. Phalloidin is known to impose a higher stiffness[21] on thin filaments but does not alter their function.[22,23]

3.6. Number of Observed Myosin Molecules

To determine the number of Alexa-labeled phalloidin molecules under observation, the instrument was calibrated to determine the fluorescence intensity caused by a known number of molecules of Alexa-labeled phalloidin. This number was determined by fluorescence correlation spectroscopy (FCS). At delay time zero, the autocorrelation function (ACF) of fluctuations caused by diffusion of free AP is equal to the inverse of the number of molecules contributing to the fluctuations [$N = 1/\mathrm{ACF}(0)$].[16,24,25] A calibration was made by plotting the number of AP molecules versus the rate of photon arrival. It indicated that the number of photons collected in a second from a single Alexa633-labeled phalloidin molecule illuminated with ∼1 μW of laser power was 1200. An example of the fluorescent signal is shown in Figure 2S of the Supporting Information. Typically, there were three to six molecules in the observational volume (OV). The OV (1.7 μm^3) was estimated by measuring the fwhm of axial and lateral dimensions of an image of 20 nm fluorescent beads and then making a three-dimensional (3D) Gaussian approximation[26] However, it must be emphasized that as long as the number of molecules is mesoscopic, the exact number does not matter; i.e., three molecules should give the same result as 30 molecules, etc.

Each experiment lasted 20 s and included 2 million experimental data points. Because a characteristic lifetime of one fluctuation is on the order of milliseconds,[27] each data set was binned (smoothed) to contain 20000 fluctuations. If X is the number of fluctuations detected, the precision of the measurement is approximately equal to $1/\sqrt{X}$. Hence, the precision of our experiment is ∼0.5%.

3.7. Time-Resolved Anisotropy Measurements

To ascertain whether the phalloidin probe is immobilized so that the transition dipole of the fluorophore reflects the orientation of the protein, we measured the decay of anisotropy of AP inserted into myofibrils. Anisotropy is defined as $r = (I_{\parallel} - I_{\perp})/(I_{\parallel} + 2I_{\perp})$. The fluorescence anisotropy was measured by the time domain technique using a FluoTime 200 fluorometer (PicoQuant, Inc.) at room temperature. The excitation was provided by a 635 nm pulsed diode laser, and the observation was conducted through a 670 nm monochromator with a supporting 650 nm long pass filter. The full width at half-maximum (fwhm) of the pulse response function was <100 ps, and the time resolution was <10 ps. The intensity decays were analyzed by a multiexponential model using FluoFit (PicoQuant, Inc.).

3.8. Data Collection

The myofibrils were placed on a scanning stage of a PicoQuant MT 200 inverse time-resolved fluorescence instrument coupled to an Olympus IX 71 microscope. The stage was rotated to align vertically a myofibril under observation. Before each experiment, the fluorescence of an isotropic solution of a small dye with a long fluorescence lifetime (rhodamine 700, which has zero anisotropy) was measured to make sure that the parallel (∥) and perpendicular (⊥) channels received an equal amount of emitted light. A 640 nm laser beam modulated at 20 MHz was focused by an Olympus 60×, NA 1.2 water immersion objective to the diffraction limit on the fluorescent part of a myofibril. The power delivered to each half-sarcomere was adjusted within a range of 1–2 μW to obtain a similar photon rate for each myofibril. If the power is not equal, the differences between data sets become statistically interpretable; ∼25–50 myofibrils were examined. We measured the polarization of fluorescence (PF) rather than steady-state anisotropy (R). The PF is the normalized ratio of the difference between ∥ and ⊥ components of the fluorescent light emitted by the dye.

The relation between the two is PF = $R/(2 + R)$. Dos Remedios, Morales, and others have shown that PF is a sensitive indicator of the conformation of the transition dipole of the fluorophore.[2,3,28−32]

3.9. Statistical Analysis

The rate constants were measured from the slope of the autocorrelation function. A typical ACF was a single rectangular hyperbola that was linearized as shown in Figure 3S of the Supporting Information. The slope was determined by the best square fit by Origin (version 8.6, OriginLab Corp., Northampton, MA). Comparisons between groups were performed using an unpaired Student's *t* test (Sigma Plot 11, Systat Software, Inc., San Jose, CA). The differences were deemed significant when $P < 0.05$. SigmaPlot 11 was used to compute histograms. Origin was used to compute autocorrelation functions.

4. RESULTS

4.1. Distribution of Actin Orientations

Experiments were conducted in rigor. Rigor XBs are rigidly attached to actin monomers. Therefore, their fluorescence transition dipoles are mostly immobilized, and their steady-state anisotropy (SSA) values are high (Figure 4b). Deviations of polarization values from the mean arise from the fact that not all rigor bonds are precisely the same. The probability distribution of polarized fluorescence data is best represented in the form of a histogram, a plot of polarization versus probability of it occurring within a given experiment. Examples of histograms of the experiments on LVs and RVs are shown in the top and bottom panels, respectively, of Figure 1. The degree of actin disorder is best expressed by the value of the full width at half-maximum of a histogram (fwhm). It measures the width of the distribution at the point where the maximal probability is the largest. All data are summarized in Table 1. fwhm values of actins of RVs were significantly narrower (better ordered) than those of LVs. The difference between LVs and RVs is statistically significant (two-tailed $t = 2.986$; $P = 0.004$, with 42 degrees of freedom). The 95% confidence interval of this difference ranged from 0.03210 to 0.16590. The difference in the polarization values was extremely statistically significant (the two-tailed P value is <0.0001 with 42 degrees of freedom). The 95% confidence interval of this difference ranged from 0.22968 to 0.46232. The difference in counts per millisecond (fluorescence intensity) was statistically insignificant.

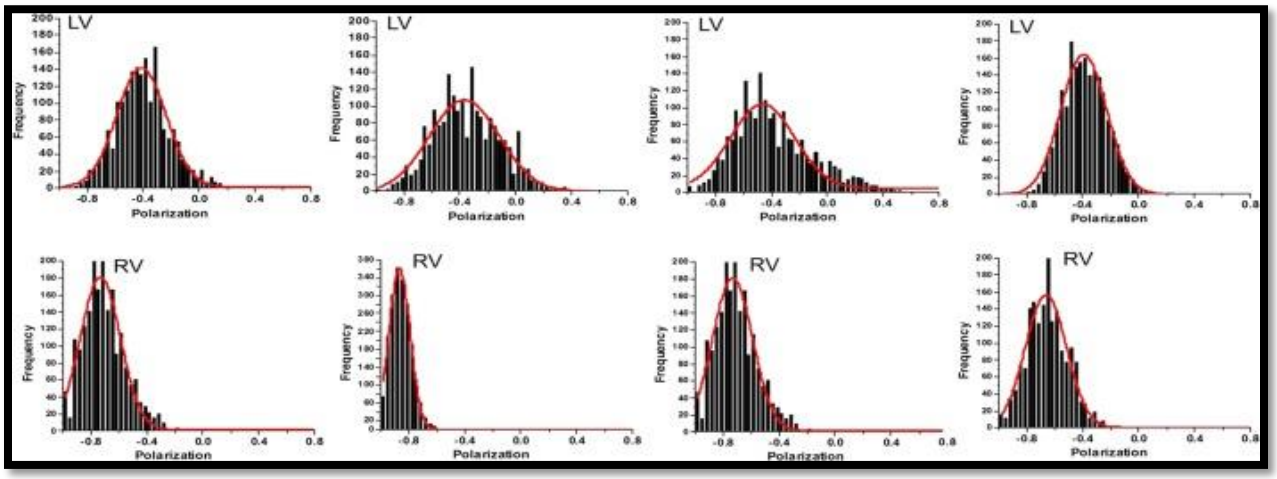

Figure 1: Examples of distributions of polarization values of actin transition dipoles in rigor.

TABLE 1. Widths of Angular Distribution of Actin transition Dipoles in Rigor LVs and RVs			
	FWHM	Polarization	Counts/ms
Rigor LV	0.438 ± 0.069	–0.416 ± 0.057	8.756 ± 2.774
Rigor RV	0.339 ± 0.144	–0.762 ± 0.276	6.171 ± 2.029
The results are averages of 25 experiments on different LVs and RVs. Errors are standard deviations			

We report the fluorescence intensity of the signal because in static experiments it is crucial that the mean fluorescence intensity be taken into account. This is because the fwhm of the Gaussian distribution of polarizations depends not only on the properties of muscle but also on the strength of the signal. Strong

Gaussian signals give small fwhms, and weak signals give large fwhms. Importantly, in our experiments, the difference between intensities of LV and RV signals was insignificant.

Another way to characterize differences between LVs and RVs is to measure their skewness and kurtosis (Table 2). Skewness is a measure of the lack of symmetry of a distribution. The skewness of an ideal Gaussian distribution is 0. Kurtosis is a measure of whether the data are peaked or flat relative to the normal distribution. High-kurtosis histograms have a distinct peak near the mean. Conversely, low-kurtosis histograms have a flat top near the mean rather than a sharp peak. The kurtosis of an ideal Gaussian distribution is 0.

TABLE 2. Skewness and Kurtosis of the Distribution of Actin Orientations

	Skewness	Kurtosis
Rigor LV	1.141 ± 0.172	0.785 ± 0.467
Rigor RV	2.187 ± 0.655	3.599 ± 2.491

From 25 experiments on different LVs and RVs. Errors are standard deviations

The difference in skewness was extremely statistically significant (t = 5.589; P < 0.0001, with 42 degrees of freedom). The 95% confidence interval of this difference ranges from −1.05619 to −0.49581. The difference in kurtosis was also extremely statistically significant (t = 5.501; P < 0.0001, with 42 degrees of freedom). The 95% confidence interval for the difference in means ranges from −4.233 to −1.959.

The fact that kurtosis of rigor distributions of RV muscles is high suggests that XBs bind to actin predominantly in a single orientation; i.e., binding is stereospecific. This seems not to be the case in LVs. The point is further argued in the Discussion.

4.2. Relaxation as a Negative Control

During relaxation, XBs do not make contact with actin filaments, which results in a disorder.[33,34] We expected histograms of the polarization of fluorescence of actin to be the same for both ventricles. This was indeed the case. The examples of distributions of actin in relaxation are shown in Figure 4S of the Supporting Information. Data are summarized in Table 3.

TABLE 3. Widths of Angular Distribution of Actin transition Dipoles in Relaxed LVs and RVs

	FWHM	Polarization	Counts/ms	Skewness	Kurtosis
Relaxation LV	0.414 ± 0.075	–0.631 ± 0.223	6.476 ± 1.849	1.743 ± 0.567	2.256 ± 2.575
Relaxation RV	0.416 ± 0.266	–0.822 ± 0.698	6.791 ± 1.923	1.790 ± 0.571	2.344 ± 3.435

The results are averages of 22 experiments with different LVs and RVs. Errors are standard deviations

None of the differences were statistically significant. The −0.00216 difference in fwhm was *not* statistically significant (t = −0.0359; P = 0.971, with 42 degrees of freedom). The 95% confidence interval for the difference in means ranges from −0.124 to 0.119. The −0.315 difference in the rate of photon arrival was *not* statistically significant (t = −0.552; P = 0.584, with 42 degrees of freedom). The 95% confidence interval for the difference in means ranges from −1.465 to 0.835. The 0.191 difference in polarization was *not* statistically significant (t = 1.198; P = 0.237, with 42 degrees of freedom). The 95% confidence interval

for the difference in means ranges from −0.131 to 0.513. The −0.0463 difference in skewness was *not* statistically significant (t = −0.269; P = 0.789, with 42 degrees of freedom). The 95% confidence interval for the difference in means ranges from −0.393 to 0.300. The −0.0888 difference in kurtosis was *not* statistically significant (t = −0.0963; P = 0.924, with 42 degrees of freedom). The 95% confidence interval for the difference in means ranges from −1.950 to 1.773.

4.3. Kinetics

Kinetics is extracted from the analysis of fluctuations.[13,16] The fluctuations occur because the transition dipole of actin changes during contraction, with myosin XBs constantly binding to and dissociating from the thin filaments. While most of these interactions have no effect on polarization (because only 1 in 1000 actin monomers is fluorescent), sometimes they do have an effect (explained in more detail in Figure3). Figure4 explains why the fluctations of the transition dipoles of the few labeled actin molecules provide insight into the mechanical cycle of XBs. Figure2 Shows representative examples of autocorrelation functions of myofibrils from a typical ventricle.

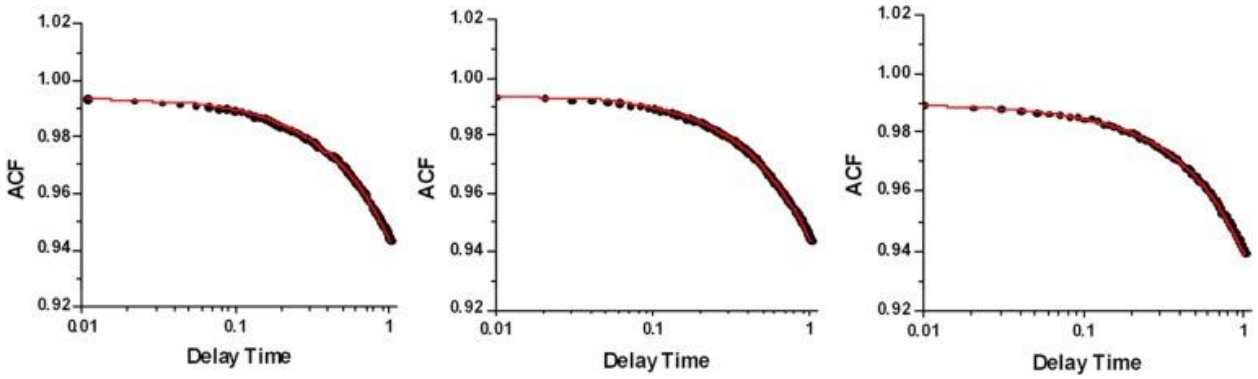

Figure 2: Examples of ACFs of contracting ventricular myofibrils. The decays were fit (red line) by a model shown in Figure4. This model allows calculation of the rate of the power stroke (k_2) and the rate of dissociation of XBs from thin filaments (k_3). Red lines are the best fits from the model of Mettikola et al.,[35]reproduced here in Figure 5S of the Supporting Information. This model includes the rate of binding of XB to thin filaments (k_1), but we were not able to resolve; it is probably too rapid. We present only averages of rates k_2 and k_3. The horizontal axes are on a logarithmic scale. Figure 3S of the Supporting Information explains how the rate constants are calculated after converting a log scale to a linear scale.

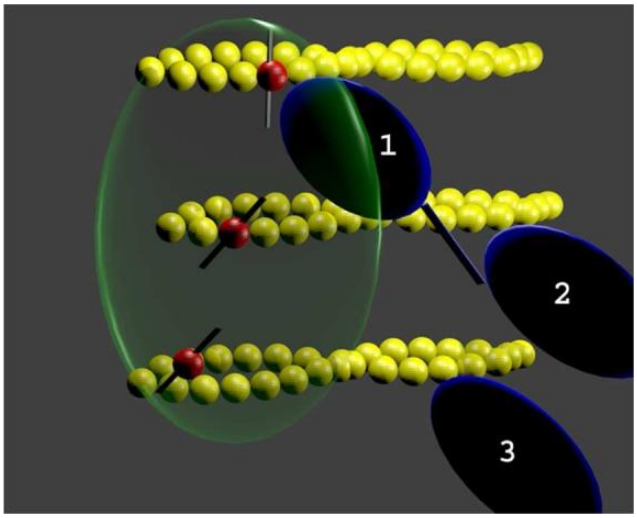

Figure 3: Sparse labeling of myofibrils. Thin filaments are irrigated with a 0.1% mixture of Alexa633-labeled phalloidin and unlabeled phalloidin. As a result, only 1 in 1000 actins is labeled (red) and 999 are not (yellow). The dipole moment of rhodamine is indicated by the black line. Only XB 1 affects the direction of the actin dipole. The myofibril is illuminated with 640 nm light. The detector sees only the volume equivalent to the transparent green

ellipsoid of revolution (not drawn to scale).

The results of fits to 27 experiments are summarized in Table 4. A good measure of the goodness of fit is adjusted R^2 (AR^2) because it accounts for the number of degrees of freedom. The best fit gives a value of 1. The AR^2 for the ACF fit was significantly better for the average value of k_3 than that of k_2 (t = 4.086; P< 0.001, with 41 degrees of freedom).

TABLE 4. Mean Values and Standard Deviations of Rate Constants from 27 Experiments

Contracting Ventricle	k_2 (s^{-1})	k_3 (s^{-1})	AR^2 for k_2	AR^2 for k_3
LV	0.159 ± 0.086	0.061 ± 0.026	0.639 ± 0.236	0.920 ± 0.103
RV	0.085 ± 0.035	0.0492 ± 0.008	0.629 ± 0.188	0.972 ± 0.022

The difference in k_2 between LVs and RVs was highly statistically significant (t = 4.275; P < 0.001, with 46 degrees of freedom). The 95% confidence interval for the difference in means ranges from 0.123 to 0.0441. The difference in k_3 was statistically significant (t = −2.239; P = 0.030, with 51 degrees of freedom). The 95% confidence interval for the difference in means ranges from 0.0346 to 0.00189.

5. DISCUSSION

5.1. Distribution of actin orientations

This report shows that on a mesoscopic scale the spatial distribution of actin monomers (and therefore the degree of order) within thin filaments in LVs and RVs is different. However, because there have been no confirmed reports of any amino acid or conformational differences in LVs and RVs of myosin heavy or light chains, it is commonly believed that the right and left ventricular muscles responsible for contraction are identical, yet the afterloads imposed on the LV and RV by aortic and pulmonary artery pressures cause different mechanical requirements of the two ventricles. As mentioned above, the whole ventricles contain at least 10^{18} molecules of actin or myosin. If one makes a sufficiently large number of independent random measurements, each with a well-defined expected value and well-defined variance, the distribution will be approximately normal.[12] Therefore, when whole ventricles are studied, there is no hope of observing differences between distributions of polarization of fluorescence (or any other property) of molecules within ventricles. Via the limitation of the number of observed molecules in *ex vivo* ventricles, it was possible to detect differences in the degree of order. The fwhm (of polarized fluorescence or any other property of observed molecules) can be significantly affected only when an individual molecule makes a substantial contribution to the overall signal. When the number is small, the orientations that are the most likely to appear first are the most probable. Less probable ones (those contained in the outliers of distributions) are less likely to appear. As a consequence, the histograms of a distribution of a few molecules are mostly populated by the most likely orientations, lacking the outliers of the distribution. The lack of outliers magnifies the differences in fwhms. The fact that kurtosis of rigor distributions of the RV is high indicates that the data are peaked relative to the normal distribution. This implies that there is a well-defined orientation of the transition dipole of actin and therefore of XB that affects this monomer and suggests that the binding of XBs to actin in RV is stereospecific.

5.2. Kinetics

There are three requirements for making kinetic measurements. First, the data must be obtained *ex vivo*, not from isolated molecules *in vitro*. An ensemble of myosin molecules in muscle cannot be viewed as a collection of independent motors because individual motors interact mechanically by accelerating ADP release and increasing the reach of the XBs when attached.[36] Second, it must be recognized that in contracting muscle the force-generating molecules act in an unsynchronized fashion. Thus, to obtain kinetic information, the molecules have to be synchronized by applying transients[27,37] or white noise.[38] The alternative is to collect data from a small assembly of force generators. We chose this alternative, because the other approaches are difficult to apply *in vivo*. Measurements from large assemblies are averages, containing no kinetic information from all molecules. In contrast, the average of a small assembly does contain kinetic information in the form of large fluctuations from the average.[13,14] Third, *ex vivo* information must be obtained with a millisecond time resolution, because XBs are expected to rotate rapidly.[27] Super-resolution microscopy using single molecules *in vivo* is a conceivable method but has a limited time resolution.[b] We have achieved the necessary time resolution by sampling a small volume of muscle containing only a few labeled molecules.

We now explain why observing the orientation of actin dipoles provides information about the kinetics of a XB. As mentioned above, the polarized fluorescence of the transition dipole of actin fluctuates because myosin XBs are constantly binding to and dissociating from actin. While most of these interactions have no effect on polarization (because only 1 in 1000 actin monomers is fluorescent), sometimes they do have an

effect. This is illustrated in Figure3. Fourteen actin monomers are connected by the tropomyosin double helix that acts as a cooperative unit.[44–49] Each interaction of the myosin head (mostly with the unlabeled actin) results in no change in the dipole orientation of labeled actin (e.g., XBs 2 and 3) because it occurs too far from the labeled actin monomer, but the few XBs that bind within the cooperative unit (e.g., XB 1) will cause a change in the orientation of the actin dipole.

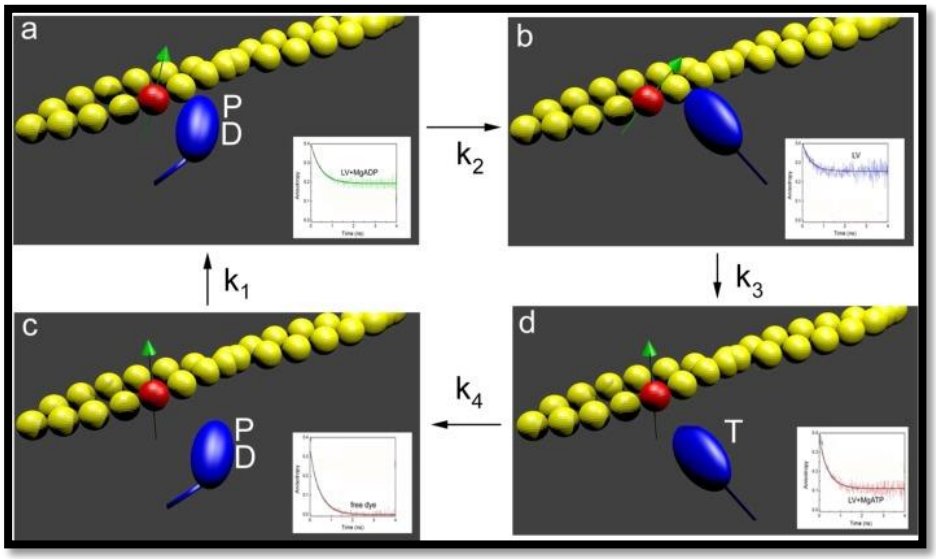

Figure 4: Conventional model of XB action showing that the steady-state orientation of labeled actin [red sphere; the orientation of phalloidin (its fluorescent transition dipole) is indicated by a green arrow] is different in different intermediate states (0.1 mg/mL myofibrils labeled with 0.01 μM AP and 10 μM UP). ATP is T, ADP D, and P_i P.

The changes in those dipole moments that are affected by interactions with myosin heads do reflect the XB cycle (remembering that labeled actins that are too far from the interacting myosin head and unlabeled actins do not contribute to the change in signal). The basic cycle is shown in Figure4. In this scheme, based on models of Lymn and Taylor,[50] Coureux, Sweeney, and Houdusse,[51] and Spudich,[52] starting from panel c, the myosin head (blue) containing products of hydrolysis is not attached to the thin filament and rotates nearly freely in the myofilament space as does the transition dipole of Alexa633-labeled phalloidin (green arrow). The closest labeled actin protomer (red sphere) also rotates rapidly because it is not restrained by a XB. Its steady-state anisotropy (SSA) is small (0.041, inset in panel c). In the next step (panel a), myosin binds to actin with a rate k_1. At the same time, the SSA of actin increases to 0.180 (inset of panel a). The next step (panel b) involves the release of phosphate and ADP (not necessarily in that order), during which a XB executes a power stroke with a rate constant k_2 to bind strongly to actin. Actin rotation now becomes restricted [SSA = 0.265 (inset of panel b)]. This is followed by XB binding of a fresh molecule of ATP and dissociation of myosin from actin at a rate k_3. Actin rotation now becomes more free [SSA = 0.133 (inset of panel d)]. It is a pseudo-first-order reaction because the concentration of ATP is much greater than the myosin concentration (i.e., the ATP concentration is constant). Hydrolysis of ATP with a rate k_4 reverses the power stroke and reprimes the head. This conformational change is not recorded.

5.*3. Observing Actin Rather Than Myosin XB's*

This approach has several important advantages. First, in mesoscopic measurements, it is crucial to be able to label a small number of molecules and to know precisely how many molecules are labeled. Irrigating myofibrils with the exact ratio of labeled and unlabeled phalloidin allows one to accomplish this. Second, it

avoids measuring the rate of repriming (back stroke). Omitting it considerably simplifies the analysis. An autocorrelation function of the four-state cycle is very complex,[53] whereas the three-state cycle proved to be manageable.[35] Third, labeling of actin with phalloidin is very reproducible[54] because labeling of actin involves only gentle irrigation of myofibrils with the protein at room temperature, whereas direct labeling of myosin involves labeling light chain 1 (LC1) and exchanging it with myofibrillar LC1 under harsh conditions (0.5 h at 37 °C in the presence of trifluoroperazine).[55] However, there are disadvantages of labeling actin. Labeling myosin directly with bifunctional rhodamine is well-understood.[19,56] Part of a XB that undergoes the most prominent rotation, its regulatory light chain, is probed directly, and in contrast to XB labeled with Alexa633-labeled phalloidin, the dipole moment of bifunctional rhodamine in rigor is 100% immobilized by thin filaments.

6. CONCLUSION

6.1. Summarizing Data about the Distribution of Actin Orientations

Statistical analysis of rigor muscle revealed that all static parameters were different in rigor LVs and RVs. In particular, the fwhm of RV muscle was significantly smaller than that of LV muscle. This may reflect the stereospecific character of rigor bond in the RV.

6.2. Summarizing Kinetic Data

The rate of power stroke (k_2) of XBs was significantly higher in the LV than in the RV. This would have led to the development of more tension. The rate of dissociation from the thin filament (k_3) was also significantly higher in LV muscle. Faster dissociation would have led to the development of less tension, because XBs would spend less time in the tension-generating state. The fact that an increase in macroscopic tension has not been observed suggests that two effects offset each other. Myosin molecules from left and right ventricular muscles may be different as a result of differences in force requirements that could lead to epigenetic changes in DNA. One possible mechanism is histone deacetylation followed by oxidation and phosphorylation, to cause histone deacetylases (HDACs) to exit the nucleus and cause observed differences between ventricles. It is conceivable that this hypothesis could be tested by knocking out genes encoding HDACs.

The detection of a few myosin molecules in an *ex vivo* ventricle with a millisecond time resolution is not technically easy. The main problem is that the signals are weak. Weak Gaussian signals with a low signal-to-noise ratio have an intrinsically large relative error. This also applies to the ratio of these signals, as shown by Midde et al.[57] It is thus remarkable that we were able to measure the fwhm and kinetic constant with relatively high accuracy, in spite of the nonuniform incorporation of AP into sarcomeres (Figure 1S of the Supporting Information), differing degrees of phosphorylation of myofibrils,[58] a relatively low steady-state anisotropy of AP, and consequently relatively small differences in anisotropy between different mechanochemical steps. The photobleaching and light scattering from a sample add to the degree of error of the results.

More work is required to address the issues mentioned above and to determine whether the observed differences between the XBs of mouse left and right ventricles are characteristic of all mammalian muscles or whether they are specific for the hearts of small rodents. Further, it should be mentioned that phosphorylation levels of myosin binding protein C (MBP-C) may influence the distribution and kinetics of XBs in ventricles. MBP-C binds to both actin and myosin heads through the N-terminus.[59] It is believed to stabilize the binding of the myosin head to the core of the thick filament. Any of the three sites for phosphorylation of cardiac MBP-C can be phosphorylated by a variety of kinases. Phosphorylation at some of these sites causes myosin heads to be released from the core of the thick filament and become disordered. It is possible that protein C acts as a signaling molecule, reporting changes in cross-bridges to actin. Indeed, recent data suggest that MyBP-C may alter the interaction between cross-bridges and actin.[60]

7. SUPPLEMENTARY DATA

Figure S1

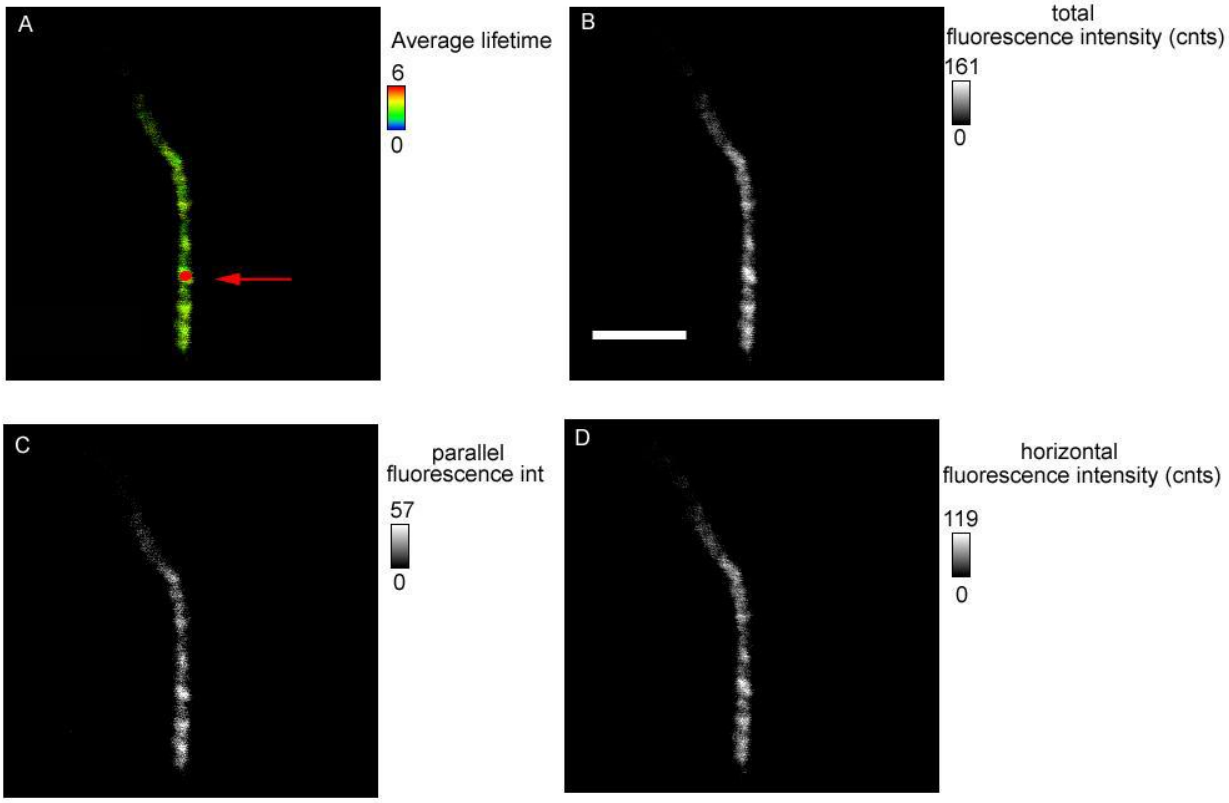

Figure S1: Image of cardiac myofibril. ***A****: Lifetime image. Scale to the right is in ns. Intensity scales in* ***B*** *(total fluorescence intensity. Scale bar is 5 µm,* ***C*** *(parallel component of fluorescence intensity) and* ***D*** *(perpendicular component of fluorescence intensity) are in B/W scale, 0 corresponding to black, 255 corresponding to white. Red circle in A pointed to by the red arrow is a projection of the confocal aperture on the image plane.*

Figure S2

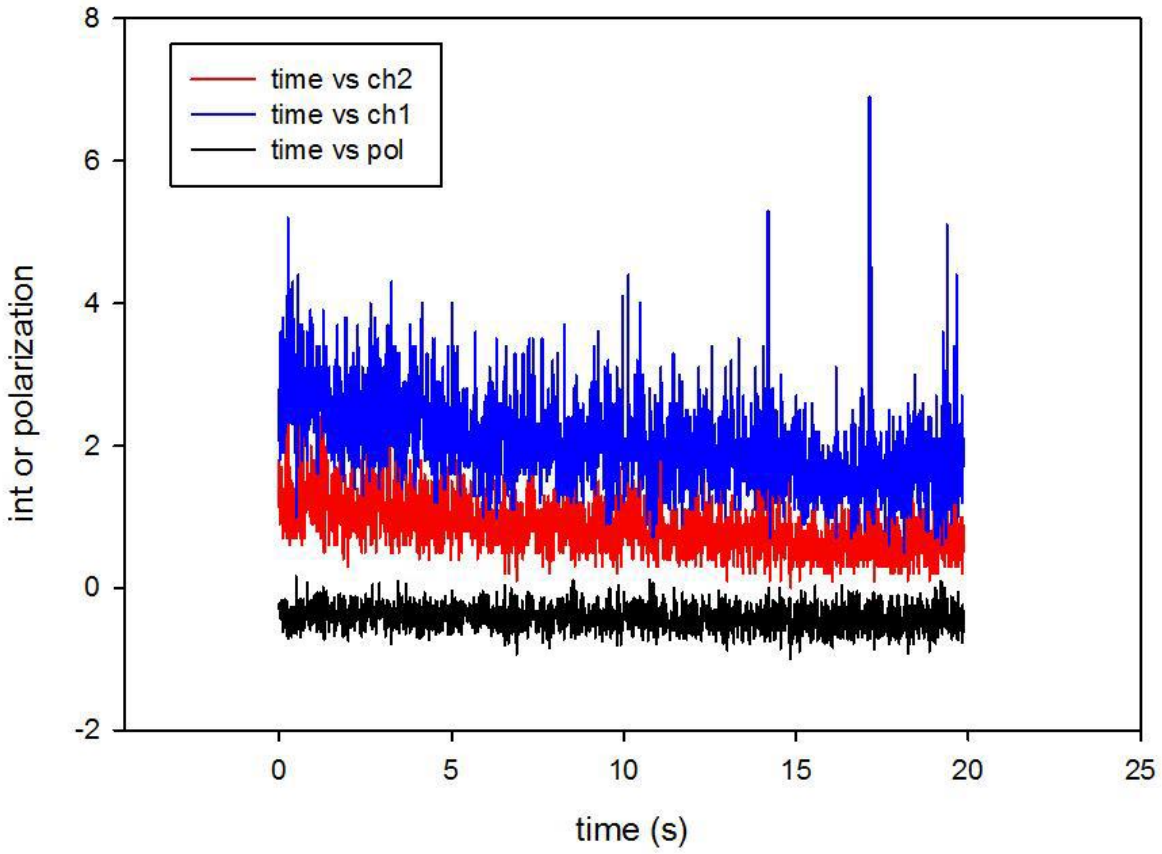

Figure S2: ***Typical time-trace of intensity of the LV****. The mean intensity of perpendicular channel (red) was 0.8580± 0.3914 (SD), mean intensity of parallel channel (blue) was 2.0544± 0.6479 and the mean polarization of fluorescence (black) was -0.4179± 0.1759.In this example the total intensity was 2.05+2*0.85=3.76 counts/ ms and the number of detected molecules was 3760/1200≈3. Typically the total fluorescence intensity was between 4,000 and 7,000 counts/s, i.e. the number of detected molecules was between 3 and 6.*

Figure S3

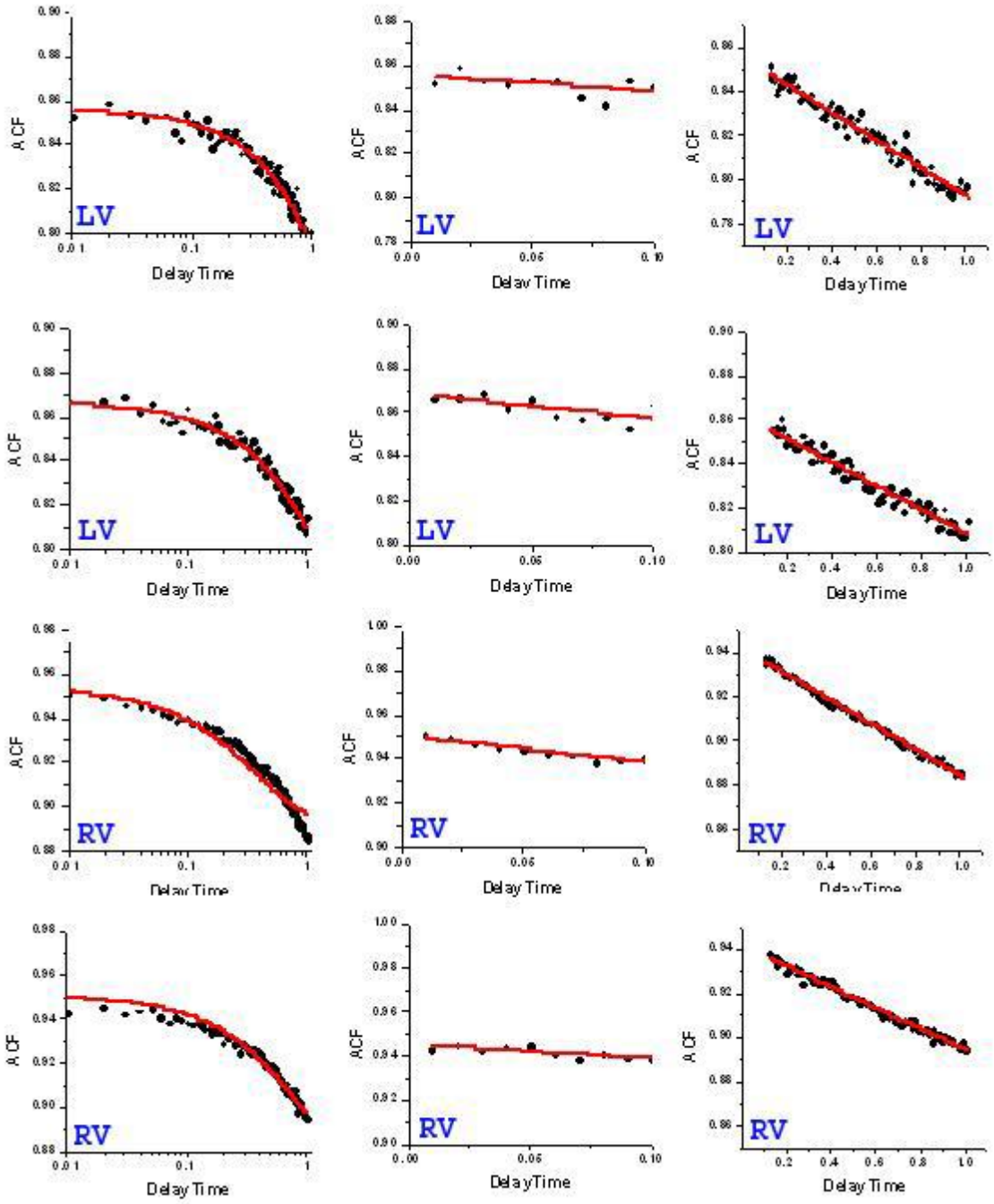

Figure S3: Calculation of the rate constants. *The horizontal scale of ACF (first column) is in log scale. It was linearized in columns 2 & 3. The slope was determined by linear best square fit by Origin version 8.6. First and last two rows are the data from LVs and RV's, respectively.*

Figure S4

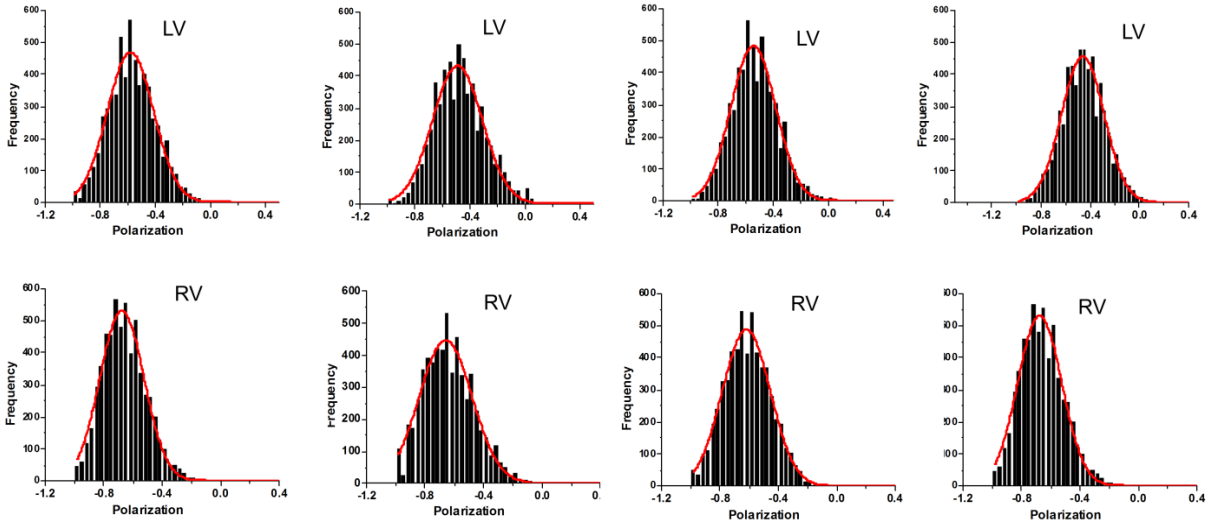

Figure S4: *Examples of distribution of polarization values of **RELAXED** LV (top panels) and RV (bottom panels). The statistical significance of the differences are in text Table 3.*

8. REFERENCES

1. Geeves M. A.; Holmes K. C. (2005) The molecular mechanism of muscle contraction. Adv. Protein Chem. 71(24), 161–193.
2. Sabido-David C.; Brandmeier B.; Craik J. S.; Corrie J. E.; Trentham D. R.; Irving M. (1998)Steady-state fluorescence polarization studies of the orientation of myosin regulatory light chains in single skeletal muscle fibers using pure isomers of iodoacetamidotetramethylrhodamine. Biophys. J.74(6), 3083–3092.
3. Hopkins S. C.; Sabido-David C.; van der Heide U. A.; Ferguson R. E.; Brandmeier B. D.; Dale R. E.; Kendrick-Jones J.; Corrie J. E.; Trentham D. R.; Irving M.; Goldman Y. E. (2002) Orientation changes of the myosin light chain domain during filament sliding in active and rigor muscle. J. Mol. Biol. 318(5), 1275–1291.
4. McMahon W. S.; Mukherjee R.; Gillette P. C.; Crawford F. A.; Spinale F. G. (1996) Right and left ventricular geometry and myocyte contractile processes with dilated cardiomyopathy: Myocyte growth and β-adrenergic responsiveness. Cardiovasc. Res. 31(2), 314–323.
5. Belin R. J.; Sumandea M. P.; Sievert G. A.; Harvey L. A.; Geenen D. L.; Solaro R. J.; de Tombe P. P. (2011) Interventricular differences in myofilament function in experimental congestive heart failure. Pfluegers Arch. 462(6), 795–809.
6. Carlsson M.; Heiberg E.; Toger J.; Arheden H. (2012) Quantification of left and right ventricular kinetic energy using four-dimensional intracardiac magnetic resonance imaging flow measurements.Am. J. Physiol. 302(4), H893–H900.
7. Itoya M.; Mallet R. T.; Gao Z. P.; Williams A. G. Jr.; Downey H. F. (1996) Stability of high-energy phosphates in right ventricle: Myocardial energetics during right coronary hypotension. Am. J. Physiol. 271(1, Part 2), H320–H328.
8. Samarel A. M. (1989) Regional differences in the in vivo synthesis and degradation of myosin subunits in rabbit ventricular myocardium. Circ. Res. 64(2), 193–202.
9. Sordahl L. A. (1976) Differences in mitochondrial functions from right and left ventricular myocardium of four mamalian species. Comp. Biochem. Physiol. 54B, 339–342.
10. Cadete V. J.; Lin H. B.; Sawicka J.; Wozniak M.; Sawicki G. (2012) Proteomic analysis of right and left cardiac ventricles under aerobic conditions and after ischemia/reperfusion. Proteomics 12(14), 2366–2377.
11. Wikman-Coffelt J.; Fenner C.; Smith A.; Mason D. T. (1975) Comparative analyses of the kinetics and subunits of myosins from canine skeletal muscle and cardiac tissue. J. Biol. Chem. 250(4), 1257–1262.
12. Rice J.. (1995) Mathematical Statistics and Data Analysis, 2nd ed., Duxbury Press, Pacific Grove, CA.
13. Elson E. L.; Magde D. (1974) Fluorescence Correlation Spectroscopy: Coceptual Basis and Theory.Biopolymers 13, 1–28.
14. Elson E. L.; Webb W. W. (1975) Concentration correlation spectroscopy: A new biophysical probe based on occupation number fluctuations. Annu. Rev. Biophys. Bioeng. 4, 311–334.
15. Qian H.; Saffarian S.; Elson E. L. (2002) Concentration fluctuations in a mesoscopic oscillating chemical reaction system. Proc. Natl. Acad. Sci. U.S.A. 99(16), 10376–10381.
16. Magde D.; Elson E. L.; Webb W. W. (1974) Fluorescence correlation spectroscopy. II. An experimental realization. Biopolymers 13(1), 29–61.

17. Herrmann C.; Lionne C.; Travers F.; Barman T. (1994) Correlation of ActoS1, myofibrillar, and muscle fiber ATPases. Biochemistry 33(14), 4148–4154.
18. Tsaturyan A. K.; Bershitsky S. Y.; Burns R.; Ferenczi M. A. (1999) Structural changes in the actin-myosin cross-bridges associated with force generation induced by temperature jump in permeabilized frog muscle fibers. Biophys. J. 77(1), 354–372.
19. Bershitsky S. Y.; Tsaturyan A. K.; Bershitskaya O. N.; Mashanov G. I.; Brown P.; Burns R.; Ferenczi M. A. (1997) Muscle force is generated by myosin heads stereospecifically attached to actin.Nature 388(6638), 186–190.
20. Barman T.; Brune M.; Lionne C.; Piroddi N.; Poggesi C.; Stehle R.; Tesi C.; Travers F.; Webb M. R. (1998) ATPase and shortening rates in frog fast skeletal myofibrils by time-resolved measurements of protein-bound and free Pi. Biophys. J. 74(6), 3120–3130.
21. Grazi E.; Cintio O.; Trombetta G. (2004) On the mechanics of the actin filament: The linear relationship between stiffness and yield strength allows estimation of the yield strength of thin filament in vivo. J. Muscle Res. Cell Motil. 25(1), 103–105.
22. dos Remedios C. G.; Moens P. D. J. (1995) Actin and the actomyosin interface: A review. Biochim. Biophys. Acta 1228, 99–124.
23. Miki M.; Barden J.; dos Remedios C.; Philips L.; Hambly B. D. (1987) Interaction of phalloidin with chemically modified actin. Eur. J. Biochem. 165, 125–130.
24. Elson E. L. (1985) Fluorescence correlataion spectroscopy and photobleaching recovery. Annu. Rev. Phys. Chem. 36, 379–406.
25. Elson E. L.; (2007) Introduction to FCS. Short Course on Cellular and Molecular Fluorescence(Gryczynski Z., editor. , Ed.) Vol. 2, pp 1–10, University of North Texas, Fort Worth, TX.
26. Buschmann V., Kramer B., and Koberling F. (2009) Quantitive FCS: Determination of confocal volume by FCS and bead scabnning with Micro Time 200, PicoQuant, Application Note Quantitative FCS version 1.1.
27. Huxley A. F.; Simmons R. M. (1971) Proposed mechanism of force generation in striated muscle.Nature 233, 533–538.
28. Dos Remedios C. G.; Millikan R. G.; Morales M. F. (1972) Polarization of tryptophan fluorescence from single striated muscle fibers. A molecular probe of contractile state. J. Gen. Physiol. 59, 103–120.
29. Nihei T.; Mendelson R. A.; Botts J. (1974) Use of fluorescence polarization to observe changes in attitude of S1 moieties in muscle fibers. Biophys. J. 14, 236–242.
30. Tregear R. T.; Mendelson R. A. (1975) Polarization from a helix of fluorophores and its relation to that obtained from muscle. Biophys. J. 15, 455–467.
31. Morales M. F. (1984) Calculation of the polarized fluorescence from a labeled muscle fiber. Proc. Natl. Acad. Sci. U.S.A. 81, 145–149.
32. Hopkins S. C.; Sabido-David C.; Corrie J. E.; Irving M.; Goldman Y. E. (1998) Fluorescence polarization transients from rhodamine isomers on the myosin regulatory light chain in skeletal muscle fibers. Biophys. J. 74(6), 3093–3110.
33. Thomas D. D.; Cooke R. (1980) Orientation of spin-labeled myosin heads in glycerinated muscle fibers. Biophys. J. 32(3), 891–906.
34. Borejdo J.; Assulin O.; Ando T.; Putnam S. (1982) Cross-bridge orientation in skeletal muscle measured by linear dichroism of an extrinsic chromophore. J. Mol. Biol. 158, 391–414.

35. Mettikolla P.; Calander N.; Luchowski R.; Gryczynski I.; Gryczynski Z.; Zhao J.; Szczesna-Cordary D.; Borejdo J. (2011) Cross-bridge Kinetics in Myofibrils Containing Familial Hypertrophic Cardiomyopathy R58Q Mutation in the Regulatory Light Chain of Myosin. J. Theor. Biol. 284, 71–81.
36. Walcott S.; Warshaw D. M.; Debold E. P. (2012) Mechanical Coupling between Myosin Molecules Causes Differences between Ensemble and Single-Molecule Measurements. Biophys. J. 103(3), 501–510.
37. Dantzig J. A.; Higuchi H.; Goldman Y. E. (1998) Studies of molecular motors using caged compounds. Methods Enzymol. 291, 307–348.
38. Kawai M.; Zhao Y. (1993) Cross-bridge scheme and force per cross-bridge state in skinned rabbit psoas muscle fibers. Biophys. J. 65(2), 638–651.
39. Hell S. W.; Wichmann J. (1994) Breaking the diffraction resolution limit by stimulated emission: Stimulated-emission-depletion fluorescence microscopy. Opt. Lett. 19, 780–782.
40. Shroff H., White H., and Betzig E. (2008) Photoactivated localization microscopy (PALM) of adhesion complexes. Current Protocols in Cell Biology, Chapter 4, Unit 4, 21, Wiley, New York.
41. Heintzmann R.; Ficz G. (2013) Breaking the resolution limit in light microscopy. Methods Cell Biol.114, 525–544.
42. Vision D.. (2013) OMX (http://www.api.com/downloads/pdfs/lifescience/DV%20OMX.pdf).
43. York A. G.; Chandris P.; Nogare D. D.; Head J.; Wawrzusin P.; Fischer R. S.; Chitnis A.; Shroff H. (2013) Instant super-resolution imaging in live cells and embryos via analog image processing. Nat. Methods 10, 1122–1126.
44. Yanagida T.; Oosawa F. (1978) Polarized fluorescence from ε-ADP incorporated into F-actin in a myosin-free single fiber: Conformation of F-actin and changes induced in it by heavy meromyosin. J. Mol. Biol. 126(3), 507–524.
45. Yanagida T.; Oosawa F. (1980) Conformational changes of F-actin-ε-ADP in thin filaments in myosin-free muscle fibers induced by Ca^{2+}. J. Mol. Biol. 140(2), 313–320.
46. Prochniewicz-Nakayama E.; Yanagida T.; Oosawa F. (1983) Studies on conformation of F-actin in muscle fibers in the relaxed state, rigor, and during contraction using fluorescent phalloidin. J. Cell Biol. 97, 1663–1667.
47. Oosawa F.; Maeda Y.; Fujime S.; Ishiwata S.; Yanagida T.; Taniguchi M. (1977) Dynamic characteristics of F-actin and thin filaments in vivo and in vitro. J. Mechanochem. Cell Motil. 4(1), 63–78.
48. Ando T. (1989) Propagation of Acto-S-1 ATPase reaction-coupled conformational change in actin along the filament. J. Biochem. 105(5), 818–822.
49. Hill T. L.; Eisenberg E.; Chalovich J. M. (1981) Theoretical models for cooperative steady-state ATPase activity of myosin subfragment-1 on regulated actin. Biophys. J. 35(1), 99–112.
50. Lymn R. W.; Taylor E. W. (1971) Mechanism of adenosine triphosphate hydrolysis by actomyosin.Biochemistry 10, 4617–4624.
51. Coureux P. D.; Sweeney H. L.; Houdusse A. (2004) Three myosin V structures delineate essential features of chemo-mechanical transduction. EMBO J. 23(23), 4527–4537.
52. Spudich J. A. (2014) Hypertrophic and Dilated Cardiomyopathy: Four Decades of Basic Research on Muscle Lead to Potential Therapeutic Approaches to These Devastating Genetic Diseases. Biophys. J. 106(3), 1236–1249.

53. Mettikolla P.; Calander N.; Luchowski R.; Gryczynski I.; Gryczynski Z.; Borejdo J. (2010)Observing cycling of a few cross-bridges during isometric contraction of skeletal muscle.Cytoskeleton 67(6), 400–411.
54. Borejdo J.; Shepard A.; Dumka D.; Akopova I.; Talent J.; Malka A.; Burghardt T. P. (2004)Changes in orientation of actin during contraction of muscle. Biophys. J. 86, 2308–2317.
55. Ling N.; Shrimpton C.; Sleep J.; Kendrick-Jones J.; Irving M. (1996) Fluorescent probes of the orientation of myosin regulatory light chains in relaxed, rigor, and contracting muscle. Biophys. J.70(4), 1836–1846.
56. Ferenczi M. A.; Bershitsky S. Y.; Koubassova N.; Siththanandan V.; Helsby W. I.; Panine P.; Roessle M.; Narayanan T.; Tsaturyan A. K. (2005) The “roll and lock” mechanism of force generation in muscle. Structure 13(1), 131–141.
57. Midde K.; Rich R.; Marandos P.; Fudala R.; Li A.; Gryczynski I.; Borejdo J. (2013) Orientation and Rotational Motion of Cross-Bridges Containing Phosphorylated and de-Phosphorylated Myosin Regulatory Light Chain. J. Biol. Chem. 288(10), 7012–7023.
58. Duggal D.; Nagwekar J.; Rich R.; Midde K.; Fudala R.; Gryczynski I.; Borejdo J. (2013)Phosphorylation of myosin regulatory light chain has minimal effect on kinetics and distribution of orientations of cross-bridges of rabbit skeletal muscle. Am. J. Physiol. 306(4), R222–R233.
59. Gomes A. V.; Potter J. D. (2004) Molecular and cellular aspects of troponin cardiomyopathies. Ann. N.Y. Acad. Sci. 1015, 214–224.
60. Colson B. A.; Locher M. R.; Bekyarova T.; Patel J. R.; Fitzsimons D. P.; Irving T. C.; Moss R. L. (2010) Differential roles of regulatory light chain and myosin binding protein-C phosphorylations in the modulation of cardiac force development. J. Physiol. 588(Part 6), 981–993.

CHAPTER V

DIFFERENCES IN THE SPATIAL DISTRIBUTION OF ACTIN IN THE RIGHT AND LEFT VENTRICLES OF HEALTHY RABBIT HEARTS

J. Nagwekar[1], D. Duggal[1], R. Rich[1], R. Fudala[1], I. Gryczynski[1], S. Raut[2], Z. Gryczynski[2] and J. Borejdo[1]*

[1] Dept of Cell Biology and Center for Commercialization of Fluorescence Technologies, University of North Texas, Health Science Center, 3500 Camp Bowie Blvd, Fort Worth, TX 76107

[2] Dept of Physics and Astronomy, Texas Christian University, 2800 S. University Dr., Fort Worth, Texas 76129

* Corresponding Authors: Julian Borejdo, Department of Cell Biology, University of North Texas Health Science Center, 3500 Camp Bowie Blvd, Fort Worth, TX 76107, USA, Tel.: (817) 735-2106, Fax: (817) 735-2118; E-mail: Julian.Borejdo@unthsc.edu

1. ABSTRACT

We examined the effect of the differences in spatial arrangement of actin in contracting muscles from the left (LV) and right (RV) ventricles of rabbit heart. Spatial arrangement is a fundamental property of muscle because it reflects the interaction of individual actin molecules with myosin cross-bridges. Macroscopic parameters of contraction, such as maximum tension, speed of shortening or ATPase activity, are unlikely to reveal differences between the ventricles because they are made on whole organs containing trillions of actin and myosin molecules. Averaging the data collected from such a large assembly is likely to conceal small differences. To eliminate complications arising from the differences in the basic myocardial architecture and fiber structures of the ventricles, and to ensure that the molecular crowding influences contraction in the same way as under the *in-vivo* conditions, we collected data from isolated myofibrils *ex-vivo*. Control anisotropy experiments revealed that the orientation of actin reflected the orientation of myosin cross-bridges. The results showed that the changes in the distribution of actin induced by the interaction of actin filaments with myosin heads were demonstrated only in LVs, not in RVs. This suggests that both ventricles interact differently with myosin cross-bridges. We think that the stress induced in the thin filaments of LV causes loosening of bonds between actin monomers which leads to greater mobility of actin monomers.

KEYWORDS: Actin orientation, heart ventricles, fluorescence polarization

2. INTRODUCTION

Left and right ventricles (LV, RV) are morphologically and physiologically different. Left ventricle pumps blood into systemic circulation while right ventricle pumps blood into the pulmonary circulation. Different force is necessary to overcome afterload of both systems. This resulted in evolutionary changes that gave rise to number of differences between ventricles. One difference is in basic fiber structures. The right ventricle (RV) consists of transverse fibers in its free wall while the left ventricle (LV) is encircled by oblique and circumferential fibers (Schwarz et al., 2013). Both fiber types differ in mechanical efficiency (Sallin, 1969; Austin, 2007). Other differences are present as well: differences have been reported in the ATPase activity (Krug et al., 1987), in the α-heavy chain composition and velocity of contraction (Brooks et al., 1987), energy usage (Itoya et al., 1996; Carlsson et al., 2012), amounts of proteins (Cadete et al., 2012), synthesis and degradation of myosin chains (Samarel, 1989), in the contractile performance in dilated cardiomyopathy (McMahon et al., 1996) and congestive heart failure (Belin et al., 2011), in ventricular development (Tam et al., 1997) (Rosenquist, 1970; de la Cruz et al., 1977; Mjaatvedt et al., 2001; Buckingham et al., 2005) and in the expression of transcription factors (Drake et al., 2011). There are number of heart diseases that are caused by the dysfunction of right or left ventricles only. For example, RV dysfunction causes pulmonary hypertension. LV dysfunction causes systolic or diastolic heart failure. Yet there are no drugs that are specific for either ventricle. The function of RV can be controlled only indirectly by pulmonary vasodilators to reduce afterload. The new one, riociguat, has little side effects and directly stimulates soluble guanylyl cyclase (Sundaram et al., 2010). The function of LV can only be controlled by invasive aortic banding (Li et al., 2003). Therefore, the goal of this work is to stimulate search for drugs that act specifically on each ventricle.

We think that the differences arise because the measurements were carried out macroscopically (i.e. on the whole tissues or parts of it). They contain typically 10^{11} - 10^{13} contractile molecules and the resulting signal is an average. Average of such a large number loses all the information about contributions of the individual molecule. In fact, the Central Limit Theorem (Bracewell, 1965) of statistics states that if a large number of independent measurements (in our case steady-state distribution of orientations of actin during ventricle contraction) are performed, each measurement having its own mean and standard deviation, then the final distribution of measurements will be a perfect Gaussian (Bracewell, 1965). While this Gaussian may have different mean, it will have 0 skewness and 0 excess kurtosis (i.e. absolute kurtosis of 3), no matter from which ventricle a sample it is taken. The averaged signal will also lose all information about the kinetic behavior of molecules. Therefore the experiments should be carried out on ventricles containing contributions from only a few molecules. The best way to accomplish this is to carry out experiments on isolated myofibrils, where only ~20 molecules of actin can be observed in a confocal volume. Although it is impossible to directly measure stress exerted by a myofibril on the ventricular wall, it is possible to measure steady-state distribution of actin orientations in the left and the right ventricles. This distribution is a fundamental property of muscle because it reflects the interaction of individual actin molecules with myosin cross-bridges. Myofibrils in a myocyte are oriented every-each way as illustrated in Fig. 1.

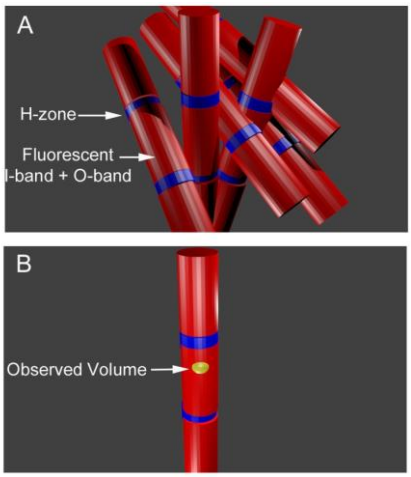

Figure 1: A diagram explaining that by using isolated myofibril a few molecules can be observed with ordinary confocal microscope. A: Fibers within myocytes have different orientations. Actin is labeled with phalloidin (red) yielding fluorescent actin in the I-bands & A-bands. The H-zone (blue) is non-fluorescent, **B**: Single myofibril is isolated from a myocyte and is placed vertically on a microscope stage. A laser beam is focused to a diffraction limit on isolated myofibril. Fluorescence is collected from the Observational Volume (yellow) which contains 20-40 actin molecules.

Observing isolated myofibril eliminates complications due to the differences between LV and RV in shape and thickness. In addition, it must be recognized that molecular crowding plays an important role in *in-vivo* or *ex-vivo* situations, especially in muscle where protein concentration is extremely high (Bagshaw, 1982). Therefore measurements must be carried out under conditions as closely as possible resembling the *in-vivo* conditions (Minton, 2001; Mourao et al., 2014).

We expect to find differences between distributions of actin in the left and right functioning ventricles. We hypothesize that precise modifiers of power output can be generated to reverse the effects of that distribution. To modify function of one ventricle only, one can take the advantage of the fact that the binding of a small molecule to large molecule such as actin may perturb its function (Spudich, 2014). Any drug that potentiates of power output is likely to have a positive effect on a ventricle pumping too weakly. Likewise, specific inhibitors that affect force to reduce power and velocity of muscle shortening are likely to be effective on a ventricle pumping too strongly.

We carried out experiments on sarcomeres of isolated myofibrils under *ex-vivo* conditions. Each sarcomere contained ~20 labeled actin molecules. We labeled ventricular actin with fluorescent phalloidin and measured the distribution of its steady-state orientations during contraction, relaxation and rigor. Both ventricles had consistently different distributions during contraction but identical distribution during rigor or relaxation. We conclude that while mammalian ventricular muscles may be expressed from the same genes, show the same composition of the beta-myosin heavy chain and show no differences in stress development, twitch duration, work performance and power development on the macroscopic level, there is a significant functional difference between them on the molecular level.

3. MATERIALS AND METHODS

3.1. Chemicals and Solutions

All chemicals were from Sigma-Aldrich (St Louis, MO). Alexa 633 phalloidin (AP) and unlabeled phalloidin (UP) was from Molecular Probes (Eugene, OR). Ca-rigor solution contained 50 mM KCl, 10 mM Tris-HCl pH 7.5, 2 mM $MgCl_2$, 0.1 mM $CaCl_2$. Contracting solution contained 50 mM KCl, 10 mM Tris-HCl pH7.5, 5 mM $MgCl_2$, 0.1 mM $CaCl_2$, 5 mM ATP, 20 mM creatine phosphate and 10 units/ml of 1 mg/ml creatine kinase. Relaxing solution had the same composition as contracting solution, but with 0.1 mM Ca^{2+} replaced with 2 mM EGTA. Glycerinating solution contained 50 mM KCl, 10 mM Tris-HCl pH7.5, 5 mM $MgCl_2$, 2 mM EGTA, 5 mM ATP, 20 mM creatine phosphate and 10 units/ml of 1 mg/ml creatine kinase.

3.2. Preparation of Ventricles

University of North Texas HSC Institutional Animal Care and Use Committee (IACUC) specifically approved this study (approval # 2013/2014-46-A08) starting Oct 8 2014. Healthy 6 month old female rabbits (Charles River, Mass) were sacrificed by injection of 10-20 mg/kg Ketamine, 5mg/kg Xylazine and 2ml IA Phentobarbital and were immediately placed in a cold dissecting solution (50 mM KCl, 5 mM MgEGTA, 15% glycerol). Left and right ventricles were dissected in the cold room, tied to wooden sticks and placed for 24 hrs in glycerinating solution at 0^oC. After 24 hrs, glycerinating solution was replaced with a fresh glycerinated solution and placed at -20^oC. Myofibrils (MF) were made from glycerinated hearts no earlier than 2 weeks at -20^oC.

3.3. Preparation of myofibrils

Experiments were done on isolated myofibrils. **Fig. 2S** explains that by using a sample containing isolated myofibril, observation of a few actin molecules is possible employing conventional confocal microscope. To prepare myofibrils, ventricles were washed 3 times for 30 min each with ice-cold EDTA-rigor solution (50 mM KCl, 10 mM Tris-HCl pH 7.5, 5 mM EDTA), in order to wash out ATP present in the skinning solution without causing contraction. They were then washed thoroughly with Ca-rigor solution and homogenized in the Cole-Palmer LabGen 125 homogenizer for 10 s followed by further 10 s homogenization after a cool down period of 30 s.

3.4. Cross-linking

MFs shorten rapidly when washed upon adding contracting solution (**movie, Fig. 3S**). Such shortening would make it impossible to perform steady-state experiment (i.e. collect data from half-sarcomere for 20 s). To inhibit shortening, 1 mg/ml myofibrils were incubated for 20 min at room temperature with 20 mM water-soluble cross-linker 1-ethyl-3-[3-(dimethylamino)-propyl]-carbodiimide (EDC) [25-28]. The reaction was stopped by adding 20 mM DTT. The pH of the solution remained unchanged at 7.5 throughout the time course of reaction. The absence of shortening was verified by observing myofibrils irrigated with contraction solution in a Nomarski microscope.

3.5. Labeling of myofibrils

50 µL of 1 mg/mL myofibrils at room temperature were placed on #1 cover-glass, allowed to adhere for 10 min and washed for 10 min with a labeling solution (10 nM AP, 10 µM UP, 50 mM Ca-rigor solution) by

applying labeling solution at one end of the cover slip and sucking with #1 filter paper at the opposite end. The number of actin molecules in the observational volume (OV) is calculated in the paragraph below.

3.6. Signal from a single molecule of actin

To determine the number of actin molecules under observation, the instrument had to be calibrated to determine fluorescence intensity (counts/s) produced by a known number of molecules of Alexa-phalloidin. This number was determined by Fluorescence Correlation Spectroscopy (FCS). The autocorrelation function (ACF) at delay time 0 of fluctuations caused by free Alexa phalloidin molecules entering and leaving the OV is equal to the inverse of the number of molecules contributing to fluctuations N = 1/ACF(0) [29-31]. 15 nM Alexa phalloidin was illuminated with 18 μW of laser at 532 nm. A calibrations curve was constructed by plotting the power of the laser vs. the rate of photon arrival per molecule of the dye (**Fig. 4S**). From this curve it was determined that the number of photons collected in a second from a single Alexa633 phalloidin molecule was ~220. A typical total fluorescence intensity was ~4,000 photons/s and number of fluorescent actins contributing to the signal was ~20. Each experiment lasted 20 s and contained 2 million experimental data points. Signal of contracting muscle contained fluctuations (**Fig. 2**) due to periodic kicks actin receives from interactions with myosin cross-bridges. Since a characteristic life-time of one fluctuation is of the order of milliseconds [32], each data set was binned (smoothed) to contain 20,000 fluctuations. If X is the number of fluctuations detected, the precision of measurement is approximately equal to $1/\sqrt{X}$. Hence precision of our experiment is ~0.5%.

3.7. Time resolved anisotropy measurements

The lifetime and fluorescence anisotropy were measured by the time-domain technique using a FT300 fluorescence lifetime spectrometer (PicoQuant, Inc.) at a room temperature. The excitation was provided by a continuum laser (Fionium Whitelase Sc400-4), and the observation was conducted through a 660 nm monochromator with a supporting 650 nm long pass filter. The Full Width at Half Maximum (FWHM) of the pulse response function was less than 100 ps and the time resolution was <10 ps. The intensity decays were analyzed by a multi-exponential model using FluoFit software (PicoQuant, Inc.). To ascertain whether the phalloidin probe is immobilized so that the transition dipole of the fluorophore reflects the orientation of actin monomer, we measured the decay of anisotropy of AP inserted into myofibrils. Anisotropy is defined as $r = (I_{\parallel} - I_{\perp})/(I_{\parallel} + 2I_{\perp})$.

3.8. Data collection

Before each experiment, fluorescence of an isotropic solution of a small dye with long fluorescence lifetime (rhodamine 700 which has 0 anisotropy) was measured to make sure that the parallel (∥) and perpendicular (⊥) channels received equal amount of emitted light. The myofibrils were placed on a scanning stage of PicoQuant MT 200 inverse time-resolved fluorescence instrument coupled to Olympus IX 71 microscope. The stage was rotated to vertically align myofibril under observation (**Fig. 6S**). 543 nm laser beam modulated at 20 MHz was focused by an Olympus x60, NA=1.2 water immersion objective to the diffraction limit on the fluorescent part of a myofibril. The power delivered to each half-sarcomere was adjusted within 10-20 μW range to obtain the similar photon rate for each myofibril. If the power is not equal, the differences between data sets become statistically interpretable (see Discussion). ~20-50 myofbrils were examined. The OV (1.7 μm^3) was estimated by measuring FWHM of axial and lateral dimensions of an image of 20 nm fluorescent beads and making 3D Gaussian approximation following [33].

3.9. Statistical analysis

Comparisons between groups were performed using an unpaired Student's t-test (Sigma Plot 11; Systat Software, Inc., San Jose, CA, USA). The differences were deemed significant when $P<0.05$. SigmaPlot 11 was used to compute histograms. Origin v.8.6 (Northampton, MA) was used to compute autocorrelation functions.

4. RESULTS

4.1. Macroscopic data

We first confirm the macroscopic data (obtained from myofibrils in solution containing $>10^{10}$ actin molecules) that no difference between ventricles can be observed. Fig. 2 shows the steady-state anisotropies of fluorescence decays of Alexa633 phalloidin bound to thin filaments. Anisotropy is a measure of the orientation of the emission dipole of Alexa633 dye, and since the dye is fairly rigidly attached to actin (Fig. S1) it is also an indicator of actin orientation.

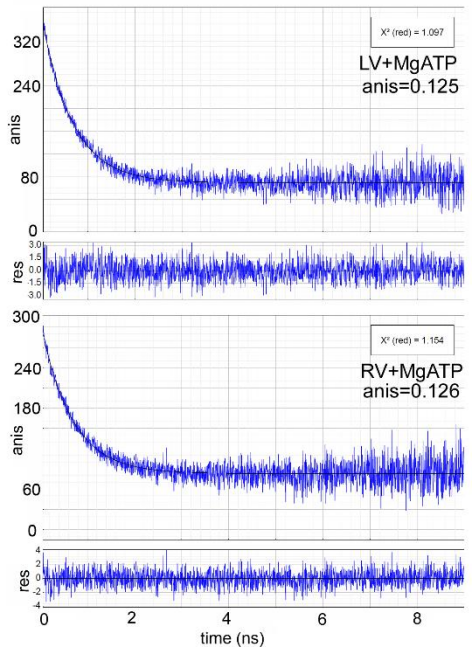

Figure 2: Anisotropy decay curves of myofibrils from the left (top panel) and the right (bottom panel) ventricles showing that macroscopic measurements are unable to distinguish between ventricles. Left and right ventricles yielded 57% and 67% contribution, respectively, of slowly rotating actin. The bottom graphs show residual values of non-linear fits. 0.5 mg/mL ventricular myofibrils, 50 nM Alexa633 phalloidin, 0.5 µM unlabeled phalloidin, room temperature. Time scale is shifted so that 0 ns occurs 21 ns after the laser pulse.

The steady-state anisotropies in Fig. 2 of left (top) and right (bottom) ventricles are the same. The same result was obtained from comparison of ATPase activities of whole myofibrils from the left (2.665± 0.029 ATP/min/myosin molecule) and right (2.395± 0.116 ATP/min/myosin molecule) ventricles. Thus the macroscopic data is incapable of demonstrating differences between ventricles**.**

4.2. Microscopic Data

We carried out experiments on 23-40 isolated myofibrils under *ex-vivo* conditions. An example of a fluorescently labeled myofibril is shown in Fig. 3. Alexa633-phalloidin stains the entire A+I bands, because in contrast to skeletal muscle cardiac muscle does not contain nebulin (Ao and Lehrer, 1995).

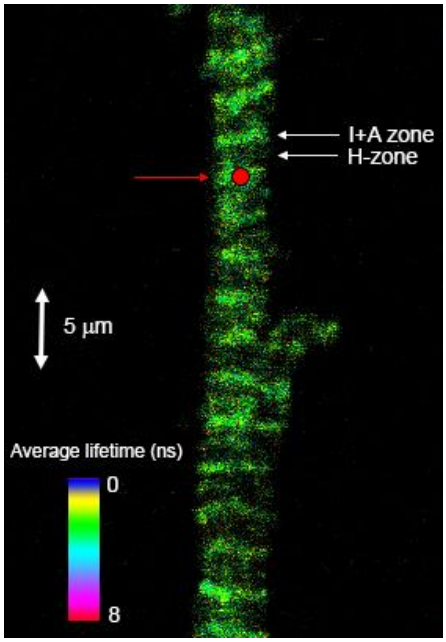

Figure 3: Fluorescence lifetime image of sparsely labeled myofibril. Thin filaments are irrigated with a 0.1% mixture of Alexa633-Phalloidin (AP) to Unlabeled-Phalloidin (UP) resulting in one actin out of 1000 actin monomers being labeled. The myofibril is illuminated with 635 nm light. From the image the lifetime is ~3 ns. In the cuvette the intensity average is 3 ns and amplitude average is 2.1 ns. The red circle indicated by a red arrow is a projection of the confocal aperture on the image plane. The detector sees only this volume (~1.7 μm^3) (OV in 3D is the ellipsoid-of-revolution). The number of fluorescent actin molecules in this volume is ~20 (see text).

A typical fluorescent signal from one sarcomere is shown in Fig. 4. During contraction the orientation of actin is not constant because it receives periodic kicks from the myosin cross-bridges which drive it between various configurations. The signal fluctuated between two specific orientations of actin (Fig. S2). In the absence of nucleotides, the anisotropy of actin was small (comparable to the free dye, Fig. S2A). It showed a small increase in the presence of MgADP and a large increase in the presence of MgATP (Fig. S2B and C). Thus the time course of actin orientations is best represented schematically by Fig. S2D. This ON-OFF cycle is an oversimplification, because cross-bridges execute more complicated cycle (Coureux et al., 2004), but is sufficient to demonstrate difference between ventricles.

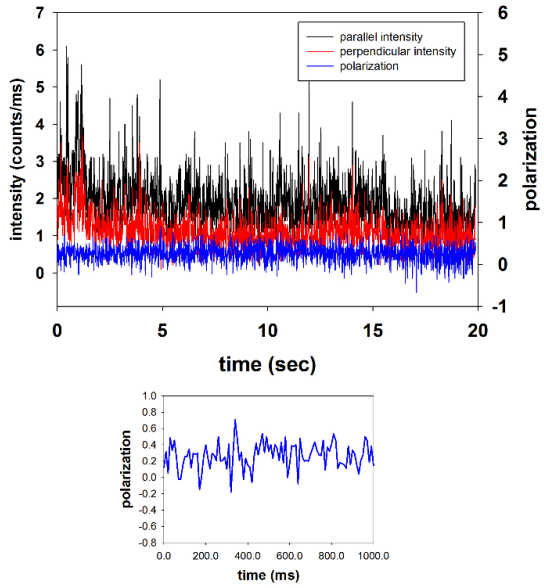

Figure 4: Traces of polarized fluorescence intensities (parallel in black, perpendicular in red, left scale) and polarization of fluorescence (blue, right scale) obtained from actin in the contracting overlap band of a sarcomere of the left ventricle; Bottom: first 1000 ms of the time course of polarization of fluorescence change.

To be able to better compare the results with those of previous experiments (Nagwekar et al., 2014), we measured polarized fluorescence of actin during 20 s of ventricle contraction. Anisotropy is related to polarization of fluorescence (PF) by the relation: anis=2PF/(3-P). Polarization of fluorescence is the normalized ratio of the difference between $\parallel$ and $\perp$ components of the fluorescent light emitted by the dye. It is a reliable measure of the conformation of the transition dipole of the fluorophore (Dos Remedios et al., 1972; Nihei, 1974; Tregear and Mendelson, 1975; Morales, 1984; Hopkins et al., 1998; Sabido-David et al., 1998; Hopkins et al., 2002).

During the first 2 seconds the intensities decline due to photobleaching, but this has no effect on polarization of fluorescence because the orthogonal intensities decline at the same rate. The total intensity of this typical contracting signal was small, because we deliberately labeled every 1000th actin monomer to decrease the number of observable molecules. The total intensity in Fig. 4 was $I_{\parallel}+2\ I_{\perp}$ i.e. 1.9+2*1.1=4.1 counts/ms. Since the number of photons collected in a second from a single Alexa633 phalloidin molecule was ~220 (see Materials and Methods), in this (typical) case the number of fluorescent (detected) actin molecules was 4100/220≈20. It should be emphasized, however, that as long as the number of molecules is mesoscopic (i.e. small), the exact number does not matter.

The width of the orientation distribution of Alexa633 fluorophore bound to actin was Gaussian, which is best quantitated by Full Width at Half Maximum (FWHM) or Standard Deviation (SD). We have chosen to measure the former, although for a Gaussian it makes no difference because the two a simply related (FWHM=2Sqrt(2ln2)=2.355 SD). Skewness and kurtosis indicate how well the distribution matches a perfect Gaussian distribution. Thus negative or positive skewness indicates how much the distribution is slanted to the left or right, respectively. The size of kurtosis indicates the degree to which outliers (values

near the tail) contribute to the distribution (absolute and reduced kurtosis of a perfect Gaussian distribution is 3 and 0, respectively).

During contraction the mean FWHMs of RVs were significantly smaller than of LVs (i.e. actin orientations in LV were significantly wider than in RVs. The distributions are shown here as histograms – plots of frequency of occurrence of a given orientation (i.e. polarization of fluorescence), show significant differences in skewness and kurtosis. Distributions of LVs differed less from a perfect Gaussian than RV. Examples of histograms of measurements of 35 experiments from LVs and 30 experiments of RVs are shown in Fig. 5. (experiments were performed in myofibrils from different hearts). The histograms of all LV experiments are shown in Fig. S5 a-c and of RV experiments in Fig. S6 a-b.

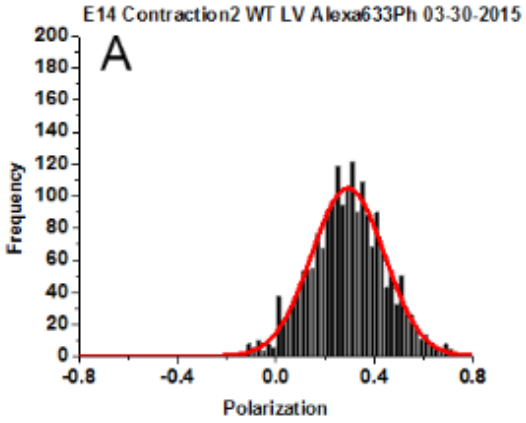

Figure 5: An example of distribution of polarization values of the transition dipole of actin in the I+A bands of contracting LV sarcomere. To obtain histogram polarization, the data (such as shown in blue in Fig. 3 and 4) is imported into the Origin program and the Hist function is applied. The orientation of ~20 labeled actin molecules was measured 2000 times.

All data are summarized in Table 1.

TABLE 1. The widths of distribution of actin during contraction of LVs and RVs myofibrils

Contracting Ventricle	FWHM *	Counts/ms	Polarization	Skewness*	Kurtosis *	AR^2
LV	0.439±0.048	5.2±1.6	0.275±0.111	1.458±0.108	1.017±0.453	0.903±0.053
RV	0.374±0.033	6.0±1.7	0.301±0.020	1.594±0.101	1.304±0.388	0.954±0.022

Table 1: The widths of distribution of Alexa633 dipole angles bound to actin during contraction of LVs and RVs myofibrils. The results present 35 experiments on LVs and 30 experiments on RVs. Errors are SD. Statistically significant differences between LV and RV are marked with the asterisk.

0.065 difference in FWHM was extremely statistically significant ($t = 5.875$, $P<0.0001$) with 63 degrees of freedom (degrees of freedom is the number of possible values of FWHM, skewness or kurtosis that can be varied in calculations). 95 percent confidence interval for difference of means was 0.041 to 0.083. -0.8 difference in the counts/ms was NOT statistically significant ($t = -1.983$, $P=0.052$) with 63 degrees of freedom. 95 percent confidence interval for difference of means was -1.659 to 0.006. -0.136 difference in

skewness was statistically significant (t = -5.097, P<0.001) with 61 degrees of freedom. 95 percent confidence interval for difference of means was -0.189 to -0.0827. -0.287 difference in kurtosis was statistically significant (t = -2.671, P=0.010) with 61 degrees of freedom. 95 percent confidence interval for difference of means was -0.502 to -0.072. The mean values of polarizations were not statistically significant (t = -1.235, P = 0.221). The value of AR^2 indicates goodness of non-linear fit to an ideal Gaussian (value of 1.00 indicates ideal fit).

It is crucial that difference between the mean fluorescence intensity be not significant. This is because the FWHM of the Gaussian distribution depends not only on the properties of muscle, but also on the strength of the signal (Borejdo and Midde, 2012). Strong Gaussian signals give relatively small FWHM and weak signals give relatively large FWHM.

To summarize the contraction results: FWHM, mean polarization, skewness and kurtosis are characteristics of the orientation distribution of actin molecules. These parameters are different in LV and RV.

4.3. Rigor

In rigor all myosin heads are attached to actin**.** All data are summarized in Table 2. For the sake of brevity the individual histograms are not shown.

TABLE 2. The widths of distribution of actin during rigor of LVs and RVs myofibrils

Contracting Ventricle	FWHM *	Counts/ms	Polarization	Skewness*	Kurtosis *	AR^2
LV	0.392±0.051	5.3±1.2	0.325±0.030	1.576±0.103	1.331±0.382	0.932±0.057
RV	0.401±0.047	5.3±1.2	0.312±0.044	1.518±0.121	1.110±0.371	0.940±0.038

Table 2. *The widths of distribution of Alexa633 dipole angles bound to actin in rigor of cross-linked LVs and RVs myofibrils. The results present 23 experiments on LVs and 25 experiments on RVs. Errors are SD. There were no statistically significant differences between LV and RV.*

In contrast to contraction, none of the differences were statistically significant. The difference of -0.00876 of FWHM was not statistically significant (t = -0.594, P=0.556) with 43 degrees of freedom. The 95 percent confidence interval for difference of means was -0.038 to 0.021. The difference of 0.0137 in the mean polarization was not statistically significant (t = 1.203, P=0.235) with 43 degrees of freedom. The 95 percent confidence interval for the difference of means was -0.009 to 0.036. The difference of 0.0585 of skewness was not statistically significant (t = 1.735, P=0.090) with 43 degrees of freedom. The 95 percent confidence interval for difference of means was -0.009 to 0.126. The difference of 0.221in kurtosis was not statistically significant (t = 1.964, P=0.056) with 43 degrees of freedom. 95 percent confidence interval for difference of means was -0.006 to 0.447.

4.4. Relaxation

This is the negative control. In relaxation cross-bridges do not make contact with actin filaments and are disordered (Borejdo et al., 1982; Cooke et al., 1982). The histograms of polarization of fluorescence of actin were the same for both ventricles except in the case of Mean Polarization which was dramatically different. The fact that polarization is significantly different suggests that organization of thin filaments or binding of phalloidin are different in LV and RV. Data are summarized in Table 3.

TABLE 3. The widths of distribution of actin during relaxation of LVs and RVs myofibrils						
Contracting Ventricle	FWHM *	Counts/ms	Polarization	Skewness*	Kurtosis *	AR^2
LV	0.376±0.051	5.7± 1.1	0.273±0.061	1.595±0.117	1.354±0.350	0.951±0.033
RV	0.398±0.040	4.8± 1.0	0.337±0.045	1.544±0.087	1.198±0.292	0.935±0.044

Table 3. The widths of distribution of Alexa633 angles bound to actin in relaxed LVs and RVs. The results of 26 experiments on LVs and RVs. Errors are SD.

Similarly to rigor, none of the differences (except counts and polarization) were statistically significant. The -0.0218 difference in FWHM was not statistically significant (t = -1.705, P=0.094) with 50 degrees of freedom. 95 percent confidence interval for the difference of means was -0.047 to 0.004. The 0.815 difference in counts was significant (t = 2.866, P =0.006) with 47 degrees of freedom. The 95 percent confidence interval for difference of means was 0.243 to 1.387. The -0.0632 difference in the mean polarization was statistically significant (t = -4.223, P<0.001) with 50 degrees of freedom. The 95 percent confidence interval for difference of means was -0.093 to -0.033. 0.0510 difference in skewness was statistically insignificant (t = 1.784, P=0.080) with 50 degrees of freedom. The 95 percent confidence interval for difference of means was -0.006 to 0.108. 0.156 difference in kurtosis was statistically insignificant (t = 1.742, P=0.088) with 50 degrees of freedom. The 95 percent confidence interval for difference of means was -0.024 to 0.336.

5. DISCUSSION

The main conclusion of this paper is that there exist significant functional differences between ventricles on a molecular level. The orientation distribution of actin molecules in thin filaments revealed statistically significant differences in the width and overall shape of a distribution of orientations of actin between the two ventricles during contraction. FWHMs were significantly smaller for RVs than for LVs and skewness and kurtosis for LV was significantly smaller than for RV. The fact that those effects were absent in rigor and relaxed ventricles suggests that it was active interaction of myosin cross-bridges with thin filaments that caused these differences. It is interesting to note that the mean polarization values in relaxed ventricles were dramatically different in LV and RV. This may be a result of the fact that different portions of a sarcomere were sampled in both ventricles, or it may reflect genuine differences in distribution of actin. The former possibility is less likely, because position within sarcomere from which data was collected was random.

Despite macroscopic observations that there have been no confirmed reports of any β-myosin heavy chain composition or conformational differences between myosin molecules in the LV and the RV, our data revealed that there were statistically significant differences in the width of the distribution of a few actin molecules in working LV and RV. The differences could be observed because our data originated from only a few molecules of *ex-vivo* working myofibrils. We thus avoided complications due to differences in basic fiber structures and physiology of both ventricles, we were able to measure distributions specific to conformational transitions and to make sure that the data was collected under conditions where molecular crowding was not eliminated.

Notice that the distribution parameters of RVs were nearly the same in relaxation, rigor and in contraction. In particular, polarizations of RV were nearly identical. Since no tension was applied to the ventricles in relaxation or rigor, this implies that RV felt little effect of tension during systole. This is not surprising, considering that the hydrostatic pressures in the systemic circulation (systolic 120 mm Hg, diastolic 80 mm Hg,) are much higher than in the pulmonary circulation (systolic 25 mm Hg, diastolic 10 mm Hg). This suggests that the force exerted by cross-bridges of RVs did not result in any changes in actin orientation. In other words, the changes in distribution of actin that were induced by the interaction of actin filaments with myosin heads were demonstrated only in the LVs, not in the RVs. The absolute tension developed by LVs is greater, and in spite of the fact that the LV wall is thicker, the stress on the thin filaments of LV's is larger. This stress acts to stretch the actin filaments. We think that this stretch loosens interactions between actin monomers and causes the differences between left and right ventricle distributions, in particular causes the FWHM of LV's to be wider.

It would be interesting to correlate clinical indexes of heart performance in humans with the steady-state measurements reported here. We think that the increase in FWHM is a demonstration of a greater contractility, because it suggests that myosin cross-bridges can reach larger population of actin. We hypothesize that if one can understand the effects of a particular ventricular dysfunction on the steady-state values of FWHM, then precise modifiers of power output can be generated to reverse the effects of that dysfunction. The increased contractility of ventricles may be remedied by those drugs that park some of the heads in a state that cannot interact with actin (Spudich, 2014). The agents that shift the equilibrium towards the state where myosin cannot bind to actin (OFF state) would reduce the number of strongly bound myosin and muscle force. Similarly, the agents that shift the equilibrium towards the state where myosin can bind to actin (ON state) would increase the number of strongly bound myosin and muscle force.

Observation of a single molecule of actin would have been much simpler experiment. Unfortunately, it is impossible in *ex-vivo* experiments due to a significant contributions from the background fluorescence. In addition to the very strong autofluorescence due to an extremely dense environment (Bagshaw, 1982), the background consists of a constant fluorescence coming from actin that are always present in the OV: in contrast to the regular FCS, actin molecules do not translate and fluorescent signal does not fluctuate between zero and maximum. In our experiments only the PF fluctuates around the mean. Further, the laser beam cannot be focused on the same spot for much more than 20 sec to avoid photobleaching.

Observing a single actin molecule *in-vitro* is possible (Forkey et al., 2003; Forkey et al., 2005). However, single molecules *in-vitro* cannot be viewed as an independent motors (Walcott et al., 2012) (Pate and Cooke, 1991; Baker et al., 2002).

The advantage of our measurements is that they were carried out on isolated myofibrils where actin is in its native environment. The fluorescent label had a minimal effect on myofibril contractility (data not shown). Labeling of actin allowed us to control exactly how many molecules occupied the OV. Notice that the number of observed actin molecules determined experimentally agrees within an order of magnitude with the number calculated theoretically: the concentration of actin in a muscle is 0.6 mM (Bagshaw, 1982). There are ~6 x 10^4 actin molecules in the OV. Since 1 out of 1000 actin molecules carries the fluorescent label, the calculation suggests that we observe ~60 fluorescent actin molecules – close to the experimentally observed value of 20. Labeling of actin is very gentle (it involves only irrigation of myofibrils with the protein at room temperature), in contrast with labeling of myosin, which involves labeling light chain 1 (LC1) and exchanging it with myofibrillar LC1 under harsh conditions (1/2 hr at 37^{o}C in the presence of trifluoroperazine) (Ling et al., 1996).

Our earlier results showed that the functional differences between ventricles are present in mice hearts (Nagwekar et al., 2014). The present work extends this to the medium size mammals. We are at present testing whether the differences are present in human heart. We hope that these findings will justify the search for ventricle-specific drugs.

6. SUPPLEMENTARY DATA

Figure S1

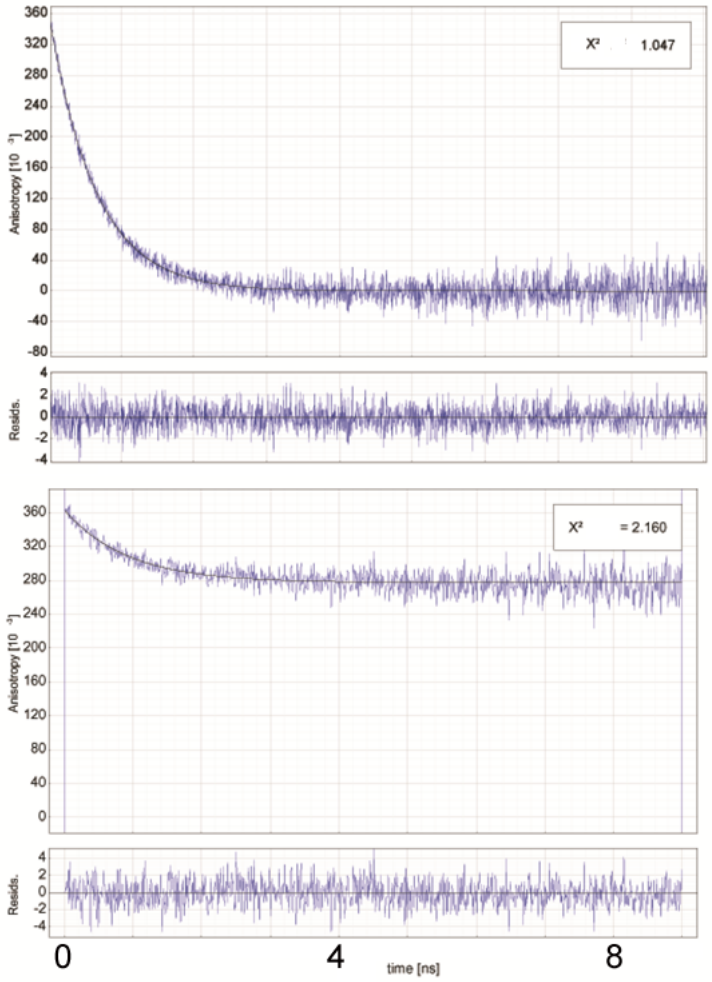

Figure S1: Anisotropy decay of Alexa633 phalloidin bound to actin. Phalloidin alone (top panel) has estimated steady-state anisotropy as 0.066, initial anisotropy 0.358 and correlation time of 0.645 ns. 100% of the signal was due phalloidin. In contracting solution phalloidin bound F-actin with estimated steady-state anisotropy 0.294 (initial anisotropy 0.362) and correlation time of 0.917 ns. 93% of the signal was due to bound phalloidin (i.e. 93% of phalloidin rotated as F-actin). F-actin in contracting solution.

Figure S2

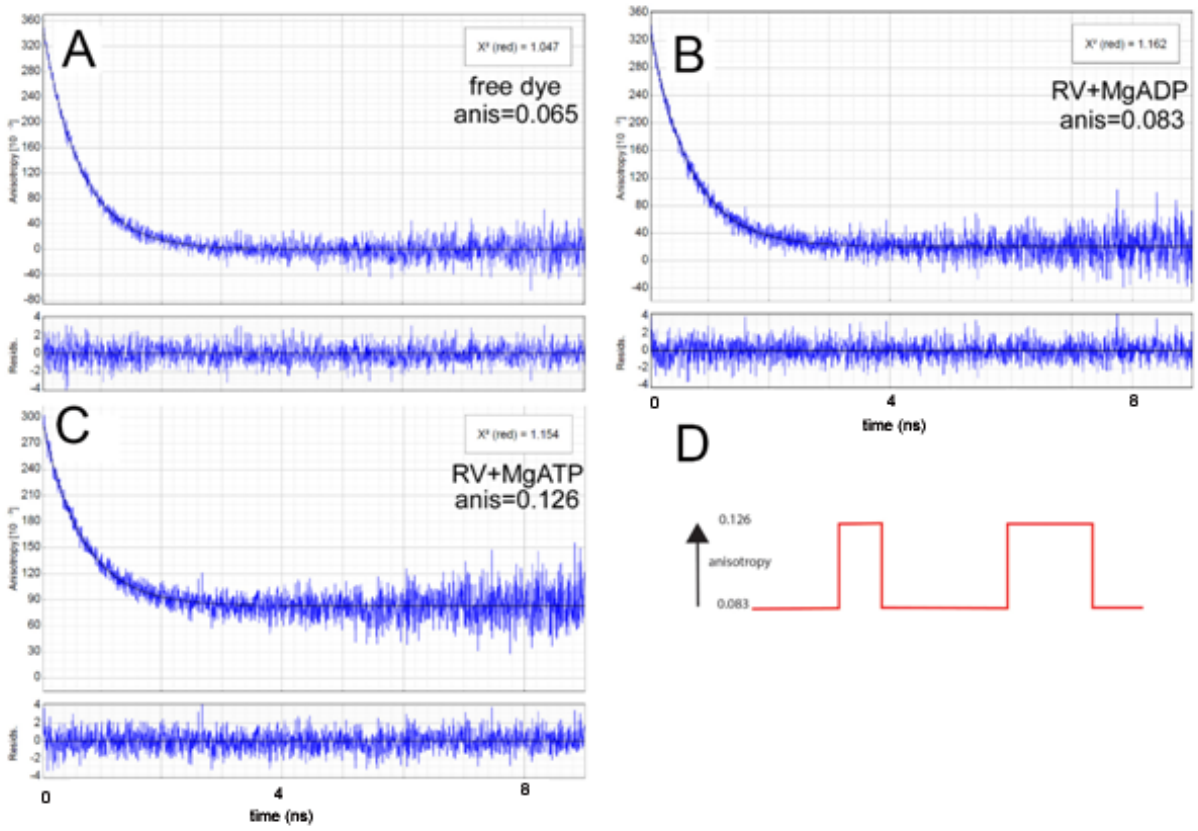

Figure S2: Anisotropy decay of Alexa633 phalloidin bound to thin filaments of right ventricle. Under the conditions simulating rigor (**A**) (26% contribution of slowly rotating actin) and contraction (**B**) (67% contribution of slowly rotating actin), steady-state anisotropies are low and high, respectively. (**C)** Free dye (correlation time (0.630 ns) of rapidly rotating actin is 100%) has steady-state anisotropy close to 0. (**D**) is a schematic diagram of expected signal from contracting ventricles. The observed signal is a sum of 20-40 such curves with max and min anisotropy values of random duration. Bottom graphs show residual values of non-linear fits. 0.5 mg/mL ventricular myofibrils, 50 nM Alexa633 phalloidin, 0.5µM unlabeled phalloidin, room temperature).

Figure S3

contraction cardiac myofibrils from rabbit heart right ventricle

Figure S4

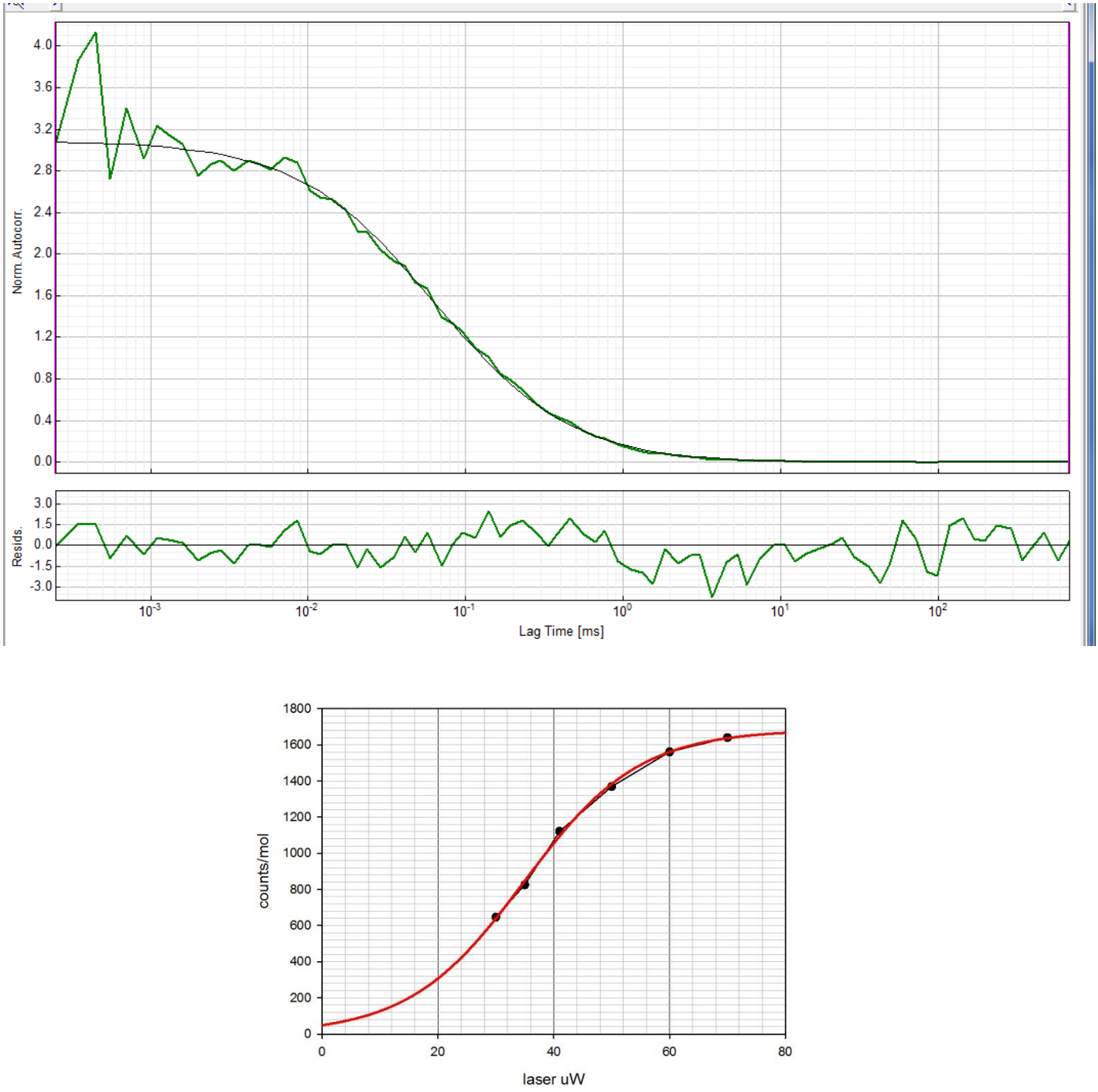

Figure S4: Top: ACF of freely diffusing Alexa633-phalloidin. Bottom: Calibration – the relation between laser power and photon counts per molecule.

Figure S5a

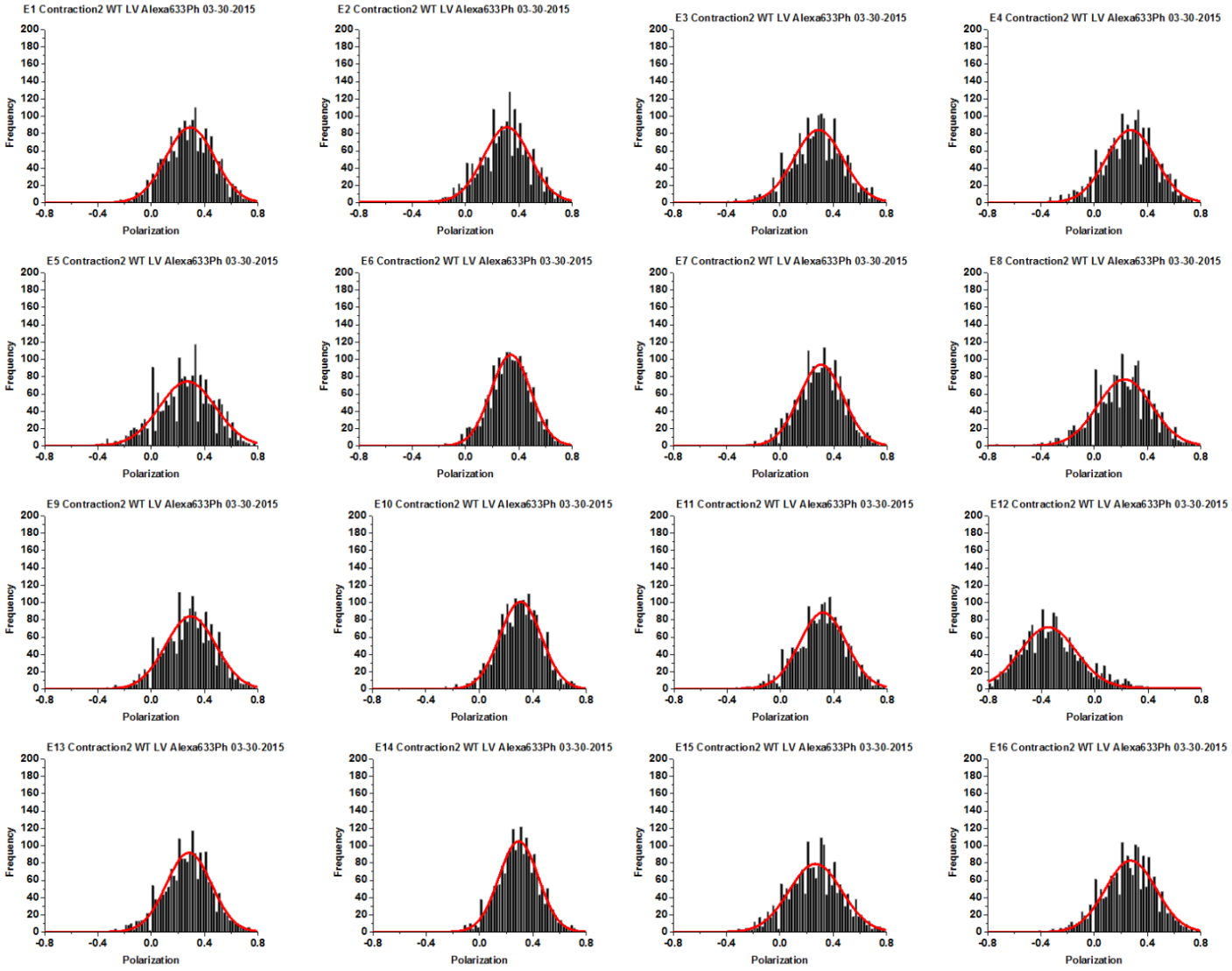

Figure S5a: All histograms of contracting myofibrils from LV. Experiments were performed in different myofibrils from different hearts.

Figure S5b

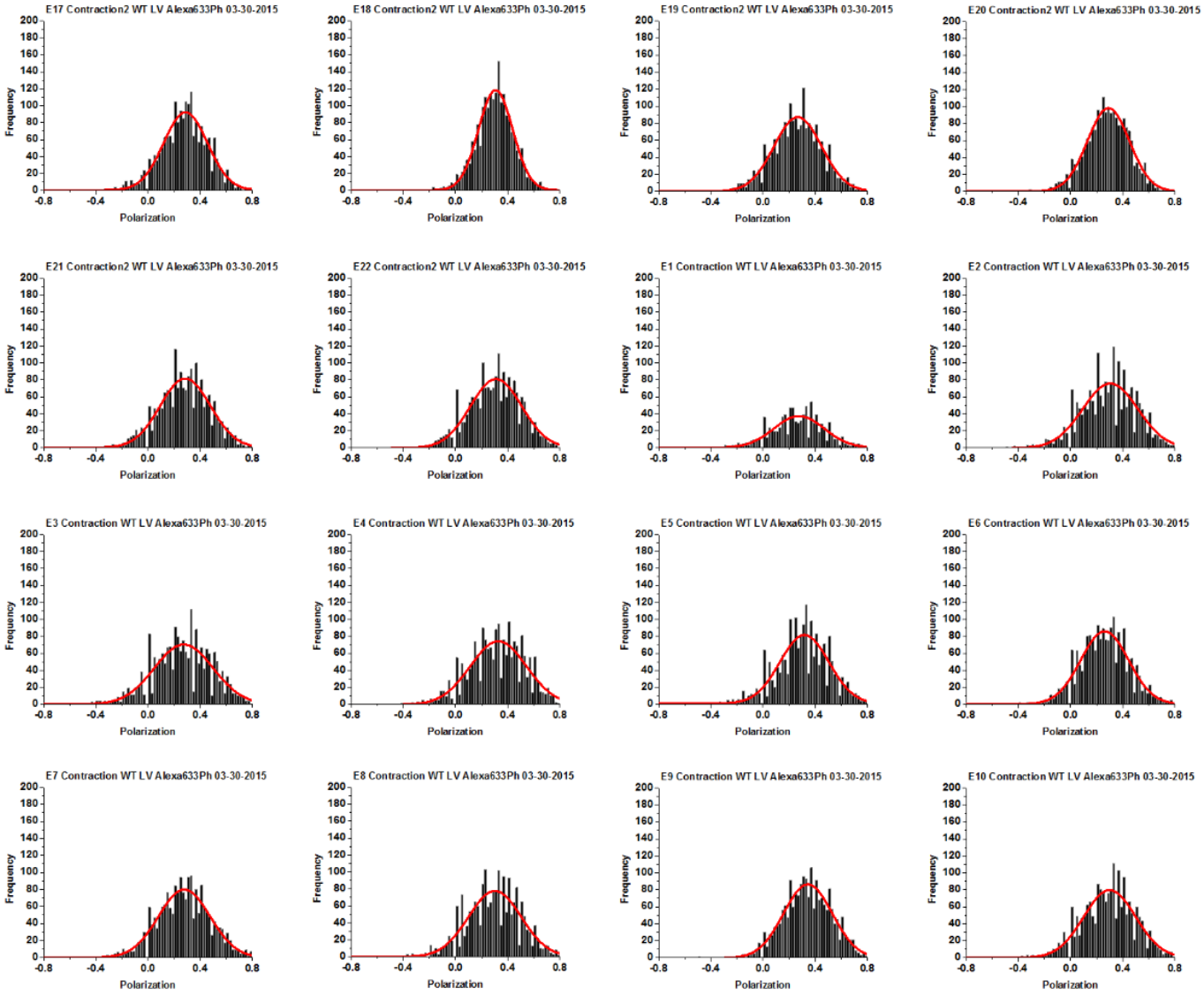

Figure S5b: All histograms of contracting myofibrils from the LV

Figure S5c

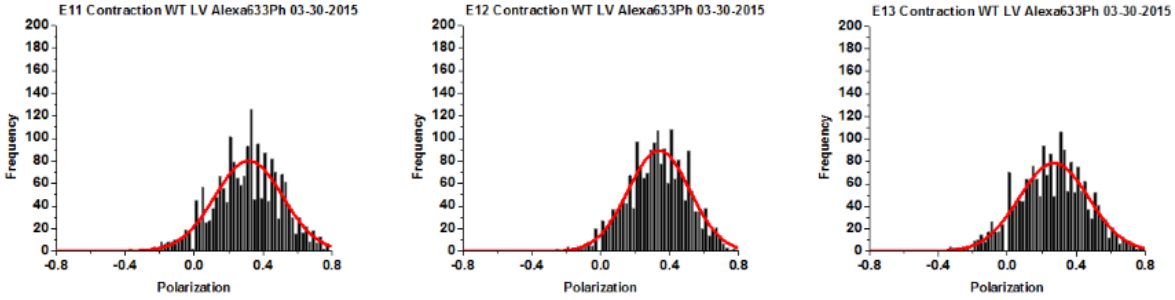

Figure S5c: cntd - all histograms of contracting myofibrils from the LV

Figure S6a

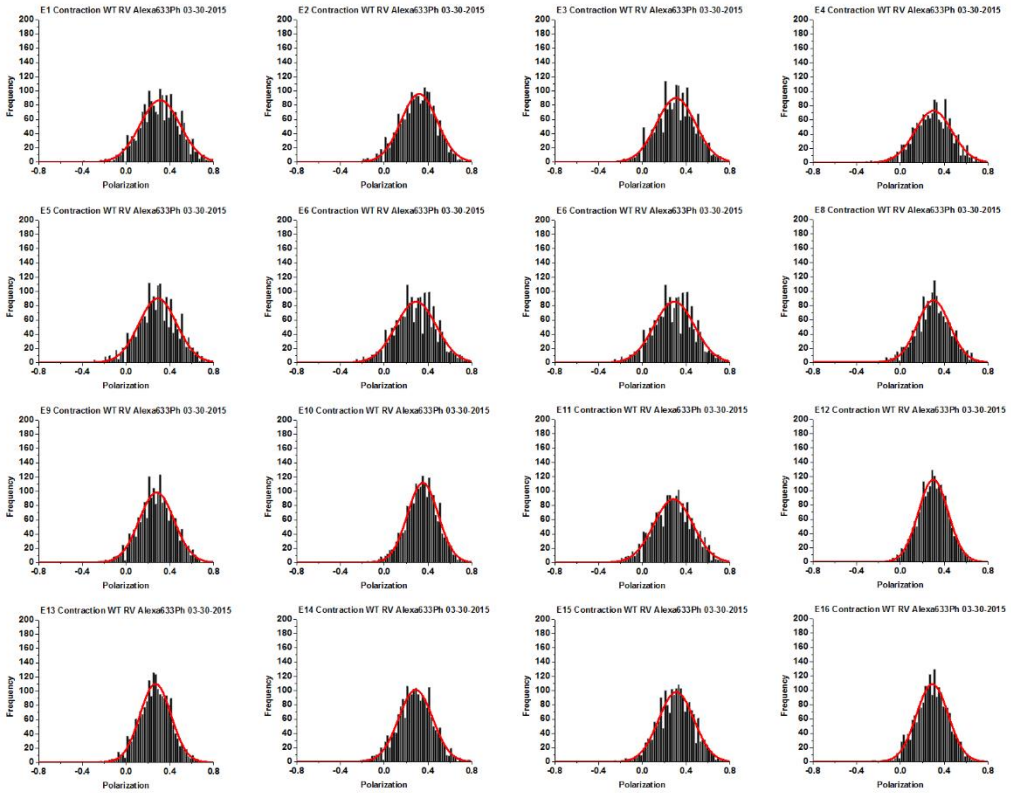

Figure S6a: All histograms of contracting myofibrils from the RV

Figure S6b

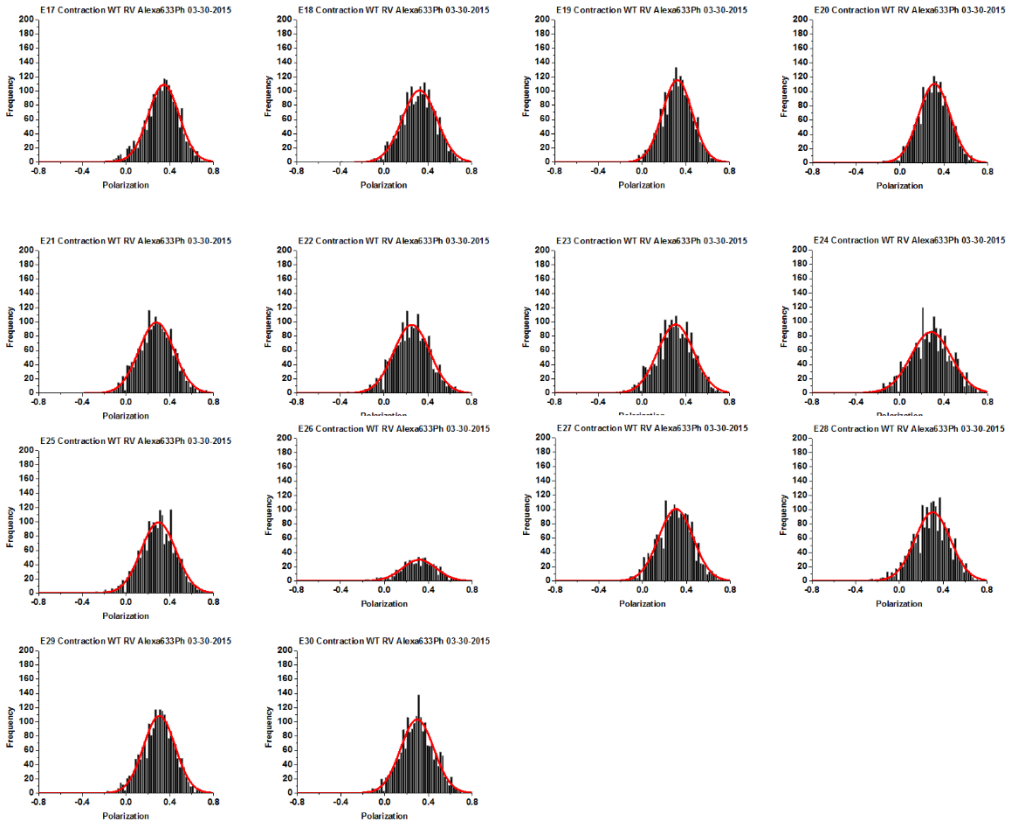

Figure S6b: All histograms of contracting myofibrils from the RV

7. REFERENCES

1. Galkin VE, Orlova A, Egelman EH (2012) Actin filaments as tension sensors. Curr Biol 22: R96-101.
2. Ando T (1989) Propagation of Acto-S-1 ATPase reaction-coupled conformational change in actin along the filament. J Biochem (Tokyo) 105: 818-822.
3. Ingber DE (2003) Mechanobiology and diseases of mechanotransduction. Ann Med 35: 564-577.
4. McGough A, Pope B, Chiu W, Weeds A (1997) Cofilin Changes the Twist of F-Actin: Implications for Actin Filament Dynamics and Cellular Function. J Cell Biol 138: 771-781.
5. Jimenez J, Tardiff JC (2011) Abnormal heart rate regulation in murine hearts with familial hypertrophic cardiomyopathy-related cardiac troponin T mutations. Am J Physiol Heart Circ Physiol 300: H627-635.
6. Duggal D, Nagwekar J, Rich R, Huang W, Midde K, et al. (2015) Effect of a Myosin Regulatory Light Chain mutation K104E on Actin-Myosin Interactions. Am J Physiol Heart Circ Physiol: ajpheart.00834.02014.
7. Wessels MW, Willems PJ (2008) Mutations in sarcomeric protein genes not only lead to cardiomyopathy but also to congenital cardiovascular malformations. Clin Genet 74: 16-19.
8. Matsson H, Eason J, Bookwalter CS, Klar J, Gustavsson P, et al. (2008) Alpha-cardiac actin mutations produce atrial septal defects. Hum Mol Genet 17: 256-265.
9. Wikman-Coffelt J, Fenner C, Smith A, Mason DT (1975) Comparative analyses of the kinetics and subunits of myosins from canine skeletal muscle and cardiac tissue. J Biol Chem 250: 1257-1262.
10. Borchert B, Tripathi S, Francino A, Navarro-Lopez F, Kraft T (2010) The left and right ventricle of a patient with a R723G mutation of the beta-myosin heavy chain and severe hypertrophic cardiomyopathy show no differences in the expression of myosin mRNA. Cardiol J 17: 518-522.
11. McMahon WS, Mukherjee R, Gillette PC, Crawford FA, Spinale FG (1996) Right and left ventricular geometry and myocyte contractile processes with dilated cardiomyopathy: myocyte growth and beta-adrenergic responsiveness. Cardiovasc Res 31: 314-323.
12. Belin RJ, Sumandea MP, Sievert GA, Harvey LA, Geenen DL, et al. (2011) Interventricular differences in myofilament function in experimental congestive heart failure. Pflugers Arch 462: 795-809.
13. Krug H, Punkt K, Bittorf L (1987) The higher myosin ATPase activity in the right heart ventricle of the rat, proved by histophotometry. Acta Histochem 82: 115-119.
14. Brooks WW, Bing OH, Blaustein AS, Allen PD (1987) Comparison of contractile state and myosin isozymes of rat right and left ventricular myocardium. J Mol Cell Cardiol 19: 433-440.
15. Carlsson M, Heiberg E, Toger J, Arheden H (2012) Quantification of left and right ventricular kinetic energy using four-dimensional intracardiac magnetic resonance imaging flow measurements. Am J Physiol Heart Circ Physiol 302: H893-900.
16. Itoya M, Mallet RT, Gao ZP, Williams AG, Jr., Downey HF (1996) Stability of high-energy phosphates in right ventricle: myocardial energetics during right coronary hypotension. Am J Physiol 271: H320-328.
17. Cadete VJ, Lin HB, Sawicka J, Wozniak M, Sawicki G (2012) Proteomic analysis of right and left cardiac ventricles under aerobic conditions and after ischemia/reperfusion. Proteomics 12: 2366-2377.
18. Samarel AM (1989) Regional differences in the in vivo synthesis and degradation of myosin subunits in rabbit ventricular myocardium. Circ Res 64: 193-202.
19. Schwarz K, Singh S, Dawson D, Frenneaux MP (2013) Right ventricular function in left ventricular disease: pathophysiology and implications. Heart Lung Circ 22: 507-511.

20. Austin EH, 3rd (2007) The ventricular myocardial band of Torrent-Guasp - the controversy: an editorial. Semin Thorac Cardiovasc Surg Pediatr Card Surg Annu: 87-88.
21. Sallin EA (1969) Fiber orientation and ejection fraction in the human left ventricle. Biophys J 9: 954-964.
22. Minton AP (1981) Excluded volume as a determinant of macromolecular structure and reactivity. Biopolymers 20: 2093-2120.
23. Minton AP (1998) Molecular crowding: analysis of effects of high concentrations of inert cosolutes on biochemical equilibria and rates in terms of volume exclusion. Methods Enzymol 295: 127-149.
24. Minton AP (2001) The influence of macromolecular crowding and macromolecular confinement on biochemical reactions in physiological media. J Biol Chem 276: 10577-10580.
25. Herrmann C, Lionne C, Travers F, Barman T (1994) Correlation of ActoS1, myofibrillar, and muscle fiber ATPases. Biochemistry 33: 4148-4154.
26. Tsaturyan AK, Bershitsky SY, Burns R, Ferenczi MA (1999) Structural changes in the actin-myosin cross-bridges associated with force generation induced by temperature jump in permeabilized frog muscle fibers. Biophys J 77: 354-372.
27. Bershitsky SY, Tsaturyan AK, Bershitskaya ON, Mashanov GI, Brown P, et al. (1997) Muscle force is generated by myosin heads stereospecifically attached to actin. Nature 388: 186-190.
28. Barman T, Brune M, Lionne C, Piroddi N, Poggesi C, et al. (1998) ATPase and shortening rates in frog fast skeletal myofibrils by time-resolved measurements of protein-bound and free Pi. Biophys J 74: 3120-3130.
29. Magde D, Elson EL, Webb WW (1974) Fluorescence correlation spectroscopy. II. An experimental realization. Biopolymers 13: 29-61.
30. Elson EL (1985) Fluorescence correlataion spectroscopy and photobleaching recovery. Annu Rev Phys Chem 36: 379-406.
31. Elson EL (2007) Introduction to FCS; Gryczynski Z, editor. Fort Worth: UNT. 1-10 p.
32. Huxley AF, Simmons RM (1971) Proposed mechanism of force generation in striated muscle. Nature 233: 533-538.
33. Buschmann V, Kramer B, Koberlink (2009) Quantitive FCS: Determination of confocal volume by FCS and bead scabnning with Micro Time 200. PicoQuant, Application note Quantitative FCS v 11.
34. Ao X, Lehrer SS (1995) Phalloidin unzips nebulin from thin filaments in skeletal myofibrils. J Cell Sci 108: 3397-3403.
35. Nagwekar J, Duggal D, Rich R, Raut S, Fudala R, et al. (2014) Spatial Distribution of Actin and Mechanical Cycle of Myosin are Different in Right and Left Ventricles of Healthy Mouse Hearts. Biochemistry, in press (Editors Choice). Biochemistry in press (Editors Choice).
36. Dos Remedios CG, Millikan RG, Morales MF (1972) Polarization of tryptophan fluorescence from single striated muscle fibers. A molecular probe of contractile state. J Gen Physiol 59: 103-120.
37. Nihei T, Mendelson, R.A., & Botts, J. (1974) Use of fluorescence polarization to observe changes in attitude of S1 moieties in muscle fibers. Biophys J 14 236-242.
38. Tregear RT, Mendelson RA (1975) Polarization from a helix of fluorophores and its relation to that obtained from muscle. Biophys J 15: 455-467.
39. Morales MF (1984) Calculation of the polarized fluorescence from a labeled muscle fiber. Proc Nat Acad Sci USA 81: 145-149.
40. Sabido-David C, Brandmeier B, Craik JS, Corrie JE, Trentham DR, et al. (1998) Steady-state fluorescence polarization studies of the orientation of myosin regulatory light chains in single

skeletal muscle fibers using pure isomers of iodoacetamidotetramethylrhodamine. Biophys J 74: 3083-3092.
41. Hopkins SC, Sabido-David C, Corrie JE, Irving M, Goldman YE (1998) Fluorescence polarization transients from rhodamine isomers on the myosin regulatory light chain in skeletal muscle fibers. Biophys J 74: 3093-3110.
42. Hopkins SC, Sabido-David C, van der Heide UA, Ferguson RE, Brandmeier BD, et al. (2002) Orientation changes of the myosin light chain domain during filament sliding in active and rigor muscle. J Mol Biol 318: 1275-1291.
43. Borejdo J, Midde K (2012) Mesoscopic Analysis of Motion and Conformation of Cross-Bridges. In: Garnier J, editor. Biophysical Reviews.
44. Cooke R, Crowder MS, Thomas DD (1982) Orientation of spin labels attached to cross-bridges in contracting muscle fibres. Nature 300: 776-778.
45. Borejdo J, Assulin O, Ando T, Putnam S (1982) Cross-bridge orientation in skeletal muscle measured by linear dichroism of an extrinsic chromophore. J Mol Biol 158: 391-414.
46. Bagshaw CR (1982) "Muscle Contraction". Chapman & Hall, London.
47. Ling N, Shrimpton C, Sleep J, Kendrick-Jones J, Irving M (1996) Fluorescent probes of the orientation of myosin regulatory light chains in relaxed, rigor, and contracting muscle. Biophys J 70: 1836-1846.

CHAPTER VI

DIFFERENCES IN THE KINETICS AND SPATIAL DISTRIBUTION OF ACTIN IN THE LEFT AND RIGHT VENTRICLES OF HUMAN HEARTS

J. Nagwekar[1], D. Duggal[1], S. Raut[2], R. Rich[3], H. Das[4], I. Gryczynski[1], R. Fudala[1], Z. Gryczynski[2], J. Borejdo[1]*

[1] Dept of Cell Biology and Center for Commercialization of Fluorescence Technologies, University of North Texas, Health Science Center, 3500 Camp Bowie Blvd, Fort Worth, TX 76107

[2] Dept of Physics and Astronomy, Texas Christian University, 2800 S. University Dr., Fort Worth, Texas 76129

[3] Dept of Mathematics and Physics, Texas Wesleyan University, Fort Worth 76105

[4] Center for Neuroscience Discovery, Institute for Health Aging and Institute of Cancer Research, UNT Health Science Center

*Running title: Differences between Orientation of Cross-Bridges in Human Right and Left Ventricles

*To whom correspondence should be addressed: Julian Borejdo, Department of Cell Biology, University of North Texas Health Science Center, 3500 Camp Bowie Blvd, Fort Worth, TX 76107, USA, Tel.: (817) 7352106, Fax: (817) 735-2118; E-mail: Julian.Borejdo@unthsc.edu

1. ABSTRACT

The left and right ventricles (LV, RV) are morphologically and physiologically different because they are play vastly different roles in the human circulatory system: the RV pumps blood into the pulmonary system and LV into the systemic systems, both of which offer different resistances to contracting ventricles. It is therefore not surprising that large differences are seen when ventricles are examined on a macroscopic level. This does not mean, however, that the ventricles are different on a molecular level, i.e. that the contractile proteins that are responsible for the ventricular contraction are different in the LV and RV. If this is true it should be possible to develop drugs affecting only one, not both, ventricles. Such drugs are currently not available, and would be of clinical importance because there exist a number of heart diseases caused by dysfunction of one ventricle only. For example, pulmonary hypertension is mainly due to RV dysfunction. Systolic or diastolic heart failure is mainly due to LV dysfunction. Because of these macroscopic differences, experiments can't be carried out on the whole organs. Moreover, the whole ventricles (or papillary muscles) contain a large number of contractile molecules (10^{11}-10^{13}). Measurements which originate from such a large assembly yield the average values and all the kinetic information about molecular action is absent from macroscopic data. Similarly, all the details of the steady-state measurements are lost. Therefore, the experiments need to be carried out on a few molecules of contractile proteins: we observed the A-band of a sarcomere - a volume where a force producing interaction between actin and myosin molecules takes place. We measured kinetics and distribution of ~16 actin molecules of isometrically contracting A-bands. Experiments were done *ex-vivo* – in the A-bands of myofibrils isolated from human non-failing and failing ventricles. We show that the kinetics and the steady-state distribution of actin were different in contracting left and right ventricle of the non-failing human heart. In contrast, these parameters obtained from failing hearts were the same. These results suggest that there exists genuine differences in the way actin interacts with myosin cross-bridges in both ventricles of non-failing hearts, and suggests how the absence of such differences in failing ventricles can be offset.

Keywords: Cross-bridge orientation, heart ventricles, fluorescence polarization

2. INTRODUCTION

We are interested in the question of whether the ventricular contractile proteins are different in the left (LV) and right (RV) ventricle. If differences emerge, it should be possible to develop drugs affecting only one, not both, ventricles. Such drugs would be of clinical importance because there exist number of heart diseases caused by dysfunction of one ventricle only, e.g. pulmonary hypertension is mainly due to the RV dysfunction, and systolic and diastolic heart failure is mainly due to the LV dysfunction.

The question of differences is impossible to answer by making macroscopic measurements (such as tension or ATPase activity) because systemic and pulmonary systems offer different resistances to contracting left and right ventricles resulting in gross morphological and physiological differences between ventricles. Therefore, significant macroscopic differences between ventricles are expected to be observed. Indeed, a non-failing RVs of rat hearts have higher myosin ATPase activity than the LV [1]. Papillary RV muscles have differences in the α-heavy chain composition and contract more rapidly at light loads than those from the LV [2]. Differences in energy usage were observed in healthy LVs and RVs [3, 4]. There were differences in the amounts of proteins like ATP synthase, Heat Shock Protein (HSP), Myosin Binding Protein C (MBPC) and MLC2 [5]. Fractional synthesis and degradation of myosin heavy chains and light chains [6] were seen. Finally, differences between ventricles were observed in the contractile performance in hearts affected by dilated cardiomyopathy [7] and congestive heart failure [8] and in ventricular development.

In view of the above, in order to detect molecular differences, the experiments cannot be performed on the whole ventricles or papillary muscles. Moreover, whole organs contain huge number of contractile molecules (10^{11}-10^{13}). Measurements originated from such a large assembly yield average values, and all the kinetic information about molecular action is absent [9, 10]. Similarly, all the details of the steady-state measurements are lost: if a large number of molecules are examined, each having its own mean and standard deviation, the final distribution of measurements will be a perfect Gaussian, irrespective of the data points being taken from the left or right ventricular myofibril. Subtle changes may be missed no matter from which ventricle a sample is taken. Indeed, macroscopic anisotropy experiments (Supplementary Fig. S1) reveal that it is impossible to detect subtle differences between data obtained from many molecules.

PRINCIPLE OF UNDERLYING MEASUREMENTS

To avoid problems associated with a large number of molecules in a ventricle, we carried out experiments on the A-band of contracting sarcomere of *ex-vivo* myofibrils isolated from human ventricles. The A-band is where the force-producing interactions between actin and myosin take place. Carrying out experiments on isolated myofibrils *ex-vivo* allows direct access to the A-band. Moreover, it avoids the problems associated with the fact that isolated motor molecules *in-vitro* cannot be viewed as independent motors [11]. Fig. 1 explains how this is done: myofibrils in myocytes are oriented every-which way (A) and are not suitable for angular measurements such as are done here. Measurements must be carried out on myofibrils that are perfectly oriented vertically (B). Single myofibril is selected, oriented strictly vertically on a microscope stage and the laser light of a confocal microscope is focused on a sarcomere. The microscope sees only a femtoliter volume, called Observational Volume (OV), embedded in the A-band of a sarcomere (B). In a typical A-band there are still ~10^4 actin molecules, which is too large a number to measure kinetics or distribution. To reduce this number, every 1000^{th} actin monomer in a thin filament is labeled with a

fluorescent phalloidin (C). Actin is labeled with a long-wavelength fluorescent probe (Alexa633-phalloidin) to minimize autofluorescence [12]. The remaining 999 monomers are labeled with non-fluorescent phalloidin which reduces the number of observed fluorescent actins to ~16.

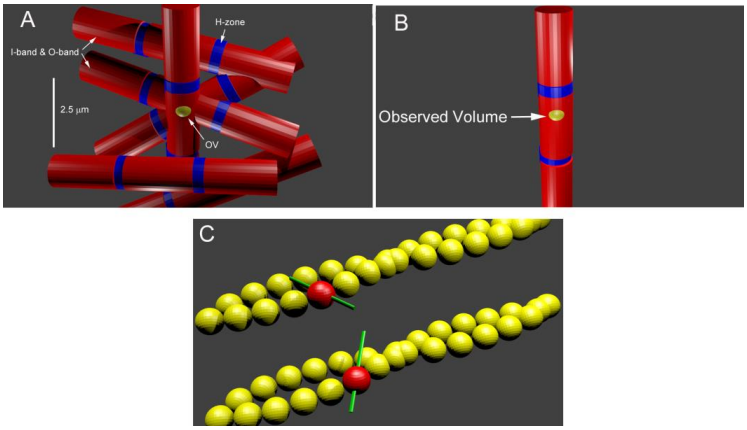

Figure 1. ***Diagram explaining why it is essential to carry out measurements on isolated myofibrils of a heart. A****: A laser beam is focused to a diffraction limit on a myocyte. A myocyte contains hundreds of myofibrils arranged every which way; actin is labeled with fluorescent dye (red) leaving only the H-zones to be non-fluorescent (blue);* ***B****: Fluorescence is collected from the Observational Volume (OV) of a confocal microscope (yellow ellipsoid) which is positioned at the A-band of contracting sarcomere. OV is ~0.5 µm in diameter. Myofibril is perfectly vertically aligned. Myofibril contracts (i.e. develops normal force), but does not move or change shape (shorten, swell or become dehydrated) because it is cross-linked;* ***C****: The OV contains only a few fluorescent actin molecules because only one in thousand actin monomers are labeled with a fluorophore (red). The transition dipoles of the fluorophores labeling actin are represented by green rods Actin containing non-fluorescent phalloidin is yellow. The schematic diagram of the instrument is shown in the Supplementary* ***Fig. S2****.*

As a result of the ATP-induced interaction of myosin cross-bridges with thin filaments, a momentum is transferred from myosin to actin, which brings on actin rotation [13, 14] [15, 16]. As a consequence, the transition dipole of Alexa633-phalloidin bound tightly to actin monomer changes orientation. We show that the kinetics describing interaction of thin filaments with myosin heads were different in contracting left and right ventricles of non-failing human heart. The same was true for the mean distribution of orientations of actin. In contrast, these parameters were the same in failing hearts (before heart transplant). Our results suggest that on the molecular level there exist genuine differences between the LV and RV in the way actin and myosin molecules interact with each other.

3. CHEMICALS AND METHODS

3.1. Chemicals and solutions

Alexa633 phalloidin (AP) and unlabeled phalloidin (UP) were from Molecular Probes (Eugene, OR). All other chemicals were from Sigma-Aldrich (St Louis, MO). Ca-rigor solution contained 50 mM KCl, 10 mM Tris-HCl pH 7.5, 2 mM $MgCl_2$, 0.1 mM $CaCl_2$. Contracting solution contained in addition 5 mM ATP, 20 mM creatine phosphate and 10 units/ml of 1 mg/ml creatine kinase. Glycerinating solution contained 50 mM KCl, 10 mM Tris-HCl pH7.5, 5 mM $MgCl_2$, 2 mM EGTA, 5 mM ATP, 20 mM creatine phosphate and 10 units/ml of 1 mg/ml creatine kinase.

3.2. Preparation of ventricles

Non-failing hearts were obtained through Kentucky Organization of Donor Associates (KODA). Failing hearts were obtained from patients about to undergo a heart transplant. Left and right ventricles were sent from the University of Kentucky to UNTHSC on dry ice. Immediately upon arrival they were tied to wooden sticks (in a cold room) and placed for 24 hrs in glycerinating solution at 0^oC. After 24 hrs, the glycerinating solution was replaced with a fresh solution and placed at -20^oC. Myofibrils (MF) were made from ventricles which had spent at least 2 weeks in glycerinating solution and were used within 2 days.

3.3. Preparation of myofibrils

Human ventricles were washed 3 times for 30 min each with ice-cold EDTA-rigor solution (50 mM KCl, 10 mM Tris-HCl pH 7.5, 5 mM EDTA), in order to wash out ATP present in the glycerinating solution without causing contraction. They were then washed thoroughly with Ca-rigor solution and homogenized in the Cole-Palmer LabGen 125 homogenizer for 10 s followed by further 10 s homogenization after a cool down period of 30 s.

3.4. Actin labeling and measurements

1 mg/mL myofibrils at room temperature in an Eppendorf tube were incubated for 10 min with the labeling solution (100 nM AP+10 μM UP in Ca-rigor solution). They were then spun for 3 min, resuspended in Ca-rigor solution, a 50 μL drop was placed on an ethanol cleaned #1 coverslip and washed as described below. The coverslip was placed on a scanning stage of a PicoQuant MT 200 inverse time-resolved Single Molecule fluorescence microscope. They were allowed to adhere for 10 min before a final wash with Ca-rigor solution. Washing was done by placing drops of solution on one end of a coverslip and sucking out excess solution on the other side with the Whatman #1 filter paper. 10 μW laser beam at 635 nm modulated at 20 MHz was focused by an Olympus x100, NA=1.2 water immersion objective to the diffraction limit on A-band of a myofibril.

3.5. Cross-linking

Non-failing myofibrils contract rapidly when washed with contracting solution; failing myofibrils also contracted, albeit slowly (data not shown). Such shortening would make it impossible to collect data from a half-sarcomere for 20 s. Myofibrils must be prevented from any movement while preserving the ability to contract (develop force). To do so, 1 mg/ml myofibrils were incubated for 20 min at room temperature with 20 mM water-soluble cross-linker 1-ethyl-3-[3-(dimethylamino)-propyl]-carbodiimide (EDC) (3, 5, 21, 42). The reaction was stopped by adding 20 mM DTT. The pH of the solution remained unchanged at 7.5

throughout the time course of reaction. As a control we observed cross-linked myofibrils under a Nomarski microscope and noted that they did not shorten or become dehydrated during the experiment. We also confirmed that they retained full ATPase activity (3, 5, 21, 42).

3.6. Instrument

The data was collected on Pico-Quant MT 200 instrument coupled to Olympus IX 71 microscope. A single MF was illuminated with 10 μW laser beam at 635 nm modulated at 20 MHz focused to a diffraction limit on an A-band by an Olympus x100, NA=1.2 water immersion objective. The experimental apparatus, and its operation, is illustrated in **Fig. S2**. To ensure accuracy, the instrument was first calibrated to make sure that the parallel (∥) and perpendicular (⊥) channels received equal amounts of emitted light. Fluorescence of an anisotropic solution of a long fluorescence lifetime dye (rhodamine 700) was measured before each experiment. Long lifetime assures that polarization does not change following a short laser pulse, i.e. that fluorescence is fully polarized. Each experiment lasted 20 s during which the instrument collected 2,000,000 data points (every 10 μsec). To smooth the data, 2M points were placed in 2,000 10 msec long bins, each containing an average of 1000 data points. Each data point was a little different because actin changes orientation due to the momentum transfer (kicks) by myosin. Huxley at al. determined that a characteristic life-time of one fluctuation is on the order of milliseconds, so during 20 s the orientation will change X=20,000 times (25). The precision of measurement is therefore approximately $1/\sqrt{X} = 0.7\%$.

3.7. Time resolved anisotropy measurements

The measurements are performed on FT300 fluorescence lifetime spectrometer (PicoQuant GmbH, Germany). The excitation source was Fianium super-continuum white light source (Fianium Ltd, Whitelase SC400-4). White light was passed through a monochromator to get 635 nm light at 10MHz repetition rate. The emission was observed at 665 nm through a long pass 650 nm filter by fast microchannel photomultiplier tube. The resolution was kept at 4ps per channel, and the pulse width was less than 100ps. For measuring anisotropy decays, the fluorescence intensity decays were collected while orienting the emission polarizer in vertical and horizontal respective to the vertically oriented excitation polarizer. For measuring the fluorescence lifetime of the sample, the emission polarizer was kept at 54.7^0. The vertical (parallel) and horizontal (perpendicular) intensity decays were used to calculate the time dependent anisotropy using the equation:

$$r(t) = \frac{I_{Parallel}(t) - I_{Perpandicular}(t)}{I_{Parallel}(t) + 2I_{Perpandicular}(t)}$$

The obtained anisotropy decay was analyzed using Fluofit 4.0 program provided by PicoQuant and was fitted using formula:

$$r(t) = \sum R_i \, e^{-t/\phi_i}$$

Where, r is the total anisotropy, Ri is the fractional anisotropy amplitude associated with component, φi is the rotation correlation time and t is the time in nanoseconds.

3.8. Statistical analysis

Comparisons between groups were performed using an unpaired Student's t-test (OriginLab Corporation, Northampton, MA). The differences were deemed significant when $P<0.05$. Origin 8.5 was also used to compute histograms and autocorrelation functions.

4. RESULTS

4.1. Principle of measurement

We are concerned only with the contracting ventricles. The experimental procedure involved observing a single myofibril oriented vertically (in the lab reference plane). **Fig. 3** shows a typical fluorescent lifetime image of a human labeled myofibril of the RV. The red circle represents the Observational Volume of the microscope, i.e. the projection of a confocal pinhole on the image plane. Its diameter (0.5μm) is equal to the diameter of the confocal pinhole (50 μm) divided by the magnification of the objective (100x). The data was collected only from the part of a myofibril which was strictly vertical; e.g. it was not collected from a part of a myofibril pointed to by the white arrow.

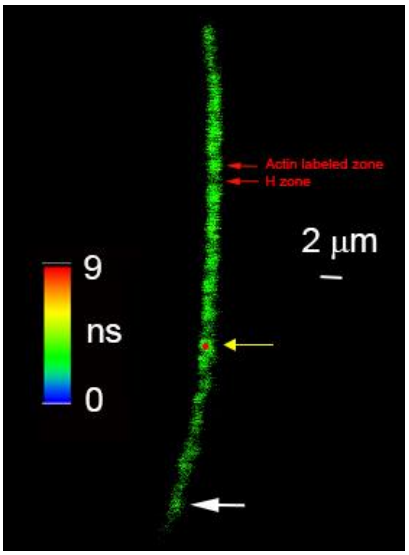

Fig. 2. *Fluorescent lifetime image of a myofibril from a non-failing human RV in rigor. The color bar indicates lifetime (in nanoseconds) of a given pixel. The horizontal bar is 2 μm. The actin labeled zone extends on both sides of the Z-line and includes two I-bands and an A-band. It is ~2 μm long. Typically, the data was collected from 3-4 confocal volumes.*

Number of observed actin molecules. To determine this number it is necessary to measure fluorescence intensity produced by a known number of molecules of Alexa633-phalloidin. This number was determined by Fluorescence Correlation Spectroscopy (FCS). The autocorrelation function of fluctuations of freely diffusing Alexa633-phalloidin molecules entering and leaving the OV at delay time 0 is equal to the inverse of the number of molecules contributing to the fluctuations N = 1/ACF(0) (18, 30). 15 nM Alexa-phalloidin was illuminated with 1-70 μW of laser power at 635 nm. A calibration curve was constructed by plotting the power of the laser vs. the rate of photon arrival per molecule of the dye. From this curve it was determined that the number of photons collected in a second from a single Alexa633-phalloidin molecule was ~400. At this power the average number of observed photons in a typical experiment (**Fig. 7B**) in a parallel channel $I_{\parallel}$ was 3,500± 600 per second. The average number of photons per sec in perpendicular channel $I_{\perp}$ was 1,500±400 (the average polarization of fluorescence was 0.4011± 0.135). The average total fluorescence intensity was $I_{\parallel} + 2*I_{\perp}$ = 6,500±1,000 counts/s. Therefore the average number of observed actin molecules was 6500/400=~16.

4.2. Kinetics of actin in contracting non-failing ventricles

The transition dipole of Alexa633 embedded in actin is not constant during contraction because actin receives periodic thrusts (momentum transfers) from myosin cross-bridges that drive it between two different configurations. We follow the orientation of this dipole by measuring steady-state anisotropy (SSA) of myofibrils. XBs (and therefore dipole moments) of large collection of myofibrils can be frozen in various physiological states by adding appropriate nucleotides. We measured SSA of Alexa633 phalloidin bound to actin of the LV during the ATPase cycle (**Fig. 3**). At first the transition dipole of Alexa633 rotates like a free dye with the average steady-state anisotropy of 0.064 (**Fig. 5A).** Weak binding (simulated by addition of ADP) of actin to a ventricle increases anisotropy (decreases rotation) of the dye: the transition dipole of Alexa633 rotates with the average SSA of 0.228 (**Fig. 4B**). Next, the XB executes a power stroke precipitated by dissociation of ADP that is associated with force production (20, 24). After the power stroke, ATP rapidly replaces ADP which causes further increase of anisotropy (to 0.218, **Fig. 4C**). Transition to rigor causes anisotropy to decrease to the initial value (**Fig. 4D**). XB remains attached to thin filament but the drop of anisotropy occurs because phalloidin becomes not well immobilized by thin filaments (it is immobilized only in the presence of a nucleotides) or because the bond that connects Alexa633 to phalloidin becomes flexible in the absence of a nucleotide.

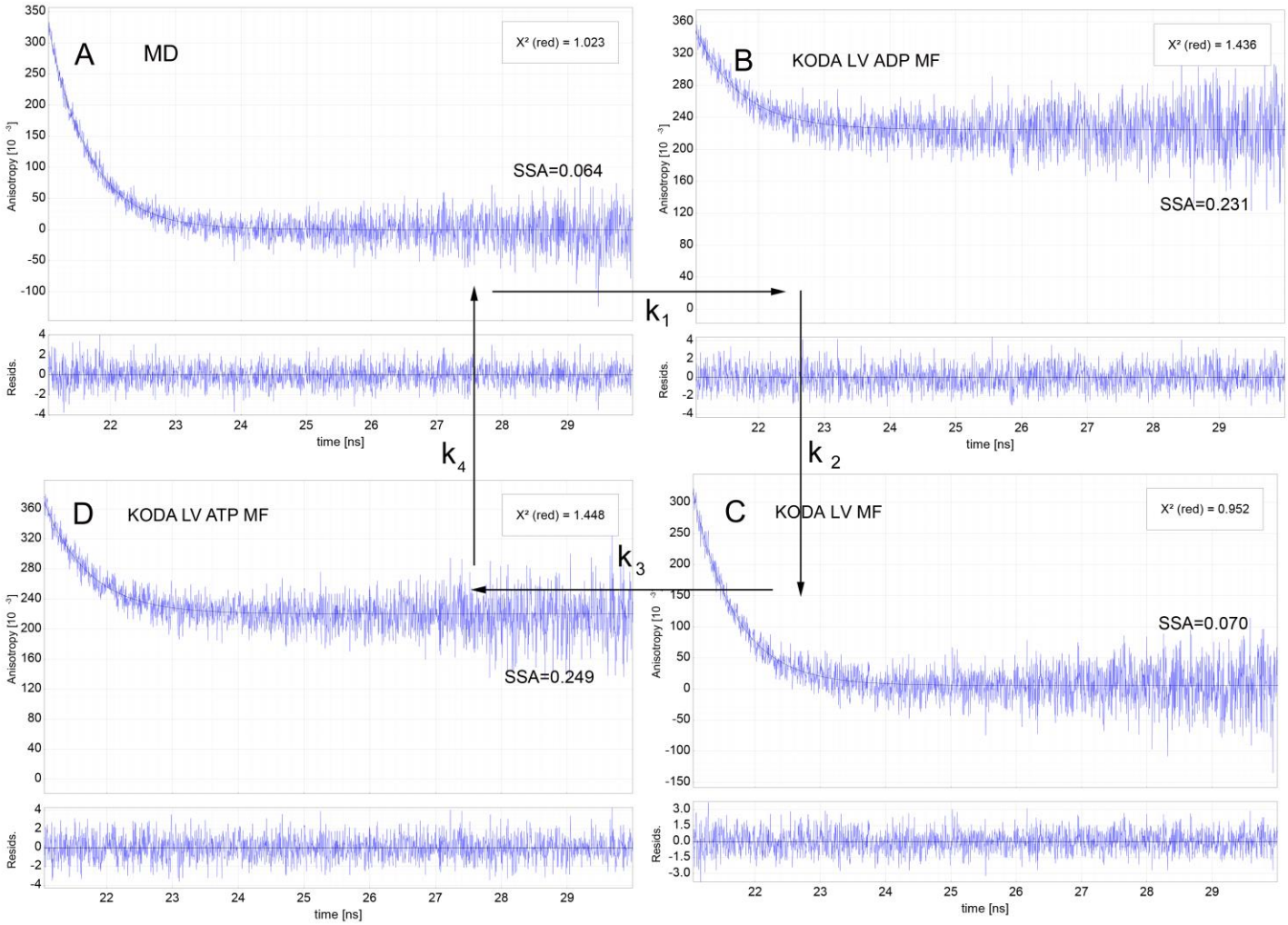

Fig. 3 *Anisotropy decay of contracting non-failing LV myofibrils labeled with Alexa633-phalloidin. Free dye has low anisotropy (**A**). It increases upon weak binding (**B**) and increases a little upon undergoing*

*power stroke (**C**). It decreases when ATP is removed (**D**).0.1 mg/mL myofibrils from the left ventricle, 2 mM MgADP, 5 mM MgATP. Excitation at 635 nm by laser. The emission observed at 665 nm through long pass 650 nm filter by a fast microchannel photomultiplier tube. Changes of steady-state anisotropy of Alexa633 bound to actin of the RV are similar (not shown).*

In the interest of simplicity we ignore small changes between the Myosin (M), M+ATP (MT) and M+ADP (MD), and between anisotropy in the presence of nucleotides. The anisotropy fluctuates between the average values of a_1= 0.240 for the period of time t_1, and a_2= 0.067 for a period of time t_2. Changes of steady-state anisotropy suggest the following acto-myosin mechanochemical cycle: Myosin containing ADP (MD) binds to actin with a rate k_1 to form high fluorescence state AMD*. This binding is very rapid and cannot be visualized in our experiments because time resolution of the apparatus is 10 msec. AMD* is a weakly bound pre-power stroke state which does not generate tension. It lasts for a time period t_{PRE} and transforms with a rate k_{PRE} to a strongly bound tension generating post-power stroke state AM which lasts for a time t_{POST}. AM relaxes with a rate k_{POST} to a dissociated short-lived state AMT*. Myosin hydrolyzes ATP to ADP with a rate k_4. Neither MT nor MD states can be visualized in our experiments because they have the same anisotropy. **Fig. 5** is a schematic representation of these changes.

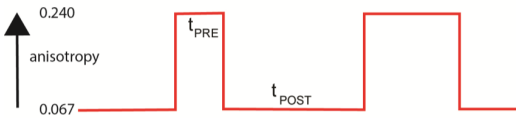

Fig. 4. *Schematic representation of anisotropy change and associated rate constants.*

The experiment follows the time course of changes in polarization of fluorescence (PF) - a quantity that is closely related to steady-state anisotropy. We chose to measure polarization of fluorescence rather than anisotropy because it has been used reliably for many years to measure conformation of the transition dipole of the fluorophore (13, 22, 23, 34, 36, 37, 41). (The anisotropy, r, is related to PF by r=2PF/(3-PF). A typical example of the fluorescence signal is shown in **Fig. 5**.

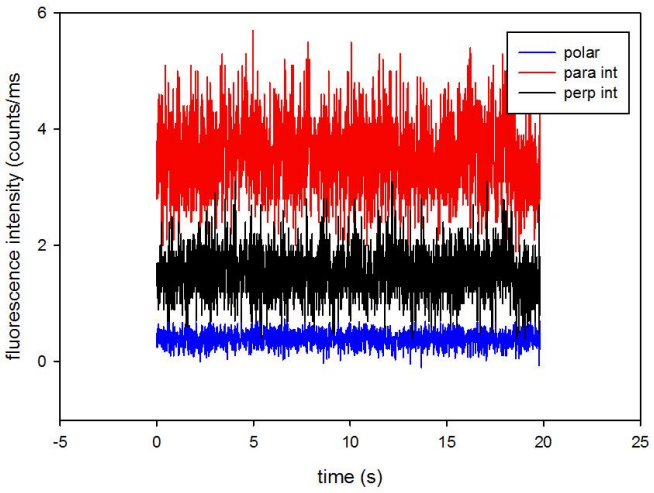

Fig. 5. *The time course of evolution of intensities of fluorescent light of Alexa633 imbedded in ventricular actin. The intensity of fluorescent light polarized parallel to myofibrillar axis is in red. The intensity of fluorescent light polarized perpendicular to myofibrillar axis is in black. From the orthogonal intensities we calculate polarization of fluorescence (PF, blue). It is the normalized ratio of the difference between ∥ and ⊥ components of the fluorescent light emitted by the dye). Contraction of the myofibril from non-failing ventricle.*

To obtain the rates of the transitions, a method first introduced by Magde and Elson (14, 16, 30), is applied to the polarization data such as shown in **Fig. 5** (blue).

Autocorrelation function (ACF) of polarization of fluorescence PF is calculated by taking an average of the sum of products of instantaneous values of PF and values of PF delayed by an increasing delay time □. The time evolution of the two-state process can be described by a theoretical expression given by eq. 1. (derived in (33)).

$$R_2(t) = \frac{(a_1k_2 + a_2k_1)^2}{(k_1 + k_2)^2} + k_1k_2\frac{(a_1 - a_2)^2}{(k_1 + k_2)^2}\exp(-(k_1 + k_2)t)$$

***Eq. 1**. Analytical form of ACF. Note $R_2(t)$=ACF, $k_1=k_{PRE}$, $k_2=k_{POST}$*

From the fit of this equation to the ACF obtained from experiments one obtains the rates of the two rate constants: k_{PRE} - the rate characterizing lifetime of the pre-power stroke state and k_{POST} - the rate characterizing lifetime of the post-power stroke state. One example of 33 measurements of ACF from non-failing RV's is shown in **Fig. 6**.

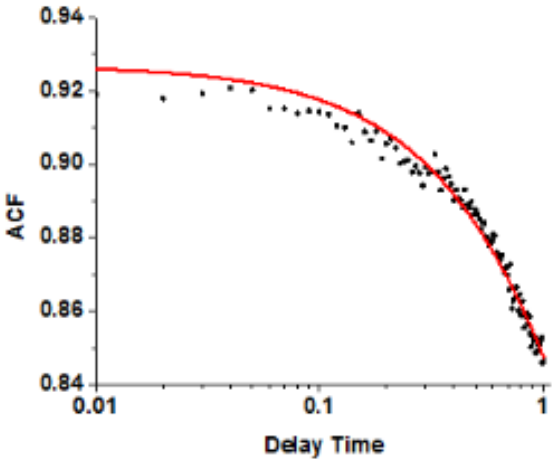

Fig. 6**. An example of a typical autocorrelation function of Alexa633 embedded in cardiac actin of contracting non-failing RV. The fact that the ACF is not flat confirms that the number of molecules contributing to the observed signal is small (mesoscopic): If the number was not small, the ACFs would have been a flat line. However, it should be emphasized that as long as the number of molecules is small, the exact number does not matter. Observing 16 or 80 molecules would have yielded the same result. The fact that the function is not decaying to zero is due to the fact that the background fluorescence is large. It is contributed by the autofluorescence and by the fact that molecules do not leave OV after conformational change (i.e. in contrast to translational diffusion where fluorescence fluctuates between 0 and maximum, here it fluctuates between minimum and maximum around non-zero mean.

We obtained data from 2 LVs and RVs of non-failing ventricles. (These are difficult to obtain because the patients have to die from causes other than heart problems and have to donate body to science). The data from one ventricle was rejected because the female patient was diabetic, which is known to cause, among other dysfunctions such as oxidative stress and increased glycosylation, LV dysfunction (12). All data from the remaining non-failing ventricle (33 & 32 experiments on RV and LV, respectively) are summarized in **Table 1**.

Contraction of ventricle of non-failing heart	k_{PRE}	k_{POST}
LV	1.84±0.75 } ★	0.20±0.10 } ★
RV	1.44±0.75	0.15±0.07

***Table 1**: The difference between LV and RV for k_{PRE} was statistically **significant** (t = 2.081, P=0.041) with 63 degrees of freedom. The difference between LV and RV for k_{POST} was statistically **significant** (t = 2.310, P=0.024) with 62 degrees of freedom. The errors are SD. The★ indicates that the difference is statistically significant.*

The rate k_{PRE} is the rate of power stroke. The reason it is so small in our experiments is that they were carried out under **isometric** conditions. This rate is high only in rapid release (25) or isotonic experiments.

4.3. Kinetics of actin in contracting failing ventricles

Failing ventricles also partially contracted and yielded tighter fit to theoretical autocorrelation functions. We obtained 6 failing ventricles (those are easier to obtain than non-failing ventricles because the patients survive and receive heart transplant). Data from one ventricle was rejected because patient suffered from non-compaction. One example of the 153 measurements of ACF from remaining 5 failing RV's is shown in **Fig. 7**.

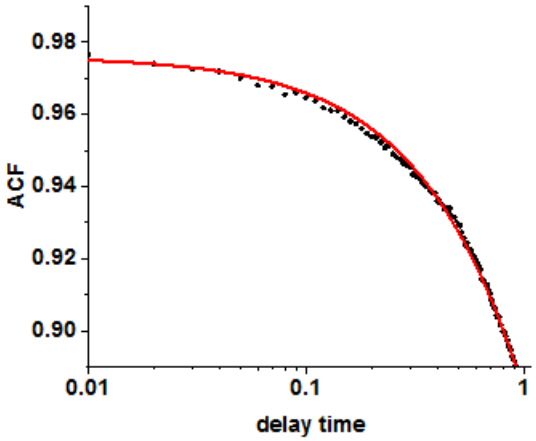

Fig. 7. An example of a typical autocorrelation function of Alexa633 embedded in cardiac actin of failing LV.

In general, fits to failing ventricles were better than to non- failing ones. Data from LV 668C5.

We analyzed by a 2-state model data from 5 LV and RV of failing ventricles. All data (153 and 148 experiments on RV and LV, respectively) from the failing ventricles are summarized in **Table 2** and shown individually in **Fig. 8**.

Contraction of ventricles of failing heart	k_{PRE}	k_{POST}
LV	0.98±0.54 } —	0.28±0.05 } —
RV	1.37±0.94 } —	0.13±0.26 } —

***Table 2**: The difference between LV and RV for the rate constant k_{PRE} was statistically **insignificant** (P=0.469, t=0.794) and 95 degrees of freedom. The difference between LV and RV for the rate constant k_{POST} was statistically **insignificant** (P=0.238, t=1.274) and 95 degrees of freedom. The errors are SD. The — indicates that the difference is not statistically insignificant.*

Muscle 117DD

LV		RV	
k_{PRE}	k_{POST}	k_{PRE}	k_{POST}
ND	ND	ND	ND

Fig. 8. *Summary of 2-state actin kinetics in contracting failing hearts. Kinetics of the ventricle 117DD was not determined (ND) because the ACF's could not be well fitted patient.* Not Statistically Significant, Statistically Significant

Muscle 43149

LV		RV	
k_{PRE}	k_{POST}	k_{PRE}	k_{POST}
0.40±0.20	0.06±0.07	0.63±0.34	0.06±0.04

Muscle 668C5

LV		RV	
k_{PRE}	k_{POST}	k_{PRE}	k_{POST}
0.80±0.46	0.07±0.02	1.92±1.11	0.14±0.07

Muscle 98868

LV		RV	
k_{PRE}	k_{POST}	k_{PRE}	k_{POST}
1.29±0.57	0.11±0.06	0.84±0.58	0.08±0.03

Muscle 74B28

LV		RV	
k_{PRE}	k_{POST}	k_{PRE}	k_{POST}
0.58±0.55	0.06±0.05	0.90±0.72	0.09±0.05

4.4. Spatial distribution of actin from contracting non-failing ventricles

The spatial distribution during muscle contraction of Alexa633 fluorophore bound to actin was Gaussian. A Gaussian curve is best characterized by a Full Width at Half Maximum (FWHM). Like Standard Deviation, FWHM indicates the width of the distribution of orientations of dipole moment of Alexa633. Examples of measurements of spatial distribution from 33 experiments of contracting LVs and 32 experiments of contracting RVs from healthy donor ventricles are represented in **Fig. 10**. The distributions are shown are the histograms – plots of frequency of occurrence of a given orientation (polarization of fluorescence).

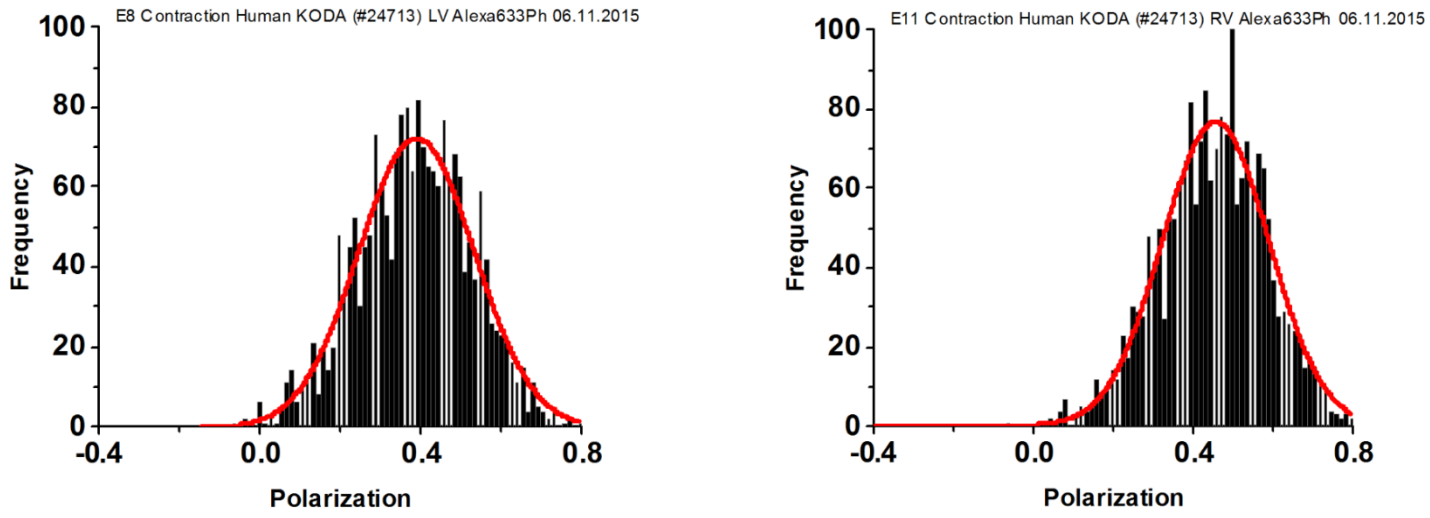

Fig. 9. *Left panel: An example of distribution of polarization values of Alexa633 in the A-bands of contracting LV sarcomere. The orientation of ~16 actin monomers in 33 different preparations of ventricles was measured 2000 times. Right panel: An example of a distribution of polarization values of Alexa633 in the A-bands of contracting RV sarcomere. The orientation of ~16 actin monomers in 32 different preparations of ventricles was measured 2000 times.*

Data from all experiments on LV and RV are summarized in **Table 3**. The distributions show significant differences in the value of mean FWHM. AR^2 values indicate how well the fitted curve (red) matches a perfect Gaussian (a perfect fit has AR^2 value of 1). The data shows that distributions of LVs differed more from a perfect Gaussian than RV.

Contraction of ventricle of non-failing heart	**FWHM**	**AR^2**
LV	0.339±0.027 } ★	0.906±0.043 } ★
RV	0.318±0.022	0.924±0.025

Table 3. *The distribution of Alexa633 dipole angles bound to actin in thin filaments during contraction of myofibrils from non-failing human heart. Errors are SD. AR^2measures goodness of fit (closer to 1 the better). Stars indicate statistically significant differences.*

The difference of -0.00945 in the mean value of polarization was statistically **significant** (t = -2.095, P=0.040) with 61 degrees of freedom. The 95 percent confidence interval for difference of means was from -0.018 to -0.00042. The difference of 0.0423 in the value of skewness was **significant** (t = 2.606, P=0.011) with 61 degrees of freedom. 95 percent confidence interval for difference of means was from 0.00983 to 0.0747. The difference of -0.0344 in the value of AR^2 was statistically significant (t = -3.718, P<0.001) with 61 degrees of freedom. The 95 percent confidence interval for difference of means was from -0.0529 to -0.0159.

4.5. Spatial distribution of actin from contracting failing ventricles.

In contrast to the distribution of actin in ventricles of contracting non-failing hearts, ventricles from failing hearts showed no differences in distribution. Examples of measurements of 148 experiments from LVs and 153 experiments from RVs are shown in **Fig. 10**.

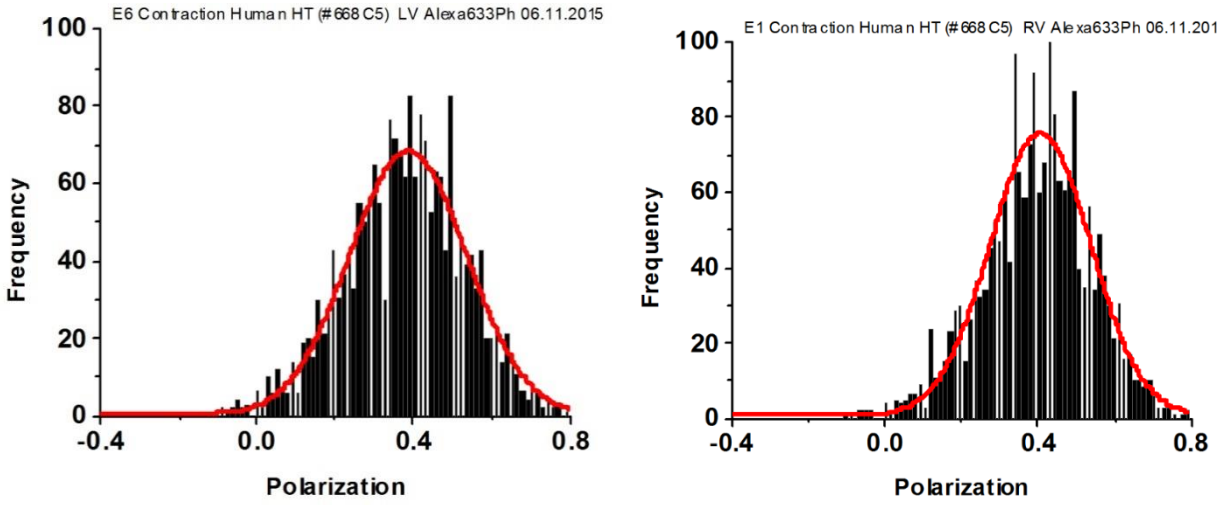

***Fig. 10**. Examples of distribution of polarization values of the A-bands of contracting LV (left panel) and RV (right panel) sarcomeres.*

All data is summarized in **Table 4** and shown in **Fig. 12**.

Contraction of ventricles of failing heart	FWHM	AR^2
LV	0.348±0.030	0.896±0.042
RV	0.356±0.035	0.888±0.082

Table 4. *The average values of distribution of Alexa633 dipole angles bound to actin in thin filaments during contraction of 148 LVs and 153 RVs myofibrils from failing human heart. Errors are SD. AR^2measures goodness of fit (closer to 1 the better). ▬ signs indicate statistically insignificant differences.*

The difference in the mean value of FWHM was statistically **insignificant** (t = 0.393, P=0.704) with 61 degrees of freedom. The difference in the mean value of polarization was statistically **insignificant** (t = 0.098, P=0.924) with 61 degrees of freedom. The difference in the value of skewness was **insignificant** (t = 0.446, P=0.667) with 61 degrees of freedom. The difference in the value of AR^2 was statistically **insignificant** (t = 0.388, P=0.707) with 61 degrees of freedom.

Muscle 117DD

FWHM	
LV	**RV**
0.369±0.103	**0.369±0.044**

***Fig. 11**. Summary of actin distribution in contracting failing hearts.* Not Statistically Significant, Statistically Significant

Muscle 43149

FWHM	
LV	RV
0.337±0.032	0.357±0.024

Muscle 668C5

FWHM	
LV	RV
0.356±0.027	0.351±0.025

Muscle A3CD2

FWHM	
LV	RV
0.345±0.031	0.369±0.056

Muscle 98868

FWHM	
LV	RV
0.355±0.033	0.355±0.028

Muscle 74B28

FWHM	
LV	RV
0.349±0.035	0.351±0.043

5. DISCUSSION

Kinetic and steady-state data summarized in **Tables 1-4** and brought together in **Tables 5 & 6** below to emphasize the main point of this paper: kinetics and steady-state orientation of actin differ significantly between the LV and RV in the non-failing heart, while they do not differ in the ventricles of the failing heart.

Contracting ventricles of non-failing and failing heart	k_{PRE}	k_{POST}
Non-failing LV	1.84±0.75 } ★	0.20±0.10 } ★
Non-failing RV	1.44±0.75	0.15±0.07
failing LV	0.98±0.54 } ▬	0.28±0.05 } ▬
failing RV	1.37±0.94	0.13±0.26

Table 5. *Difference in the mean rate constants between non-failing and failing ventricles. The errors are SD. The brackets and ★ indicate statistical significance of the difference with P<0.05. The brackets and ▬ indicate no statistical significance.*

Contracting ventricles of non-failing and failing heart	**FWHM**
Non-failing LV	0.339±0.027 } ★
Non-failing RV	0.318±0.022
Failing LV	0.351±0.010 } ▬
Failing RV	0.358±0.083

Table 6. *Difference in the steady state values between non-failing and failing ventricles. The errors are SD. The brackets and ★ indicate statistical significance of the difference with P<0.05. The brackets and ▬ indicate no statistical significance.*

Even though major macroscopic differences between ventricles can be seen in the non-failing heart, there have been no confirmed reports of composition or thin filament packing differences between actin molecules in the LV and the RV. Actin is expressed from the same genes (45) in both ventricles. We think that the observed difference between the non-failing LV and RV are due to the different mechanical requirements of the two ventricles. The hydrostatic pressures in the systemic circulation (systolic 120 mm Hg, diastolic 80 mm Hg,) are much higher than in the pulmonary circulation (systolic 25 mm Hg, diastolic 10 mm Hg). We think that we were able to reveal the differences because we worked on mesoscopic, not macroscopic, samples. We sampled only a few molecules of actin of contracting myofibrils *ex-vivo*. This avoided problems associated with differences in basic fiber structures and physiology between ventricles, and assured that it was possible to measure kinetic rates of conformational transitions and steady-state during contraction. Although representing contractile cycle by a simple PRE and POST power stroke process is an oversimplification, it allows us to get a glimpse of the kinetics that rule the interactions between actin and myosin *ex-vivo* and highlight the differences between the LV and the RV. Finally, since the data was collected under *ex-vivo* conditions, we were able to eliminate the effects of molecular crowding and packing of actin in thin filaments.

The changes in tension per cross-bridge and tension per ventricle brought about by changes in the rate constants and steady-state values are summarized in Table below:

k_{PRE}	Tension/filament	LV Tension	RV Tension
↑	↑	↑	?
↓	↓	↓	↓
k_{POST}	Tension/filament	LV Tension	RV Tension
↑	↓	↓	↓
↓	↑	↑	?
FWHM	↑	↑	↑
	↓	↓	↓

Table 7. *Changes in tension resulting from changes in the rate constants and FWHM..*

Since there was no difference in the failing ventricles, we discuss only the changes in non-failing LVs relative to non-failing RVs. t_{PRE} in LV is smaller than in RV. This causes the increase in tension in LV because pre-power stroke (non-tension generating) is short and tension generating state is populated faster. Since the number of cross-bridges in RVs is smaller, we are unable to deduce what changes this increase may cause in RV. k_{POST} is also larger in LV than in RV. This causes the tension/filament and ventricular tension to decrease because tension generating state is depleted faster. FWHM is larger in LV than RV. This causes the tension/filament and tension/ventricle to increase because XB has now more actin binding sites to interact with. Small FWHM in non-failing RV is suggests that pressure and wall thickness are smaller in RV than LV and that stress/area ratio experienced by actin filaments in RV maybe be larger. Thus the resulting compression of actin monomers may be greater in RV (it may, on occasion, be compensated for by ventricular enlargement - hypertrophy). Greater compression implies that the phalloidin carrying Alexa633 fluorophore is unable to vigorously respond to the thrust exerted by myosin, thus causing actin distribution during contraction of the non-failing RV to be narrower than the LV. Since our measurements were carried out on isolated myofibrils, they suggest the presence of fundamental differences in the function of muscles of both the ventricles.

Comparison between failing and non-failing hearts has a significant diagnostic value. One patient was very unusual – both rate constants and FWHM values were off-the-chart. This patient suffered from non-compaction (19), and was omitted from analysis. In spite of clinical differences of the remaining 5 patients (one had high Body/Mass Index , one had unusually low End Diastolic Volume and End Systolic Volume and that one had unusually low Ejection Fraction) , the comparison between non-failing and failing ventricles may be useful:

Contracting ventricles of non-failing and failing heart	k_{PRE}	k_{POST}
Non-failing LV	1.84±0.75 } ★	0.20±0.10 } ★
failing LV	0.98±0.54 }	0.28±0.05 }
Non-failing RV	1.44±0.75 } —	0.15±0.07 } —
failing RV	1.37±0.94 }	0.13±0.26 }

Table 8. *Differences in the mean rate constants between non-failing and failing ventricles. The errors are SD. The brackets and ★ indicate statistical significance with P<0.05 of the difference. The brackets and ~~and~~ indicate no statistical significance.*

k_{PRE} of non-failing LVs was larger in comparison with failing LVs. This leads to the increase in LV tension. k_{POST} of non-failing LV was smaller in comparison with failing LV. This also leads to the increase in LV tension. To offset these differences, drugs that increase tension in the LV of failing ventricle, such as omecamtiv mecarbil (31) should be applied to the LV of failing heart patients. This drug is known to bind between the nucleotide-binding pocket and the converter domain of the myosin head (40). The alternative is to modulate function of actin: there are hundreds of proteins that affect function of actin. To name just a few: tropomyosin-troponin regulatory system which is affected by allosteric interactions with a drug Tirasemtiv, being developed as a potential treatment for muscle weakness and wasting (39), WASP-Arp2/3 proteins cap the pointed end of actin and is able to cross-link actin into Y branches and can cause produce "actin-cages" modifying motion of certain pathogens (27), gelsolin that has a strong severing activity of F-actin by capping /uncapping the barbed ends (43), ADF/coffilin family changes twist of F-actin increase the POST rate of pointed end and thus has weak severing activity (49). In addition, there is a whole host of actin-interacting proteins which control Ca^{2+} concentration in the cell.

There were no differences in the width of actin distributions between non-failing and failing ventricles. Thus in contrast to the kinetic measurements, measuring the steady-state distribution of myosin has no value when diagnosing reasons for heart failure.

Observing a single molecule of actin would have been the ultimate experiment. If it were possible, the rate constants could have been determined directly, from traces such as shown in the top panel of Fig. 4. Observing a single actin molecule *in-vitro* is possible (46). However, observing a single molecule *ex-vivo* proved impossible because the background contains very strong autofluorescence (due to an extremely dense environment (2)) and a constant fluorescence coming from actin that are always present in the OV. Unlike the regular FCS, the actin molecule does not translate but remains fixed in the OV, so the fluorescent signal does not fluctuate between zero and maximum. The PF fluctuates around non-zero mean. A further complication is that the laser beam cannot be focused on the same spot for much more than 20 sec to avoid photobleaching. Observing16 molecules *ex-vivo*, rather than a single molecule, introduces complications that in order to derive rate constants the autocorrelation function has to be computed and analyzed.

It must be emphasized that there is significant advantage of labeling actin rather than myosin head. Labeling actin is gentle (it involves only irrigation of myofibrils with the protein at room temperature), in contrast with labeling of myosin, which involves labeling light chain 1 (LC1) and exchanging it with myofibrillar LC1 under harsh conditions (1/2 hr at 37^{o}C in the presence of trifluoroperazine) (1).

Our earlier results showed that the functional differences between ventricles are present in mice hearts (35). The present work extend this to the humans and suggests that the mechanism causing the differences is change in the way actin interacts with myosin to produce tension.

6. SUPPLEMENTARY DATA

Figure S1

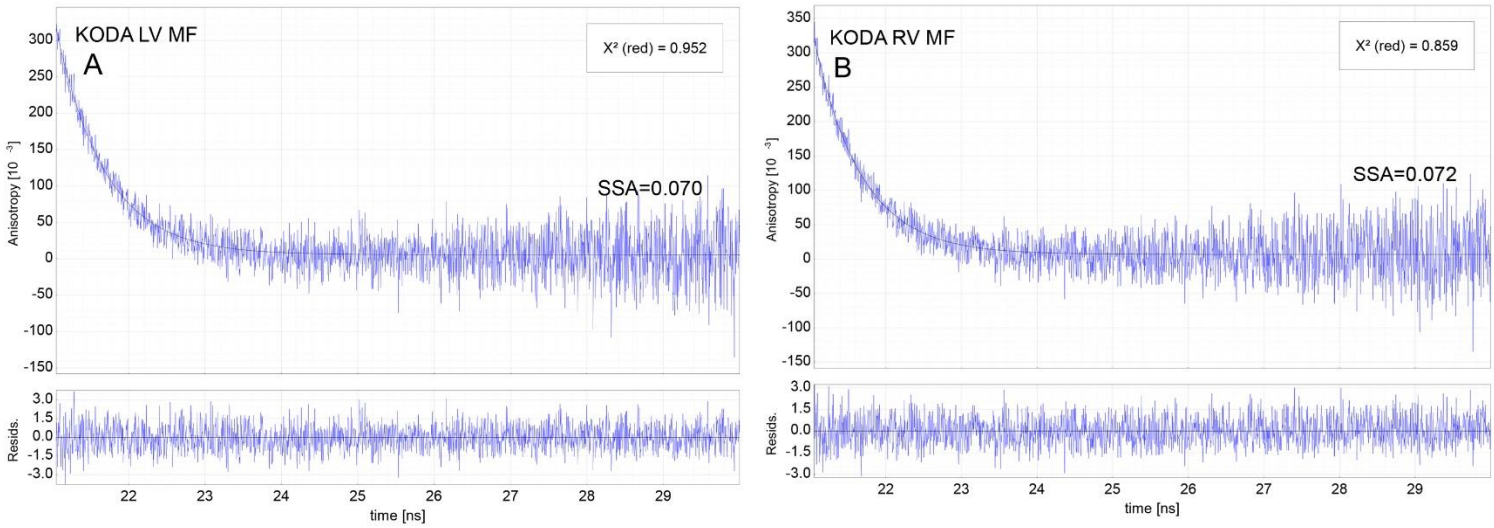

Figure S1. *There was no statistically significant differences between macroscopically measured anisotropies of non-failing LV and RV in rigor. It is true also in various physiological states. 0.1 uM ventricular myofibrils.*

Figure S2

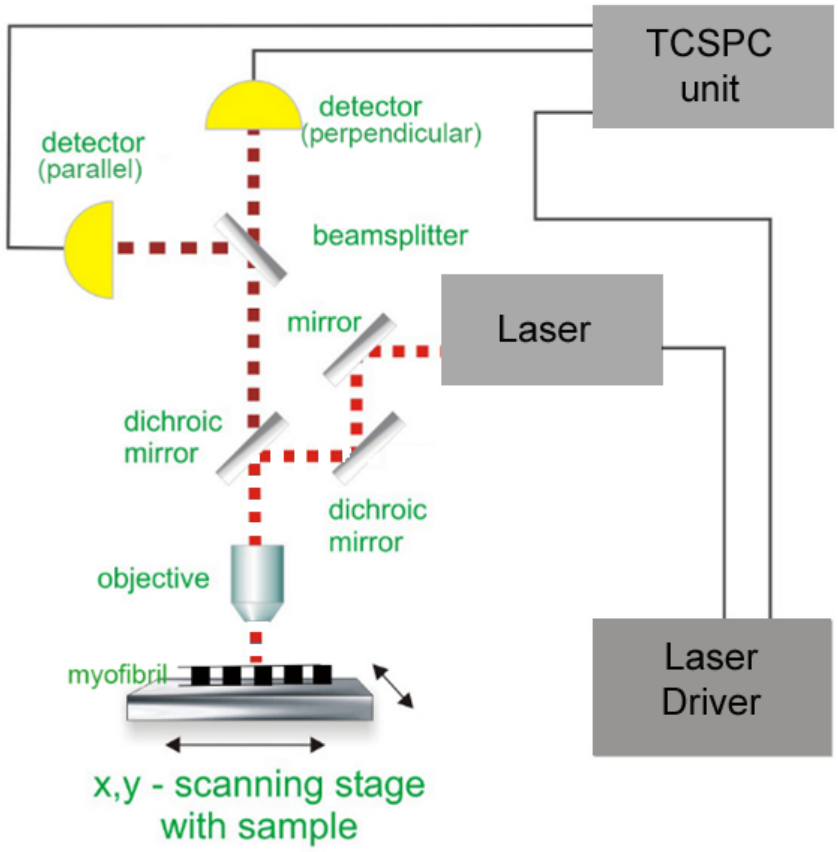

Figure S2. *Instrument used in the experiments. It is PicoQuant MT200 coupled to Olympus IX 71 microscope. Pulsed red light is directed by an objective to an A-band of a sarcomere of an isolated myofibril. X-Y scanning is disabled. Dark red light is collected by the same objective and projected onto a polarizing beam-splitter which splits the light into parallel and perpendicular components. They are collected by Time Correlated Single Photon Counter unit, binned and transferred to separate computer for processing.*

Figure S3

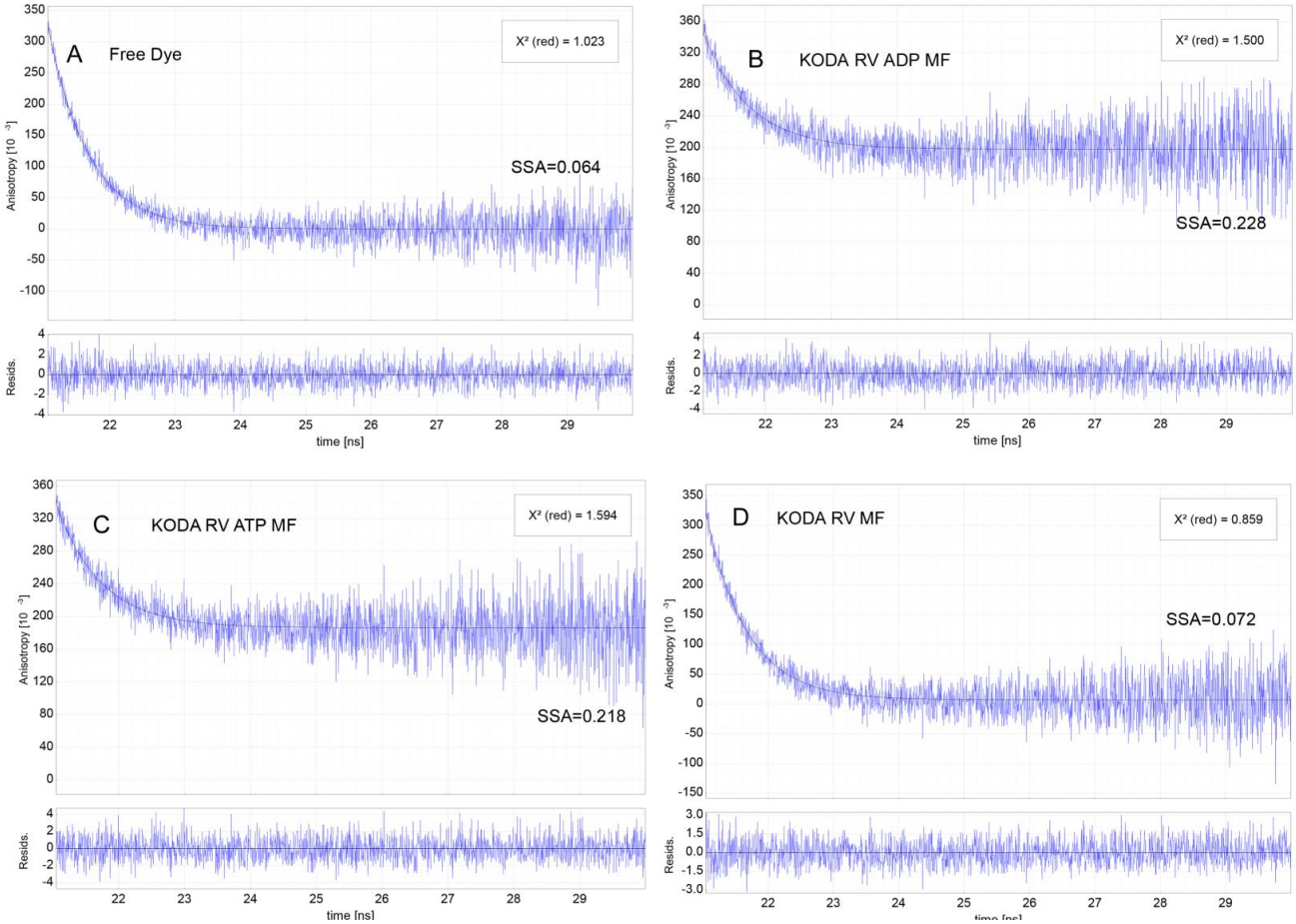

Fig. S3. *Changes in the steady-state anisotropy in different stages of ventricular contraction. 0.1 μM myofibrils from the RV labeled at 1:1000 ratio (dye : protein) with Alexa633.*

Figure S4

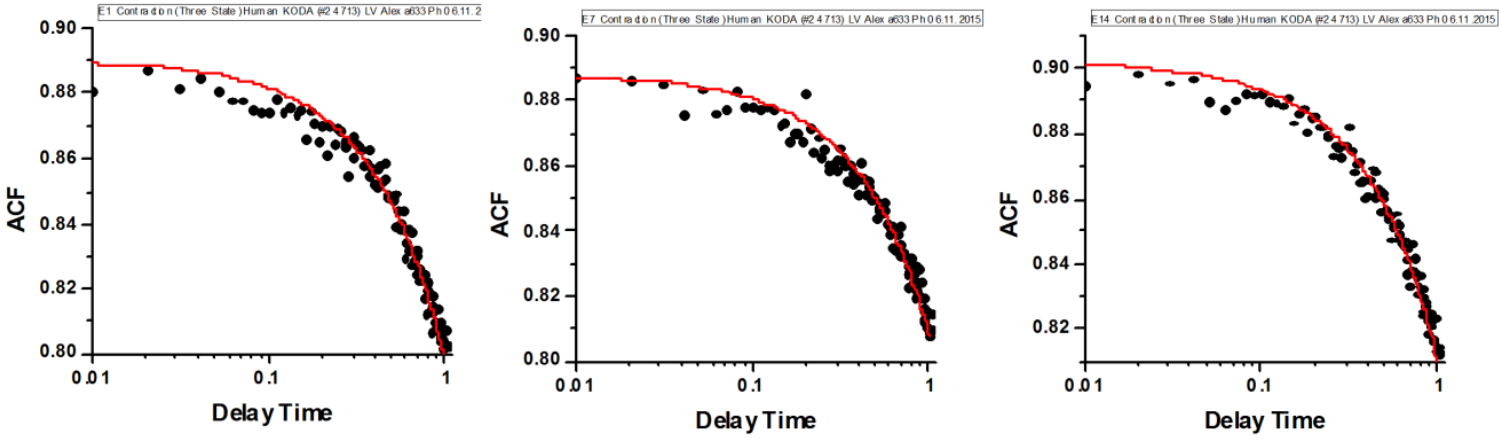

Figure S4. *Changes in the steady-state anisotropy in different stages of ventricular contraction. 0.1 μM myofibrils from the RV labeled at 1:1000 ratio (dye : protein) with Alexa633.*

7. REFERENCES

1. Allen TS-C, Ling N, Irving M, and Goldman YE. Orientation changes in myosin regulatory light chains following photorelease of ATP in skinned muscle fibers. *Biophys J* 70: 1847-1862., 1996.
2. Bagshaw CR. "Muscle Contraction". *Chapman & Hall*, London., 1982.
3. Barman T, Brune M, Lionne C, Piroddi N, Poggesi C, Stehle R, Tesi C, Travers F, and Webb MR. ATPase and shortening rates in frog fast skeletal myofibrils by time-resolved measurements of protein-bound and free Pi. *Biophys J* 74: 3120-3130., 1998.
4. Belin RJ, Sumandea MP, Sievert GA, Harvey LA, Geenen DL, Solaro RJ, and de Tombe PP. Interventricular differences in myofilament function in experimental congestive heart failure. *Pflugers Arch* 462: 795-809, 2011.
5. Bershitsky SY, Tsaturyan AK, Bershitskaya ON, Mashanov GI, Brown P, Burns R, and Ferenczi MA. Muscle force is generated by myosin heads stereospecifically attached to actin. *Nature* 388: 186-190, 1997.
6. Borovikov YS and Chernogriadskaia NA. Studies on conformational changes in F-actin of glycerinated muscle fibers during relaxation by means of polarized ultraviolet fluorescence microscopy. *Microsc Acta* 81: 383-392., 1979.
7. Borovikov YS, Kuleva, N.V. & Khoroshev, M.I. Polarization microfluorimetry study of interaction between myosin head and F-actin in muscle fibers. *Gen Physiol Biophys* 10: 441-459., 1991.
8. Bracewell R. *The Fourier Transform and Its Applications*. New York: McGraw-Hill, 1965.
9. Brooks WW, Bing OH, Blaustein AS, and Allen PD. Comparison of contractile state and myosin isozymes of rat right and left ventricular myocardium. *J Mol Cell Cardiol* 19: 433-440, 1987.
10. Cadete VJ, Lin HB, Sawicka J, Wozniak M, and Sawicki G. Proteomic analysis of right and left cardiac ventricles under aerobic conditions and after ischemia/reperfusion. *Proteomics* 12: 2366-2377, 2012.
11. Carlsson M, Heiberg E, Toger J, and Arheden H. Quantification of left and right ventricular kinetic energy using four-dimensional intracardiac magnetic resonance imaging flow measurements. *Am J Physiol Heart Circ Physiol* 302: H893-900, 2012.
12. Devereux RB, Roman MJ, Paranicas M, O'Grady MJ, Lee ET, Welty TK, Fabsitz RR, Robbins D, Rhoades ER, and Howard BV. Impact of diabetes on cardiac structure and function: the strong heart study. *Circulation* 101: 2271-2276, 2000.
13. Dos Remedios CG, Millikan RG, and Morales MF. Polarization of tryptophan fluorescence from single striated muscle fibers. A molecular probe of contractile state. *J Gen Physiol* 59: 103-120, 1972.
14. Elson EL. Fluorescence correlataion spectroscopy and photobleaching recovery. *Annu Rev Phys Chem* 36: 379-406, 1985.
15. Elson EL. Fluorescence correlation spectroscopy: past, present, future. *Biophys J* 101: 2855-2870, 2011.
16. Elson EL. *Introduction to FCS*. Fort Worth: UNT, 2007.
17. Elson EL. Quick tour of fluorescence correlation spectroscopy from its inception. *J Biomed Opt* 9: 857-864., 2004.
18. Elson EL and Magde D. Fluorescence Correlation Spectroscopy: Coceptual Basis and Theory. *Biopolymers* 13: 1-28, 1974.
19. Espinola-Zavaleta N, Soto ME, Castellanos LM, Jativa-Chavez S, and Keirns C. Non-compacted cardiomyopathy: clinical-echocardiographic study. *Cardiovascular ultrasound* 4: 35, 2006.
20. Geeves MA and Holmes KC. The molecular mechanism of muscle contraction. *Adv Protein Chem* 71: 161-193., 2005.

21. Herrmann C, Lionne C, Travers F, and Barman T. Correlation of ActoS1, myofibrillar, and muscle fiber ATPases. *Biochemistry* 33: 4148-4154., 1994.
22. Hopkins SC, Sabido-David C, Corrie JE, Irving M, and Goldman YE. Fluorescence polarization transients from rhodamine isomers on the myosin regulatory light chain in skeletal muscle fibers. *Biophys J* 74: 3093-3110, 1998.
23. Hopkins SC, Sabido-David C, van der Heide UA, Ferguson RE, Brandmeier BD, Dale RE, Kendrick-Jones J, Corrie JE, Trentham DR, Irving M, and Goldman YE. Orientation changes of the myosin light chain domain during filament sliding in active and rigor muscle. *J Mol Biol* 318: 1275-1291., 2002.
24. Houdusse A and Sweeney HL. Myosin motors: missing structures and hidden springs. *Curr Opin Struct Biol* 11: 182-194., 2001.
25. Huxley AF and Simmons RM. Proposed mechanism of force generation in striated muscle. *Nature* 233: 533-538., 1971.
26. Itoya M, Mallet RT, Gao ZP, Williams AG, Jr., and Downey HF. Stability of high-energy phosphates in right ventricle: myocardial energetics during right coronary hypotension. *Am J Physiol* 271: H320-328, 1996.
27. Johnston SA and May RC. The human fungal pathogen Cryptococcus neoformans escapes macrophages by a phagosome emptying mechanism that is inhibited by Arp2/3 complex-mediated actin polymerisation. *PLoS pathogens* 6: e1001041, 2010.
28. Krug H, Punkt K, and Bittorf L. The higher myosin ATPase activity in the right heart ventricle of the rat, proved by histophotometry. *Acta histochemica* 82: 115-119, 1987.
29. Lakowicz JR. *Principles of Fluorescence Spectroscopy*: Springer, 2006.
30. Magde D, Elson EL, and Webb WW. Fluorescence correlation spectroscopy. II. An experimental realization. *Biopolymers* 13: 29-61., 1974.
31. Malik FI, Hartman JJ, Elias KA, Morgan BP, Rodriguez H, Brejc K, Anderson RL, Sueoka SH, Lee KH, Finer JT, Sakowicz R, Baliga R, Cox DR, Garard M, Godinez G, Kawas R, Kraynack E, Lenzi D, Lu PP, Muci A, Niu C, Qian X, Pierce DW, Pokrovskii M, Suehiro I, Sylvester S, Tochimoto T, Valdez C, Wang W, Katori T, Kass DA, Shen YT, Vatner SF, and Morgans DJ. Cardiac myosin activation: a potential therapeutic approach for systolic heart failure. *Science* 331: 1439-1443, 2011.
32. McMahon WS, Mukherjee R, Gillette PC, Crawford FA, and Spinale FG. Right and left ventricular geometry and myocyte contractile processes with dilated cardiomyopathy: myocyte growth and beta-adrenergic responsiveness. *Cardiovasc Res* 31: 314-323, 1996.
33. Mettikolla P, Calander N, Luchowski R, Gryczynski I, Gryczynski Z, Zhao J, Szczesna-Cordary D, and Borejdo J. Cross-bridge Kinetics in Myofibrils Containing Familial Hypertrophic Cardiomyopathy R58Q Mutation in the Regulatory Light Chain of Myosin. *Journal of theoretical Biology* 284: 71-81, 2011.
34. Morales MF. Calculation of the polarized fluorescence from a labeled muscle fiber. *Proc Nat Acad Sci USA* 81: 145-149., 1984.
35. Nagwekar J, Duggal D, Rich R, Raut S, Fudala R, Gryczynski I, Gryczynski Z, and Borejdo J. Spatial Distribution of Actin and Mechanical Cycle of Myosin are Different in Right and Left Ventricles of Healthy Mouse Hearts. Biochemistry, in press (Editors Choice). *Biochemistry* 53 (Editors Choice). 7641-7649, 2014.
36. Nihei T, Mendelson, R.A., & Botts, J. Use of fluorescence polarization to observe changes in attitude of S1 moieties in muscle fibers. *Biophys J* 14 236-242., 1974.
37. Sabido-David C, Brandmeier B, Craik JS, Corrie JE, Trentham DR, and Irving M. Steady-state fluorescence polarization studies of the orientation of myosin regulatory light chains in single skeletal muscle fibers using pure isomers of iodoacetamidotetramethylrhodamine. *Biophys J* 74: 3083-3092, 1998.

38. Samarel AM. Regional differences in the in vivo synthesis and degradation of myosin subunits in rabbit ventricular myocardium. *Circ Res* 64: 193-202, 1989.
39. Shefner JM, Watson ML, Meng L, and Wolff AA. A study to evaluate safety and tolerability of repeated doses of tirasemtiv in patients with amyotrophic lateral sclerosis. *Amyotrophic lateral sclerosis & frontotemporal degeneration* 14: 574-581, 2013.
40. Spudich JA. Hypertrophic and dilated cardiomyopathy: four decades of basic research on muscle lead to potential therapeutic approaches to these devastating genetic diseases. *Biophys J* 106: 1236-1249, 2014.
41. Tregear RT and Mendelson RA. Polarization from a helix of fluorophores and its relation to that obtained from muscle. *Biophys J* 15: 455-467., 1975.
42. Tsaturyan AK, Bershitsky SY, Burns R, and Ferenczi MA. Structural changes in the actin-myosin cross-bridges associated with force generation induced by temperature jump in permeabilized frog muscle fibers. *Biophys J* 77: 354-372, 1999.
43. Vandekerckhove JS and Sandoval IV. Purification and characterization of a new mammalian serum protein with the ability to inhibit actin polymerization and promote depolymerization of actin filaments. *Biochemistry* 21: 3983-3991, 1982.
44. Walcott S, Warshaw DM, and Debold EP. Mechanical Coupling between Myosin Molecules Causes Differences between Ensemble and Single-Molecule Measurements. *Biophys J* 103: 501-510, 2012.
45. Wessels MW and Willems PJ. Mutations in sarcomeric protein genes not only lead to cardiomyopathy but also to congenital cardiovascular malformations. *Clinical genetics* 74: 16-19, 2008.
46. Yanagida T, Nakase M, Nishiyama K, and Oosawa F. Direct observation of motion of single F-actin filaments in the presence of myosin. *Nature* 307: 58-60., 1984.
47. Yanagida T and Oosawa F. Conformational changes of F-actin-epsilon-ADP in thin filaments in myosin-free muscle fibers induced by Ca2+. *J Mol Biol* 140: 313-320., 1980.
48. Yanagida T and Oosawa F. Polarized fluorescence from epsilon-ADP incorporated into F-actin in a myosin-free single fiber: conformation of F-actin and changes induced in it by heavy meromyosin. *J Mol Biol* 126: 507-524., 1978.
49. Yin HL and Stull JT. Proteins that regulate dynamic actin remodeling in response to membrane signaling minireview series. *J Biol Chem* 274: 32529-32530, 1999.

CHAPTER VII

A NOVEL METHOD OF DETERMINING THE FUNCTIONAL EFFECTS OF A MINOR GENETIC MODIFICATION OF A PROTEIN

Janhavi Nagwekar[1] , Divya Duggal[1] , Krishna Midde[1] , Ryan Rich[2] , Jingsheng Liang[3] , Katarzyna Kazmierczak[3] , Wenrui Huang[3] , Rafal Fudala[1] , Ignacy Gryczynski[1] , Zygmunt Gryczynski[4] , Danuta Szczesna-Cordary[3] and Julian Borejdo[1] *

[1]Department of Cell Biology, Center for Commercialization of Fluorescence Technologies, University of North Texas Health Science Center, Fort Worth, TX, USA,

[2]Department of Mathematics, Computer Science, and Physics, Texas Wesleyan University, Fort Worth, TX, USA,

[3]Department of Molecular and Cellular Pharmacology, Miller School of Medicine, University of Miami, Miami, FL, USA, 4Department of Physics and Astronomy, Texas Christian University, Fort Worth, TX, USA

* Corresponding Authors: Julian Borejdo, Department of Cell Biology, University of North Texas Health Science Center, 3500 Camp Bowie Blvd, Fort Worth, TX 76107, USA, Tel.: (817) 735-2106, Fax: (817) 735-2118; E-mail: Julian.Borejdo@unthsc.edu

1. ABSTRACT

Contraction of muscles results from the ATP-coupled cyclic interactions of the myosin cross-bridges with actin filaments. Macroscopic parameters of contraction, such as maximum tension, speed of shortening, or ATPase activity, are unlikely to reveal differences between the wild-type and mutated (MUT) proteins when the level of transgenic protein expression is low. This is because macroscopic measurements are made on whole organs containing trillions of actin and myosin molecules. An average of the information collected from such a large assembly is bound to conceal any differences imposed by a small fraction of MUT molecules. To circumvent the averaging problem, the measurements were done on isolated ventricular myofibril (MF) in which thin filaments were sparsely labeled with a fluorescent dye. We isolated a single MF from a ventricle, oriented it vertically (to be able measure the orientation), and labeled 1 in 100,000 actin monomers with a fluorescent dye. We observed the fluorescence from a small confocal volume containing approximately three actin molecules. During the contraction of a ventricle actin constantly changes orientation (i.e., the transition moment of rigidly attached fluorophore fluctuates in time) because it is repetitively being "kicked" by myosin cross-bridges. An autocorrelation functions (ACFs) of these fluctuations are remarkably sensitive to the mutation of myosin. We examined the effects of Alanine to Threonine (A13T) mutation in the myosin regulatory light chain shown by population studies to cause hypertrophic cardiomyopathy. This is an appropriate example, because mutation is expressed at only 10% in the ventricles of transgenic mice. ACFs were either "Standard" (Std) (decaying monotonically in time) or "Non-standard" (NStd) (decaying irregularly). The sparse labeling of actin also allowed the measurement of the spatial distribution of actin molecules. Such distribution reflects the interaction of actin with myosin cross-bridges and is also remarkably sensitive to myosin mutation. The result showed that the A13T mutation caused 9% ACFs and 9% of spatial distributions of actin to be NStd, while the remaining 91% were Std, suggesting that the NStd performances were executed by the MUT myosin heads and that the Std performances were executed by non-MUT myosin heads. We conclude that the method explored in this study is a sensitive and valid test of the properties of low prevalence mutations in sarcomeric proteins.

Keywords: low expressing mutations, actin, myosin light chain, phalloidin-actin, fluorescence polarization, autocorrelation function

2. INTRODUCTION

Muscle contraction results from the ATP-coupled, cyclic interactions of the myosin cross-bridges with actin filaments. Macroscopic parameters of contraction, such as maximum tension, speed of shortening, or ATPase activity are unlikely to reveal differences between wild-type (WT) and mutated (MUT) proteins when the level of transgenic protein expression is low. This is because macroscopic measurements are done on whole organs (or on a small part of a tissue) containing trillions of actin and myosin molecules. These molecules originate from muscle fibers with different fiber structures and orientations. Moreover, molecular crowding effects are different in various parts of a ventricle. Averaging data from such a large assembly of molecules with varying orientations prevent observing minute deviations expected from mutant protein that is expressed at a low level.

This paper suggests a novel method of circumventing the averaging problem in samples containing minor genetic modifications of myosin. The samples are analyzed by the mesoscopic method (1) (i.e., only a small number of molecules within a sample are analyzed). Observing only a small number of molecules avoids averaging data from a large assembly of molecules with varying orientations. To achieve mesoscopic conditions, only 1 out of 100,000 actin monomers in thin filaments of isolated cardiac myofibrils (MFs) was labeled. Figure1 illustrates how the complications arising from the fact that molecules originate from muscle fibers with different structures and orientations was eliminated.

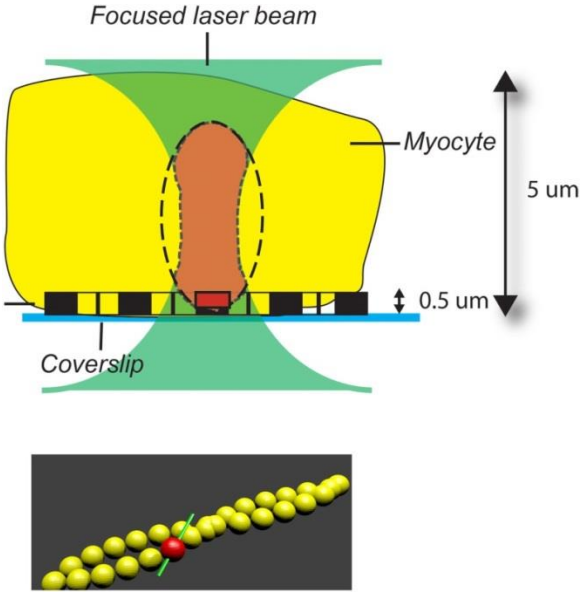

Figure 1. The illustration to show advantage of using myofibrils rather than a whole ventricle or myocytes in studies when a few molecules need to be studied in *ex vivo*. Top: a laser beam (green) is focused on a myocyte. Fluorescence is collected from the region (brown) of overlap between the volume seen by a confocal microscope (ellipsoid-of-revolution, dashed line) and the laser beam. This part of a myocyte contains hundreds of myofibrils and, therefore, more than 100,000 actin molecules. If, on the other hand, only a single myofibril is studied, the fluorescence is collected only from a volume containing actin (dark brown), which contains approximately three actin molecules; Bottom: only one (red) in 100,000 actin molecules (yellow) is labeled. The transition dipole of rhodamine is green. Not drawn to-scale.

As an experimental model we used mouse ventricles that had undergone cardiac hypertrophic cardiomyopathy HCM mutation A13T (Alanine → Threonine) in the myosin regulatory light chain (RLC). This mutation was shown by population studies to cause cardiac hypertrophy with no incidences of sudden cardiac death (2–5). A13T-RLC mutation is a good choice to study the effects of low expression because in mouse hearts it is expressed at only ~10% level (6).

The conformational change of myosin heads bound to actin filaments during contraction triggers the rotation of actin protomers because thin filaments receive periodic "kicks" (momentum transfer) from the active myosin heads (7–9). As a result, the transition dipole of rhodamine fluctuates in time. We measured the parameters characterizing these fluctuations during contraction in MUT cardiac MFs from mice, and compared it with transgenic WT-RLC. Specifically, we measured the parallel (||) and perpendicular (⊥) components of the fluorescent light emitted by rhodamine-bound actin monomers and followed the fluctuations of the orientation of the transition dipole of rhodamine by computing the normalized ratio of the difference between these components, called polarized fluorescence (PF). PF is a sensitive indicator of the orientation of the transition dipole of the fluorophore (10–16). The relative fluctuation of PF depends on the number of molecules under observation (N) as $\sqrt{N}/N$ (17–19).

A whole papillary muscle or even a single cardiac myocyte contain a large number ($>10^{11}$) of myosin molecules, i.e., the relative fluctuation is $<10^{-3\%}$ (i.e., only 1/100,000 of the signal carries the kinetic information). There is no hope of observing such small signal. By using a microscope capable of detecting single molecules, we were able to observe only approximately three actin molecules. For this number of molecules ($N = 3$), the relative fluctuation is $\sqrt{N}/N = 57\%$. We show that the autocorrelation functions (ACF) of mesoscopic fluctuations are uniquely sensitive to the deviations from the "standard" (Std) (monotonic) decay characteristic of WT. Furthermore, the distribution of orientations of the transition dipole of rhodamine also proved to be sensitive to deviations from the Std Gaussian distribution. With the techniques used today, hypertrophy induced with only 10% penetrance of the mutation would generally go undetected. This defect is easily detected by labeling a few actin molecules and studying the kinetics and orientation changes. The results showed that the A13T mutation caused 9% ACFs and 9% of spatial distributions of actin to be non-standard (NStd; i.e., assumed a shape completely incongruous with the Std), while the remaining 91% were Std. These data suggest that the NStd performances were realized by the MUT myosin heads and that the Std performances were realized by non-MUT myosin heads. We conclude that the mesoscopic method explored in this study is a sensitive and valid test of the properties of HCM-linked mutations in myosin or its light chains that occur with low prevalence in humans and are expressed at low levels in the ventricles of animal models of HCM.

3. MATERIALS AND METHODS

3.1. Chemicals, Solutions

Tetramethylrhodamine-phalloidin was purchased from Molecular Probes (Eugene, OR, USA, Cat. No. R-415). All other chemicals were from Sigma-Aldrich (St Louis, MO, USA). The composition of solutions was as in (20). Briefly, the Ca-rigor solution contained 50 mM KCl, 0.1 mM $CaCl_2$, 5 mM $MgCl_2$, 10 mM Tris pH 7.5, and 1 mM DTT. EDTA-rigor had the same composition except that it did not contain either Mg or Ca and contained in addition 5 mM EDTA. Relaxing solution had the same composition as Ca-rigor but contained 5 mM ATP and 2 mM EGTA. Contracting solution had the same composition as Ca-rigor but contained 5 mM ATP.

3.2. Reconstituted Transgenic Mice Containing Human RLC

The transgenic mice were prepared by DS-C. Human WT-RLC and A13T-RLC were expressed in the mice to obtain increasing degree of reconstituted human RLC (WT or MUT A13T). Tg-WT served as control with human RLC expression of 40%. A13T mutant is incorporated in Tg mice to give 10% expression with 90% NTg.

3.3. Preparation of Myofibrils

The investigation conforms with the Guide for the Care and Use of Laboratory Animals published by the US National Institutes of Health (NIH Publication No. 85–23, revised 1996). All animal studies were conducted in accordance with institutional guidelines (Recent Annual Animal Protocol Review, Protocol Approval # 2013/14-46-A08, approved by Dr. Michael Forster, Chairman of IACUC on 05/30/2014). Left ventricular muscle from 6-month-old Tg-A13T mice together with Tg-WT controls were shipped to Fort Worth on dry ice Kazmierczak et al. (6). Before experiments, the strips were thoroughly washed with an ice-cold EDTA-rigor solution for 0.5 h (to avoid contraction on transfer to ATP-free solution) followed by an extensive wash with Mg^{2+}-rigor solution followed by the Ca^{2+}-rigor solution. The muscle strips were then homogenized in Ca^{2+}-rigor solution using a Heidolph Silent Crusher S homogenizer for 20 s (with a break to cool after 10 s). Freshly prepared MFs were used in each experiment.

3.4. Labeling

Myofibrils were labeled with 0.1 nM rhodamine-phalloidin (RP) + 10 μM unlabeled-phalloidin (UP) in Ca^{2+}-rigor solution as described in (21). Since the ratio of fluorescent to non-fluorescent phalloidin was 1:100,000, only 1 in 10^5 actin monomers carried a fluorophore. UP was used to avoid uneven labeling. In the absence of UP, MFs closest to the tip of pipette that was used to add fluorophore were predominantly labeled. Phalloidin had no effect on the ATPase activity of labeled MFs: 1.33 ± 2.65 μM Pi/min/mg myofibrillar myosin without phalloidin, 1.81 ± 2.70 μM Pi/min/mg myofibrillar myosin with phalloidin. In addition, myofibrils shortened at the same speed when observed under Nomarski microscope.

3.5. Number of Observed Molecules

Calibration shown in supplementary Figure S1 in Supplementary Material reveals that one molecule of rhodamine resulted in the detection of 9 photons/10 ms. Figure Figure22 shows the intensities of the

perpendicular (ch1) and parallel (ch2) channels of contracting WT MF. The average intensities were 23 and 26 counts/10 ms (note that Figure 2 is a bar plot). The number of molecules observed in one channel was 24 counts/9 count/molecule = ~2.7 molecules/10 ms/channel.

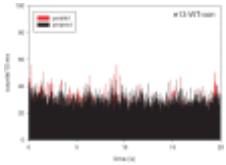

Figure 2: A typical time course of polarized intensity of contracting myofibrils (MFs) from the right ventricle of WT heart. The graph is a bar plot. The vertical scale is the number of counts during 10 ms. The intensities perpendicular ($\|_\perp$) and parallel ($I_\|$) to myofibrillar axis are black and red, respectively.

This number agrees well with the predicted number: the concentration of actin in muscle is 0.6 mM, (22) and the confocal volume is 10^{-15}L. There are 3.6×10^5 actin monomers in this volume. Since only 1 in 100,000 monomers are labeled, we estimate that there are approximately three to four fluorescent actin molecules in the detection volume (OV). It is important to note, however, that we only need to know that this number is small. The results must be the same whether the number is 3 (57% fluctuation) or 30 (18% fluctuation). The latter is also easily detectable by the avalanche photodiode used by our microscope.

3.6. Cross-Linking

In contracting solution (in the presence of Ca^{2+} and ATP) MFs shorten, making it impossible to record steady-state polarization. To prevent MFs from shortening they were cross-linked with water-soluble cross-linker 1-ethyl-3-[3-(dimethylamino) -propyl] carbodiimide (EDC) (23, 24). MFs (1 mg/ml) were incubated with 20 mM EDC for 20 min at room temperature. The reaction was stopped by adding 20 mM DTT. The lack of shortening was checked by confocal microscopy after labeling MFs with 1 μM RP. Control experiments in skeletal muscle showed that cross-linking made no difference to the shape of histograms, i.e., that cross-bridges cycled normally) (23, 24). Phalloidin had no effect on the ATPase activity of EDC cross-linked MFs: it was 2.44 ± 0.58 μM Pi/min/mg myofibrillar myosin without phalloidin and 2.33 ± 1.35 μM Pi/min/mg myofibrillar myosin with phalloidin.

3.7. Sample Preparation

Cardiac MFs attached weakly to the glass and were easily displaced by washing. To help them attach strongly, the coverslips were thoroughly cleaned with 100% ethanol, and spin coated with Poly-L-lysine solution (Sigma-Aldrich 0.1%) at 3,000 rpm for 120 s using a spincoater P6700 (Specialty Coating Systems, Indianapolis, IN, USA).

3.8. Probability Distribution Measurements

The measurements were done on an MT200 confocal system (PicoQuant, Berlin, Germany) coupled to an Olympus IX 71 microscope. The 2-M data points were collected every 10 μs for 20 s and smoothed by binning 1,000 points together. Before each experiment, the instrument was optimized with 50 nM solution of long fluorescent lifetime dye (rhodamine 700), making sure that the geometrical correction factor G (ratio of the orthogonal components) was the same as measured in the specialized instrument (PicoQuant FT 200). The excitation was by a 532 nm CW laser. To ensure that the exciting light was strictly linearly polarized, a polarizer was inserted before the entrance of the light to the microscope. The laser polarization was vertical

on the microscope stage. The laser power incident on a sample was 100 μW. The confocal aperture was 50 μm and magnification of the objective was 60× (NA = 1.2). The emitted (fluorescent) light was split 50/50 by a birefringent prism and each component was detected by a separate avalanche photodiode (APD). The || and ⊥ (with respect to the laboratory frame of reference) analyzers were inserted before each APD. Channels 1 and 2 measured the polarized intensities oriented ⊥ and || to the myofibrillar axis, respectively. MFs were always placed with the axis pointing vertically on the microscope stage. Adopting the notation of (12), ${}_{\|}I_{\|}$ (recorded in ch2) is the polarized intensity obtained with the exciting light polarized parallel to muscle axis and detected through analyzer oriented parallel to the axis, and ${}_{\|}I_{\perp}$(recorded in ch1) is the polarized intensity obtained with exciting light polarized parallel to muscle axis and detected through the analyzer oriented perpendicular to the axis. We, thus, measured ${}_{\|}I_{\perp}$ (ch1) and ${}_{\|}I_{\|}$ (ch2). We calculated parallel polarization of fluorescence as $PF_{\|} = ({}_{\|}I_{\|} - {}_{\|}I_{\perp})/({}_{\|}I_{\|} + {}_{\|}I_{\perp}) = (\text{ch2} - \text{ch1})/(\text{ch2} + \text{ch1})$.

3.9. Time Resolved Anisotropy

Fluorescence anisotropy was measured by the time-domain technique using FluoTime 200 fluorometer (PicoQuant, Inc.). The excitation was by a 532-nm laser pulsed diode, and the observation was through a monochromator at 590 nm with a supporting 590-nm-long wave pass filter. The FWHM of pulse response function was 370 ps. Time resolution was better than 10 ps. The intensity decays were analyzed in terms of a multi-exponential model using FluoFit software (PicoQuant, Inc.). All experiments were performed at room temperature (~23°C).

3.10. Anisotropy Decay

To ascertain whether the phalloidin probe is immobilized by the protein so that the transition dipole of the fluorophore reflects the orientation of the protein, we measured the decay of anisotropy, defined as $r = (I_{\|} - I_{\perp})/(I_{\|} + 2I_{\perp})$ using green 532 nm excitation. We first measured the fluorescence lifetime of RP (100 nM) in rigor solution (not shown). About 92.19% of the intensity decay could be fitted by a single exponential function convolved with the instrument response function, giving the intensity weighted lifetime of 2.453 ns. The decay of anisotropy of RP alone was fitted by a single exponential function $r(t) = R_{\infty} + R_o \times \exp(-t/\theta_1)$ where R_{∞} was the value of anisotropy at infinite time, R_o was the amplitude of the anisotropy at time 0, and θ_1 was the rotational correlation time. The best fit gave $R_{\infty} = 0$, $R_o = 0.241$, and a correlation time $\theta_1 = 0.703$ ns (black circles, Figure S2 in Supplementary Material). The decay of anisotropy of RP + MFs (red circles) was fitted by a sum of two exponential functions $r(t) = R_{\infty} + R_1 \times \exp(-t/\theta_1) + R_2 \times \exp(-t/\theta_2)$ with the best fit giving $R_{\infty} = 0.121$, $R_o = R_1 + R_2 + R_{\infty} = 0.258$, a long correlation time $\theta_1 = 2.040$ ms, and a short correlation time $\theta_2 = 0.443$ ns. The long correlation time (82.15% of the total) was due to the rotation of rhodamine immobilized by actin filaments and a short correlation time (17.85% of total) was due to the rotation of mobile phalloidin, consistent with the rotation of a molecule with $M_w = 1{,}250$. Thus, the mobile fraction was contributed by the minority of fluorophores and we conclude that RP labeling is appropriate for measuring polarization of fluorescence in muscle.

3.11. Statistical Analysis

It was carried out using Systat software (SigmaPlot 11.02 and Origin v. 8.5, Northampton, MA, USA). Goodness of fit was assessed by SE or reduced (χ^2) and by adjusted coefficient of determination (AR^2). The distribution functions were fitted by 3-parameter Gaussian function.

4. RESULTS

4.1. Mesoscopic measurements

Measurements were done on MFs, as illustrated in Figure3. The MF was labeled with 0.1 nM RP + 10 μM UP. In contrast to skeletal muscle, where nebulin prevents phalloidin from labeling all-but the pointed ends of actin filaments (25, 26), in the nebulin-free heart muscle the entire I-bands are labeled. The dark areas do not contain actin (H-bands). The red circle is a 2D projection of the confocal aperture on the image plane. Its diameter (0.84 μm) is equal to the diameter of the confocal aperture (50 μm) divided by the magnification of the objective (60×). As expected from the aligned array of polar actin filaments (8), the parallel ($I_{\parallel}$) and the perpendicular ($I_{\perp}$) polarization images (B and C) have different intensities, indicating that the fluorescence is highly anisotropic. The fluorescence signal was collected through the pinhole (red circle) after the initial photobleaching. We estimated in Section "Materials and Methods" that approximately three actin molecules contributed to this signal.

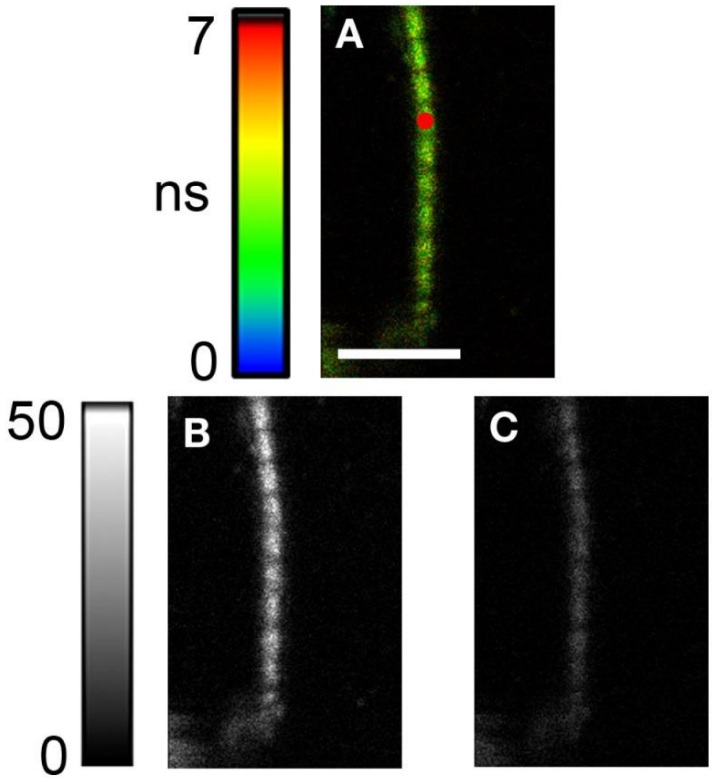

Figure 3. **Image of A13T myofibril in rigor labeled with rhodamine-phalloidin**. **(A)** FLIM (Fluorescent Lifetime Image), **(B)** parallel, and **(C)** and perpendicular intensity images of a A13T myofibril in rigor. Lifetime scale, in nanosecond, is at left of **(A)**. The intensity scale [left of **(B,C)**] is in arbitrary units with 0 corresponding to white and 255 to black. Notice that muscle in rigor is very anisotropic, because **(B)** is more intense than **(C)**. By contrast, contracting muscle is isotropic (Figure1). The red circle is the projection of the confocal aperture on the sample plane (diameter is 50/60 = 0.84 μm). Images were acquired with the PicoQuant Micro Time 200 confocal lifetime microscope. Excitation with a 470 nm pulsed laser, emission through LP500 filter. Sarcomere length 3.0 μm. Scale bar in A is 5 μm.

4.2. Contraction Kinetics

The orientation of the transition dipole of rhodamine embedded in actin protomer changes constantly during contraction because during acto-myosin interactions, actin is being constantly "kicked" by the myosin heads. The manifestation of these kicks is seen in PF changes (or changes of anisotropy) as occurring in three stages: (1) when myosin heads bind to thin filaments, (2) when isomerization of bound myosin heads occur, and (3) when myosin heads dissociate from thin filaments. These steps are schematically illustrated in Figure4.

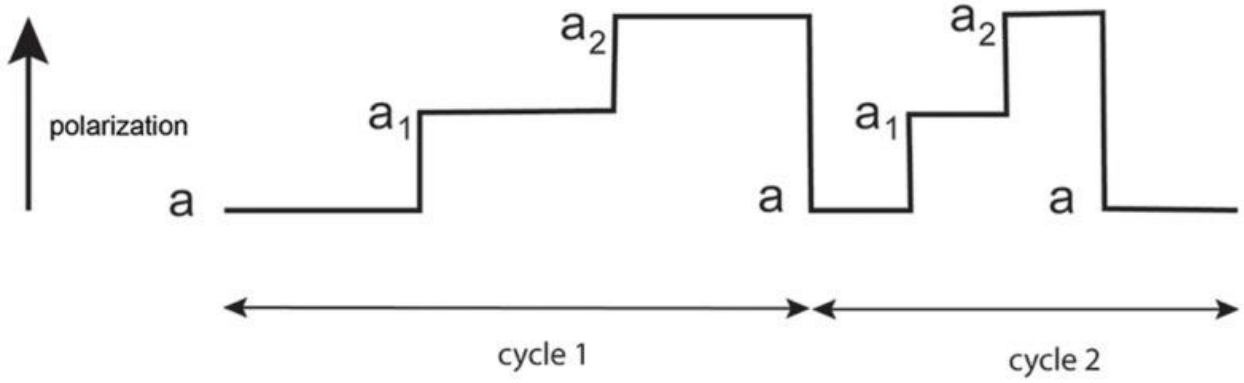

Figure 4: Schematic representation of changes of polarized fluorescence of transition dipole of rhodamine bound to actin. Note that duration of each intermediate state is random. a1, a2, and a3 are the values of steady-state anisotropy determined from anisotropy decay curves such as shown in Figure S2 in Supplementary Material. Anisotropy of actin is initially low because it is not immobilized by a cross-bridge (XB). It subsequently increases because actin rotation is now restricted by a weakly bound myosin heads. It then further increases because actin rotation is restricted by isomerization of the myosin head (power stroke) that causes strong binding to actin.

Figure 5 shows the time course of PF from the actual experiment. It results from summation of individual fluctuations (like the ones shown schematically in Figure 4) during 20-s experiment

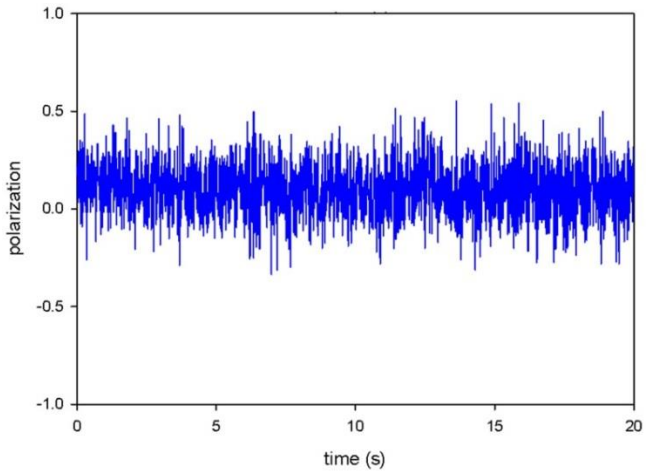

Figure 5. **Actual fluctuations of polarized fluorescence of phalloidin transition dipole in contracting myofibril**. The overall signal has characteristics of a random Gaussian signal.

Fluctuations are characterized by an ACF(τ) (17, 18). The rate of decay of ACF from the maximal value to 0 is a reflection of how quickly the average fluctuation crosses the equilibrium baseline (19). To extract the rate constants from the time course, such as shown in Figure Figure5,5, we solved the differential equations (27) describing the ACF of a three-state process. The resulting ACF determines the rates of $a_1 \rightarrow a_2$, $a_2 \rightarrow a_3$, and $a_3 \rightarrow a_1$ transitions (rates k_1–k_3). Note, however, that all experimental ACFs were similar to two-parameter hyperbolic decay, i.e., we were able to define only two kinetic constants. This is due to the fact that the rate of cross-bridge binding to actin is very rapid (28) and the time resolution of the present method is 10 ms. Thus, the rapid process (k_1) was undetectable. We, therefore, report only k_2 (the rate of cross-bridge isomerization or power stroke) and k_3 (the rate of cross-bridge detachment from thin filaments).

4.3. Kinetics of Orientation change During Contraction

We first measured the correlation functions of contracting Tg-WT MFs.Figure6A shows an example of the ACF functions out of the total of 33 experiments. As shown in Kazmierczak et al. (6), WT L4 hearts expressed 40% transgene (human ventricular RLC) and were 60% NTg in comparison to 10% A13T: 90% NTg in A13T hearts. The fit of Std WT MFs to ACF was excellent and we have not observed any NStd populations. This result suggests that WT and NTg XBs present in WT hearts were not kinetically different.

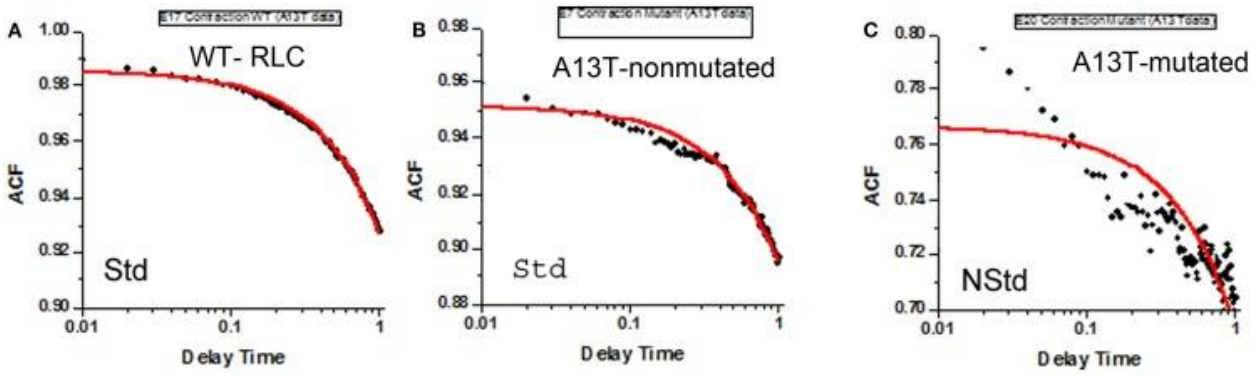

Figure 6. Representative trace of normalized autocorrelation function of polarization of fluorescence. **(A)** Data are from 33 contracting sarcomeres prepared from the left ventricle of Tg-WT. Traces are labeled Std for Standard (based on adjusted coefficient of determination, see text). The fact that the correlation decays in time in this figure, and Figures Figures6B,C6B,C indicate that the orientation of absorption/emission dipoles change in time. The fact that ACF decays to a value >0 is due to the fact that mean polarization was non-zero. Delay time is in seconds. All 33 experiments are shown in Figure S3 in Supplementary Material. **(B)**Representative trace of normalized autocorrelation function of polarization of fluorescence of contracting sarcomeres prepared from the left ventricle of Tg-A13T mice which apparently was non-transfected (labeled "Std" for Standard. All 33 experiments are shown in Figure S4 in Supplementary Material. **(C)**Representative trace of normalized autocorrelation function of polarization of fluorescence of a contracting myofibril prepared from the left ventricle of Tg-A13T mice expressing ~10% of transgene (labeled "NStd" for non-standard. All traces of normalized autocorrelation functions of Tg-A13T mouse myofibrils are shown in Figure S4 in Supplementary Material.

The correlation function could be classified as "Std" and "NStd." To quantify the difference between them, we computed the adjusted coefficient of determinations (AR^2) of the non-linear fit to the ACF. AR^2 is a

good measure of goodness of fit because it takes into account scaling of the dependent variable. The closer AR^2 is to the value of 1, the better the fit. ACFs shown in Figures Figures 6A,B had AR^2 of 0.90 and 0.93, respectively, and, thus, they were classified as Std.

The quantitative comparison of the kinetics of Std WT and Std A13T correlation functions is shown in Table1. There was no statistically significant difference between either parameter.

TABLE 1. The kinetic constants of contracting WT and A13T-mutated left ventricular muscle

	k_2 (s^{-1})	k_3 (s^{-1})
WT-RLC (standard)	1.03 ± 0.72	0.09 ± 0.09
A13T-non-mutated (standard)	1.45 ± 0.76	0.19 ± 0.45

The errors are SD of 30 experiments. The non-standard data have been excluded from the total Tg-A13T data.

The −0.355 difference in k_2 was statistically *insignificant* ($t = -1.954$, $P = 0.056$) with 57 degrees of freedom. Ninety-five percent confidence interval for difference of means was −0.721 to 0.00880. The −0.101 difference in k_3 was statistically *insignificant* ($t = -1.214$, $P = 0.229$) with 60 degrees of freedom. Ninety-five percent confidence interval for difference of means was −0.267 to 0.0654. This supports the conclusion that the Std data from MUT A13T ventricle represent the behavior of NTg XBs in Tg-A13T muscles.

We next analyzed NStd ACFs. There were no NStd ACFs of WT muscle. As shown in Figure S4 in Supplementary Material, 3 (possibly 5) out of 33 experiments on A13T sarcomeres showed NStd ACFs. Examples of ACFs are shown in Figure6C. ACFs had AR^2 of 0.36 and 0.30 and, thus, they were classified as NStd. The average ± SD of ACFs of all Std fits was 0.88 ± 0.07, whereas average of "NStd" fits was 0.33 ± 0.03.

No meaningful fit to the ACFs of NStd A13T muscles could be made. The quantitative comparison of the kinetics of Std A13Tand NStd A13T correlation functions was impossible. (For example, SD was large, 64% of the mean). Table2 shows the kinetic constants of Std ACFs only.

TABLE 2. Top row: mean $\mathbf{k}_2$ *and* $\mathbf{k}_3$ *of standard fit.*

	k_2 (s^{-1})	k_3 (s^{-1})
A13T-non-mutated (standard)	1.45 ± 0.76	0.19 ± 0.45
A13T-mutated (non-standard)	-----	-----

They are the same as Std Tg-A13T of Table 1. Bottom row, no meaningful fit to the ACFs of non-standard A13T muscles could be obtained. Errors are SD

4.4. Steady-State Distribution of Orientations During Contraction

A histogram is a plot of the number of times a given polarization of fluorescence that occurred during 20 s contraction, plotted against the value of polarization of fluorescence. Figure7A shows an example of "Std" histogram of PF selected from a pool of 33 Std histograms of contracting WT MFs. Figure7B shows an example of the histogram of PF selected from 30 histograms of contracting A13T MFs that could be classified as "Std." Figure7C shows an example of a histogram of PF of contracting A13T MFs selected

from three histograms that could be classified as "NStd." The histograms were fitted with a Gaussian curve $y = a \times \exp[-0.5(x - x_o/b)^2]$. All the histograms of Tg-WT mice are shown in Figure S5 in Supplementary Material. All the histograms of Tg-A13T mouse are shown in Figure S6 in Supplementary Material. All the histograms of Tg-A13T mice are shown in color in Figure S6 in Supplementary Material.

A histogram can be quantitatively characterized by the values of skewness and kurtosis. A positive skewness means that the tail of the curve points toward positive values of the histogram (20). A negative skewness means that the tail of the curve points toward the negative values of the histogram. A positive kurtosis is expressed by long tails and lower peaks compared to the Gaussian curves. A negative kurtosis means that the tails are smaller and the peaks are taller than those of Gaussian curves. Of the 33 experiments carried out on WT-RLC MFs (Figure S5 in Supplementary Material) all showed Std behavior. Of the 33 experiments on A13T MFs (Figure S6 in Supplementary Material), 30 showed Std behavior and 3 experiments (9%) showed NStd behavior. These three experiments were quantitatively different to the remaining 30 curves. It showed different histogram characteristics. These characteristic parameters (peak polarizations, skewness, and kurtosis) of a Gaussian curve are summarized in Table 3. It compares parameters of the 33 WT-RLC and 30 histograms of the A13T-non-MUT Std only data (three NStd experiments were excluded).

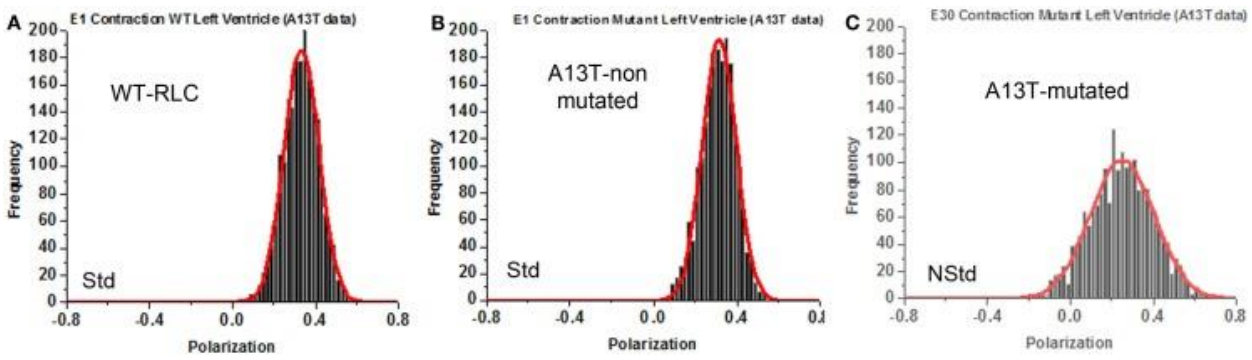

Figure 7. **Representative histogram of histograms of polarization of fluorescence of contracting sarcomeres prepared from left ventricle of mice**. **(A)** Data from 33 experiments from WT ventricle mice that were classified as "standard." **(B)** Representative histogram of 30 histograms of polarization of fluorescence of contracting sarcomeres prepared from the left ventricles of Tg-A13T mice that were classified as "standard." These muscles were negative for the A13T mutation. **(C)** Representative histogram of polarization of fluorescence of contracting sarcomeres prepared from the left ventricles of Tg-A13T mice that were positive for mutation (labeled "NStd" for non-standard.

The 0.00695 difference in the mean polarization was statistically insignificant ($t = 0.882$, $P = 0.381$) with 61 degrees of freedom. The 95% confidence interval for the difference of means was −0.00880 to 0.0227. Surprisingly, the 0.502 difference in skewness was statistically significant ($t = 4.444$, $P < 0.001$) with 61 degrees of freedom. The 95% confidence interval for the difference of means was 0.276–0.728. Similarly, the 3.135 difference in kurtosis was statistically significant ($t = 4.434$, $P < 001$) with 61 degrees of freedom. The 95% confidence interval for difference of means was 1.721–4.548. These results suggest that the very process of making transgenic animals produces some, albeit minor, differences in the distribution and suggests that Std histograms were contributed by ventricles that did not undergo A13T exchange.

TABLE 3. Polarization values of 33 WT-RLC and 30 A13T-non-mutated and 3 A13T-mutated myofibrils from the left ventricle of contracting heart			
	Mean polarization	Skewness	Kurtosis*
WT-RLC (standard)	0.321 ± 0.033	2.886 ± 0.574	7.749 ± 3.734
A13T-non-mutated (standard)	0.314 ± 0.028	2.383 ± 0.260	4.610 ± 1.259
A13T-mutated (non-standard)	0.250 ± 0.037	1.623 ± 0.262	1.450 ± 1.021
** indicates that the change was significant at 5% level.*			

Table3 also shows comparison between non-MUT and A13T-MUT MFs. The −0.064 difference in the mean polarization was statistically highly significant ($t = -4.008$, $P < 0.001$) with 31 degrees of freedom. The 95 percent confidence interval for difference of means was −0.0994 to −0.0324. The 3.160 difference in kurtosis was statistically highly significant ($t = -4.926$, $P < 0.001$) with 31 degrees of freedom. The 95 percent confidence interval for difference of means was −4.631 to −1.919. The −0.760 difference in skewness was statistically highly significant ($t = -5.967$, $P < 0.001$) with 31 degrees of freedom. The 95 percent confidence interval for difference of means was −0.057 to −0.518. These results show that the NStd histograms differed very significantly from Std ones and suggest that NStd histograms represented the ~10% MUT A13T preparations. No NStd histograms were observed for WT muscles.

5. DISCUSSION

The method described in this report has several advantages compared with the method where a large number of molecules are observed. It avoids signal averaging, which would have resulted in perfect Gaussian distributions, no matter which sample population was observed (due to Central Limit Theorem of statistics). It would have caused loss of equilibrium kinetic rates. [Kinetic rates of a large assembly of molecules can only be obtained when equilibrium is disturbed (29, 30)].

A method that relies on the measurements of a few molecules of actin can readily distinguish between the MUT vs. non-MUT molecules by observing changes in the orientation of the transition dipole of a few actin-bound rhodamine fluorophores. Since the dye is firmly attached to actin, the orientation changes are due to the fact that during muscle activity actin receives the periodic "kicks" from myosin heads. The number of these kicks is small: actin monomers in a thin filaments form a highly cooperative units that are connected by a tropomyosin double helix (7, 31–35). Each unit will interact with the myosin cross-bridge at least 100 times during our experiment lasting 20 s. This number is arrived at as follows: there are ~362 actin monomers and 180 myosin heads in one actin filament. ATPase activity of myosin is ~4/s/myosin head. The duty ratio of myosin is 20% (i.e., only 20% of myosins interact with actin during contraction). Therefore, $180/5 = 36$ myosins interact with one actin filament ~2,880 times in 20 s. Each actin filament is ~1 μ (1,000 nm) long, and each cooperative unit is 38.5 nm long. There are $1{,}000/38.5 = 26$ cooperative units in an actin filament. Each cooperative unit, thus, interacts with myosin head $\sim 2{,}880/26 = 110$ (~100) times/20 s. Because actin is labeled sparsely, most of the units do not contain a fluorescent dye, and, therefore, most of the interactions will not be registered by the photodiode. But once in a while, XBs will encounter the unit that contains the fluorophore, and this interaction will be registered. This number will be small, leading to a large fluctuation (57%). If mutations in the RLC make a difference to this interaction, 1 out of 10 interactions, like in A13T muscle, will be NStd. This means that at least 10 experiments are necessary to have a reasonable chance of detecting the temporal effect of the A13T mutation. Indeed, we observed NStd behavior of actin in 9% out of 33 experiments.

The comparison of Std WT and Std A13T data showed no difference in kinetic constants(Table1), indicating similar behavior of NTg XBs (present in 60 and 90% in Tg-WT) and Tg-A13T muscles, respectively. Since the fit of the MUT muscle excluded three highly NStd sets of data, the remaining 30 experiments for A13T (Std) showed no significant differences compared with WT (Table1). The fit of Std A13T MFs to the ACF was slightly poorer than fit of WT data in spite of exclusion of highly NStd experimental curves (Figure6A,B). Even though muscle had high content of NTg XB, we expected no significant differences between the kinetics of WT and A13T preparations. This expectation was met (Table(Table1)1) and is supported by physiological data on Tg-WT and NTg muscle fibers (6).

Figure6 shows that there is a large qualitative difference between the cross-bridge behavior of the MUT and WT cross-bridges. Even though the differences could not be quantified, because of a poor fit to NStd correlation functions, the difference is obvious by inspection. Interestingly, even though the A13T mutation is sparsely expressed in the A13T myocardium, it triggered macroscopic changes in the heart morphology manifested by cardiac fibrosis and the functional changes, such as significantly enhanced contractile force and reduced actin-activated myosin ATPase activity, are compared to NTg/WT hearts (6). Based on these obvious macroscopic changes, it was speculated that this particular HCM-causing mutation works most likely through a "poison-peptide" mechanism (6).

The RLC-A13T mutation that was chosen here as a model is one of the mutations of the sarcomeric proteins associated with familial hypertrophic cardiomyopathy (FHC) (3, 36). FHC is an autosomal-dominant disease, characterized by left ventricular hypertrophy, myofibrillar disarray, and sudden death. It is caused by missense mutations in various genes that encode for β-myosin heavy chain (37), myosin-binding protein C (38), ventricular RLC, and essential light chain (3, 36). The MUT proteins are rarely expressed at 100% level, but A13T mutation is an extreme example of very low expression. The A13T mutation is located near the phosphorylation site (Ser-15) of the human cardiac RLC. Even though it was expressed only at 10% level, it had threefold lower K_{Ca} than wild-type light chain (39). The phosphorylation of this mutant increased the Ca^{2+} affinity sixfold (39). Our method of detecting such a low level of expression may find application in a diagnostic laboratory. All that is needed is a confocal microscope equipped with polarization optics and a laser. The method described here is highly sensitive. Its validity in the mutation of myosin RLC has been tested, but it may be applicable also in studies of other genetic mutations expressed in mouse myocardium at a very low levels. It seems reasonable to use this new approach for re-analyzing already existing models that develop HCM. It would be even more applicable in studies of a disease causing mutation that may work through other mechanisms (3, 40, 41). Finding the mechanisms of heart failure due to HCM mutations is clinically important not only for patients with HCM who have the A13T mutation or other RLC mutations, but also for other patients with mutations elsewhere in the sarcomere (41). Since reverting HCM-causing mutations to their WT state is not currently possible, revealing specific disease mechanisms may lead to identification of protein-specific therapeutic targets that could prevent disease progression and improve quality of life of HCM patients (42). Due to the high sensitivity of the method described here, it may be applicable in studies of a wide range of cardiomyopathy causing mutations that are expressed at various levels in animal models of heart disease.

The most challenging part of the technique is the detection of the weak fluorescent signal. Because measurements are done *ex vivo*, the contribution of the background to the total signal is considerable. Since autofluorescence decreases at higher wavelengths (43), the choice of a red dye, rhodamine, is a necessary one. In the future, we propose to use even redder dye, rhodamine633, which has an additional advantage that it can be excited with an inexpensive 633 nm laser (or even with a red laser pointer).

It should be noted that labeling of actin has significant advantages over labeling cross-bridges. First, it is mild, involving only addition of RP under physiological conditions, whereas labeling of the cross-bridges involves incubation under extreme conditions (37°C, in the presence of anti-schizophrenia drug trifluoperazine) (44). Second, labeling actin is very quantitative. The ratio of fluorescent to non-fluorescent phalloidin determines exactly the fraction of actin monomers that are labeled. Even though the bond between actin and phalloidin is non-covalent, it is strong enough to make rhodamine firmly fixed with respect to the thin filament axis [our anisotropy decay measurements (Figure S2 in Supplementary Material) are in line with earlier measurements].

6. SUPPLEMENTARY DATA

Figure S1

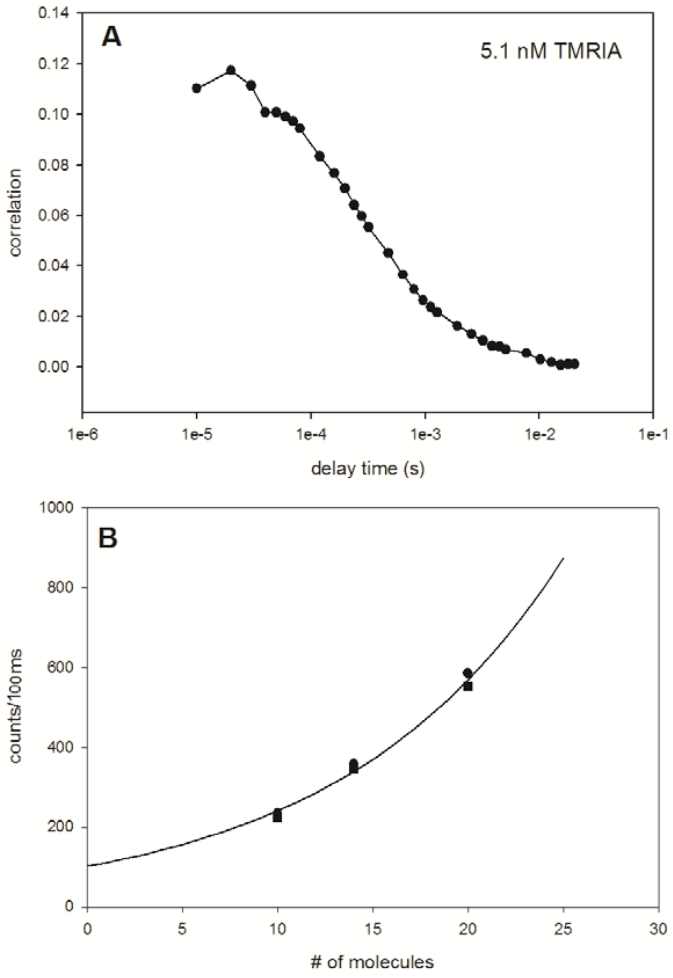

Figure S1. ***Number of observed molecules***. It is essential to make sure that this number of observed molecules is known precisely and that it be small. To measure this number we need to compare the rate at which photons are arriving from muscle with the rate at which photons are arriving from a single molecule of rhodamine. To this end we measured number of free TMRIA molecules diffusing in and out of the confocal volume of our microscope. We then systematically decreased the number of observed molecules and recorded the associated signal intensity. To determine the number of observed molecules we measured a autocorrelation function (ACF) by the Fluorescence Correlation Spectroscopy (FCS). The value of the correlation function at a delay time 0 [G(0)] is equal to the inverse of the number of molecules N contributing to the signal, N=1/G(0) [1, 2]. Correlation functions were obtained for the solution of TMRIA (tetramethylrhodamine-5-iodoacetamide dihydroiodide) in the range 50-0.5 nM. An example of the autocorrelation function obtained at a concentration of 5.1 nM is shown in **Fig. 1SA**. The G(0) was 0.11, giving the number of molecules ~9. **Fig. 1SB** shows the amplitude of the signal plotted against the average number of molecules in the DV obtained by FCS. We were unable to measure autocorrelation functions at low dye concentrations (<5.1 nM TMRIA) so the curve needed to be extrapolated to a single molecule. Extrapolation was by an exponential growth, single exponent, 2 parameters fit y=abx. The fit revealed that the number of photons contributed by 1 molecule was 9/10 ms or 900 counts/s per channel.

Figure S2

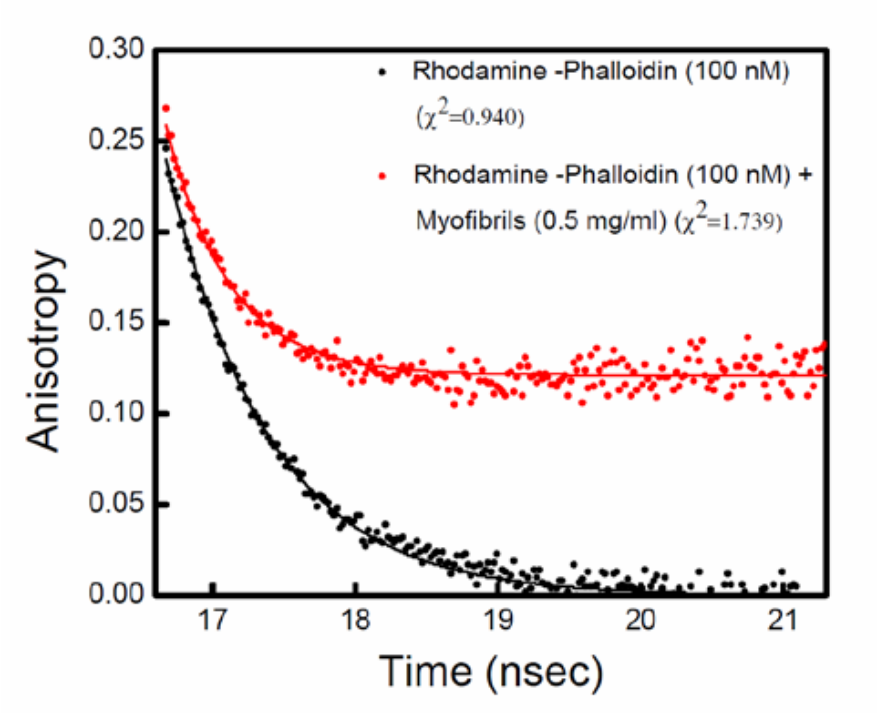

Figure S2. Decay of anisotropy of 0.1 μM RP alone (black) and of 0.1 μM RP+0.5 mg/mL Tg-WT myofibrils (red).

Figure S3

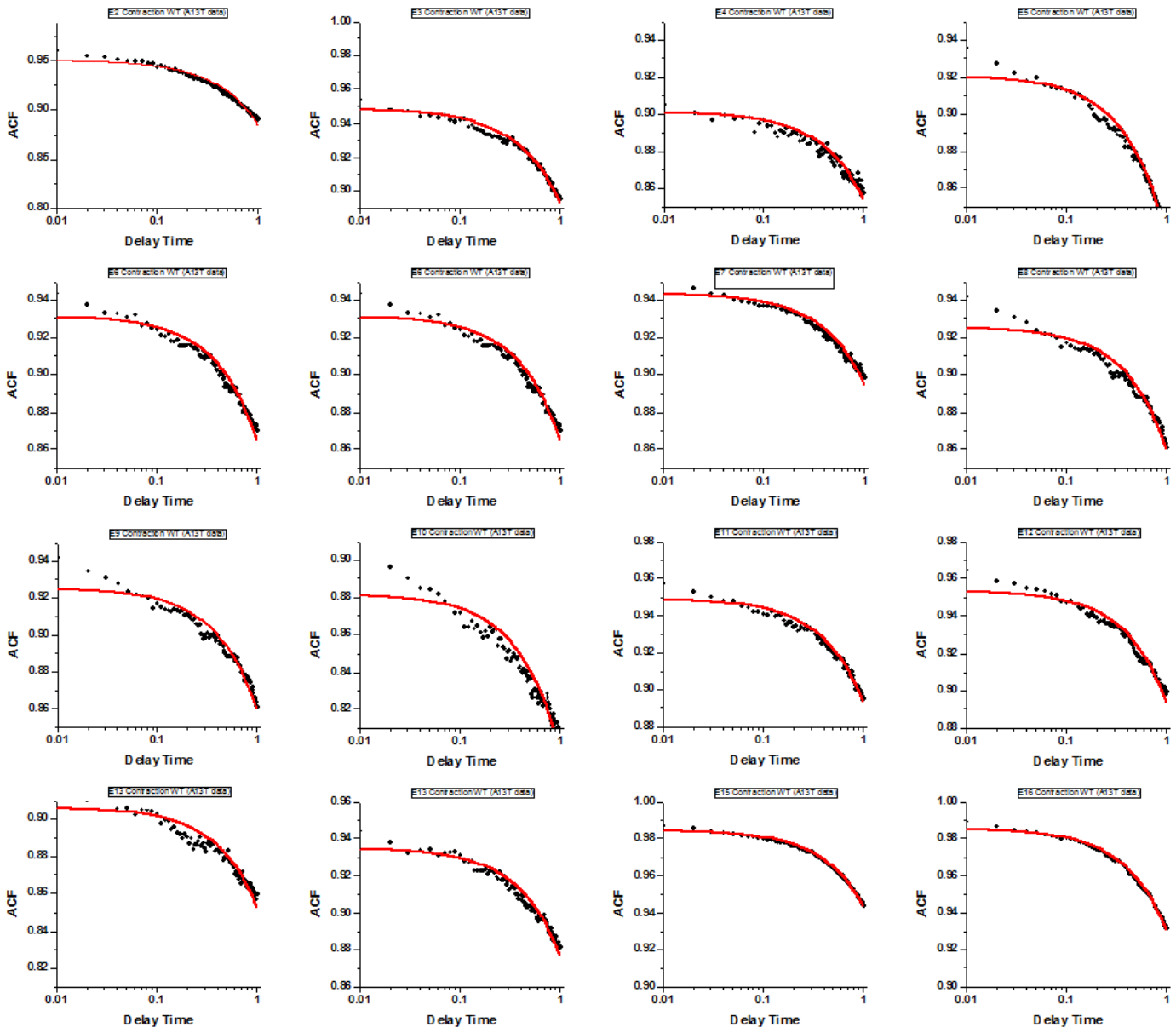

Figure S3: Normalized autocorrelation functions of all 33 experiments of polarization of fluorescence of contracting myofibril prepared from the left ventricle of Tg-WT mouse. Circles are experimental data. A red line is the fit to the analytical solution for ACF (equation of Fig. 3S). The fact that the correlation decays in time indicates that the orientation of absorption/emission dipoles change in time. The fact that ACF decays to a value >0 is due to the fact that mean polarization was non-zero. Delay time is in seconds. There are no nonstandard ACF's.

Figure S3 cntd.

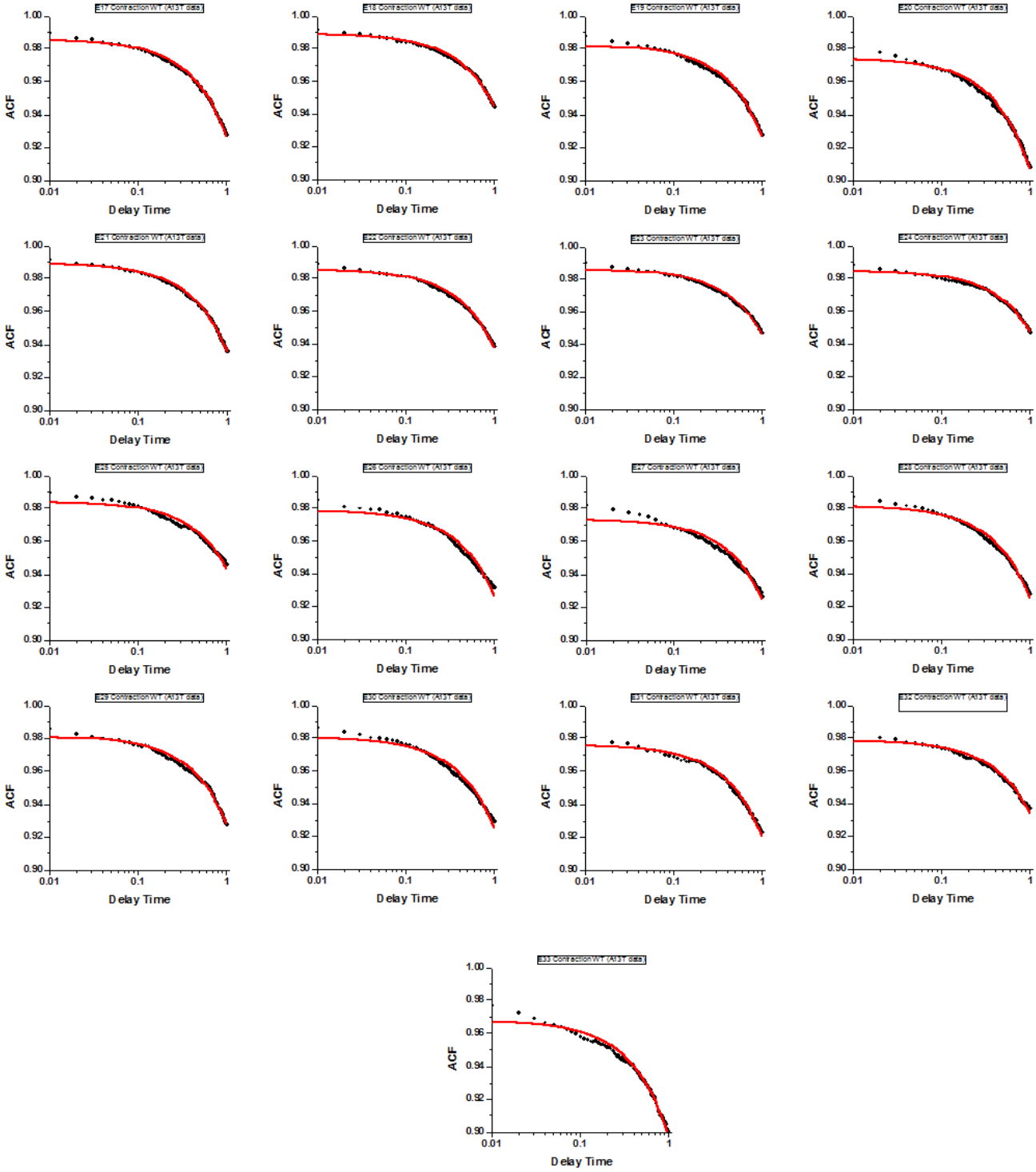

Figure S4.

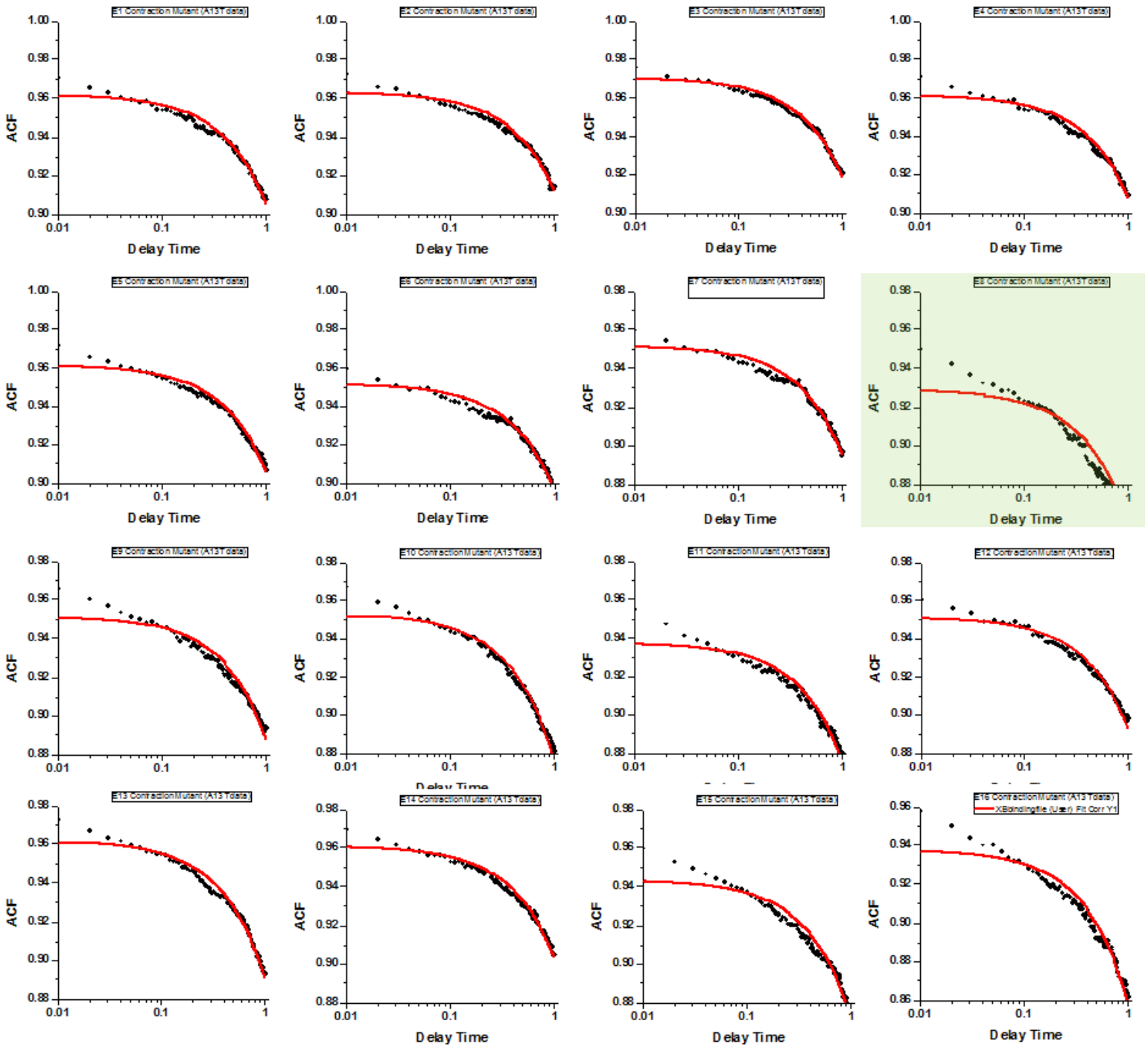

Figure S4: Traces of normalized autocorrelation functions of all 33 experiments of polarization of fluorescence of contracting myofibril prepared from the left ventricle of Tg-A13T mouse. Circles are experimental data. A red line is the fit to the equation for ACF (equation of Fig. 3S). The fact that the correlation decays in time indicates that the orientation of absorption/emission dipoles change in time. The fact that ACF decays to a value >0 is due to the fact that mean polarization was non-zero. Delay time is in seconds. ACF's judged by AR^2 to be nonstandard are outlined in blue. The nonstandard ACF's are outlined in color.

Figure S4 continued

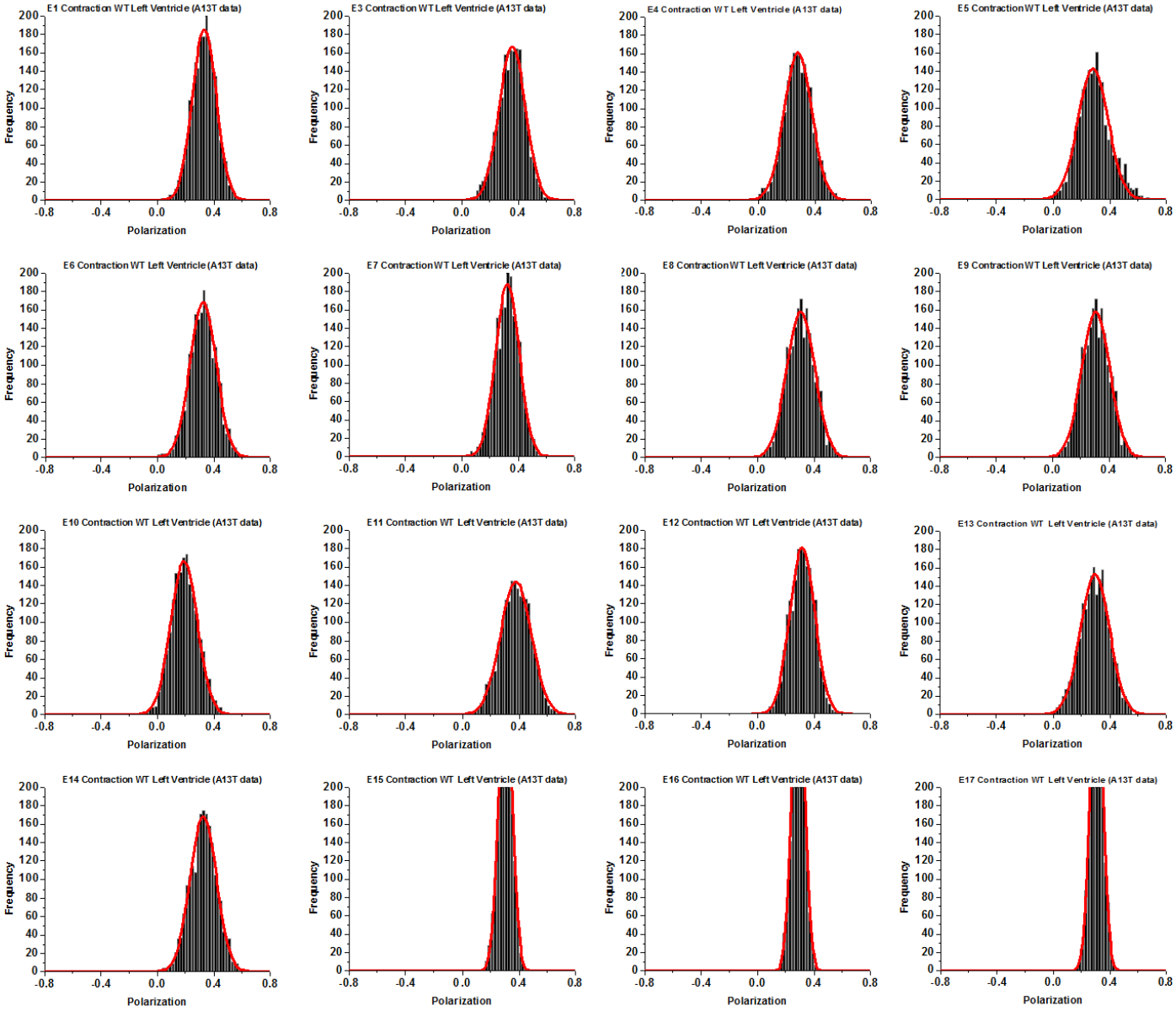

Figure S5

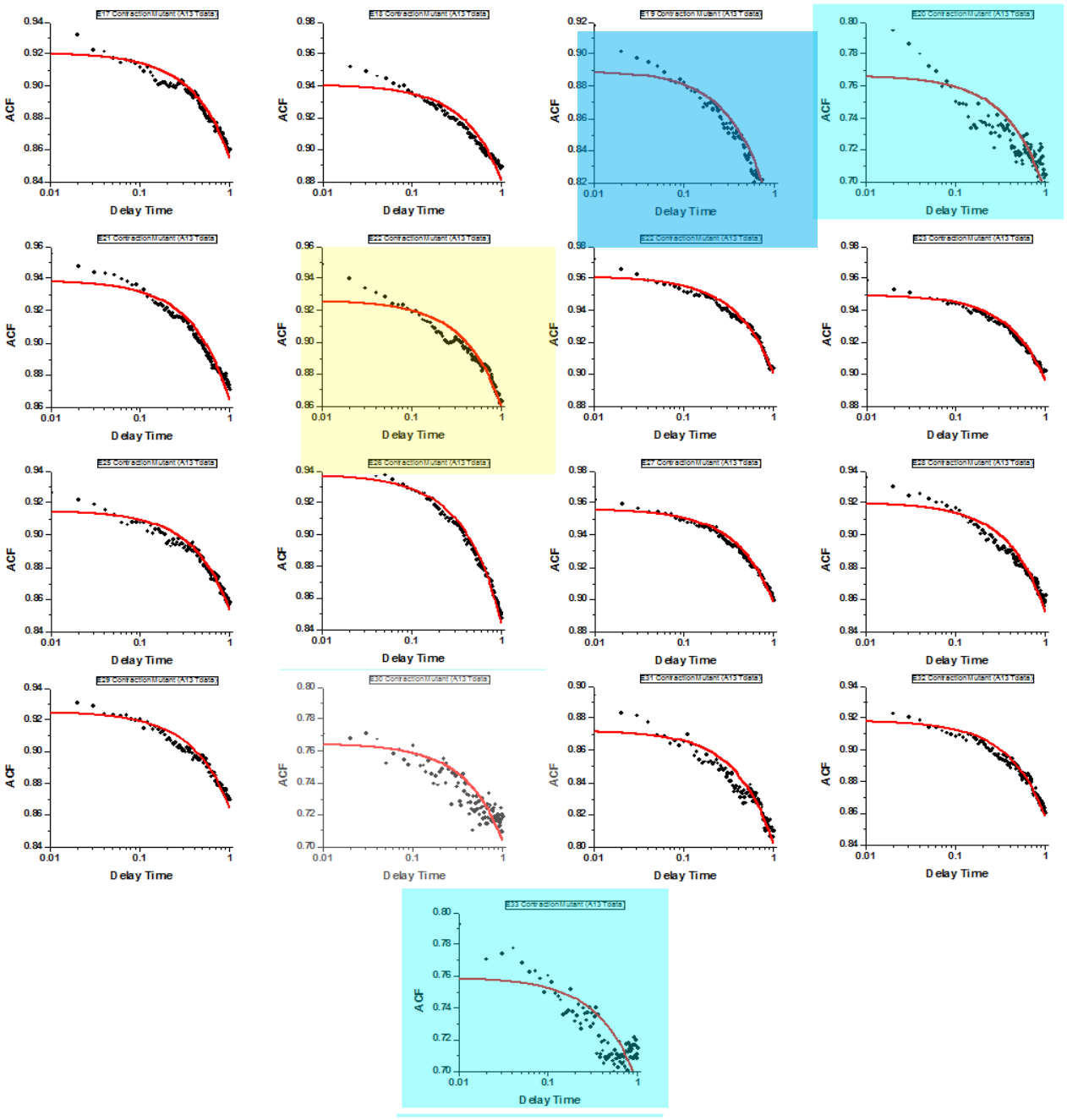

Figure S5. Histograms of all 32 experiments of polarization of fluorescence of contracting myofibrils prepared from the left ventricle of **Tg-WT** mouse. A red line is the fit to a Gaussian curve $y=a\exp[-0.5(x-x_o/b)^2]$. Histograms judged to be nonstandard are outlined in blue. One experiment was omitted.

Figure S5 Continued

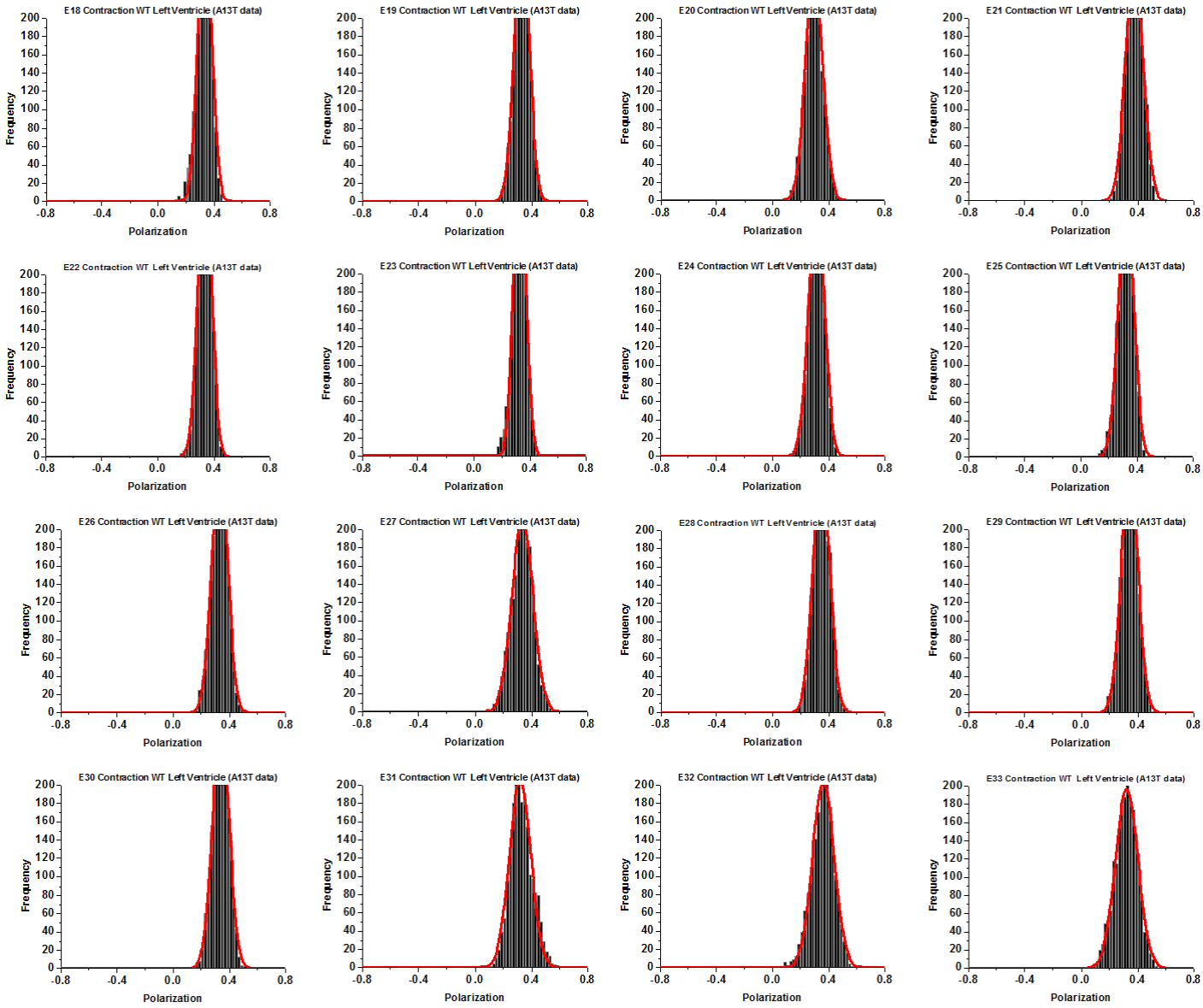

Figure S6

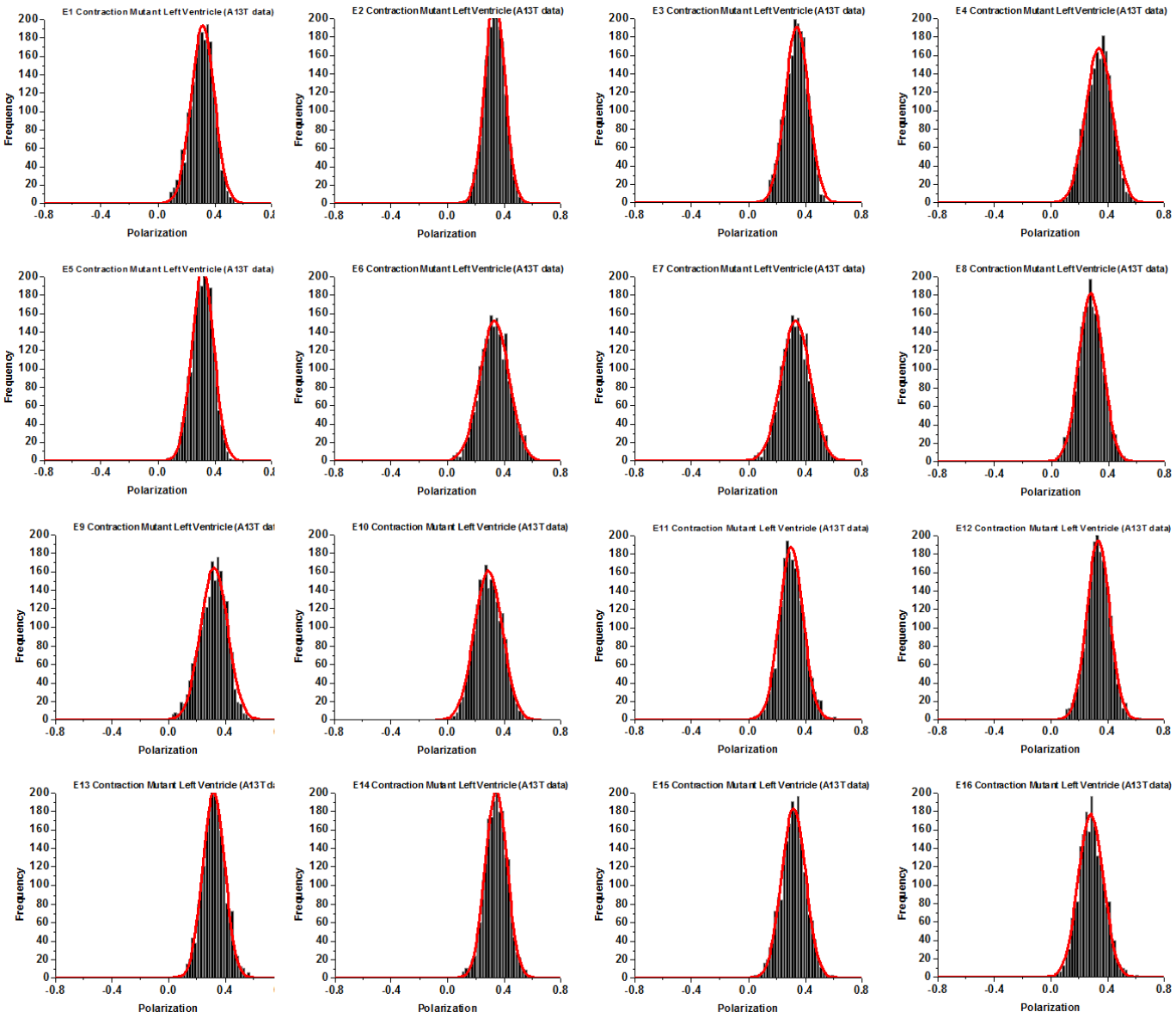

Figure S6. Histograms of all 33 experiments of polarization of fluorescence of contracting myofibrils prepared from the left ventricle of Tg-A13T mouse. A red line is the fit to a Gaussian curve $y=a\exp[-0.5(x-x_o/b)^2]$. Histograms judged to be nonstandard are outlined in blue.

Figure S6 continued

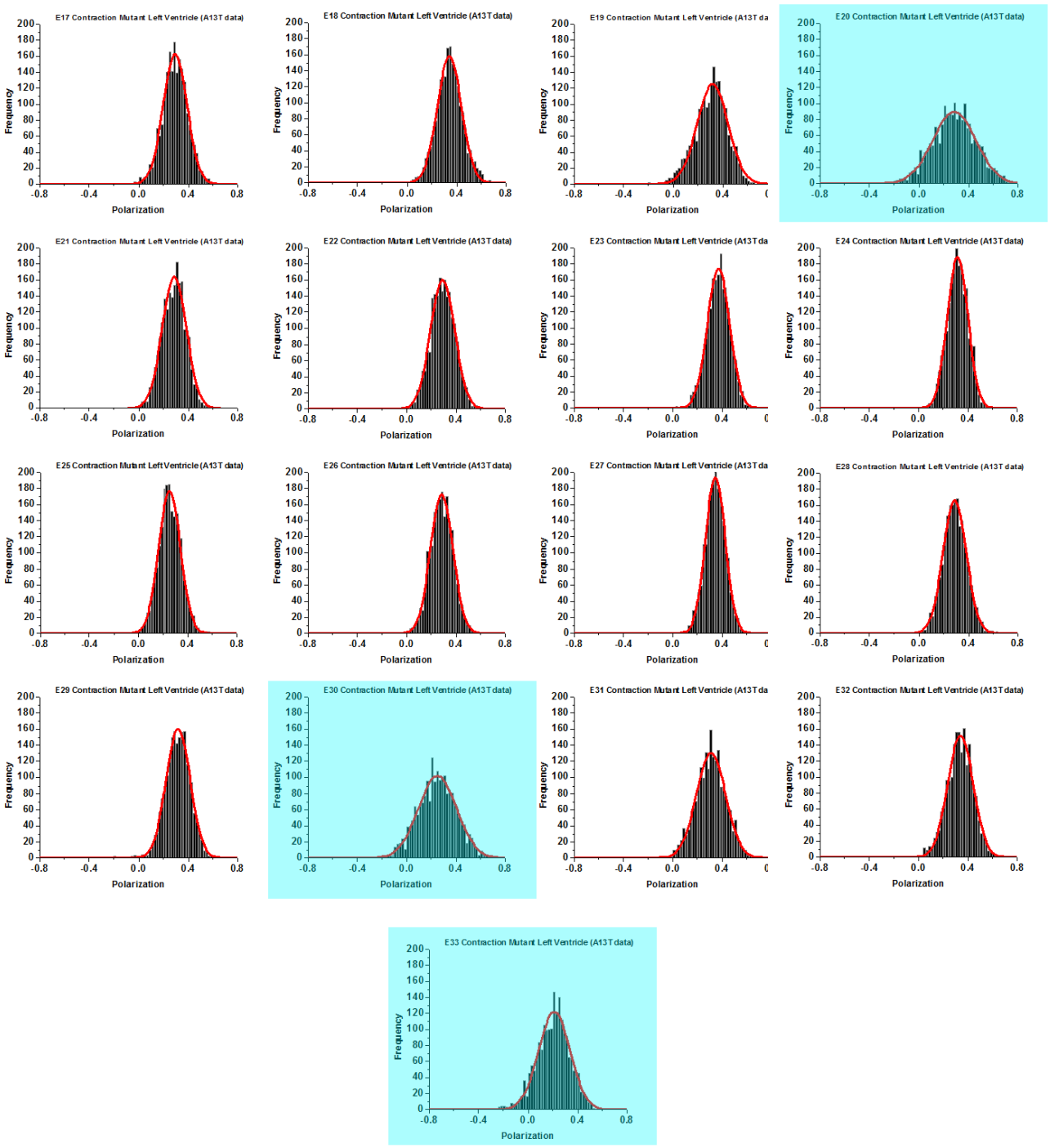

7. REFERENCES

1. Qian H, Saffarian S, Elson EL.. Concentration fluctuations in a mesoscopic oscillating chemical reaction system. Proc Natl Acad Sci U S A (2002) 99(16):10376–81.10.1073/pnas.152007599

2. Kabaeva ZT, Perrot A, Wolter B, Dietz R, Cardim N, Correia JM, et al. Systematic analysis of the regulatory and essential myosin light chain genes: genetic variants and mutations in hypertrophic cardiomyopathy. Eur J Hum Genet (2002) 10(11):741–8.10.1038/sj.ejhg.5200872

3. Poetter K, Jiang H, Hassanzadeh S, Master SR, Chang A, Dalakas MC, et al. Mutations in either the essential or regulatory light chains of myosin are associated with a rare myopathy in human heart and skeletal muscle. Nat Genet (1996) 13:63–9.10.1038/ng0596-63

4. Hougs L, Havndrup O, Bundgaard H, Køber L, Vuust J, Larsen LA, et al. One third of Danish hypertrophic cardiomyopathy patients have mutations in MYH7 rod region. Eur J Hum Genet (2005)13:161–5.10.1038/sj.ejhg.5201385

5. Andersen PS, Havndrup O. Myosin light chain mutations in familial hypertrophic cardiomyopathy: phenotypic presentation and frequency in Danish and South African populations. J Med Genet (2001)38(12):E43.10.1136/jmg.38.12.e43

6. Kazmierczak K, Muthu P, Huang W, Jones M, Wang Y, Szczesna-Cordary D.. Myosin regulatory light chain mutation found in hypertrophic cardiomyopathy patients increases isometric force production in transgenic mice. Biochem J (2012) 442(1):95–103.10.1042/BJ20111145

7. Prochniewicz-Nakayama E, Yanagida T, Oosawa F.. Studies on conformation of F-actin in muscle fibers in the relaxed state, rigor, and during contraction using fluorescent phalloidin. J Cell Biol (1983) 97:1663–7.10.1083/jcb.97.6.1663

8. Borovikov YS, Chernogriadskaia NA.. Studies on conformational changes in F-actin of glycerinated muscle fibers during relaxation by means of polarized ultraviolet fluorescence microscopy. Microsc Acta(1979) 81(5):383–92.

9. Borejdo J, Muthu P, Talent J, Akopova I, Burghardt TP.. Rotation of actin monomers during isometric contraction of skeletal muscle. J Biomed Opt (2007) 12(1):014013.10.1117/1.2697286

10. Dos Remedios CG, Millikan RG, Morales MF.. Polarization of tryptophan fluorescence from single striated muscle fibers. A molecular probe of contractile state. J Gen Physiol (1972) 59:103–20.10.1085/jgp.59.1.103

11. Nihei T, Mendelson RA, Botts J.. Use of fluorescence polarization to observe changes in attitude of S1 moieties in muscle fibers. Biophys J (1974) 14:236–42.10.1016/S0006-3495(74)85911-4

12. Tregear RT, Mendelson RA. Polarization from a helix of fluorophores and its relation to that obtained from muscle. Biophys J (1975) 15:455–67.

13. Morales MF.. Calculation of the polarized fluorescence from a labeled muscle fiber. Proc Natl Acad Sci U S A (1984) 81:145–9.10.1073/pnas.81.1.145

14. Sabido-David C, Hopkins SC, Saraswat LD, Lowey S, Goldman YE, Irving M.. Orientation changes of fluorescent probes at five sites on the myosin regulatory light chain during contraction of single skeletal muscle fibres. J Mol Biol (1998) 279(2):387–402.10.1006/jmbi.1998.1771

15. Hopkins SC, Sabido-David C, Corrie JE, Irving M, Goldman YE.. Fluorescence polarization transients from rhodamine isomers on the myosin regulatory light chain in skeletal muscle fibers. Biophys J (1998)74(6):3093–110.10.1016/S0006-3495(98)78016-6

16. Hopkins SC, Sabido-David C, van der Heide UA, Ferguson RE, Brandmeier BD, Dale RE, et al.Orientation changes of the myosin light chain domain during filament sliding in active and rigor muscle. J Mol Biol (2002) 318(5):1275–91.10.1016/S0022-2836(02)00189-4

17. Elson EL, Magde D. Fluorescence correlation spectroscopy: coceptual basis and theory. Biopolymers(1974) 13:1–28.10.1002/bip.1974.360130102

18. Elson EL, Webb WW. Concentration correlation spectroscopy: a new biophysical probe based on occupation number fluctuations. Annu Rev Biophys Bioeng (1975) 4(00):311–34.10.1146/annurev.bb.04.060175.001523

19. Elson EL.. Quick tour of fluorescence correlation spectroscopy from its inception. J Biomed Opt(2004) 9(5):857–64.10.1117/1.1779234

20. Borejdo J, Szczesna-Cordary D, Muthu P, Calander N.. Familial hypertrophic cardiomyopathy can be characterized by a specific pattern of orientation fluctuations of actin molecules. Biochemistry (2010)49:5269–77.10.1021/bi1006749

21. Mettikolla P, Luchowski R, Gryczynski I, Gryczynski Z, Szczesna-Cordary D, Borejdo J..Fluorescence lifetime of actin in the FHC transgenic heart. Biochemistry (2009) 48(6):1264–71.10.1021/bi801629d

22. Bagshaw CR. Muscle Contraction. London: Chapman & Hall; (1982).

23. Herrmann C, Lionne C, Travers F, Barman T.. Correlation of ActoS1, myofibrillar, and muscle fiber ATPases. Biochemistry (1994) 33(14):4148–54.10.1021/bi00180a007

24. Bershitsky SY, Tsaturyan AK, Bershitskaya ON, Mashanov GI, Brown P, Burns R, et al. Muscle force is generated by myosin heads stereospecifically attached to actin. Nature (1997) 388(6638):186–90.10.1038/40651

25. Szczesna D, Lehrer SS.. The binding of fluorescent phallotoxins to actin in myofibrils. J Muscle Res Cell Motil (1993) 14(6):594–7.10.1007/BF00141556

26. Ao X, Lehrer SS.. Phalloidin unzips nebulin from thin filaments in skeletal myofibrils. J Cell Sci(1995) 108(Pt 11):3397–403.

27. Mettikolla P, Calander N, Luchowski R, Gryczynski I, Gryczynski Z, Zhao J, et al. Cross-bridge kinetics in myofibrils containing familial hypertrophic cardiomyopathy R58Q mutation in the regulatory light chain of myosin. J Theor Biol (2011) 284:71–81.10.1016/j.jtbi.2011.06.014

28. Geeves MA, Holmes KC. The molecular mechanism of muscle contraction. Adv Protein Chem (2005)71(24):161–93.10.1016/S0065-3233(04)71005-0

29. Dantzig JA, Higuchi H, Goldman YE. Studies of molecular motors using caged compounds. Methods Enzymol (1998) 291:307–48.10.1016/S0076-6879(98)91021-7

30. Dantzig JA, Barsotti RJ, Manz S, Sweeney HL, Goldman YE.. The ADP release step of the smooth muscle cross-bridge cycle is not directly associated with force generation. Biophys J (1999) 77(1):386–97.10.1016/S0006-3495(99)76897-9

31. Yanagida T, Oosawa F. Polarized fluorescence from epsilon-ADP incorporated into F-actin in a myosin-free single fiber: conformation of F-actin and changes induced in it by heavy meromyosin. J Mol Biol (1978) 126(3):507–24.10.1016/0022-2836(78)90056-6

32. Yanagida T, Oosawa F. Conformational changes of F-actin-epsilon-ADP in thin filaments in myosin-free muscle fibers induced by Ca2+. J Mol Biol (1980) 140(2):313–20.10.1016/0022-2836(80)90108-4

33. Oosawa F. Actin-actin bond strength and the conformational change of F-actin. Biorheology (1977)14(1):11–9.

34. Ando T.. Propagation of Acto-S-1 ATPase reaction-coupled conformational change in actin along the filament. J Biochem (1989) 105(5):818–22.

35. Hill TL, Eisenberg E, Chalovich JM.. Theoretical models for cooperative steady-state ATPase activity of myosin subfragment-1 on regulated actin. Biophys J (1981) 35(1):99–112.10.1016/S0006-3495(81)84777-7

36. Flavigny J, Richard P, Isnard R, Carrier L, Charron P, Bonne G, et al. Identification of two novel mutations in the ventricular regulatory myosin light chain gene (MYL2) associated with familial and classical forms of hypertrophic cardiomyopathy. J Mol Med (1998) 76(3–4):208–14.10.1007/s001090050210

37. Geisterfer-Lowrance AA, Kass S, Tanigawa G, Vosberg HP, McKenna W, Seidman CE, et al. A molecular basis for familial hypertrophic cardiomyopathy: a beta cardiac myosin heavy chain gene missense mutation. Cell (1990) 62(5):999–1006.10.1016/0092-8674(90)90274-I

38. Watkins H, Conner D, Thierfelder L, Jarcho JA, MacRae C, McKenna WJ, et al. Mutations in the cardiac myosin binding protein-C gene on chromosome 11 cause familial hypertrophic cardiomyopathy. Nat Genet (1995) 11(4):434–7.10.1038/ng1295-434

39. Szczesna D, Ghosh D, Li Q, Gomes AV, Guzman G, Arana C, et al. Familial hypertrophic cardiomyopathy mutations in the regulatory light chains of myosin affect their structure, Ca2+ binding, and phosphorylation. J Biol Chem (2001) 276(10):7086–92.10.1074/jbc.M009823200

40. Szczesna D.. Regulatory light chains of striated muscle myosin. Structure, function and malfunction.Curr Drug Targets Cardiovasc Haematol Disord (2003) 3(2):187–97.10.2174/1568006033481474

41. Alcalai R, Seidman JG, Seidman CE.. Genetic basis of hypertrophic cardiomyopathy: from bench to the clinics. J Cardiovasc Electrophysiol (2008) 19(1):104–10.

42. Yuan CC, Muthu P, Kazmierczak K, Liang J, Huang W, Irving TC, et al. Constitutive phosphorylation of cardiac myosin regulatory light chain prevents development of hypertrophic cardiomyopathy in mice.Proc Natl Acad Sci U S A (2015) 112(30):E4138–46.10.1073/pnas.1505819112

43. Lakowicz JR. Principles of Fluorescence Spectroscopy. New York, NY: Plenum; (1986).

44. Sweeney HL.. Function of the N-terminus of the myosin essential light chain of vertebrate striated muscle. Biophys J (1995) 68:112s–9s.

CHAPTER VIII

BACKGROUND TO OTHER PROJECTS

My previous projects explored the role and influence of actin in the Contraction-Relaxation cycle of cardiac muscles in different mammalian species and in human hearts. The projects gave a clear understanding of the mechanistic function of actin with respect to its contractile protein myosin. This directed the further research into exploring the role of myosin in different aspects of cardiovascular research in an attempt to comprehend the muscle behavior better. According to previous reports, it is quite well known that the acto-myosin structure and function differed in the two ventricles of the hearts of mice, rabbits and human when experiments were performed with labeled actin molecules. Therefore, it was imperative to investigate the role of single point mutations in the complementing contractile protein to actin called myosin, which helps assimilate the contraction mechanism cycle in cardiac muscles of healthy hearts of mammals.

The course of action to develop heart failure can thrive at many levels in one's lifetime. One such pernicious event to lead a heart towards its failing is a mutation in its sarcomeric proteins. Mutations in a part of myosin molecule called the regulatory light chain (RLC) and another sarcomeric protein of troponin I were thus explored. Since normal structure and function of both the proteins are crucial in the smooth working of sarcomeres in myofibrils, mutations in these proteins may prove detrimental to the working of the heart. Lysine to Glutamate (K104E) mutation in RLC and Arginine to Cysteine (R21C) mutation in Troponin I (TnI) was investigated.

It has been shown that phosphorylation of striated muscles play a crucial role in advancing the contraction-relaxation cycles. To understand the role of myosin further, myosin regulatory light chain (RLC) and the influence of phosphorylation on its regulation was investigated in another set of striated muscles – skeletal muscles.

These projects will be discussed in this section of the thesis.

CHAPTER IX

PHOSPHORYLATION OF MYOSIN REGULATORY LIGHT CHAINS HAS MINIMAL EFFECT ON KINETICS AND DISTRIBUTION OF ORIENTATIONS OF CROSS BRIDGES OF RABBIT SKELETAL MUSCLE

Divya Duggal,[*] Janhavi Nagwekar,[*] Ryan Rich, Krishna Midde, Rafal Fudala, Ignacy Gryczynski, and Julian Borejdo

Corresponding author.

[*]D. Duggal and J. Nagwekar contributed equally to this article.

Address for reprint requests and other correspondence: J. Borejdo, Dept. of Molecular Biology & Immunology and Center for Commercialization of Fluorescence Technologies, Univ. of North Texas, Health Science Center, 3500 Camp Bowie Blvd., Fort Worth, TX 76107(e-mail: Julian.Borejdo@unthsc.edu)

1. ABSTRACT

Force production in muscle results from ATP-driven cyclic interactions of myosin with actin. A myosin cross bridge consists of a globular head domain, containing actin and ATP-binding sites, and a neck domain with the associated light chain 1 (LC1) and the regulatory light chain (RLC). The actin polymer serves as a "rail" over which myosin translates. Phosphorylation of the RLC is thought to play a significant role in the regulation of muscle relaxation by increasing the degree of skeletal cross-bridge disorder and increasing muscle ATPase activity. The effect of phosphorylation on skeletal cross-bridge kinetics and the distribution of orientations during steady-state contraction of rabbit muscle is investigated here. Because the kinetics and orientation of an assembly of cross bridges (XBs) can only be studied when an individual XB makes a significant contribution to the overall signal, the number of observed XBs was minimized to ~20 by limiting the detection volume and concentration of fluorescent XBs. The autofluorescence and photobleaching from an *ex vivo* sample was reduced by choosing a dye that was excited in the red and observed in the far red. The interference from scattering was eliminated by gating the signal. These techniques decrease large uncertainties associated with determination of the effect of phosphorylation on a few molecules ex vivo with millisecond time resolution. In spite of the remaining uncertainties, we conclude that the state of phosphorylation of RLC had no effect on the rate of dissociation of cross bridges from thin filaments, on the rate of myosin head binding to thin filaments, and on the rate of power stroke. On the other hand, phosphorylation slightly increased the degree of disorder of active cross bridges.

Keywords: Phosphorylation, Skeletal muscles

. INTRODUCTION

Ca^{2+} binding to thin filaments is a major factor contributing to the initiation of skeletal muscle contraction. But it is thought that in addition to Ca^{2+}, another factor, phosphorylation of the regulatory light chain (RLC) of myosin, may play an important regulatory role. Phosphorylation of skeletal myosin RLC is accomplished by skeletal myosin light-chain kinase (MLCK) with Ca^{2+}-calmodulin acting as a coenzyme. A single twitch or short tetanus induces a small amount of phosphorylation of RLC (10). Phosphorylation and phosphatase-induced dephosphorylation of RLC ensure that the level of phosphorylation during the steady-state contraction is relatively constant. It is well known that the level of phosphorylation increases during heavy use and fatigue (10, 26). The current thinking is that RLC transmits the influence through myosin heavy chain (MHC) and by stabilizing the lever arm. It has been suggested that phosphorylation of RLC may cause charge repulsion with the thick filament core in a heart (46, 72) and, thus, move heads closer to thin filaments. Moving heads closer to actin would increase the likelihood of MHC interacting, which, in turn, is expected to increase the rate of force development. Indeed, Metzger et al. (49) have shown that phosphorylation of RLC in skeletal muscle increased the rate of tension redevelopment at lower [Ca^{2+}] but was unaffected at maximum [Ca^{2+}]. The same was true in in vitro studies of isolated striated (38, 72) thick filaments. Colson et al. (9) used synchrotron low-angle X-ray diffraction to show that phosphorylation of either RLC or cMyBP-C resulted in displacement of cross bridges (XBs) away from the thick filament backbone in cardiac muscle. The other effect of phosphorylation of RLC is the stabilization of the lever arm, which would make it easier to transmit force (63).

Ca^{2+} withdrawal from the myofilament space is a major contributing factor in relaxation (24). It has been shown to influence order and ATPase of XBs in relaxed muscle (67). Dephosphorylated muscle having low ATPase activity and high degree of XB order has been suggested to exist in a new super-relaxed state (SRX) (11). It applies to both skeletal (67) and cardiac muscle fibers (31). We have recently confirmed and quantified these findings by examining the local order of a few XBs in a relaxed half-sarcomere (51).

In this communication, we examine the influence of RLC phosphorylation on the movement and distribution of the orientations of XBs during contraction at the level of individual molecules. There are three fundamental reasons for examining contraction using a small number of XBs.

Steady-state kinetic information about XBs can be obtained from fluctuations of orientations of XBs (in our case, the polarization of fluorescence). The relative size of fluctuations is large only when the number of XBs is sufficiently small (22, 23). This allows determination of the kinetics of contraction by the so-called "mesoscopic" approach, first applied to biological problems by Elson et al. (22, 23). The reason why it is necessary to observe only a small number of molecules at any time is fully explained by Midde et al. (51). In our experiments, a typical number of molecules was 20, and the corresponding fluctuation was ~22%. The use of a small number of molecules eliminates problems associated with nonuniformity of contracting sarcomeres (74), as fully explained by Midde et al. (51). Finally, our method recognizes that only when an individual XB makes a significant contribution to the overall signal, i.e., the total number of XBs is small, its contribution can significantly affect the total distribution of orientations.

Since the kinetics and orientation of an assembly of XBs can only be studied when an individual XB makes a significant contribution to the overall signal, we minimized the number of observed XBs by limiting the detection volume and concentration of fluorescent XBs. The ideal number of molecules to observe is $n = 1$, because then 100% of the signal carries kinetic information.[1] We have chosen to investigate ~20 molecules, because with current technology, the signal from a single molecule in an ex vivo sample is not enough to

collect data with millisecond time resolution and overcome complications due to light scattering and autofluorescence.

There has been many measurements of the dynamics of single motor proteins in vitro because they do not suffer from complications due to high-protein concentration, light scattering, autofluorescence, and the presence of physical barriers, which are encountered by motor proteins (65). Thus, important information about the kinetics of heavy meromyosin (80), myosin V, (25) kinesin (42, 82), myosin VI (81), gizzard heavy meromyosin (2, 41, 61), myosin X (69), plant myosin XI (76), and dynein (60) have been gathered. But it is not clear how the in vitro measurements relate to the in vivo situation in which high protein concentrations lead to exclusion effects (53) and in which motor proteins encounter obstacles when actively transporting material throughout the cell (65). In the case of muscle, the situation is further complicated by the high density of muscle proteins (1).

To ensure that only a few XBs contribute to the signal, we genetically produced light chain 1 (LC1). It was labeled at cysteine 178 with the reactive dye SeTau-maleimide and deliberately exchanged inefficiently with the native LC1 of myofibrils. This inefficient exchange ensured that there were only a few XBs in the detection volume (DV). We recorded the parallel ($\parallel$) and perpendicular ($\perp$) components of fluorescent light emitted by the dye and calculated polarization of fluorescence (PF), the normalized ratio of the difference between these two. We show that the dye is immobilized during critical transient states of the contraction cycle, in spite of the fact that it is attached to LC1 at only one point, rather than more firm attachment at two points (12). PF is known to be a sensitive indicator of the orientation of the transition dipole of a fluorophore (16, 17, 32, 33, 54, 57, 66, 77). We show that PF is different in different transient states of contraction cycle, and, hence, its fluctuations reflect transitions between different states. Autocorrelation analysis of fluctuations in the PF signal revealed the kinetics of a single fluorophore. Statistical analysis revealed the distribution of orientations of XBs during contraction. Although we report that phosphorylation of RLC has no statistically significant effect on the kinetics, a small effect on the degree of order (probability distribution of orientations) of cross bridges of contracting rabbit psoas muscle was observed. In particular, phosphorylation has no effect on the rate of dissociation of cross bridges from thin filaments and on the rate of execution of the power stroke.

3. MATERIALS AND METHODS

3.1. Chemicals and solutions.

The glycerinating solution contained 50% glycerol, 150 mM KCl, 10 mM Tris·HCl pH 7.5, 5 mM $MgCl_2$, 5 mM EGTA, 5 mM ATP, 1 mM DTT, 2 mM PMSF, and 0.1% β-mercaptoethanol. The rigor solution contained 50 mM KCl, 10 mM Tris·HCl at pH 7.5, and 2 mM $MgCl_2$. EDTA rigor had the same composition, except Mg was replaced with 5 mM EDTA. Ca rigor was the same as ordinary rigor, except it contained 0.1 mM $CaCl_2$. Contracting solution contained 50 mM KCl, 10 mM Tris·HCl, at pH 7.5, 5 mM $MgCl_2$, 0.1 mM $CaCl_2$, 5 mM ATP, 20 mM creatine phosphate, and 10 units/ml of 1 mg/ml creatine kinase. The relaxing solution was the same as contracting, except Ca was replaced by 2 mM EGTA, and it did not contain ATP-regenerating solution. All chemicals were from Sigma-Aldrich (St. Louis, MO). Labeling dye SeTau-647-mono-maleimide was purchased from SETA BioMedicals (Urbana, IL).

3.2. Preparation of myofibrils.

Rabbit psoas muscle bundles were washed three times with ice-cold EDTA-rigor solution for 30 min. The purpose of this step was to wash out ATP present in the glycerinating solution without causing contraction. It was followed by an extensive wash with rigor solution (not EDTA-rigor) and homogenization by the Cole-Palmer LabGen 125 homogenizer for 10 s. After a cool down period of 30 s, it was homogenized for a further 10 s. The reason that it was homogenized in rigor solution was to avoid foam, which forms when the homogenization is carried out in EDTA rigor.

3.3. Preparation of phosphorylated and dephosphorylated muscle.

Muscle fibers were naturally dephosphorylated after a few weeks in glycerinating solution. Fibers were phosphorylated by overnight incubation in ice in a solution containing 5 mM ATP, 12.5 mM $MgCl_2$, 0.1 mM $CaCl_2$, 5 μM calmodulin, 0.5 μM MLCK, 20 mM PO_4, and 30 mM KCl. Fibers were further dephosphorylated by overnight incubation in ice in solution containing 5 mM ATP, 2.0 mM $MgCl_2$, 0.1 mM $CaCl_2$, 1 mM EGTA, 20 mM PO_4, and 30 mM KCl. Phosphorylation by incubation in glycerinating solution with phosphatase enzyme inhibitor [20 mM sodium fluoride and 20 mM phosphate (67) were not used to avoid complications due to the direct effect of fluoride on myosin (45, 62, 64)]. Isoelectric focusing gel of phosphorylated (by the addition of MLCK, *lane 2*, and dephosphorylated, *lane 1*) myofibrillar lysate of psoas muscle stained with Pro Q showed that phosphorylated RLC band was 1.52 times stronger than the dephosphorylated band.

3.4. Isoelectric focusing.

To assess the degree of phosphorylation, muscle proteins were analyzed by isoeletric focusing. Total protein concentration was analyzed by the Bradford assay after homogenizing phosphorylated and dephosphorylated muscle in 8 M urea. For isolectric focusing, a sample was diluted to 2.5 mg/ml in a buffer [9 M urea, 130 mM DTT, 20% glycerol, 250 μl of 40% carrier ampholines pH 4–6 (Bio-Rad, Hercules, CA), 10% Triton X-100]. Denaturing isoelectric focusing gel (10 M urea, 18% acrylamide/bis-acrylamide, 20% glycerol, 10% Triton-X 100, 1 ml of 40% ampholines, 60 μl of 10% APS, and 30 μl of TEMED) was run overnight at constant 350 V and fixed with 7% TCA, 50% methanol for 2 h following the procedure of Cooke and colleagues (56, 67). The gel was washed with double-distilled water for 10 min and stained with Diamond Pro-Q phosphoprotein gel stain (Invitrogen) for 3 h in the dark. It was destained with 50 mM sodium acetate and 20% acetonitrile by shaking at room temperature for at least 30 min.

3.5. Expressing LC1.

Recombinant vector (pQE60) containing LC1 with a single cysteine residue (Cys178) was donated by Dr. Susan Lowey (University of Vermont). It was transfected into *Escherichia coli* M15-competent cells. Recombinant clones were selected by resistance to ampicillin. That the sequencing was correct was confirmed by an independent company (Iowa State University of Science and Technology). To overexpress LC1, Luria broth containing 100 μg/ml of ampicillin was used, and induction was achieved with isopropylthiogalactoside. His-tagged LC1 was affinity-purified on a Ni-NTA column. The fractions were eluted by imidazole and were run on SDS-PAGE. This was followed by a Western blot analysis with anti-LCN1 antibodies (Abcam, Cambridge, MA). LC1 fractions were pooled and dialyzed against 50 mM KCl and 10 mM phosphate buffer pH 7.0. SDS-PAGE showed that the dialyzed protein exhibited a single ∼25-kDa band. Protein concentration was determined using the Bradford assay. In some experiments, commercial skeletal human LC1 was used (Prospec, Ness Ziona, Israel).

3.6. Choice of the dye.

The fluorophore of choice must be excited in the red to bypass most contributions by autofluorescence (37), and, therefore, the following two dyes were suitable choices: SeTau 647 or Alexa Fluor 647. SeTau was selected mainly because it was more resistant to photobleaching and brighter than Alexa Fluor 647. Fig. 1 compares the photobleaching of a solution of 1 μM SeTau 647 and 0.7 μM Alexa Fluor 647. At these concentrations, both dyes have the same extinction coefficients at the excitation wavelength used (640 nm). Further reasons to select SeTau were that it has a large Stokes shift (44 nm) compared with Alexa Fluor 647 (20 nm) and high extinction coefficient and quantum yield (0.65).

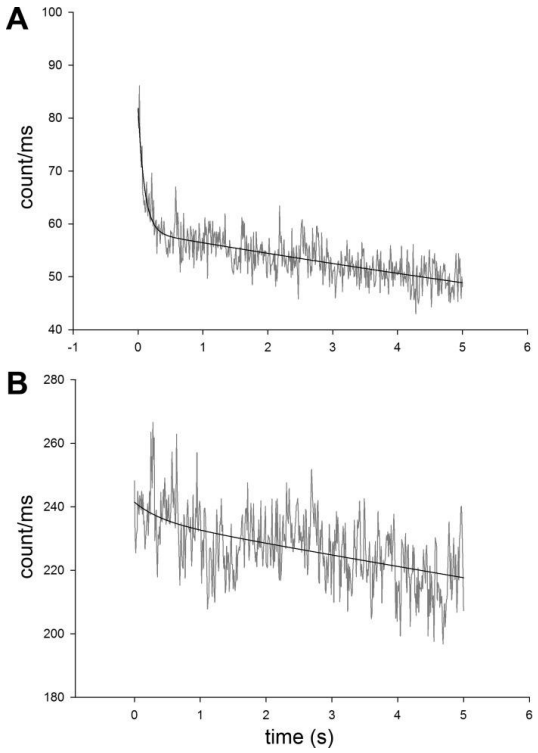

Figure.1. Comparison of photobleaching of Alexa Fluor 647 (*A*) and SeTau (*B*). The photobleaching occurred in two phases: the rate of the first phase, lasting ∼0.5 s was 10.1 s^{-1} for Alexa Fluor 647. It was 4.2 times slower for SeTau. The rate of the second phase was 0.036 s^{-1} for Alexa Fluor 647 and ∼3 times

slower for SeTau. Note that the mean count rate of SeTau was 4.2 times larger than that of Alexa Fluor 647. The laser (640 nm) power was 0.9 mW before the objective.

The initial rate of photobleaching was 10.1 s^{-1} for Alexa Fluor 647 and 2.4 s^{-1} for SeTau. The diffusion of dye molecules were slowed down by the addition of 80% glycerol to increase the time they spent in the laser beam before diffusing out. Photobleaching is more dramatic in the case of muscle, in which molecules are not merely slowed down, but the same XBs are illuminated for the entire experiment (20 s). The protection from photobleaching of SeTau is achieved by nanoencapsulation of the squaraine moiety of the dye chromophore system in a mixed aliphatic-aromatic macrocycle. Although SeTau has a slightly lower extinction coefficient at 640 nm than Alexa Fluor 647, its overall fluorescence is more than compensated by its high quantum yield (0.65) and by the fact that its quantum yield increases 70% beyond that of Alexa Fluor 647 upon protein binding. All in all, after a 1-s exposure to 640 nm excitation, the fluorescence intensity of SeTau was 4.2 times larger than fluorescence intensity of Alexa Fluor 647. All of these attributes are necessary for extracting the maximum number of photons from a few molecules.

3.7. Labeling of LC1.

LC1 (and not RLC) was chosen as the site of labeling to ensure that the phosphorylation site is not disturbed by the dye. Labeling RLC can conceivably disturb the extension of the NH_2 terminal of RLC and phosphorylation of Ser-15. It was labeled at position 178 with a 5 molar excess of protein over SeTau overnight on ice. After initial purification by dialysis against 50 mM KCL, 10 mM phosphate buffer pH 7.0, labeled LC1, was passed through a Sephadex G50 LP column to eliminate free dye. The dye and protein were complexed in a 0.2:1 ratio.

3.8. Cross-linking.

Contracting myofibrils must be completely still while recording polarized fluorescence. Otherwise, fluctuations could be attributed to the "number" fluctuations, i.e., the change in the number of fluorescent XBs in the detection volume as the myofibril moves through the volume. In addition, we want to avoid muscle shortening during LC1 exchange. Although the exchange solution contains ATP and EGTA, it is possible that some troponin C becomes defective during the exchange and some myofibrils become Ca-insensitive. To completely immobilize myofibrils without affecting their ATPase, we treated myofibrils with a water-soluble cross-linker 1-ethyl-3-[3-(dimethylamino)-propyl]-carbodiimide (EDC) (3,30, 78). 20 mM EDC was added to 1 mg/ml myofibrils in Ca-rigor solution. Myofibrils were incubated for 20 min at room temperature. The reaction was stopped by adding 20 mM DTT. The pH of the solution (7.5) remained unchanged throughout the 20-min reaction. We measured ATPase by malachite green phosphate assay method, and confirmed that under our conditions X-linking had no effect on ATPase. The absence of shortening was verified by labeling the myofibrils with a 10-nM rhodamine-phalloidin and observing contraction in a TIRF microscope. No shortening was observed.

3.9. LC1 exchange into myofibrils.

To ensure a small number of XBs in the DV, we incubated myofibrils under very mild conditions [20 min at 30°C (79)] with very low concentration (5–10 nM) of SeTau-LC1 (the usual exchange takes place at 37°C for 1/2 h.). 1 mg/ml of freshly prepared myofibrils were incubated with fluorescently tagged LC1 in the exchange solution [similar to the one used in (39)]: 15 mM KCl, 5 mM EDTA, 5 mM DTT, 10 mM KH_2PO_4, 5 mM ATP, 1 mM trifluoperazine (TFP), and 10 mM imidazole (pH 7).

3.10. Data collection.

Myofibrils are inefficiently exchanged, as described above, with SeTau-LC1. The 640-nm excitation light beam is focused to the diffraction limit on the overlap band of a myofibril. Fluorescence is collected a few nanoseconds after the initial pulse of exciting light is delivered. Fig. 2 explains how this procedure eliminates the contribution of scattered light: Because scattered light has no fluorescence lifetime, this eliminates the contribution of light scattering from our experiment.

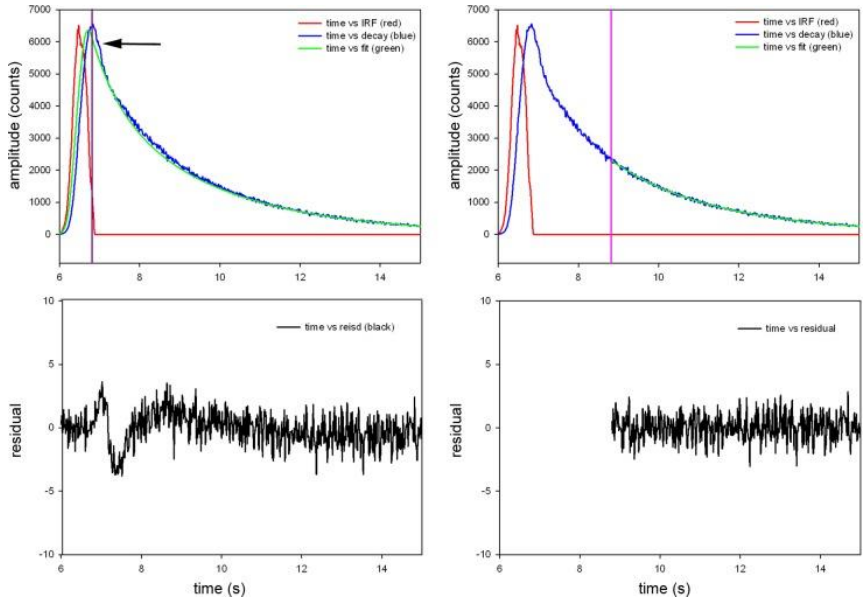

Figure 2: Fluorescence decay of parallel polarized light from rigor myofibril. *A*: no gate applied, i.e., the signal collection is started at the peak of the signal (violet line) and continued through the complete fluorescence decay. This includes scattered light (arrow). *B*: the residuals have significant dip at the time corresponding to scattering of light and are not well fitted by a straight horizontal line. *C*: gating applied. In TCSPC systems, photons are collected one-by-one. Here, photons detected within 8.8 ns of the start of the measurement (an arbitrarily determined point in time with relation to the excitation pulse) are eliminated from our measurements. All that remains are photons collected 8.8 ns or later from the start of the measurement (indicated by the violet line). *D*: residuals of the gated signal are quite flat. The same procedure is applied to perpendicular polarized light.

The laser beam is next redirected to a neighboring half-sarcomere, adjusting the laser power to make sure that each sarcomere provides a similar photon rate. If this power adjustment is not done, the differences between FWHMs of PF become statistically uninterpretable (51) (also see DISCUSSION below). The process is repeated 20–30 times, i.e., we obtain 40,000–60,000 PF values from each myofibril.

The detection volume was estimated by measuring the FWHM of an image of 20-nm fluorescent beads in the axial and lateral dimensions, which were 700 nm and 400 nm, respectively. The theoretical detection volume (DV) is equal to $(\pi/2)^{3/2}\cdot(0.400\ \mu m)^2\cdot(0.700\ \mu m) = 0.6\ \mu m^3$. Because of edge effects, the actual DV is 2.8 times greater = 1.7 μm^3 (7). The concentration of myosin in muscle is 0.1 mM (1); therefore, the DV contains $\sim 3\times10^5$ myosin XBs. The number of observed (fluorescent) XBs in this volume is estimated to be 4 (because of the inefficient exchange) (see RESULTS). A PicoQuant MicroTime 200 confocal system (PicoQuant, Berlin, Germany) coupled to an Olympus IX71 microscope was used to acquire the fluorescence data, as described earlier (51). Before each experiment, fluorescence of an isotropic solution of a dye with long fluorescence lifetime (50 nM rhodamine 700) was measured, after first splitting into the

parallel and perpendicular channels. Since rhodamine 700 is small (and, hence, its solution is nearly isotropic), the signal into each detector was attenuated to make sure that they gave identical readings. The PicoQuant is the time-resolved instrument capable of lifetime imaging with single-molecule detection sensitivity. Each photon is recorded individually by the time-correlated single photon counting electronics in time-tagged time-resolved mode. A 640-nm pulsed laser provided linearly polarized excitation parallel to the myofibrillar axis, which was always vertical. Fluorescence was collected 7.36 ns after the beginning of the excitation pulse, or 8.8 ns after the arbitrary chosen start point of the measurements (see above). A 60×, 1.2 NA water immersion objective of the Olympus IX71 collected fluorescent light and passed it through a 650-nm-long pass interference filter before going through the confocal pinhole. A birefringent prism separated the vertically and horizontally polarized fluorescent light, and Avalanche Photodiodes measured the emitted light. Figure 3 shows images of a contracting myofibril.

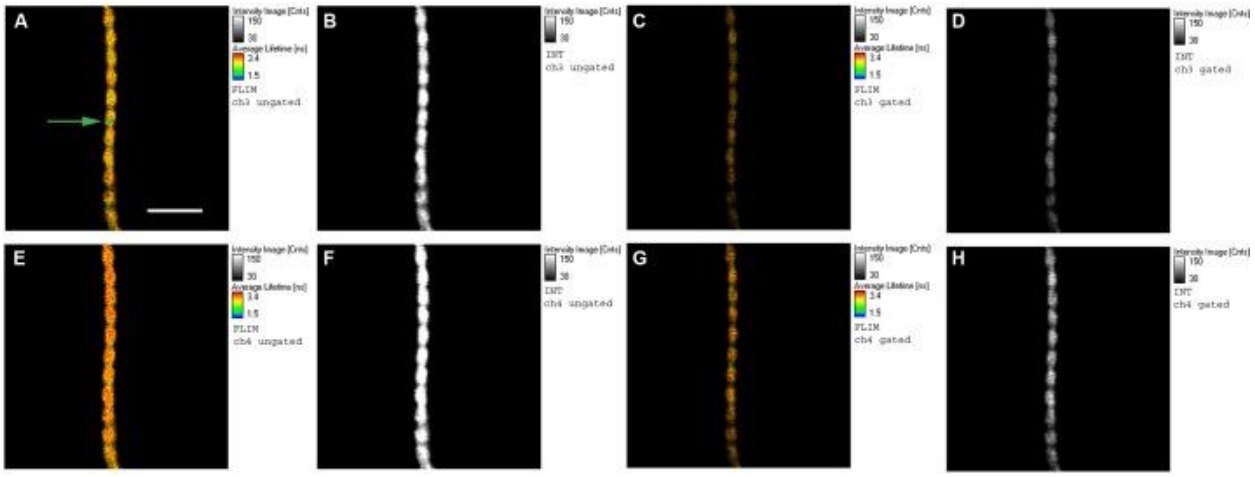

Figure 3: Images of contracting phosphorylated myofibril, effect of gating. *A*, *B*, *E*, and *F*: ungated images. *C*, *D*, *G*, and *H*: the same images after gating. The color scale (in FLIM images) and contrast scale (in intensity images) are much improved by gating. The green circle pointed to by the green arrow in *A* is a projection of the confocal aperture on the sample plane. Top row: images obtained with analyzer perpendicular to the myofibrillar axis. Bottom row: images obtained with analyzer parallel to the myofibrillar axis. Notice that perpendicular images are weaker than parallel images, indicating that a sample is anisotropic. *A*, *C*, *E*, *G*: FLIM images. *B*, *D*, *F*, *H*: intensity images. The fluorescent lifetime scales are in nanoseconds, with 1.5 ns corresponding to blue and 3.4 ns to red. The intensity scales are in counts with 30 corresponding to black and 150 to white. Native myofibrillar LC1 was exchanged with 10 nM SeTau-LC1. Scale bar = 5 μm, sarcomere length = 2.1 μm. Sarcomere length does not change during contraction because of cross-linking (30, 78). Images were acquired on a PicoQuant Micro Time 200 confocal lifetime microscope. The sample was excited with a 640-nm pulsed laser and observed through a LP 650 filter.

3.11. Statistical analysis.

Origin v.8.6 (Northampton, MA) was used to compute autocorrelation functions and fit the data by a nonlinear (Levenberg-Marquardt) algorithm for χ^2 minimization. SigmaPlot 11 (Systat Software, San Jose, CA) was used to compute histograms.

4. RESULTS

4.1 The number of observed myosin molecules.

Fluorescence correlation spectroscopy (FCS) analyzes the fluctuations in the signal as fluorescent molecules in solution diffuse through the detection volume. It is well established that the autocorrelation function of fluctuations at delay *time 0* is equal to the inverse of the number of molecules contributing to fluctuations $n = 1/\mathrm{ACF}(0)$ (19, 21, 44). Six ACF's were obtained from solutions of the fluorophore in the range of 1.29–77.3 nM. Extrapolating the plot of concentration vs. 1/ACF(0) to 1 molecule revealed that a single molecule of SeTau illuminated with 0.2 μW of laser power corresponded to ~75 counts per channel [i.e., total fluorescence ($I_{total} = I_{\parallel} + 2^* I_{-}$) from one molecule of SeTau at 0.2 μW laser power was 225 counts/s (51)]. We use this fact to estimate the number of molecules contributing to the signal. Fig. 4*A* shows the intensities of perpendicular and parallel channels of a typical contracting myofibril. The polarized intensities in ∥ (ch3) and − (ch2) channels were 2.45 and 1.13 counts/ms, respectively, giving total intensity $I_{total} = I_{\parallel} + 2 \cdot I_{-} = 4.71$ counts/ms. Therefore, with the power of the laser of 0.2 μW, the number of observed molecules is 20. The actual power used varied between 0.2 and 0.4 μW (to keep the count in ch1 at ~2 counts/ms), so we estimate that there were between 20 and 40 XBs in the DV. However, it should be emphasized that as long as the number of cross bridges is mesoscopic, the exact number does not matter, i.e., 20 molecules should give the same result as 40 molecules.

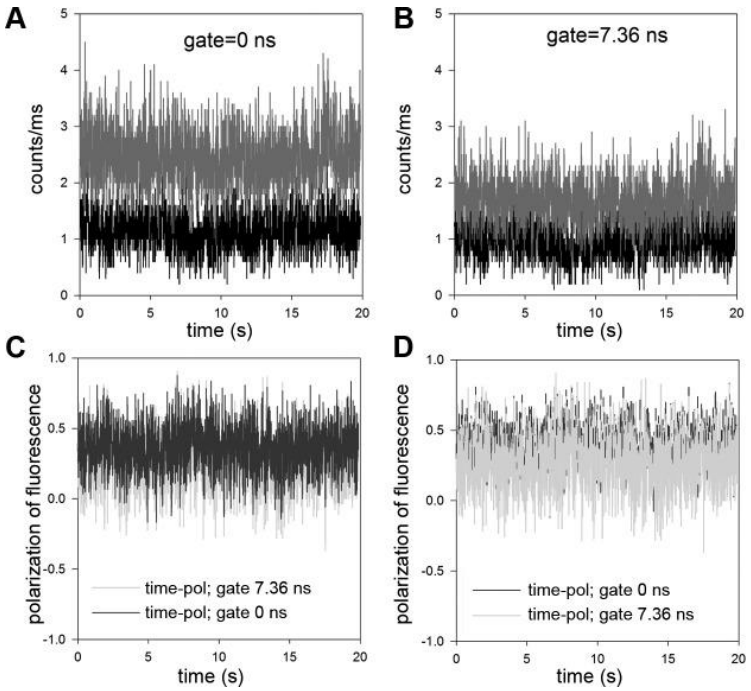

Figure 4: *A*: typical time course of intensity of contracting MLCK phosphorylated psoas muscle myofibril. Ch3 (red) and Ch2 (black) are the fluorescence intensities polarized parallel ($I_{\parallel}$) and perpendicular ($I_{\perp}$) to the myofibrillar axis, respectively. The direction of excitation polarization is ∥ to the myofibrillar axis. The gate time was set to 0 ns. *B*: same time course but with the gate set to 7.36 ns. Note the decrease of intensity due to elimination of light scattering. *C*: polarization of fluorescence of ungated (blue) and gated (green) at 7.36-ns signals. To emphasize the differences, the ungated signal is plotted on top of the gated signal in*D*. Laser intensity was 0.2–0.4 μW.

Approximately 20 rotating cross bridges imply that the fluctuating signal is 22% of the mean. The precision of measurement is approximately equal to $1/\sqrt{X}$, where X is the number of fluctuations detected. Therefore, to get 1% precision we have to analyze 10,000 fluctuations. The characteristic life-time of fluctuation due to rotations of the lever arm is of the order of milliseconds (34). Therefore, 10,000 fluctuations will occur in 10 s. We collected the data over 20 s.

4.2 Kinetics

XBs constantly change orientation while undergoing the mechanochemical cycle, thus causing fluctuations of PF. PF fluctuate about their equilibrium values with certain rate constants. The transitions between various enzymatic and mechanical states of muscle are governed by a Poisson process. A single fluctuation cannot predict a chemical rate constant, but the rates of many fluctuations are the same as rate constants that govern macroscopic dynamic processes (58). For certain processes, the effect of fluctuations on the rate constants were analytically predicted (22). Here, we attempt to predict rate constants from fluctuation caused by a rotating XB. An autocorrelation function, ACF(τ), of FP fluctuations accomplishes this when fluctuations are due only to XBs. By definition, $ACF(\tau) = \langle \delta FP(t)\delta FP(t+\tau) \rangle$ where $\langle\ \rangle$ denote averaging over a long time period (20). The system is in a steady state [dependence of ACF(τ) on t is eliminated]. Fluctuations of PF as in Fig. 3*D* can arise from *1*) random noise, *2*) a change in the number of fluorophores in the DV (22, 44), and *3*) a change of orientation of the SeTau transition dipole imbedded in LC1. The contribution *1*) to fluctuations is eliminated because random noise is uncorrelated. The contribution *2*) is not significant because each myofibril is cross-linked and does not change in length, so no fluorophores can enter or leave DV during contraction. In any case, a change in signal can only be caused by rotation, and myofibrils do not twist during contraction. We conclude that the fluctuations arise solely because of a change in orientation of the SeTau transition dipole embedded in LC1. The autocorrelation function is initially large because the average product of a fluctuation amplitude at some time t_o and at short time later, τ, must be large, because the amount of fluctuation at time t_o [$\delta F(t_o)$] is not much different than $\delta F(\tau)$. The average of the product [$\delta F(t_o)\delta F(t+\tau)$] is close to its maximal value of $[\delta F(\tau)]^2$. Since the signal average is 0, when τ is large, the amplitude is likely to be the same above and below the average, i.e., on the average $\delta F(t_o) = -\delta F(\tau)$. Therefore, the autocorrelation function at long τ tends to decay to 0. The rate of decay of autocorrelation function from maximal value to 0 is a reflection of how quickly the average fluctuation crosses the 0 baseline.

The exact shape of the autocorrelation function depends on the model assumed for the chemical reaction that drives the cycling of the XBs. In the past, we used a simple ON-OFF model, where cross bridges were either immobilized (attached) to thin filaments or mobile (detached) from thin filaments (51). Here, we use a more realistic model. The model must include transitions between three fundamental states as illustrated in Fig. 5. Each state has to be characterized in terms of mobility of LC1-SeTau. This is done by measuring the *time 0* anisotropy, steady-state anisotropy, and the lifetime of SeTau in each of the transient states. A FluoTime 200 fluorometer (PicoQuant) was used, and measurements were done at room temperature (50). The sample was excited by a 635-nm pulsed (at 20 MHz) diode laser and observed through a 670-nm monochromator with an additional 650-nm long-pass filter. The time resolution was <10 ps, and the FWHM of the pulse response function was less than 100 ps. The anisotropy decays and lifetimes were analyzed by a multiexponential model using FluoFit software (PicoQuant). Typical records of anisotropy decay of SeTau coupled to LC1 showed that the anisotropy decay was composed entirely of a single exponential decay. Records of SeTau-LC1 coupled to myofibrils gave steady state anisotropy = 0.071.

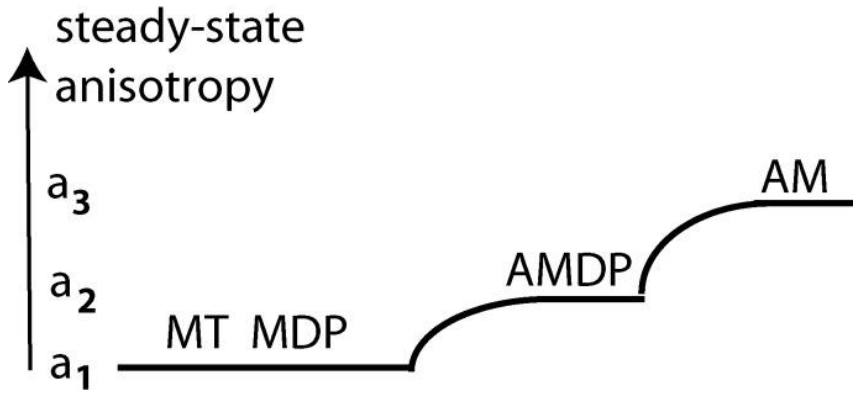

Figure 5: The three-state model of muscle contraction. M, myosin; D, ADP; P, inorganic phosphate; A, F-actin; T, ATP. The polarizations of fluorescence associated with different cross bridge states. a_1, a_2 and a_3 are amplitude of polarizations.

The cycle begins with a prehydrolytic state MT, in which myosin (M) has dissociated from thin filament by binding ATP (T), which is hydrolyzed to assume a posthydrolytic MDP state (43). After hydrolysis, the products remain bound to M. The MDP state is characterized by partially open cleft between upper and lower subdomains of the 50-KDa domain, as well as a lever arm in the UP position (13). This complex, as well as MT, are free to rotate in the myofilament space and have low steady-state anisotropy a_1 (Table 1). Next, the XB binds to actin to assume a prepower stroke state AMD, which becomes partially immobilized.Table 1 shows that its steady state anisotropy becomes 0.116,[2] which is represented in Fig. 5 by value ofa_2. The AMDP state is characterized by a partially open cleft between the upper and lower subdomains of a 50-kDa domain and a lever arm in the UP position (13). Next, dissociation of P from AMDP state initializes a XB power stroke involving transition to a rigor-like AMD state and a final rigor (AM) state. This state has the highest steady-state anisotropy a_3. AMD and AM states are characterized by a closed cleft and the lever arm in the DOWN position. Table 1 shows that the absence of a nucleotide further increases steady-state anisotropy. Transition from AMDP to AM is a power stroke. This is represented in Fig. 5 as a transition a_2 to a_3. This may occur in several steps (13, 34). Finally, the XB rapidly dissociates from actin by binding fresh molecule of ATP, (assuming low anisotropy a_1), after which the cycle repeats itself.

Anisotropies of intermediate states of XB cycle

	Time zero anisotropy, R_0	**Steady-State Anisotropy, a**	**Correlation Time (ns)**
LC1	0.325	0.077	0.777
AM	0.225	0.210	1.484
MT	0.232	0.071	0.780

AMDP	0.236	0.116	0.999

XB, cross bridge; LC1, light chain 1; AM, actin-myosin; MT, myosin with ATP; AMDP, actin-myosin with ADP ATP; ns, not significant.

Table 1 shows that the dye does not need to be attached at two points to the light chain, although the procedure described by Corrie et al. (12) is more attractive. Of course, it needs to have a well-defined PF in different enzymatic and mechanical states of the muscle.

The autocorrelation function of such a system is (47):

Origin 8.6 was used to fit the experimental data (circles) to the R_3. The red lines in **Fig. 6** are the best nonlinear fit to *Eq. 1*. Shown are four representative traces from 28 experiments on MLCK-phosphorylated muscle. Fluoride has a strong effect on enzymatic properties of myosin (8, 45, 62, 64). To avoid using fluoride to inhibit dephosphorylation, phosphorylation was achieved by adding MLCK, as described in the MATERIALS AND METHODS.

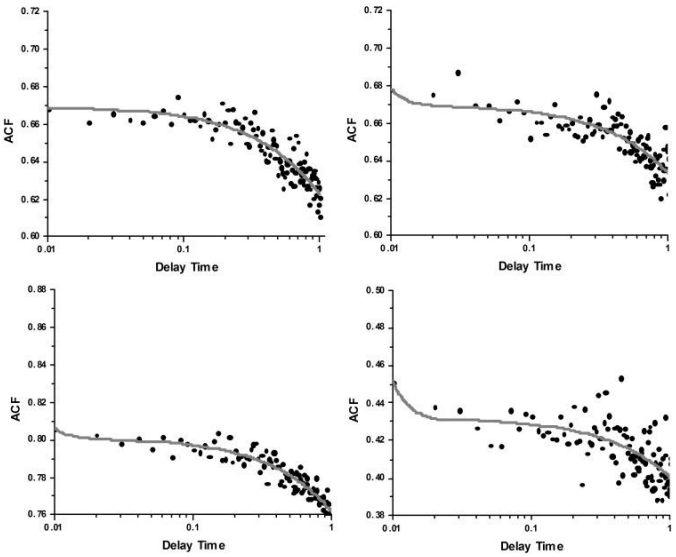

Representative traces of normalized autocorrelation functions of polarization of fluorescence of contracting MLCK phosphorylated psoas myofibril. Circles are experimental data, and a red line is the fit to *Eq. 1*. The fact that the correlation decays in time indicates that the orientation of absorption-emission dipoles change in time. The fact that ACF decays to a value >0 is due to the fact that mean polarization was nonzero (approximately −0.23). Delay time is in seconds.

The data could not be fitted with two-state (ON and OFF) mode. The fit was not so good for dephosphorylated myofibrils. The average values of *a* and *k* were determined by experiment. It remains to assign experimental *k* values to the model. The average values are summarized in Table 2.

Experimental values of the kinetic coefficients from 26 experiments on dephosphorylated and phosphorylated XBs in contracting psoas myofibrils

Myofibrils	k_1, s^{-1}	k_2, s^{-1}	k_3, s^{-1}
Dephosphorylated	961 ± 560	1.9 ± 2.7	0.19 ± 0.14
MLCK phosphorylated	689 ± 484	0.30 ± 0.30	0.18 ± 0.20

MLCK, myosin light-chain kinase.

The assignment of k_1 is obvious: it is the fastest of the processes; therefore, it must be myosin head dissociation from thin filaments: AM → MT. k_2 and k_3 are symmetrical in *Eqs. 1–3*. However, the rate of myosin binding to actin is more likely to be higher than the rate in the power stroke. Since the rate k_2 is higher (at least for dephosphorylated muscle) than k_3, we assign k_2 as the rate of myosin head binding to actin and k_3 as the power stroke rate.

None of the differences in *k*s of phosphorylated and dephosphorylated myofibrils were statistically significant, primarily because the SD of measurements was so large. The difference in k_1 of −261.782 was not statistically significant ($t = -1.625$, $P = 0.112$ with 41 degrees of freedom). The 95% confidence interval for difference of means was −543.615 to 128.311. The difference in k_2 of −1.642 was not statistically significant at 95% confidence level. The difference in k_3 of −0.0122 was not statistically significant ($t = -0.223$ with 40 degrees of freedom, $P = 0.824$). The 95 percent confidence interval for difference of means was −0.123 to 0.0986.

We conclude that phosphorylation of RLC induces no obvious changes in the mechanochemical cycle of myosin. We can only say that, under ex vivo conditions, the mean rate of XB dissociation of actin is 825 s^{-1}, the mean rate of myosin binding to thin filaments is 1.1 s^{-1}, and the mean rate of the power stroke is 0.19 s^{-1}.

4.3 Distribution of XB orientations

The easiest way to characterize spatial distributions of the transition dipole orientations of the dye is to plot polarization values vs. the number of times that a given orientation occurs during a 20-s experiment. **Fig. 7** shows representative probability distributions of dephosphorylated myofibrils.

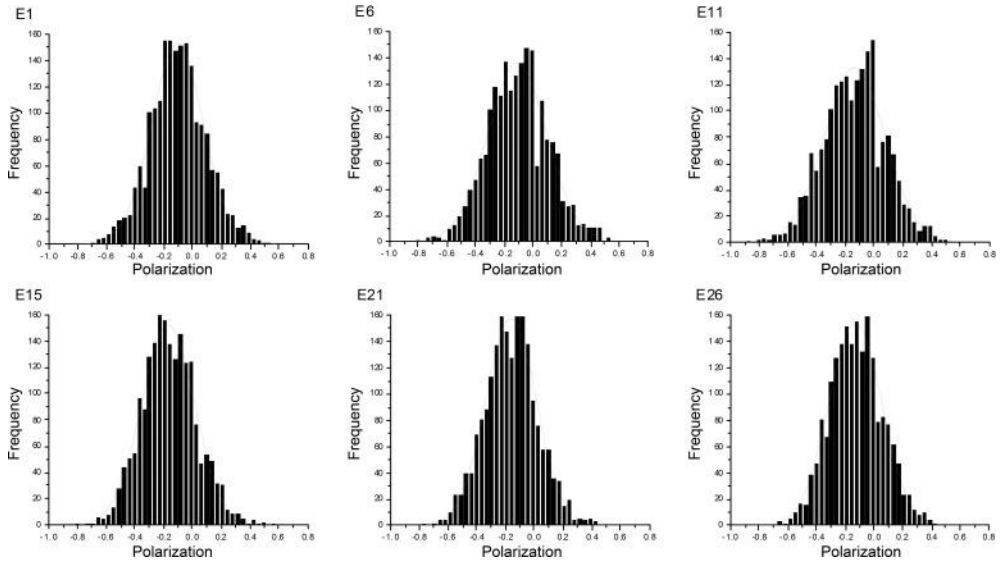

Selected examples of the probability distributions of orientations of cross bridges (XBs) of contracting myofibrils containing dephosphorylated RLC. Dephosphorylation was affected by the addition of EGTA to WT myofibrils.

The difference in FWHM, while small in absolute terms (6%), was statistically significant ($P = 0.012$, $t = 2.634$ with 45 degrees of freedom). The difference of the mean polarization of −0.107 was also statistically significant ($t = -10.209$ with 45 degrees of freedom, $P = <0.001$). 95 percent confidence interval for difference of means was −0.128 to −0.0859. We conclude that phosphorylation makes a small difference to the degree of order of active cross bridges (Table 3).

Comparison of FWHMs of 28 probability distributions of phosphorylated and dephosphorylated myofibrils

Myofibrils	FWHM	Mean Polarization	Mean Intensity, counts/ms
Dephosphorylated	0.47 ± 0.04	−0.13 ± 0.03	2.305 ± 0.336
MLCK phosphorylated	0.50 ± 0.03	−0.23 ± 0.03	1.416 ± 0.387

FWHM, full-width half-maximum.

5. DISCUSSION

We studied the effect of phosphorylation on skeletal cross-bridge kinetics and the distribution of orientations during steady-state contraction of muscle. By sacrificing the idea of measuring the signal from an individual XB and instead concentrating on detecting the signal from a few molecules, we gained the ability to increase the time resolution of ex vivo measurements in muscle to a few milliseconds. To achieve this, we exchanged fluorescent LC1 with native LC1 of myofibrils under exceedingly mild conditions (seeMATERIALS AND METHODS). Such mild labeling required the use of a microscope with single-molecule sensitivity such as the PicoQuant MicroTime 200. In a typical experiment, we observed about 20 XBs. Minimization of inhomogeneities was possible by focusing the exciting laser light on a single half-sarcomere. The dye of choice was SeTau, which was excited in the red and observed in the far red. Using SeTau dye decreased photobleaching, increased signal intensity, and decreased autofluorescence. The fluorescent signal was gated, assuring no interference from scattering.

5.1 Kinetics.

Determination of k_1, k_2, and k_3. Dissociation of the myosin head from the thin filaments is the most rapid process occurring during contraction. Since dissociation is the only rapid process detected by our method, it was natural to assign it to k_1. The SD of the means of phoshorylated and dephosphorylated myofibrils was so large as to make the differences between the means statistically insignificant. The average value of k_1 was 825 s^{-1}. Similarly, the large value of the SD of the means of k_2 of dephosphorylated myofibrils was so large as to make the difference statistically insignificant. The mean rate of myosin binding to thin filaments was 1.1 s^{-1}. Finally, there was no statistical difference between the rates of power strokes in phosphorylated and dephosphorylated myofibrils k_3 (the average rate was 0.19 s^{-1}).

The detection of a few myosin molecules in ex vivo ventricle with millisecond time resolution is not technically easy. The main problem is that the signals are weak. Weak Gaussian signals with low signal-to-noise (S/N) ratio have intrinsically large relative FWHM, and this applies as well to the ratio of these signals, such as polarization of fluorescence, as shown by (51). In addition, there are at least five reasons for such a large FWHM or SD of measurements: *1*) Nonuniform incorporation of LC1 into sarcomeres (Fig. 3); *2*) incomplete degree of phosphorylation of myofibrils (Supplemental Fig. S1); *3*) low steady-state anisotropy of SeTau and relatively small differences in anisotropy between different mechochemical steps (Table 1); *4)* large variability between samples (Ventricles are prepared in Florida and stored for various periods at −80°C). They are then shipped on ice to Texas and stored for a few days at −20°C before the experiment is performed. Each of these steps imposes some variability on the quality of the sample; and *5*) the fitting program must estimate six parameters. This allows it a great freedom in selecting the best fit. Most of these reasons are beyond our control; e.g., nonuniformity of muscle labeling (#1) is caused by extremely low concentration of the dye, #3 is an intrinsic property of SeTau and replacing it with Alexa Fluor 647 would result in even smaller S/N, #5 could have been reduced by enforcing limits on the "a" values, but it would have imposed additional arbitrary elements on the model. More experiments are needed to decrease SD, e.g., to make more measurements at room temperature, perform additional measurements at 37°C, and better control #2 and #4.

No effect of phosphorylation of RLC is consistent with the earlier conclusion of Metzger et al. (49) that phosphorylation of RLC plays no role in the rate of tension redevelopment and maximum isometric tension at saturating concentrations of Ca^{2+}. It is also consistent with the earlier result from this laboratory, which suggested that the duty cycle was unaffected by phosphorylation (51), suggesting that isometric force was

not changed by phosphorylation of RLC. Also, no effect on force was observed at saturating Ca^{2+}concentrations in skeletal (73) and cardiac (55) muscle, consistent with earlier results (4). The fact that the rate was so slow leads to the conclusion that prevention of shortening by cross-linking slows down, but does not prevent XBs from executing power strokes, suggesting that they can reach neighboring target zones. If they were unable to reach neighboring target sites, no fluctuations due to rotation of XBs would have occurred, i.e., ACF would have been flat. The mechanical cycle goes on in spite of cross-linking, like the enzymatic cycle (29). Further, we can conclude that XBs act independently from each other, i.e., they are unsynchronized. If they were synchronized, the ACF would be periodic, because the autocorrelation function of a periodic signal is periodic (5).

Overall, our kinetic results suggest that phosphorylation at saturating [Ca^{2+}] has no effect on maximal isometric tension (59, 68, 71). The situation is different at low [Ca^{2+}] at which phosphorylation is able to increase force because the fraction of XBs in force generating state is low (6, 70). The situation is also different in muscles carrying familiar hypertrophy mutations, which show obvious differences in kinetics compared with wild-type muscles (18, 27, 28, 36, 47, 48, 52) and even between α-and β-cardiac myosins (40).

5.2 Distribution.

Comparison of the probability distributions of orientations of XBs containing phosphorylated and dephosphorylated RLC can be misleading unless the means of distributions are the same (51). This is because the relative FWHM of a distribution[3] is sharply dependent on the strength of the signal[4]. Because of the stochastic nature of the Gaussian signal, a small mean is associated with a broad distribution (large relative FWHM) and a large mean is associated with a narrow distribution (small relative FWHM). The same is true for the ratio of two Gaussian signals (like polarization of fluorescence). Therefore, if the means are different, an impression is created that the distributions are different. Meaningful comparison of FWHMs or SDs of the ratio of two Gaussian signals requires that they have nearly equal means. (It is not always possible to achieve exactly the same mean, especially when the signal is as weak as in our case).

The absence of an effect from phosphorylation on the kinetic rate and FWHM is illustrated schematically inFig. 8. The white, blue, and red spheres symbolize LC1, and phosphorylated and dephosphorylated RLC, respectively. The transition dipole of SeTau is shown as a white arrow. The violet cones represent a three-dimensional Gaussian distribution of SeTau transition moments. The absence of an effect on kinetics is represented by the fact that the left (phosphorylated) XB is in the same transitional state (here dissociated from thin filament) as the right (dephosphorylated) one. The small effect on FWHM is represented by the fact that the violet cone within which phosphorylated XB rotates is slightly (6%) more open.

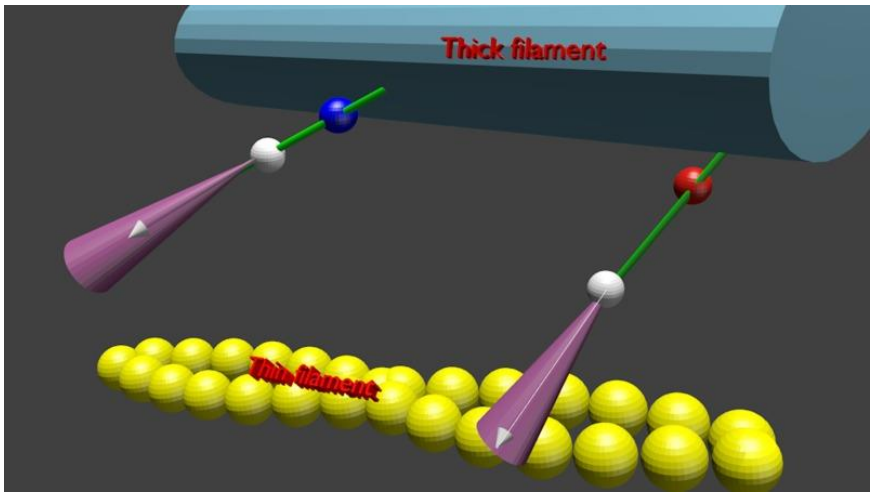

Fig:8 Schematic representation of the fact that phosphorylation of RLC has no effect on kinetics and minimal effect on distribution of XBs. Phosphorylated and dephosphorylated RLC are shown as blue and red spheres, respectively. The white sphere is LC1, and white arrows are the transition dipoles of the dye. The violet cone is the cone of angles within which the transition dipole fluctuates. The thick filament is shown in dark blue, actin filament in yellow, and myosin neck in green.

We have previously found that relaxed XBs of muscle in which RLCs were dephosphorylated were organized more tightly than XBs of muscle in which RLCs were phosphorylated (51). We also found small differences in the kinetics and orientational distribution of XBs. The differences observed in active XBs are likely due to the fact that in earlier work, muscles were phosphorylated by the addition of phosphatase inhibitors. These contain a high concentration of fluoride that may affect the kinetics and distribution of XBs during contraction. Also, the kinetic constants were obtained from a two-state (ON-OFF) model, which may be too great of an oversimplification.

5.3. Perspectives and Significance

There is convincing evidence that in cardiac muscle, phosphorylation enrichment increases isometric force and peak power output and both maximum shortening speed and the shortening velocity at peak power. This suggests that reduced RLC phosphorylation is a key aspect of impaired contractile function in the diseased myocardium (e.g., Refs. 15 and 75). The future research on this subject must, therefore, concentrate on the role of phosphorylation of cardiac RLC. Phosphorylation of skeletal RLC is perhaps a remaining vestige of evolution of cardiac myosin. The mechanical changes observed earlier [e.g., (10, 46, 72)] are perhaps inevitable consequences of adding a negative charge to the lever arm of myosin.

6. REFERENCES

1. Bagshaw CR. Muscle Contraction. London: Chapman & Hall, 1982

2. Beausang JF, Sun Y, Quinlan ME, Forkey JN, Goldman YE. Orientation and rotational motions of single molecules by polarized total internal reflection fluorescence microscopy (polTIRFM). Cold Spring Harb Protoc 2012, 2012

3. Bershitsky SY, Tsaturyan AK, Bershitskaya ON, Mashanov GI, Brown P, Burns R, Ferenczi MA.Muscle force is generated by myosin heads stereospecifically attached to actin. Nature 388: 186–190, 1997

4. Borejdo J, Midde K. Rapid measurements of orientation and rotation of a small number of cross-bridges in ex vivo muscle. In: Advanced Fluorescence Microscopy Techniques, edited by Conn M, editor. , New York: Elesevier, In press

5. Bracewell R. The Fourier Transform and Its Applications. New York: McGraw-Hill, 1965

6. Brenner B. Effect of Ca^{2+} on cross-bridge turnover kinetics in skinned single rabbit psoas fibers: implications for regulation of muscle contraction. Proc Natl Acad Sci USA 85: 3265–3269, 1988

7. Buschmann V, Krämer B, Koberling F. Quantitative FCS: Determination of confocal volume by FCS and bead scanning with MicroTime 200. PicoQuant, Application Note Quantitative FCS v 1.1, 2009

8. Chase PB, Martyn DA, Kushmerick MJ, Gordon AM. Effects of inorganic phosphate analogues on stiffness and unloaded shortening of skinned muscle fibres from rabbit. J Physiol 460: 231–246, 1993

9. Colson BA, Locher MR, Bekyarova T, Patel JR, Fitzsimons DP, Irving TC, Moss RL. Differential roles of regulatory light chain and myosin binding protein-C phosphorylations in the modulation of cardiac force development. J Physiol 588: 981–993, 2010

10. Cooke R. Modulation of the actomyosin interaction during fatigue of skeletal muscle. Muscle Nerve 36: 756–777, 2007

11. Cooke R. The role of the myosin ATPase activity in adaptive thermogenesis by skeletal muscle.Biophys Rev 3: 33–45, 2011

12. Corrie JE, Craik JS, Munasinghe VR. A homobifunctional rhodamine for labeling proteins with defined orientations of a fluorophore. Bioconjug Chem 9: 160–167, 1998

13. Coureux PD, Sweeney HL, Houdusse A. Three myosin V structures delineate essential features of chemo-mechanical transduction. EMBO J 23: 4527–4537, 2004

14. Dantzig JA, Higuchi H, Goldman YE. Studies of molecular motors using caged compounds. Methods Enzymol 291: 307–348., 1998

15. Dias FA, Walker LA, Arteaga GM, Walker JS, Vijayan K, Pena JR, Ke Y, Fogaca RT, Sanbe A, Robbins J, Wolska BM. The effect of myosin regulatory light chain phosphorylation on the frequency-dependent regulation of cardiac function. J Mol Cell Cardiol 41: 330–339, 2006

16. Dos Remedios CG, Millikan RG, Morales MF. Polarization of tryptophan fluorescence from single striated muscle fibers. A molecular probe of contractile state. J Gen Physiol 59: 103–120, 1972

17. Dos Remedios CG, Yount RG, Morales MF. Individual states in the cycle of muscle contraction. Proc Natl Acad Sci USA 69: 2542–2546, 1972

18. Dumka D, Talent J, Akopova I, Guzman G, Szczesna-Cordary D, Borejdo J. E22K mutation of RLC that causes familial hypertrophic cardiomyopathy in heterozygous mouse myocardium: effect on cross-bridge kinetics. Am J Physiol Heart Circ Physiol 291: H2098–H2106, 2006

19. Elson EL. Fluorescence correlataion spectroscopy and photobleaching recovery. Annu Rev Phys Chem36: 379–406, 1985

20. Elson EL. Fluorescence correlation spectroscopy: past, present, future. Biophys J 101: 2855–2870, 2011

21. Elson EL. Introduction to FCS. Fort Worth, TX: University of North Texas, 2007

22. Elson EL, Magde D. Fluorescence correlation spectroscopy: conceptual basis and theory. Biopolymers13: 1–28, 1974

23. Elson EL, Webb WW. Concentration correlation spectroscopy: a new biophysical probe based on occupation number fluctuations. Annu Rev Biophys Bioeng 4: 311–334, 1975

24. Endo M. Professor Ebashi's journey toward the discovery of troponin: a personal recollection. Adv Exp Med Biol 592: 7–9, 2007

25. Forkey JN, Quinlan ME, Shaw MA, Corrie JE, Goldman YE. Three-dimensional structural dynamics of myosin V by single-molecule fluorescence polarization. Nature 422: 399–404, 2003

26. Greenberg MJ, Mealy TR, Jones M, Szczesna-Cordary D, Moore JR. The direct molecular effects of fatigue and myosin regulatory light chain phosphorylation on the actomyosin contractile apparatus. Am J Physiol Regul Integr Comp Physiol 298: R989–R996, 2010

27. Greenberg MJ, Watt JD, Jones M, Kazmierczak K, Szczesna-Cordary D, Moore JR. Regulatory light chain mutations associated with cardiomyopathy affect myosin mechanics and kinetics. J Mol Cell Cardiol46: 108–115, 2009

28. Hernandez OM, Szczesna-Cordary D, Knollmann BC, Miller T, Bell M, Zhao J, Sirenko SG, Diaz Z, Guzman G, Xu Y, Wang Y, Kerrick WG, Potter JD. F110I and R278C troponin T mutations that cause familial hypertrophic cardiomyopathy affect muscle contraction in transgenic mice and reconstituted human cardiac fibers. J Biol Chem 280: 37183–37194, 2005

29. Herrmann C, Lionne C, Travers F, Barman T. Correlation of ActoS1, myofibrillar, and muscle fiber ATPases. Biochemistry 33: 4148–4154, 1994

30. Herrmann C, Sleep J, Chaussepied P, Travers F, Barman T. A structural and kinetic study on myofibrils prevented from shortening by chemical cross-linking. Biochemistry 32: 7255–7263, 1993

31. Hooijman P, Stewart MA, Cooke R. A new state of cardiac Myosin with very slow ATP turnover: a potential cardioprotective mechanism in the heart. Biophys J 100: 1969–1976, 2011

32. Hopkins SC, Sabido-David C, Corrie JE, Irving M, Goldman YE. Fluorescence polarization transients from rhodamine isomers on the myosin regulatory light chain in skeletal muscle fibers. Biophys J 74: 3093–3110, 1998

33. Hopkins SC, Sabido-David C, van der Heide UA, Ferguson RE, Brandmeier BD, Dale RE, Kendrick-Jones J, Corrie JE, Trentham DR, Irving M, Goldman YE. Orientation changes of the myosin light chain domain during filament sliding in active and rigor muscle. J Mol Biol 318: 1275–1291, 2002

34. Huxley AF, Simmons RM. Proposed mechanism of force generation in striated muscle. Nature 233: 533–538, 1971

35. James J, Robbins J. Signaling and myosin-binding protein C. J Biol Chem 286: 9913–9919, 2011

36. Kerrick WG, Kazmierczak K, Xu Y, Wang Y, Szczesna-Cordary D. Malignant familial hypertrophic cardiomyopathy D166V mutation in the ventricular myosin regulatory light chain causes profound effects in skinned and intact papillary muscle fibers from transgenic mice. FASEB J 23: 855–865, 2009

37. Lakowicz JR. Principles of Fluorescence Spectroscopy: New York: Springer, 2006

38. Levine RJ, Kensler RW, Yang Z, Sweeney HL. Myosin regulatory light chain phosphorylation and the production of functionally significant changes in myosin head arrangement on striated muscle thick filaments. Biophys J 68: 224S, 1995

39. Ling N, Shrimpton C, Sleep J, Kendrick-Jones J, Irving M. Fluorescent probes of the orientation of myosin regulatory light chains in relaxed, rigor, and contracting muscle. Biophys J 70: 1836–1846, 1996

40. Lowey S, Bretton V, Gulick J, Robbins J, Trybus KM. Transgenic mouse alpha-and beta-cardiac myosins containing the R403Q mutation show isoform-dependent transient kinetic differences. J Biol Chem288: 14780–14787, 2013

41. Lu H, Ali MY, Bookwalter CS, Warshaw DM, Trybus KM. Diffusive movement of processive kinesin-1 on microtubules. Traffic 10: 1429–1438, 2009

42. Lu H, Kennedy GG, Warshaw DM, Trybus KM. Simultaneous observation of tail and head movements of myosin V during processive motion. J Biol Chem 285: 42068–42074, 2010

43. Lymn RW, Taylor EW. Mechanism of adenosine triphosphate hydrolysis by actomyosin. Biochemistry10: 4617–4624, 1971

44. Magde D, Elson EL, Webb WW. Fluorescence correlation spectroscopy. II. An experimental realization. Biopolymers 13: 29–61, 1974

45. Maruta S, Homma K, Ohki T. Conformational changes at the highly reactive cystein and lysine regions of skeletal muscle myosin induced by formation of transition state analogues. J Biochem 124: 578–584, 1998

46. Matsubara I. X-ray diffraction studies of the heart. Annu Rev Biophys Bioeng 9: 81–105, 1980

47. Mettikolla P, Calander N, Luchowski R, Gryczynski I, Gryczynski Z, Zhao J, Szczesna-Cordary D, Borejdo J. Cross-bridge kinetics in myofibrils containing familial hypertrophic cardiomyopathy R58Q mutation in the regulatory light chain of myosin. J Theor Biol 284: 71–81, 2011

48. Mettikolla P, Luchowski R, Gryczynski I, Gryczynski Z, Szczesna-Cordary D, Borejdo J. Fluorescence lifetime of actin in the FHC transgenic heart. Biochemistry 48: 1264–1271, 2009

49. Metzger JM, Greaser ML, Moss RL. Variations in cross-bridge attachment rate and tension with phosphorylation of myosin in mammalian skinned skeletal muscle fibers. Implications for twitch potentiation in intact muscle. J Gen Physiol 93: 855–883, 1989

50. Midde K, Rich R, Hehreiter V, Raut S, Luchowski R, Hinze C, Fudala R, Gryczynski I, Gryczynski Z, Borejdo J. Rotation of myosin lever arms during isometric contraction of skeletal myofibrils. In: Skeletal Muscle: Physiology, Classification and Disease, edited by Willems M., editor. Chichester, United Kingdom Nova Science Publishers, 2012

51. Midde K, Rich R, Marandos P, Fudala R, Li A, Gryczynski I, Borejdo J. Orientation and rotational motion of cross-bridges containing phosphorylated and dephosphorylated myosin regulatory light chain. J Biol Chem 288: 7012–7023, 2013

52. Miller T, Szczesna D, Housmans PR, Zhao J, de Freitas F, Gomes AV, Culbreath L, McCue J, Wang Y, Xu Y, Kerrick WG, Potter JD. Abnormal contractile function in transgenic mice expressing a familial hypertrophic cardiomyopathy-linked troponin T (I79N) mutation. J Biol Chem 276: 3743–3755, 2001

53. Minton AP. The influence of macromolecular crowding and macromolecular confinement on biochemical reactions in physiological media. J Biol Chem 276: 10577–10580, 2001

54. Morales MF. Calculation of the polarized fluorescence from a labeled muscle fiber. Proc Nat Acad Sci USA 81: 145–149, 1984

55. Muthu P, Kazmierczak K, Jones M, Szczesna-Cordary D. The effect of myosin RLC phosphorylation in normal and cardiomyopathic mouse hearts. J Cell Mol Med 10: 1582–4934, 2011

56. Naber N, Cooke R, Pate E. EPR spectroscopy shows oriented myosin heads in relaxed muscle fibers.Biophys J 100: 130a–130a, 2011

57. Nihei T, Mendelson RA, Botts J. Use of fluorescence polarization to observe changes in attitude of S1 moieties in muscle fibers. Biophys J 14: 236–242, 1974

58. Onsager L. Reciprocal relations in irreversible processes. Phys Rev 37: 405–426, 1931

59. Persechini A, Stull JT, Cooke R. The effect of myosin phosphorylation on the contractile properties of skinned rabbit skeletal muscle fibers. J Biol Chem 260: 7951–7954, 1985

60. Qiu W, Derr ND, Goodman BS, Villa E, Wu D, Shih W, Reck-Peterson SL. Dynein achieves processive motion using both stochastic and coordinated stepping. Nat Struct Mol Biol 19: 193–200, 2012

61. Quinlan ME, Forkey JN, Goldman YE. Orientation of the myosin light chain region by single molecule total internal reflection fluorescence polarization microscopy. Biophys J 89: 1132–1142, 2005

62. Raucher D, Fajer PG. Orientation and dynamics of myosin heads in aluminum fluoride induced pre-power stroke states: an EPR study. Biochemistry 33: 11993–11999, 1994

63. Rayment I, Holden HM, Whittaker M, Yohn CB, Lorenz M, Holmes KC, Milligan R. Structure of the actin-myosin complex and its implications for muscle contraction. Science 261: 58–65, 1993

64. Regnier M, Chase PB, Martyn DA. Contractile properties of rabbit psoas muscle fibres inhibited by beryllium fluoride. J Muscle Res Cell Motil 20: 425–432, 1999

65. Ross JL, Shuman H, Holzbaur EL, Goldman YE. Kinesin and dynein-dynactin at intersecting microtubules: motor density affects dynein function. Biophys J 94: 3115–3125, 2008

66. Sabido-David C, Hopkins SC, Saraswat LD, Lowey S, Goldman YE, Irving M. Orientation changes of fluorescent probes at five sites on the myosin regulatory light chain during contraction of single skeletal muscle fibres. J Mol Biol 279: 387–402, 1998

67. Stewart MA, Franks-Skiba K, Chen S, Cooke R. Myosin ATP turnover rate is a mechanism involved in thermogenesis in resting skeletal muscle fibers. Proc Natl Acad Sci USA 107: 430–435, 2010

68. Stull JT, Kamm KE, Vandenboom R. Myosin light chain kinase and the role of myosin light chain phosphorylation in skeletal muscle. Arch Biochem Biophys 510: 120–128, 201

69. Sun Y, Sato O, Ruhnow F, Arsenault ME, Ikebe M, Goldman YE. Single-molecule stepping and structural dynamics of myosin X. Nat Struct Mol Biol 17: 485–491, 2010

70. Sweeney HL, Stull JT. Alteration of cross-bridge kinetics by myosin light chain phosphorylation in rabbit skeletal muscle: implications for regulation of actin-myosin interaction. Proc Natl Acad Sci USA 87: 414–418, 1990

71. Sweeney HL, Stull JT. Phosphorylation of myosin in permeabilized mammalian cardiac and skeletal muscle cells. Am J Physiol Cell Physiol 250: C657–C660, 1986

72. Sweeney HL, Yang Z, Zhi G, Stull JT, Trybus KM. Charge replacement near the phosphorylatable serine of the myosin regulatory light chain mimics aspects of phosphorylation. Proc Natl Acad Sci USA 91: 1490–1494, 1994

73. Szczesna D, Zhao J, Jones M, Zhi G, Stull J, Potter JD. Phosphorylation of the regulatory light chains of myosin affects Ca^{2+} sensitivity of skeletal muscle contraction. J Appl Physiol 92: 1661–1670, 2002

74. Telley IA, Stehle R, Ranatunga KW, Pfitzer G, Stussi E, Denoth J. Dynamic behaviour of half-sarcomeres during and after stretch in activated rabbit psoas myofibrils: sarcomere asymmetry but no ‘sarcomere popping’. J Physiol 573: 173–185, 2006

75. Toepfer C, Caorsi V, Kampourakis T, Sikkel MB, West TG, Leung MC, Al-Saud SA, MacLeod KT, Lyon AR, Marston SB, Sellers JR, Ferenczi MA. Myosin regulatory light chain (RLC) phosphorylation change as a modulator of cardiac muscle contraction in disease. J Biol Chem 288: 13446–13454, 2013

76. Tominaga M, Kojima H, Yokota E, Nakamori R, Anson M, Shimmen T, Oiwa K. Calcium-induced mechanical change in the neck domain alters the activity of plant myosin XI. J Biol Chem 287: 30711–30718, 2012

77. Tregear RT, Mendelson RA. Polarization from a helix of fluorophores and its relation to that obtained from muscle. Biophys J 15: 455–467, 1975

78. Tsaturyan AK, Bershitsky SY, Burns R, Ferenczi MA. Structural changes in the actin-myosin cross-bridges associated with force generation induced by temperature jump in permeabilized frog muscle fibers.Biophys J 77: 354–372, 1999

79. Ushakov DS, Caorsi V, Ibanez-Garcia D, Manning HB, Konitsiotis AD, West TG, Dunsby C, French PM, Ferenczi MA. Response of rigor cross-bridges to stretch detected by fluorescence lifetime imaging microscopy of myosin essential light chain in skeletal muscle fibers. J Biol Chem 286: 842–850, 2011

80. Warshaw DM, Hayes E, Gaffney D, Lauzon AM, Wu J, Kennedy G, Trybus K, Lowey S, Berger C.Myosin conformational states determined by single fluorophore polarization. Proc Natl Acad Sci USA 95: 8034–8039, 1998

81. Yildiz A, Park H, Safer D, Yang Z, Chen LQ, Selvin PR, Sweeney HL. Myosin VI steps via a hand-over-hand mechanism with its lever arm undergoing fluctuations when attached to actin. J Biol Chem 279: 37223–37226, 2004

82. Yildiz A, Tomishige M, Vale RD, Selvin PR. Kinesin walks hand-over-hand. Science 303: 676–678, 2004

CHAPTER X

EFFECT OF A MYOSIN REGULATORY LIGHT CHAIN MUTATION K104E ON ACTIN-MYOSIN INTERACTIONS

[1]D. Duggal*,[1] J. Nagwekar*, [1]R. Rich, [2]W. Huang, [1]K. Midde, [1]R. Fudala, [1]H. Das, [1]I. Gryczynski, [2]D. Szczesna-Cordary, [1]J. Borejdo

[1] Department of Cell Biology & Immunology and Center for Commercialization of Fluorescence Technologies, University of North Texas, Health Science Center, Fort Worth, Texas; and

[2] Department of Molecular & Cellular Pharmacology, University of Miami Miller School of Medicine, Miami, Florida; and 3 Department of Pharmacology and Neuroscience, Institute of Aging and Alzheimer's Disease Research, Institute of Cancer Research, Fort Worth, Texas

*** D. Duggal and J. Nagwekar contributed equally to this work.**

Address for reprint requests and other correspondence: J. Borejdo, Dept. of Molecular Biology & Immunology and Center for Commercialization of Fluorescence Technologies, Univ. of North Texas, Health Science Center, 3500 Camp Bowie Blvd., Fort Worth, TX 76107 (e-mail: Julian.Borejdo @unthsc.edu).

1. ABSTRACT

Familial hypertrophic cardiomyopathy (FHC) is the most common cause of sudden cardiac death in young individuals. Molecular mechanisms underlying this disorder are largely unknown; this study aims at revealing how disruptions in actin-myosin interactions can play a role in this disorder. Cross-bridge (XB) kinetics and the degree of order were examined in contracting myofibrils from the ex vivo left ventricles of transgenic (Tg) mice expressing FHC regulatory light chain (RLC) mutation K104E. Because the degree of order and the kinetics are best studied when an individual XB makes a significant contribution to the overall signal, the number of observed XBs in an ex vivo ventricle was minimized to 20. Autofluorescence and photobleaching were minimized by labeling the myosin lever arm with a relatively long-lived red-emitting dye containing a chromophore system encapsulated in a cyclic macromolecule. Mutated XBs were significantly better ordered during steady-state contraction and during rigor, but the mutation had no effect on the degree of order in relaxed myofibrils. The K104E mutation increased the rate of XB binding to thin filaments and the rate of execution of the power stroke. The stopped-flow experiments revealed a significantly faster observed dissociation rate in Tg-K104E vs. Tg-wild-type (WT) myosin and a smaller second-order ATP-binding rate for the K104E compared with WT myosin. Collectively, our data indicate that the mutation-induced changes in the interaction of myosin with actin during the contraction - relaxation cycle may contribute to altered contractility and the development of FHC.

Keywords: left ventricle; mutation of regulatory light chain; polarization of fluorescence

2. INTRODUCTION

Interactions of myosin with actin and associated proteins (sarcomeric proteins) are responsible for muscle contraction (19, 24, 48). These interactions include the mode of attachment of actin to myosin during different physiological states and the kinetics of conformational changes of myosin when interacting with actin. Familial hypertrophic cardiomyopathy (FHC) has been recognized to be caused by mutations in all major sarcomeric proteins of the heart, including the myosin regulatory light chain (RLC) (1). Compared with the myosin heavy chain, mutations in the RLC are rare, but often associated with malignant outcomes (18, 27, 41). It is therefore important to find out whether these FHC-linked mutations result in alterations of the mode of attachment of myosin to actin, and/or whether they lead to alterations of kinetics of acto-myosin interactions. These changes may ultimately contribute to the development of FHC. In this report we have focused on the K104E (lysine to glutamic acid) substitution in the myosin RLC expressed in the heart of transgenic (Tg) mice (25). The mutation was identified in a Danish population by Andersen et al. (2) and was associated with left ventricular and septal hypertrophy and diastolic filling abnormalities. In the three-dimensional RLC structure, the residue K104 is close to both the Ca2-Mg2 binding loop and to the myosin light chain kinase-specific serine-15 phosphorylation site (45). It is therefore possible that this single-point mutation results in alteration of the order with which myosin cross bridges (XBs) interact with actin filaments. Furthermore, because the lever arm and the catalytic domain of a XB are in constant communication (46), the malfunction of the RLC caused by K104E may affect the acto-myosin interaction, most critically the force production and the rates of force development and relaxation. In this report we aimed at measuring the effect of the K104E mutation on the degree of order of XBs in a small observational volume containing fluorescently labeled myofibrils prepared from previously generated Tg-K104E mice expressing the human ventricular RLC-K104E in the heart (25). The degree of order and XB kinetics are best studied when an individual XB makes a significant contribution to the overall signal, because the mean values of a large number of independent random measurements, each with a well-defined expected value and well-defined variance, are approximately normally distributed (47). Therefore, because the whole ventricle contains at least 1018 molecules of actin or myosin (left ventricle of our B6 mice typically weighs 30 mg), there is no hope of observing differences between spatial distributions of XBs within ventricles. On the other hand, if only a few XBs are observed, the differences in distribution become clear. An argument that a small number of molecules must be studied when measuring XB kinetics is different: force-generating molecules are unsynchronized, and macroscopic measurements generate only the average values. However, when only a few molecules are studied, the value of a variable is affected by fluctuations around the average (16, 17, 44). The relative size of fluctuations depends on the number of molecules under observation N as N/N. Even if "only" a million XBs were studied, the fluctuation would have been 0.1%. In our experiments, a typical number of molecules was 20, and the corresponding fluctuations were 20%. The alternative is to apply rapid transients (11, 26) to synchronize XBs. In the present work we used both approaches. We report here that the K104E mutation in RLC imposed alterations in the degree of order and kinetics of myosin XBs in contracting myofibrils from the left ventricle of Tg-K104E mice. The mutation resulted in a significantly better order of XBs during steady-state contraction and during rigor, but it had no effect on the degree of order in the relaxed myofibrils. These changes paralleled significantly increased rates of XB binding to the thin filaments and the rate of execution of the power stroke. The stopped-flow experiments revealed significantly faster observed dissociation rates (kobs) in Tg-K104E vs. Tg-wild-type (WT) myosin at low MgATP concentrations, and the linear regression analysis of the kobs-MgATP concentration ([MgATP]) dependence showed a smaller second-order ATPbinding rate for the K104E compared with WT myosin.

3. MATERIALS AND METHODS

3.1. Chemicals and solutions.

All chemicals were from Sigma-Aldrich (St. Louis, MO). The dye SeTau-647-monomaleimide was from SETA BioMedicals (Urbana, IL). Glycerinating solution contained 50% glycerol, 150 mM KCl, 10 mM Tris·HCl, pH 7.5, 5 mM $MgCl_2$, 5 mM EGTA, 5 mM ATP, 1 mM DTT, 2 mM PMSF, and 0.1% β-mercaptoethanol. Rigor solution contained 50 mM KCl, 10 mM Tris·HCl, pH 7.5, and 2 mM $MgCl_2$. EDTA-rigor contained 50 mM KCl, 10 mM Tris·HCl, pH 7.5, and 5 mM EDTA. Ca-rigor contained 50 mM KCl, 10 mM Tris·HCl, pH 7.5, 2 mM $MgCl_2$, and 0.1 mM $CaCl_2$. Contracting solution contained 50 mM KCl, 10 mM Tris·HCl, pH 7.5, 5 mM $MgCl_2$, 0.1 mM $CaCl_2$, 5 mM ATP, 20 mM creatine phosphate, and 10 U/ml of 1 mg/ml creatine kinase. Relaxing solution contained 50 mM KCl, 10 mM Tris·HCl, pH 7.5, 5 mM $MgCl_2$, 5 mM ATP, and 2 mM EGTA.

3.2. Preparation of mouse cardiac myosin and glycerinated left ventricular muscle strips.

Myosin was isolated from the left (LV) and right (RV) ventricles of Tg-K104E and Tg-WT mice as described in Kazmierczak et al. (**28**). Briefly, after death, whole hearts were isolated, and the atria were removed. LV and RV were flash-frozen and stored at −80°C until processed. The ventricular tissue was later thawed in an ice-cold Guba Straub-type buffer (pH 6.5) consisting of 300 mM NaCl, 100 mM NaH_2PO_4, 50 mM Na_2HPO_4, 1 mM $MgCl_2$, 10 mM EDTA, 0.1% NaN_3, 10 mM $Na_4P_2O_7$, 1 mM DTT, and 1 μl/ml protease inhibitor cocktail (Sigma-Aldrich) in a volume of 0.75 ml buffer/0.2 g tissue. Ventricles kept on ice were first minced by hand and then homogenized for 2 min at a frequency of 30 Hz in a Mixer-Mill MM301 (Retsch). The homogenate was then incubated on ice for 40 min before centrifugation for 1 h at 200,000 g. The supernatant was then diluted 60-fold (by volume) with 2 mM DTT and incubated on ice for 1 h. The samples were centrifuged again for 10 min at 8,000 g, and the pellets were then resuspended in a minimal volume of buffer containing 0.4 M KCl, 10 mM MOPS (pH 7.0), 5 mM DTT, and 1 μl/ml protease inhibitor cocktail. Samples were then diluted 1:1 with glycerol, mixed gently, and stored at −20°C for up to ∼10 days. On average, one myosin preparation was obtained from a pool of approximately five hearts. All animal studies were conducted in accordance with the University of Miami Miller School of Medicine institutional guidelines, and we have received required Institutional Animal Care and Use Committee approval. Muscle strips were prepared from flash-frozen hearts of Tg-WT mice (**52**) and Tg-K104E mice (**25**). LV were isolated and dissected into small muscle bundles in a cold room in ice-cold pCa 8 solution containing 30 mM butanedione monoxime and 15% glycerol (**42**). They were then chemically skinned in 50% glycerol and 50% pCa 8 solution {10^{-8} M Ca^{2+} concentration, 1 mM free Mg^{2+} concentration [total MgPr (propionate) = 3.88 mM], 7 mM EGTA, 2.5 mM [MgATP], 20 mM MOPS, pH 7.0, 15 mM creatine phosphate, and 15 U/ml of phosphocreatine kinase, ionic strength = 150 mM adjusted with KPr} containing 1% Triton X-100 for 24 h at 4°C. Mouse LV muscle bundles were then transferred to the same solution without Triton X-100 and shipped to the laboratory in Fort Worth, TX (Borejdo).

3.3. Preparation and cross-linking of myofibrils.

To observe a few XBs, it is preferable to observe myofibril preparations rather than isolated myocytes. Myofibrils are much thinner (∼0.5 μm) than the depth-of-view of a confocal microscope (∼3 μm) with the result that the volume from which fluorescence is detected (hence the number of XBs) is smaller than if the fluorescence was collected from the entire confocal volume (This procedure reduces the number of observed

XBs from thousands to 20–40.). In addition, because they are much thinner than myocytes, they are easier to penetrate by fluorescent peptide and thus prevent the problems associated with the nonuniformity of labeling of sarcomeres. To prepare myofibrils, LV was washed three times with ice-cold EDTA-rigor solution for 30 min to wash out ATP present in the glycerinating solution without causing contraction. It was then washed thoroughly with rigor solution and homogenized by the Cole-Palmer LabGen 125 homogenizer for 10 s followed by further 10-s homogenization after a cool down period of 30 s. Contracting myofibrils were immobilized without affecting their ATPase by cross-linking with the water-soluble cross-linker 1-ethyl-3-[3-(dimethylamino)-propyl]carbodiimide (EDC) (**4**, **5**, **22**, **50**). Myofibrils (1 mg/ml) were incubated for 20 min at room temperature with 20 mM EDC in Ca-rigor solution. The reaction was stopped by adding 20 mM DTT. The pH of the solution (7.5) remained unchanged throughout the 20-min reaction. The absence of shortening was verified by labeling the myofibrils with 10 nM rhodamine-phalloidin and observing contraction in a TIRF microscope.

3.4. Myosin light chain 1 labeling and exchange into myofibrils.

Recombinant myosin light chain 1 (LC1) was purchased from Prospec (ProSpec-Tany TechnoGene, Rehovot, Israel). It was labeled at position 182 with five molar excess of dye (SeTau-647-maleimide) overnight in ice. Labeled LC1 was purified by passing through a Sephadex G50 LP column to eliminate the free dye. LC1 (and not RLC) was chosen as the site of labeling to ensure that the mutation site was located on a different polypeptide chain so as not to cause any disturbance to the mutation. Freshly prepared myofibrils (1 mg/ml) were exchanged with an exchange solution as described previously (**32**) with 10 nM SeTau-LC1 under mild conditions (20 min at 30°C; see Ref. **51**). The exchange was deliberately made highly inefficient so that only a small fraction of native LC1s were fluorescent. Myosin exchanged with fluorescent LC1 and bound to myofibrils has high anisotropy, in contrast to free LC1, i.e., it is well immobilized by myofibril even though it is bound at one site only.

3.5. Choice of the dye.

The fluorophore of choice was SeTau-647. It is excited in the red and hence bypasses most contributions of autofluorescence (**30**). SeTau is also very resistant to photobleaching (the initial rate of photobleaching was 2.4/s) because of nanoencapsulation of the squaraine moiety of the dye chromophore system in a mixed aliphatic-aromatic macrocycle. SeTau has a large Stokes shift (44 nm), high extinction coefficient, and quantum yield (0.65). Its overall fluorescence intensity was 4.2 times larger than fluorescence intensity of Alexa647.

3.6. Data collection and statistical analysis.

The fluorescence was measured by a PicoQuant MT 200 inverse time-resolved fluorescence instrument coupled to an Olympus IX 71 microscope. Before each experiment, fluorescence of an isotropic solution of a long fluorescence lifetime dye (i.e., with 0 anisotropy, such as rhodamine 700) was measured to make sure that the emitted light was split equally by a birefringent prism into the parallel and perpendicular The 640-nm excitation beam was focused by an Olympus ×60, 1.2 numerical aperture water immersion objective to the diffraction limit on the overlap band of a myofibril. For each overlap band, the fluorescence intensity was measured 20,000 times over 20 s. The normalized ratio of the difference between parallel and perpendicular channels is known as polarization of fluorescence (PF). PF is known to be a sensitive indicator of the orientation of fluorophore's transition dipole moment (**12**, **23**, **24**, **40**, **43**, **48**, **49**). A

histogram of PFs, i.e., a plot of PF vs. frequency with which it occurs over 20 s, was constructed from these 20,000 measurements. Myofibrils (~20–30) were examined for each physiological state (i.e., rigor, contraction, or relaxation), location (i.e., LV or RV), and state of mutation (i.e., WT or MUT) of a ventricle. The differences between full width at half-maximum (FWHM) values of PF of different populations of ventricles are statistically interpretable only when the signal from each half-sarcomere is similar (**38**). This is because the relative value of FWHM of a strong random signal is small (relative to a signal), and FWHM of a weak signal is relatively large. To make sure that a signal was equal, the power was adjusted within the 1- to 2-μW range. Comparisons between groups were performed using an unpaired Student's t-test (Sigma Plot 11; Systat Software, San Jose, CA) or Origin version 8.6 (Northampton, MA). The significance was defined as $P < 0.05$. SigmaPlot 11 was used to compute histograms. Origin was used to compute autocorrelation functions (ACFs).

3.7. The number of observed myosin molecules.

The detection volume (DV) was estimated by measuring the width of axial and lateral dimensions of an image of 20-nm fluorescent beads. It was 1.7 μm^3 and contained $\sim 3 \times 10^5$ XBs. The number of observed (fluorescent) XBs in this volume was reduced by four orders of magnitude (see below). Data are expressed as means of n experiments ± SD. A calibration curve that plotted the number of SeTau molecules in the DV vs. fluorescence intensity was constructed. The number of molecules in the DV was estimated using fluorescence correlation spectroscopy. The ACF of fluctuations of fluorescence (because of free SeTau entering and leaving the DV) at delay time 0 is equal to the inverse of the number of molecules contributing to the fluctuations (**14**, **15**,**35**). Six correlation functions were obtained from solutions of the fluorophore in the range 1.29–77.3 nM. Extrapolating the plot to one molecule revealed that a single molecule of SeTau illuminated with 0.2 μW of laser power gave 225 counts/s (**38**). We used this fact to estimate the number of molecules contributing to the signal as 20–40. However, it should be emphasized that, as long as the number of XBs is mesoscopic (i.e., when the number of observed molecules is so small that fluorescence is affected by fluctuations around the average; see Ref. **44**), the exact number does not matter, i.e., 20 molecules should give the same result as 40 molecules, etc. The precision of measurement is approximately equal to $1/\sqrt{\text{the number of fluctuations}}$. To measure with 1% precision we must analyze 10,000 fluctuations. The characteristic lifetime of one fluctuation is of the order of 1 ms (**26**), and 10,000 fluctuations occur in 10 s. We collected the data over 20 s.

3.8. Stopped-flow measurements.

Three Tg-WT and seven Tg-K104E mouse hearts were used for mouse cardiac myosin preparation (see above). Myosins at 0.25 μM were mixed with 0.25 μM pyrene-labeled F-actin (stabilized by 0.25 μM phalloidin) in rigor buffer containing 0.4 M KCl, 1 mM DTT, and 10 mM MOPS, pH 7.0. The complexes were mixed in a 1:1 ratio (vol/vol) with varying concentrations of MgATP (10–80 μM) dissolved in the same buffer, and the dissociation of Tg-K104E vs. Tg-WT myosin from F-actin was observed by monitoring the time course of the change in pyrene fluorescence. Measurements were performed at 21°C using a BioLogic (Claix, France) model SFM-20 stopped-flow instrument outfitted with a Berger ball mixer and an FC-20 observation cuvette. The data were collected and digitized using a JASCO 6500 Fluorometer. The estimated dead time was 8.2 ms. The pyrene-F-actin was excited at 347 nm, and emission was monitored at 404 nm using monochromators set to 20-nm bandwidths. Typically, 8–14 stopped-flow records were averaged and fit to a single exponential equation to obtain the rate of a given MgATP concentration. A

plot of the observed myosin dissociation rates as a function of [MgATP] was linear, and the slope corresponded to the rate constant expressed in molar per second.

4. RESULTS

4.1 The degree of order (distribution of XB orientations).

An informative way to characterize spatial distribution of XBs is to construct a histogram of polarization values vs. the number of times that a given polarization (i.e., orientation) occurs during a 20-s experiment. **Figure 1** is a typical example of histograms of contracting Tg-WT (left) and contracting MUT myofibrils (right). The graphs are Gaussian. The regular residuals are shown (**Figure 1**). Goodness of fit to an ideal Gaussian was assessed by adjusted coefficient of determination, AR^2. It is a better measure of goodness of fit than χ^2 (typically employed to assess nonlinear curve fitting) because it takes into account scaling of the dependent variable. The closer AR^2 is to the value of one, the better the fit. **Table 1** lists average AR^2 of 25 experiments of contracting WT and 31 of contracting MUT muscles.

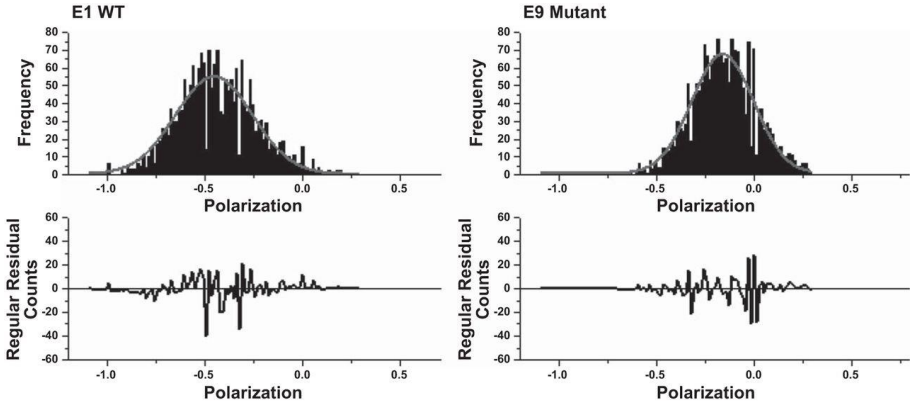

Figure 1: Random examples of the probability distribution of orientations of cross-bridges (XBs) of cardiac myofibrils of contracting wild-type (WT) and mutant (MUT) ventricles. Gray line is the best fit to a 3-parameter Gaussian. Graphs on the *bottom* show regular residuals of the counts. *Left*: WT muscle, FWHM = 0.464, adjusted coefficient of determination (AR^2) = 0.953, mean intensity = 6.3 photons/ms, mean polarization = −0.444. *Right*: MUT muscle, FWHM = 0.380, AR^2 = 0.947, mean intensity = 6 photons/ms, mean polarization = −0.156.

Table 1 compares FWHMs of probability distributions of contracting Tg-WT and Tg-K104E (MUT) myofibrils. Detailed results of 25 experiments of contracting Tg-WT are shown in Table 2. Detailed results of 31 experiments of Tg-K104E are shown in Table 3.

Table 1. Comparison of FWHM's of 25 probability distributions of Tg-WT and 31 experiments of Tg-K104E of contracting myofibrils

Contracting Muscle	FWHM	Intensity, counts/ms	Mean Polarization	AR^2
Tg-WT	0.506 ± 0.129*	5.83 ± 2.011	−0.352 ± 0.153*	0.897 ± 0.138
Tg-K104E	0.449 ± 0.046*	4.76 ± 1.112	0.148 ± 0.022*	0.886 ± 0.040

Errors are SDs of 28 experiments. FWHM, full width at half-maximum; Tg, transgenic; WT, wild type; AR^2, adjusted coefficient of determination. * Statistically significant difference.

Table 2. **Detailed results of probability distributions of contracting Tg-WT myofibrils**

Experiment No.	**FWHM**	**TI**	**Mean Orientation**	**Adjusted R^2**
1	0.464	6.39	−0.44	0.953
2	0.35	6.98	−0.627	0.978
3	0.378	8.834	−0.652	0.971
4	0.48	5.918	−0.393	0.972
5	0.821	6.017	−0.361	0.902
6	0.356	10.98	−0.369	0.985
7	0.584	5.86	−0.183	0.953
8	0.76	1.92	−0.319	0.536
9	0.635	4.08	−0.3445	0.909
10	0.511	4.87	−0.444	0.968
11	0.489	6.164	−0.4006	0.955
12	0.463	5.47	−0.291	0.951
13	0.597	3.11	−0.375	0.761
14	0.4312	6.631	−0.4407	0.951
15	0.52038	4.233	−0.291	0.916
16	0.448	5.56	−0.3044	0.946
17	0.4719	7.6	−0.3203	0.965
18	0.491	4.42	−0.397	0.935
19	0.525	4.138	−0.2306	0.874
20	0.46061	4.337	−0.0175	0.851
21	0.656	5.12	−0.012	0.855
22	0.613	4.582	−0.6209	0.411
23	0.489	7.47	−0.4001	0.965
24	0.449	9.66	−0.3359	0.975
25	0.2088	5.58	−0.232	0.976
Average	0.50608	5.837	−0.35206	0.89656
SD	0.12932	2.0114	0.153920258	0.138636

TI, total intensity

The *t*-test revealed that the 0.057 difference of FWHM was statistically significant ($t = 2.436$, $P = 0.018$) with 54 degrees of freedom. The 95% confidence interval of this difference is from 0.010 to 0.103. The 1.073 difference of intensities was statistically insignificant ($t = 2.532$, $P = 0.014$) with 54 degrees of freedom. The 95% confidence interval of this difference is from 0.223 to 1.922.

Table 3. Detailed results of probability distributions of contracting Tg-K104E myofibrils				
Experiment No.	**FWHM**	**TI**	**Mean Orientation**	**Adjusted R^2**
1	0.456	4.56	−0.131	0.887
2	0.47001	4.15	−0.167	0.881
3	0.443	5.24	−0.117	0.887
4	0.4332	4.94	−0.1455	0.909
5	0.403	5.321	−0.1553	0.91
6	0.453	4.684	−0.1466	0.905
7	0.392	6.15	−0.123	0.943
8	0.394	5.97	−0.1502	0.924
9	0.38	6.225	−0.156	0.947
10	0.473	4.06	−0.1118	0.853
11	0.423	5.29	−0.1133	0.899
12	0.403	5.388	−0.156	0.921
13	0.497	3.834	−0.1042	0.851
14	0.47	4.21	−0.1255	0.874
15	0.466	4.008	−0.1139	0.846
16	0.48859	4.136	−0.157	0.854
17	0.498	4.051	−0.222	0.897
18	0.554	2.95	−0.177	0.786
19	0.4418	5.108	−0.1859	0.899
20	0.336	8.309	−0.173	0.974
21	0.455	4.54	−0.1849	0.899
22	0.5511	3.28	−0.173	0.807
23	0.476	4.29	−0.1008	0.85
24	0.479	3.81	−0.1618	0.862
25	0.444	4.618	−0.157	0.891
26	0.428	5.232	−0.172	0.931
27	0.412	5.231	−0.184	0.907
28	0.473	4.09	−0.127	0.873
29	0.487	3.77	−0.114	0.833
30	0.456	4.34	−0.1609	0.874
31	0.408	5.139	−0.137	0.893
Average	0.4498	4.765	−0.148348	0.8860323
SD	0.04684	1.112	0.0299128	0.0401501

The differences in FWHM and polarization values were significant, but the differences in intensities were insignificant. This is important because, as already mentioned in MATERIALS AND METHODS, the stochastic nature of a Gaussian signal causes a relative FWHM to depend on the strength of the signal. Weak signal results in a large FWHM, and strong signal results in small FWHM. Thus, when comparing FWHMs of two populations, it is crucial that the difference in photon counts between the two populations be statistically insignificant (**38**). The matter is more fully discussed in the DISCUSSION. The −0.498 difference of mean polarization was statistically significant (t = 17.744, P < 0.001) with 54 degrees of freedom. The 95% confidence interval of this difference is from −0.554 to −0.441.

Figure 2 is a typical example of histograms of rigor Tg-WT (*left*) and rigor MUT myofibrils (*right*). As before, the graphs are Gaussian. The regular residuals are shown in **Fig. 2**.

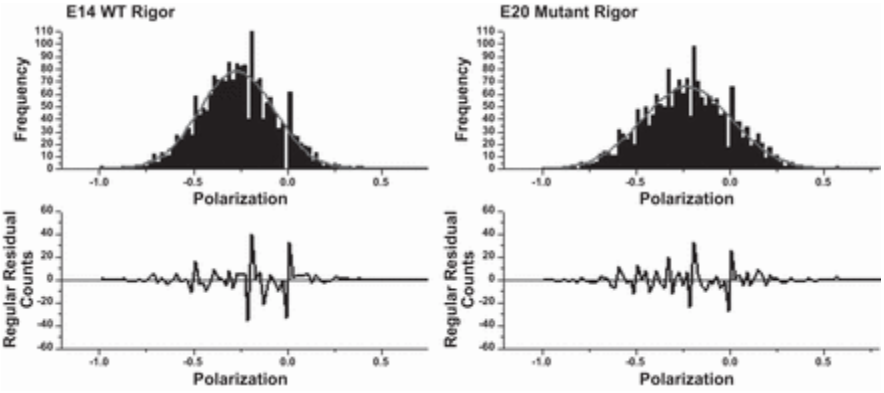

Figure 2. Random examples of the probability distribution of orientations of XBs of cardiac myofibrils of rigor transgenic (Tg)-WT and MUT ventricles. Gray line is the best fit to a 3-parameter Gaussian. Graphs on the *bottom* show regular residuals of the counts. *Left*: WT muscle, FWHM = 0.469, AR^2 = 0.932, mean intensity = 4.7 photons/ms, mean polarization = −0.269. *Right*: mutated muscle, FWHM = 0.563, AR^2 = 0.942, mean intensity = 6.817 photons/ms, mean polarization = −0.223.

Table 4 shows a comparison of FWHMs of 25 probability distributions of rigor Tg-WT and 34 experiments of Tg-K104E.

Table 4. Comparison of FWHM's of 28 probability distributions of Tg-WT and Tg-K104E of rigor myofibrils

Rigor Muscle	FWHM	Intensity, counts/min	Mean Polarization	AR^2
Tg-WT	0.579 ± 0.223*	5.68 ± 1.72	−0.226 ± 0.290	0.885 ± 0.101
Tg-K104E	0.484 ± 0.083*	5.53 ± 0.93	−0.229 ± 0.085	0.922 ± 0.032

Values are means ± SD. Errors are SDs. * Statistically significant difference.

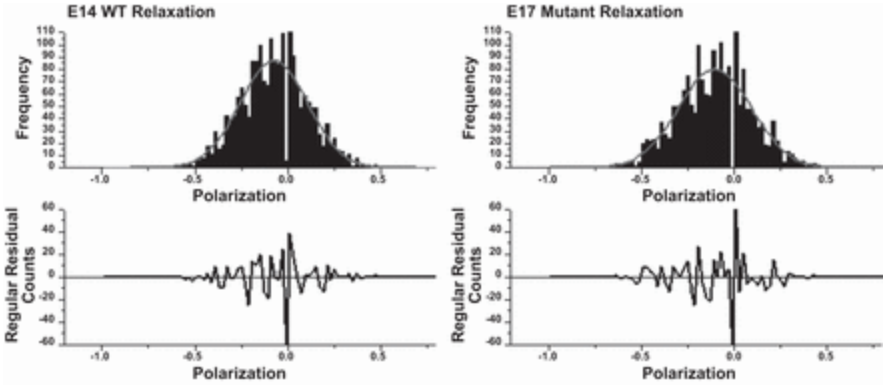

Figure 3. Random examples of the probability distribution of orientations of XBs of relaxed cardiac myofibrils of rigor Tg-WT and MUT ventricles. Gray line is the best fit to a 3-parameter Gaussian. Graphs on the *bottom* show regular residuals of the counts. *Left*: WT muscle, FWHM = 0.429, AR^2 = 0.927, mean intensity = 5.0 photons/ms, mean polarization = −0.074. *Right*: mutated muscle, FWHM = 0.467, mean intensity = 4.1 photons/ms, mean polarization = −0.100.

Table 5 is a comparison of FWHMs of 28 probability distributions of relaxed Tg-WT and Tg-K104E.

Table 5. Comparison of FWHM's of 28 probability distributions of Tg-WT and Tg-K104E of relaxed myofibrils

Relaxed Muscle	FWHM	Intensity, counts/min	Mean Polarization	AR^2
Tg-WT	0.438 ± 0.037	4.99 ± 0.770	−0.144 ± 0.085*	0.910 ± 0.054
Tg-K104E	0.440 ± 0.043	4.72 ± 0.76	−0.096 ± 0.022*	0.901 ± 0.056
Errors are SDs of 28 experiments. ↵* Statistically significant difference.				

The *t*-test revealed that the −0.0025 difference of FWHM was statistically insignificant (t = 0.251, P= 0.802) with 65 degrees of freedom. The 95% confidence interval of this difference is from −0.0223712 to 0.0173712. The −0.271 difference of intensities was statistically insignificant (t = −1.406, P = 0.165 with 63 degrees of freedom). The 95% confidence interval of this difference is from −0.655 to 0.114. The −0.0478000 difference of mean polarization was statistically significant (t = 2.893, P = 0.052 with 55 degrees of freedom). The 95% confidence interval of this difference is from −0.0807955 to −0.0148045.

4.2 XB kinetics.

Because the number of observed molecules was small, we were able to measure fluctuations in equilibrium values of PF. These fluctuations contain information about the rate constants characterizing the enzymatic cycle of actin-myosin interaction. An ACF of PF fluctuations characterizes these rate constants. The shape of the ACF depends on the model assumed for the chemical reaction that drives the cycling of XBs. We use combination of models of Lymn and Taylor (**34**) and of Coureux et al. (**10**) that includes transitions between three fundamental states as illustrated in **Fig. 4** where a XB, actin, ATP, and ADP are denoted by M, A, T, and D, respectively.

$$\mathrm{MT} \xrightarrow{k_1} \mathrm{MDP} \xrightarrow{} \mathrm{AMDP} \xrightarrow{k_2} \mathrm{AMD} \xrightarrow{k_3} \mathrm{AM} \xrightarrow{} \mathrm{AM^*} \xrightarrow{k_{obs}} \mathrm{AM^*T} \xrightarrow{} \mathrm{MT}....$$

Figure 4. Conventional model of muscle contraction. In vitro measurements (see MATERIALS AND METHODS) have shown that steady-state anisotropy associated with different cross-bridge states are 0 for MDP and MT (dissociated XBs) states, intermediate for the AMDP state, and maximum for AM and AM* states (data not shown). M, XB; A, actin; T, ATP; D, ADP.

The enzymatic (and the mechanical cycle coupled to it) begins with a state MT where M has already dissociated from thin filament by binding T and T is hydrolyzed to D and P to assume the MDP state (**34**). The products of hydrolysis remain bound to M. In this state cleft between upper and lower subdomains of a 50-kDa domain is partially closed, and the lever arm is in the up position (**10**). M and MT are free to rotate in the myofilament space and have the lowest steady-state anisotropy (and PF). MDP binds actin with a rate constant k_1 forming a weakly bound, prepower stroke state, AMDP. It is partially immobilized. In this state the cleft between the upper and lower subdomains of a 50-kDa domain is completely closed, and the lever arm is less up than previously (**10**). Next, P dissociates from AMDP forming a strongly bound rigor complex AMD. It is assumed that this transition is very rapid. The transition from AMD to AM state is a power stroke that occurs with the rate constant k_2. In AM state the cleft is completely closed and the lever arm is in the down position. The anisotropy is high. Finally, AM isomerizes to a "rigor-like" state with a rate constant k_3 (**10**). In this state the cleft is opened and the lever arm becomes uncoupled from actin. Anisotropy is rigor-like. The true relaxation is the transition from AM* to MT state characterized by the rate k_{obs}.

A representative experimental ACF is plotted in **Fig. 5**. The red line shows the best nonlinear fit to theoretically predicted expression of the ACF of a system of in **Fig. 4** (an analytical expression of ACF is shown in Ref. **36**). The kinetic constants were reported earlier by Huang et al. (**25**) and are reproduced as follows: k_1 = 205 ± 93.7/s, k_2 = 0.617 ± 0.496/s, and k_3 = 0.689 ± 0.499/s for Tg-WT myofibrils and k_1 = 779 ± 572.1/s, k_2 = 1.162 ± 1.198/s, and $k3$ = 0.300 ± 0.242/s for Tg-K104E myofibrils.

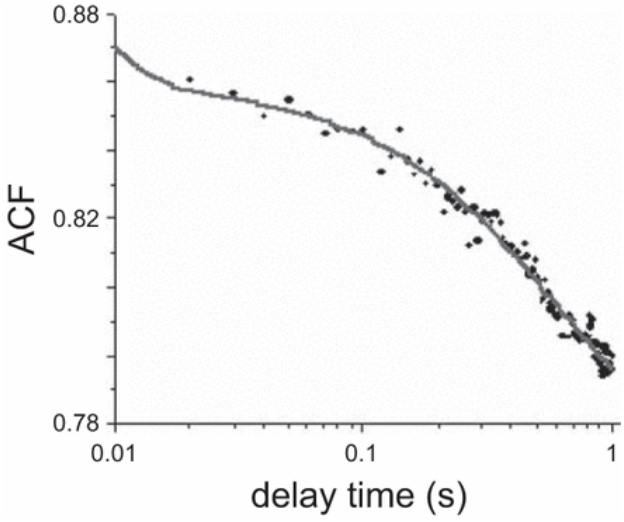

Figure 5. A representative trace of a normalized autocorrelation function (ACF) of polarization of fluorescence of contracting myofibril prepared from the left ventricle of Tg-WT mouse. Symbols are experimental data, and a gray line is the fit to equation shown in Ref. **36**. The results of each experiment are presented in **Table 4**. The fact that ACF decays to a value >0 is due to the fact that mean polarization was nonzero.

The *t*-test revealed that the −574 difference of k_1 was statistically significant ($t = -4.764$, $P < 0.001$) with 50 degrees of freedom. The −0.545 difference of k_2 was statistically significant ($t = -2.091$, $P = 0.041$) with 53 degrees of freedom. The +0.389 difference of k_3 was statistically significant ($t = 3.809$,$P = 0.001$) with 53 degrees of freedom.

The detailed results of kinetics experiments on WT and mutated ventricles are shown in **Table 6**.

Table 6. Detailed results of 23 kinetics experiments on WT ventricles and 29 experiments on mutated ventricles

k_1 WT	k_1 MUT	k_2 WT	k_2 MUT	k_3 WT	k_3 MUT
244.2160	529.4700	0.7680	0.3310	0.8530	0.1590
189.4840	471.8200	0.1140	0.0450	0.1200	0.0281
2.1650	343.5200	0.2850	3.4400	0.8770	0.2700
1.8450	347.6000	0.4020	0.0440	0.5240	0.0330
138.5100	368.3400	0.6970	0.5300	1.8400	0.3100
319.8440	1,535.0060	0.4850	0.3330	0.9630	0.1810
218.8400	376.1900	1.5280	3.3350	1.3590	0.9800
359.5600	1,644.4000	0.4440	1.0400	0.2500	0.4850
226.4500	1,442.2400	0.9170	1.2680	0.5600	0.5970
284.5820	416.8900	0.7800	0.6290	1.2700	0.0580
219.4140	337.1720	0.0530	0.0320	0.0390	0.0150
208.1330	1,477.1570	0.6300	2.0100	0.6690	0.6200
x	355.6100	0.7370	0.1670	0.5590	0.0400
200.7300	422.7700	0.2500	2.1570	0.3140	0.3320
238.0140	308.4370	0.0370	0.0710	0.0290	0.0230
263.8200	1,519.7680	0.3700	0.9530	0.3410	0.4600
213.2600	306.0660	0.1660	0.4080	0.1730	0.2340
302.3300	1,444.8200	0.8620	4.7900	1.2080	0.5600
226.8060	340.6200	0.5610	0.2700	0.4030	0.1620
−0.1250	402.2800		0.3160	0.1246	0.2180
247.4680	*x*	2.3700	2.2700	*x*	0.7900
x	450.8900	0.6400	2.3900	0.5170	0.3930
224.1660	419.7400	0.6730	2.3000	1.3670	0.3120
232.5190	304.6900	0.5211	0.0548	0.9610	0.0230
174.0300	1,690.4300	0.5260	0.8750	1.2250	0.3900
	1,036.8661		0.9740		0.5240
	1,839.0600		1.4200		0.3330
	397.8100		0.0700		0.0540
	x		2.1760		0.1219

	1,596.7300		0.7430		0.3590
	367.5150		0.6020		0.2360
Values are means ± SD. *x*, Extreme values of constants that were removed from the original data. Extremes were defined as differing by more than a factor of 5 from the mean.					

The mesoscopic method was unable to measure the rate of XB dissociation of Tg-K104E and Tg-WT myosin from thin filaments (k_{obs}). To measure this rate actin was labeled with pyrene (**31**). The time course of the change in pyrene fluorescence was monitored as a function of ATP concentrations. Myosins were stoichiometrically mixed with pyrene-F-actin, and the complexes were mixed in a 1:1 volume ratio with increasing concentrations of MgATP (10–80 μM) in a stopped-flow apparatus. An increase in the fluorescence intensity was monitored as a function of time as the myosin heads dissociated from pyrene-F-actin on the addition of MgATP. The representative time-dependent dissociation profiles for Tg-K104E myosins are presented in **Fig. 6*A***. The k_{obs}, derived from the averaged fluorescence traces and fitted with a single exponential, are presented in **Table 7**. The results revealed significantly faster k_{obs} in Tg-K104E vs. Tg-WT myosin for 10 and 25 μM MgATP and no differences between K104E and WT at higher ATP concentrations. Linear regression analysis of the plot of k_{obs} vs. increasing [MgATP] yielded the effective second-order ATP-binding rate for the K104E equal to 0.68 ± 0.01 $\mu M^{-1}/s$ compared with 0.74 ± 0.02 $\mu M^{-1}s$ for Tg-WT (**Fig. 6*B***) showing a small but significant ($P < 0.05$) change in the slope indicating a smaller MgATP binding rate for the mutant.

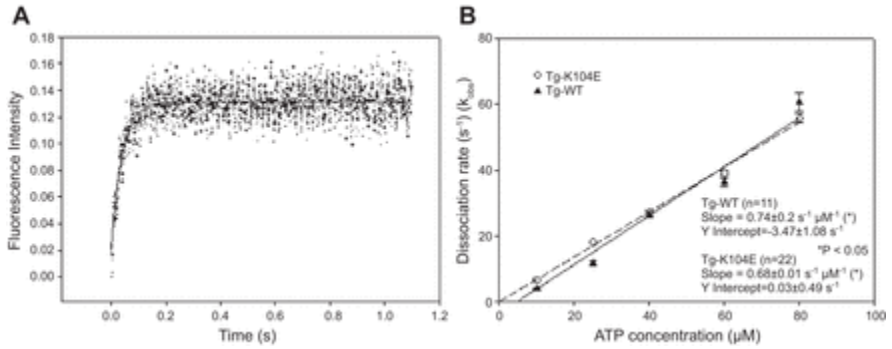

Figure 6. Fast kinetics of interaction between Tg-K104E and Tg-WT myosins with pyrene-labeled F-actin. The myosin-pyrene-actin complex was mixed with various MgATP concentrations (range from 10 to 80 μM), and the recovery of pyrene fluorescence was monitored on the dissociation of actomyosin complex. *A*: representative traces of a real-time increase of pyrene fluorescence within 1 s after MgATP was added to the Tg-WT-F-actin system. *B*: observed dissociation rates (k_{obs})-[MgATP] dependence and the effective second-order MgATP-binding rates for Tg-K104E vs. Tg-WT myosins. The average values of k_{obs} ± SE for each MgATP concentration are presented in **Table 7**

Table 7. Observed dissociation rates (s^{-1}) for Tg-WT and Tg-K104E myosins

	Myosin/[ATP], μM				
	10	**25**	**40**	**60**	**80**
Tg-WT	3.95 ± 0.081	11.75 ± 0.69	26.31 ± 0.41	36.26 ± 1.24	60.56 ± 2.84
n	11	11	11	11	11
Tg-K104E	6.71 ± 0.49*	18.08 ± 0.45*	27.26 ± 0.41	39.08 ± 0.89	55.81 ± 1.44

n	22	22	22	22	22
Errors are SEs of *n* sets of experiments with each set including at least 5 independent measurements. Concentrations refer to the amount of [ATP]. ↵* $P < 0.01$.					

5. DISCUSSION

We studied the effect of the K104E mutation in RLC on the degree of order of ventricular myosin during steady-state contraction, relaxation and rigor, and on the XB kinetics during contraction of left ventricular myofibrils. Autofluorescence and photobleaching were minimized by labeling the myosin lever arm with a relatively long-lived red-emitting dye. Inhomogenities were minimized by focusing the exciting laser light on a single half-sarcomere. The dye was immobilized during critical transient states of the contraction cycle, in spite of the fact that it was attached to LC1 at one point only, rather than two points, which is more stable (**9**). By using the mesoscopic approach, we were able to measure the average kinetics of ~20 XBs.

5.1. The degree of order.

As mentioned before, comparison of the probability distributions of orientations of Tg-WT and Tg-K104E XBs can be misleading unless the means of distributions are the same (**38**). The relative FWHM of distribution [for normal distribution FWHM = $2\sqrt{2 \ln 2}$ = 2.355 SD] is sharply dependent on the strength of the signal. A weak Gaussian signal is associated with a broad distribution, and a strong Gaussian signal is associated with a narrow distribution. The same is true for any ratio of two Gaussian signals (like PF) (**38**). Therefore, meaningful comparison of FWHMs (or SDs) of the polarization of the two Gaussian signals requires that they have nearly equal mean. In practice, we ensure this by keeping the average photon count in each series of experiments similar (by adjusting the power of the illuminating laser). Because the difference in the intensities was statistically insignificant, we could conclude that, during contraction and rigor, the Tg-WT XBs were distributed more widely than mutated Tg-XBs. The fact that the spatial distribution of contracting XBs was significantly narrower in the Tg-K104E myofibrils was not surprising since mutated muscle was found to develop less tension than WT muscle (**25**), implying that K104E-XBs cannot reach as many actin-binding sites as WT-XBs. The observation of XB order in contraction is consistent with earlier work (**7**). The difference in polarization values of XBs of relaxed K104E and WT myofibrils was significant, perhaps because some myosin-actin interaction occurs at relatively low ionic strength used here (**8**). It was surprising to find that FWHM values for both types of myofibrils were not wider in relaxation compared with rigor.

5.2. Kinetics of contracting myofibrils.

The analysis of the ACF leads to two immediate conclusions about the mode of action of XBs. First, the action of XBs is not synchronized. This is because the ACF obtained from XBs within a single half-sarcomere were not periodic. If they were periodic, the XBs would have to be synchronized because ACF of a periodic signal is periodic (**6**). Second, although cross-linking prevented shortening, it did not prevent XBs from executing the power stroke. The present work shows that XBs rotate and are able to reach the neighboring target zones. Not only enzymatic but also mechanical cycles go on, in spite of the cross-linking (**22**).

Kinetic results show that the K104E mutation exerts significant effects on the interaction between actin and myosin. It increases the rates of XB binding, execution of the power stroke, and XB dissociation from the thin filaments. In particular, the rate of XB dissociation from the thin filaments is increased. This suggests that a mutated ventricle is prone to relaxation abnormalities, ultimately leading to diastolic dysfunction in patients carrying the mutation. The molecular effects of the mutation are shown schematically in **Fig. 7**. The blue cones (that indicate the cone of angles within which the transition dipole can rotate) suggest that the degree of disorder of XBs in WT ventricle (*top*) is larger than in K104E XBs (*bottom*). This implies that K104E-XBs cannot reach as many actin-binding sites as WT-XBs, i.e., we could predict that, in vivo, the

mutated ventricles would develop less tension compared with WT. This prediction was confirmed by Huang et al. (**25**).

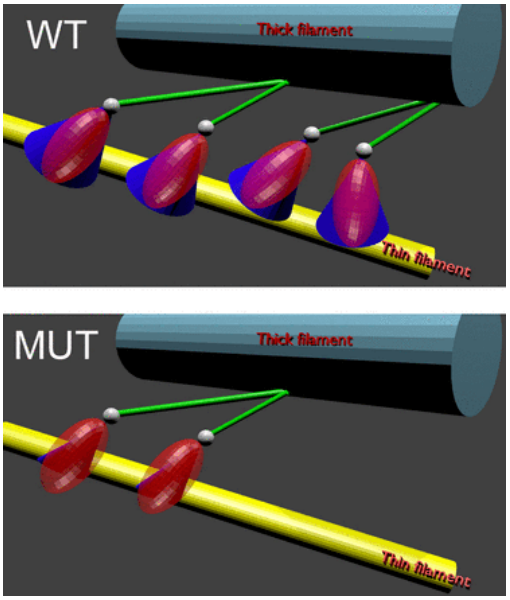

Figure 7. Schematic representation of XBs in contracting WT (*top*) and K104E (*bottom*) ventricles. WT XBs are more disorganized than K104E XBs [they rotate within larger cone of angles (blue)]. K104E XBs dissociate faster than WT (there are less XBs on *bottom*). Gray spheres are the fluorescent LC1s. Even though they can interact with actin (**3**), for simplicity it is drawn here separate from actin. Red ellipsoid represents the 50 + 20-kDa NH_2-terminal domains of the myosin head. Myosin thick filament is shown in light blue, actin filament in yellow, and the COOH-terminal domain of XB (lever arm) in green.

The difference in XB distribution and kinetics between K104E and WT may constitute a molecular hallmark of FHC. Ventricles carrying familiar hypertrophy mutations at different sites also show obvious differences in the kinetics compared with WT muscles (**13**, **20**, **21**, **29**, **36**, **37**, **39**). Differences are also present between the α- and β-cardiac myosins (**33**).

In conclusion, we report here that the K104E mutation significantly alters the degree of order and the kinetics of single myosin XBs carrying the mutated RLC. The mutation-imposed molecular changes monitored in Tg-K104E myofibrils are followed by physiological changes in heart contractility of transgenic mice. We conclude that the differences in XB distribution and kinetics between the K104E mutant and WT muscles are sufficient to trigger pathological heart remodeling and FHC.

6. REFERENCES

1. Alcalai R, Seidman JG, Seidman CE. Genetic basis of hypertrophic cardiomyopathy: from bench to the clinics. J Cardiovasc Electrophysiol 19: 104 –110, 2008.

2. Andersen PS, Havndrup O, Bundgaard H, Moolman-Smook JC, Larsen LA, Mogensen J, Brink PA, Borglum AD, Corfield VA, Kjeldsen K, Vuust J, Christiansen M. Myosin light chain mutations in familial hypertrophic cardiomyopathy: phenotypic presentation and frequency in Danish and South African populations (Abstract). J Med Genet 38: E43, 2001.

3. Andreev OA, Borejdo J. Binding of heavy-chain and essential light-chain 1 of S1 to actin depends on the degree of saturation of F-actin filaments with S1. Biochemistry 34: 14829 –14833, 1995.

Barman T, Brune M, Lionne C, Piroddi N, Poggesi C, Stehle R, Tesi C, Travers F, Webb MR. ATPase and shortening rates in frog fast skeletal myofibrils by time-resolved measurements of protein-bound and free Pi. Biophys J 74: 3120 –3130, 1998.

5. Bershitsky SY, Tsaturyan AK, Bershitskaya ON, Mashanov GI, Brown P, Burns R, Ferenczi MA. Muscle force is generated by myosin heads stereospecifically attached to actin. Nature 388: 186 –190, 1997

6. Bracewell R. The Fourier Transform and Its Applications. New York, NY: McGraw-Hill, 1965.

7. Burghardt TP, Ando T, Borejdo J. Evidence for cross-bridge order in contraction of glycerinated skeletal muscle. Proc Natl Acad Sci USA 80: 7515–7519, 1983.

8. Chalovich JM, Stein LA, Greene LE, Eisenberg E. Interaction of isozymes of myosin subfragment 1 with actin: effect of ionic strength and nucleotide. Biochemistry 23: 4885–4889, 1984.

9. Corrie JE, Craik JS, Munasinghe VR. A homobifunctional rhodamine for labeling proteins with defined orientations of a fluorophore. Bioconjug Chem 9: 160 –167, 1998.

10. Coureux PD, Sweeney HL, Houdusse A. Three myosin V structures delineate essential features of chemo-mechanical transduction. Embo J 23: 4527–4537, 2004.

11. Dantzig JA, Higuchi H, Goldman YE. Studies of molecular motors using caged compounds. Methods Enzymol 291: 307–348, 1998.

12. Dos Remedios CG, Millikan RG, Morales MF. Polarization of tryptophan fluorescence from single striated muscle fibers. A molecular probe of contractile state. J Gen Physiol 59: 103–120, 1972.

13. Dumka D, Talent J, Akopova I, Guzman G, Szczesna-Cordary D, Borejdo J. E22K mutation of RLC that causes familial hypertrophic cardiomyopathy in heterozygous mouse myocardium: effect on crossbridge kinetics. Am J Physiol Heart Circ Physiol 291: H2098 –H2106, 2006.

14. Elson EL. Fluorescence correlataion spectroscopy and photobleaching recovery. Annu Rev Phys Chem 36: 379 –406, 1985.

15. Elson EL. Introduction to FCS. Fort Worth, TX: UNT, 2007.

16. Elson EL, Magde D. Fluorescence correlation spectroscopy: coceptual basis and theory. Biopolymers 13: 1–28, 1974.

17. Elson EL, Webb WW. Concentration correlation spectroscopy: a new biophysical probe based on occupation number fluctuations. Annu Rev Biophys Bioeng 4: 311–334, 1975.

18. Flavigny J, Richard P, Isnard R, Carrier L, Charron P, Bonne G, Forissier JF, Desnos M, Dubourg O, Komajda M, Schwartz K, Hainque B. Identification of two novel mutations in the ventricular regulatory myosin light chain gene (MYL2) associated with familial and classical forms of hypertrophic cardiomyopathy. J Mol Med 76: 208 –214, 1998.

19. Geeves MA, Holmes KC. The molecular mechanism of muscle contraction. Adv Protein Chem 71: 161–193, 2005.

20. Greenberg MJ, Watt JD, Jones M, Kazmierczak K, Szczesna-Cordary D, Moore JR. Regulatory light chain mutations associated with cardiomyopathy affect myosin mechanics and kinetics. J Mol Cell Cardiol 46: 108 –115, 2009.

21. Hernandez OM, Szczesna-Cordary D, Knollmann BC, Miller T, Bell M, Zhao J, Sirenko SG, Diaz Z, Guzman G, Xu Y, Wang Y, Kerrick WG, Potter JD. F110I and R278C troponin T mutations that cause familial hypertrophic cardiomyopathy affect muscle contraction in transgenic mice and reconstituted human cardiac fibers. J Biol Chem 280: 37183–37194, 2005.

22. Herrmann C, Lionne C, Travers F, Barman T. Correlation of ActoS1, myofibrillar, and muscle fiber ATPases. Biochemistry 33: 4148 –4154, 1994.

23. Hopkins SC, Sabido-David C, Corrie JE, Irving M, Goldman YE. Fluorescence polarization transients from rhodamine isomers on the myosin regulatory light chain in skeletal muscle fibers. Biophys J 74: 3093–3110, 1998.

24. Hopkins SC, Sabido-David C, van der Heide UA, Ferguson RE, Brandmeier BD, Dale RE, Kendrick-Jones J, Corrie JE, Trentham DR, Irving M, Goldman YE. Orientation changes of the myosin light chain domain during filament sliding in active and rigor muscle. J Mol Biol 318: 1275–1291, 2002.

25. Huang W, Liang J, Kazmierczak K, Muthu P, Duggal D, Farman G, Sorensen L, Pozios I, Abraham T, Moore J, Borejdo J, SzczesnaCordary D. Hypertrophic cardiomyopathy associated Lys104Glu mutation in the myosin regulatory light chain causes diastolic disturbance in mice. J Mol Cell Card 74: 318 –329, 2014.

26. Huxley AF, Simmons RM. Proposed mechanism of force generation in striated muscle. Nature 233: 533–538, 1971.

27. Kabaeva ZT, Perrot A, Wolter B, Dietz R, Cardim N, Correia JM, Schulte HD, Aldashev AA, Mirrakhimov MM, Osterziel KJ. Systematic analysis of the regulatory and essential myosin light chain genes: genetic variants and mutations in hypertrophic cardiomyopathy. Eur J Hum Genet 10: 741–748, 2002.

28. Kazmierczak K, Muthu P, Huang W, Jones M, Wang Y, SzczesnaCordary D. Myosin regulatory light chain mutation found in hypertrophic cardiomyopathy patients increases isometric force production in transgenic mice. Biochem J 442: 95–103, 2012.

29. Kerrick WG, Kazmierczak K, Xu Y, Wang Y, Szczesna-Cordary D. Malignant familial hypertrophic cardiomyopathy D166V mutation in the ventricular myosin regulatory light chain causes profound effects in skinned and intact papillary muscle fibers from transgenic mice. FASEB J 23: 855–865, 2009.

30. Lakowicz JR. Principles of Fluorescence Spectroscopy. New York, NY: Springer-Verlag, 2006.

31. Lehrer SS, & Ishii Y. Fluorescence properties of acrylodan-labeled tropomyosin and tropomyhosin actin: evidence for myosin subfragment-1 induced changes in geometry between tropomyosin and actin. Biochemistry 27 5899 –5906, 1988.

32. Ling N, Shrimpton C, Sleep J, Kendrick-Jones J, Irving M. Fluorescent probes of the orientation of myosin regulatory light chains in relaxed, rigor, and contracting muscle. Biophys J 70: 1836 –1846, 1996.

33. Lowey S, Bretton V, Gulick J, Robbins J, Trybus KM. Transgenic mouse alpha-and beta-cardiac myosins containing the R403Q mutation show isoform dependent transient kinetic differences. J Biol Chem 288: 14780 –14787, 2013.

34. Lymn RW, Taylor EW. Mechanism of adenosine triphosphate hydrolysis by actomyosin. Biochemistry 10: 4617–4624, 1971.

35. Magde D, Elson EL, Webb WW. Fluorescence correlation spectroscopy. II. An experimental realization. Biopolymers 13: 29 –61, 1974.

36. Mettikolla P, Calander N, Luchowski R, Gryczynski I, Gryczynski Z, Zhao J, Szczesna-Cordary D, Borejdo J. Cross-bridge kinetics in myofibrils containing familial hypertrophic cardiomyopathy R58Q mutation in the regulatory light chain of myosin. J Theor Biol 284: 71–81, 2011.

37. Mettikolla P, Luchowski R, Gryczynski I, Gryczynski Z, SzczesnaCordary D, Borejdo J. Fluorescence lifetime of actin in the FHC transgenic heart. Biochemistry 48: 1264 –1271, 2009.

38. Midde K, Rich R, Marandos P, Fudala R, Li A, Gryczynski I, Borejdo J. Comaprison or orientation and rotational motion of cross-bridges containing phosphorylated and dephosphorylated myosin regulatory light chain. J Biol Chem 288: 7012–7023, 2013.

39. Miller T, Szczesna D, Housmans PR, Zhao J, de Freitas F, Gomes AV, Culbreath L, McCue J, Wang Y, Xu Y, Kerrick WG, Potter JD. Abnormal contractile function in transgenic mice expressing a familial hypertrophic cardiomyopathy-linked troponin T (I79N) mutation. J Biol Chem 276: 3743–3755, 2001.

40. Morales MF. Calculation of the polarized fluorescence from a labeled muscle fiber. Proc Nat Acad Sci USA 81: 145–149, 1984.

41. Morner S, Richard P, Kazzam E, Hellman U, Hainque B, Schwartz K, Waldenstrom A. Identification of the genotypes causing hypertrophic cardiomyopathy in northern Sweden. J Mol Cell Cardiol 35: 841–849, 2003.

42. Muthu P, Mettikolla P, Calander N, Luchowski R, Gryczynski I, Gryczynski I, Szczesna-Cordary D, Borejdo J. Single molecule kinetics in the familial hypertrophic cardiomyopathy D166V mutant mouse heart. J Mol Cell Cardiol 48: 989 –998, 2010.

43. Nihei T, Mendelson RA, Botts J. Use of fluorescence polarization to observe changes in attitude of S1 moieties in muscle fibers. Biophys J 14: 236–242, 1974.

44. Qian H, Saffarian S, Elson EL. Concentration fluctuations in a mesoscopic oscillating chemical reaction system. Proc Natl Acad Sci USA 99: 10376 –10381, 2002.

45. Rayment I, Holden HM, Whittaker M, Yohn CB, Lorenz M, Holmes KC, Milligan R. Structure of the actin-myosin complex and its implications for muscle contraction. Science 261: 58 –65, 1993.

46. Rayment I, Rypniewski W, Schmidt-Base K, Smith R, Tomchik DR, Benning MM, Winkelman DA, Wesenberg G, Holden HM. Threedimensional structure of myosin subfragment-1: a molecular motor. Science 261: 50 –58, 1993.

47. Rice J. Mathematical Statistics and Data Analysis (2nd ed.). N. Scituate, MA: Duxbury, 1995.

48. Sabido-David C, Brandmeier B, Craik JS, Corrie JE, Trentham DR, Irving M. Steady-state fluorescence polarization studies of the orientation of myosin regulatory light chains in single skeletal muscle fibers using pure isomers of iodoacetamidotetramethylrhodamine. Biophys J 74: 3083– 3092, 1998.

49. Tregear RT, Mendelson RA. Polarization from a helix of fluorophores and its relation to that obtained from muscle. Biophys J 15: 455–467, 1975.

50. Tsaturyan AK, Bershitsky SY, Burns R, Ferenczi MA. Structural changes in the actin-myosin cross-bridges associated with force generation induced by temperature jump in permeabilized frog muscle fibers. Biophys J 77: 354 –372, 1999.

51. Ushakov DS, Caorsi V, Ibanez-Garcia D, Manning HB, Konitsiotis AD, West TG, Dunsby C, French PM, Ferenczi MA. Response of rigor cross-bridges to stretch detected by fluorescence lifetime imaging microscopy of myosin essential light chain in skeletal muscle fibers. J Biol Chem 286: 842–850, 2011.

52. Wang Y, Xu Y, Kerrick WGL, Wang Y, Guzman G, Diaz-Perez Z, Szczesna-Cordary D. Prolonged Ca2 and force transients in myosin RLC transgenic mouse fibers expressing malignant and benign FHC mutations. J Mol Biol 361: 286 –299, 2006.

CHAPTER XI

DIFFERENCES IN THE DEGREE OF ORDER OF MYOSIN CROSSBRIDGES OF LEFT AND RIGHT VENTRICLES IN KNOCKED-IN R21C-TROPONIN I MICE

D. Duggal[1], J. Nagwekar[1], R. Rich[2], S. Raut[1], R. Fudala[1], H. Das[3], Z. Gryczynski[4], I. Gryczynski[1], D. Szczesna- Cordary[5] and J. Borejdo[1]*

[1]Dept of Cell Biology and Immunology and the Center for Commercialization of Fluorescence Technologies, University of North Texas, Health Science Center, 3500 Camp Bowie Blvd, Fort Worth, TX 76107.

[2]Department of Mathematics, Computer Science, and Physics, Texas Wesleyan University, 1201 Wesleyan Street, Fort Worth, TX 76105

[3] Center for Neuroscience Discovery, Institute for Healthy aging and Institute of Cancer Research, University of North Texas, Health Science Center, 3500 Camp Bowie Blvd, Fort Worth, TX 76107.

[4]Dept of Physics and Astronomy, Texas Christian University, 2800 S. University Dr., Fort Worth, Texas 76129.

[5]Dept of Molecular & Cellular Pharmacology, University of Miami Miller School of Medicine, Miami, FL 33136

D. Duggal and J. Nagwekar contributed equally to this paper.

*Corresponding author: J. Borejdo, Dept of Cell Biology & Immunology and the Center for Commercialization of Fluorescence Technologies, University of North Texas, Health Science Center, 3500 Camp Bowie Blvd, Fort Worth, TX 76107, Tel 817 735 2106, Fax 817 735 2118, Email Julian.Borejdo@unthsc.edu

* This work was supported, in whole or in part, by National Institutes of Health Grants R01 HL042325 and HL108343 (to D.S-C.), R01 AR048622 (to J. B.) and R01HL090786 (to J. B. and D. S-C.).

1. ABSTRACT

We examine the effects of the TnI R21C mutation in human cardiac troponin I, the mutation that is linked to hypertrophic cardiomyopathy on actin-myosin interactions. The study was performed on muscles from the left (LV) and right (RV) ventricles of knock-in mice. Macroscopic parameters of contraction, such as maximum tension, speed of shortening or ATPase activity, are unlikely to reveal differences between the ventricles because they are made on whole organs containing trillions of actin and myosin molecules. Since ventricles differ in their myocardial architecture, averaging the data collected from such a large assembly is likely to conceal small differences. To circumvent the averaging problem, the measurements were done on few actin molecules of a thin filament within isolated myofibril. To this end, one in thousand actin monomers were labeled with a fluorescent dye. Control anisotropy experiments revealed that the orientation of actin reflected the orientation of myosin cross-bridges. The mutation imposed significant differences in the distribution of angles that actin makes with the thin filament axis: during contraction, actin molecules in LV were arranged more tightly compared to those in RV. This work reveals phenotypic differences of the R21C mutation in the left versus right mouse ventricles even though both ventricles express the same isoform of the cardiac TnI. It also highlights the importance of functional differences between the two ventricles of cardiac disease.

Key Words: Mutation of TnI, Arrangement of Actin, Contraction of Left and Right Ventricle

2. INTRODUCTION

Muscle contraction is caused by the cyclic interactions of a myosin head with actin {(Sabido-David et al., 1998; Hopkins et al., 2002; Geeves and Holmes, 2005). These interactions, driven by hydrolysis of ATP, cause a heart to pump the blood through the body. Contraction of the right ventricle (RV) causes blood to flow into pulmonary circulation, and contraction of the left ventricle (LV) causes blood to flow into the systemic circulation through the aorta. Despite efforts by many, the contractile differences between the right and left ventricles in healthy and/or diseased muscles are poorly understood. For example, no differences were observed in stress development, twitch duration, work performance or shortening power among RV and LV in dogs (Wikman-Coffelt et al., 1975) and histologic examination revealed no differences in a patient with the R723G mutation of the beta-myosin heavy chain (Borchert et al., 2010). Further, there have been no confirmed reports of amino acid or conformational differences in LV and RV myosin heavy or light chains.

On the other hand, differences between ventricles were seen during evolutionary development (LV develops early while RV develops late), in embryological development origin (Rosenquist, 1970; de la Cruz et al., 1977; Srivastava et al., 1997), in morphological characteristics (LV is bullet shaped, RV is complex and crescentric (Friedberg and Redington, 2014)), in anatomical characteristics (LV and RV are thick- and thin-walled, respectively; (Friedberg and Redington, 2014)), in the genetics (Park et al., 2011; Cadete et al., 2012), in pumping conditions (LV and RV are high and low resistance pumps, respectively ((Schwarz et al., 2013; Friedberg and Redington, 2014) and in general physiology (LV uses more energy and shortens faster than RV (Itoya et al., 1996; Carlsson et al., 2012) Carlsson, 2012 #4598}. Samarel showed increased fractional synthesis and degradation of myosin heavy chain and light chains (but not actin) in the left compared to the right ventricular free wall (Samarel, 1989).

This report suggests that the differences exist on the molecular level as well. We have previously shown that significant differences exist in the molecular arrangement of actin monomers in the thin filament of Wild Type (WT) LV and WT-RV (Nagwekar et al., 2014) mouse tissue. These differences become more clear when ventricles of knock-in (KI) mice (Wang et al., 2012b) that are made to express human troponin I, R21C mutation are examined at the level of the myofilament (Liang et al., 2015) and at the single molecule level. This mutation has been linked to hypertrophic cardiomyopathy (HCM; a genetic autosomal dominant disorder resulting in LV and/or RV hypertrophy and sudden cardiac death (SCD) (Kimura et al., 1997; Arad et al., 2005; Alcalai et al., 2008). To be able to extract molecular data from an *ex-vivo* ventricle in spite of significant differences in morphological characteristics and myocardial architecture, it is necessary to make sure that detected actin-myosin interactions originate from only a few adjacent molecules. The simplest way to do so is to reduce the number of observed acto-myosin units by sparse labeling with a fluorophore. We were able to limit our observation to 3-4 actin molecules. Observing smaller number was impractical, because the signal from an *ex-vivo* ventricle contains significant contributions from the background and autofluorescence.

Comparison between the arrangements of actin monomers in thin filaments from LV-MUT and RV-MUT ventricles showed that the mutation affected each ventricle differently. During contraction of the LV, the arrangement was tighter than the arrangement in the RV. We speculate that this difference is due to the fact

that the maximal isometric tension is reduced in LV as compared with RV, with the consequence that thin filaments of RV are stretched (and those of LV are not). We believe that smaller stress of thin filaments of LV causes the actin protomers to be now in an opportune position for cross-linking by the cTnI. Higher stress in RV prevents cross-linking.

3. MATERIALS AND METHODS

3.1. Chemicals and solutions

All chemicals were from Sigma-Aldrich (St Louis, MO). Alexa633-Phalloidin (AP) was from Molecular Probes (Eugene, OR). Experiments were done in contracting solution containing 50 mM KCl, 10 mM Tris-HCl pH 7.5, 5 mM $MgCl_2$, 0.1 mM $CaCl_2$, 5 mM ATP, 20 mM creatine phosphate and 10 units/ml of 1 mg/ml creatine kinase; in rigor solution containing 50 mM KCl, 10 mM Tris-HCl pH 7.5, 2 mM $MgCl_2$, 0.1 mM $CaCl_2$; or in relaxing solution (which had the same composition as contracting solution but substituting 0.1 mM $CaCl_2$ for 2 mM EGTA).

3.2. Preparation of myofibrils

LVs and RVs were shipped on ice from Florida (Szczesna-Cordary) in a glycerinating solution containing 50% glycerol and 50% pCa 8 (10^{-8} M [Ca^{2+}], 1 mM free [Mg^{2+}] (total MgPr

(propionate) = 3.88 mM), 7 mM EGTA, 2.5 mM [Mg-ATP^{2-}], 20 mM MOPS, pH 7.0, 15 mM creatine phosphate, and 15 units/mL of phosphocreatine kinase, ionic strength = 150 mM adjusted with KPr), 15% glycerol, and 30 mM 2,3-Butadione Monoxide (BDM) solution. They were immediately transferred to -20^{O}C in glycerinating solution (50% glycerol, 150 mM KCl, 10 mM Tris-HCl pH 7.5, 5 mM $MgCl_2$, 5 mM EGTA, 5 mM ATP, 1 mM DTT, 2 mM PMSF and 0.1% β-mercaptoethanol). Ventricles were washed 3 times for 1/2 hr with ice-cold EDTA-rigor solution (50 mM KCl, 10 mM Tris-HCl pH 7.5, 5 mM EDTA) for 30 min in order to wash out the ATP present in the glycerinating solution without causing contraction. Muscles were then washed thoroughly with the rigor solution and homogenized in a Cole-Palmer LabGen 125 homogenizer for 10 s followed by a further 10 s homogenization after a cool down period of 30 s.

3.3. Cross-linking

To inhibit shortening, 1 mg/ml myofibrils were incubated for 20 min at room temperature with 20 mM water-soluble cross-linker 1-ethyl-3-[3-(dimethylamino)-propyl]-carbodiimide (EDC) (Herrmann et al., 1994; Bershitsky et al., 1997; Barman et al., 1998; Tsaturyan et al., 1999). The reaction was stopped by adding 20 mM DTT followed by washing with the rigor solution. The pH of the solution remained unchanged at 7.5 throughout the time course of reaction. The absence of shortening was verified by observing myofibrils irrigated with contraction solution in a Nomarski microscope. EDC had no effect on myofibrillar ATPase activity (see below). The ATPase activity was compared with and without EDC in myofibrils prepared from LV and RV of wild-type and mutant transgenic hearts.

3.4. Labeling of thin filaments

10 nM Alexa633 Phalloidin (AP) was mixed with 10 μM unlabeled phalloidin (UP) and the mixture was added to 1 mg/mL myofibrils for 10 min at room temperature. This resulted in sparse insertion of the fluorophore into a myofibril. Phalloidin had no effect on the ATPase activity of the groups being compared in this study. The determination of the actual number of fluorophores in the Observational Volume (OV) is described below.

3.5. Myofibirillar ATPase assay

The ATPase activity was measured and compared between different groups of Transgenic wild types (LV and RV) and mutant LV and RV. SensoLyte® MG Phosphate Assay Kit was used to perform the ATPase assay. 1mg/ml myofibrils were prepared in a solution containing 50mM KCl, 5mM $MgCl_2$ and calcium rigor. 20mM EDC and 10μM phalloidin were added to the samples where the effect of EDC and Phalloidin on ATPase activity was to be determined. Following sample preparation, 80μl of each sample was added to a 96-well plate. 20μl of Malachite Green was added to each well. 20mM ATP was added to each well using a multichannel pipette prior to measuring absorbance at 650 nm. Standard plot was used to measure the ATPase activity of each sample.

3.6. Effect of mutation on ATPase activity

The ATPase activities of transgenic wild types LV and RV and mutant LV and RV were measured as described above. **Table 1** lists the measured ATPase activity for all sample groups including the effect of EDC and Phalloidin. It can be seen that MUT-RV had significantly increased ATPase activity in all the four cases: with EDC, without EDC, with Phalloidin and without Phalloidin. The presence of EDC did not affect the ATPase activity significantly in Tg-WT LV, Tg- WT RV and MUT-LV. Tg-WT LV had a higher ATPase activity in the absence of EDC when compared to Tg-WT.

MF from	With EDC (uM/min/mg/ml MF)	Without EDC (uM/min/ mg/ml MF)	With Phalloidin (uM/min/ mg/ml MF)	Without Phalloidin (uM/min/ mg/ml MF)
WT R21C LV	**1.5152**	**1.9815**	**1.5205**	**1.9057**
WT R21C RV	**1.6911**	**1.7492**	**1.8347**	**1.8715**
R21C LV	**1.5721**	**1.5504**	**1.7409**	**1.8589**
R21C RV	**3.8494**	**3.6966**	**3.7976**	**3.7702**

Table 1. ***Measurements showing that neither EDC nor phalloidin have an effect on ATPase activity of ventricular muscle***. *ATPase activity of different samples in the presence and absence of EDC and Phalloidin.*

RV; while the MUL-LV had a lower ATPase activity in the absence of EDC when compared to MUT-RV. Phalloidin did not have significant effect on ATPase activity of different groups. Phalloidin slightly decreased the ATPase activity of Tg-WT LV when compared to Tg- WT RV. The results are summarized in **Fig. 1**.

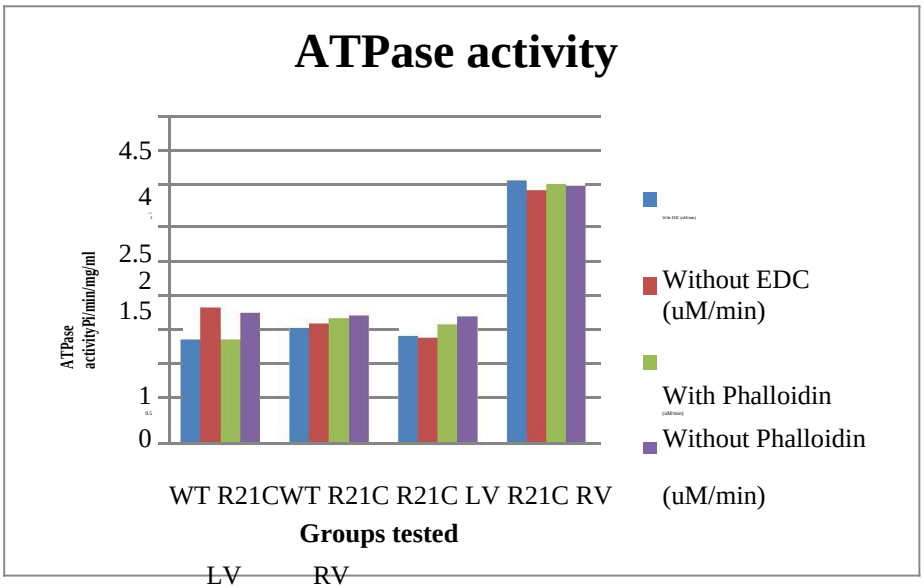

Fig. 1 Summary of data from Table 1. *The ATPase activity is in µmoles of phosphate released per minute per mg/ml of myofibril.*

ProQ Diamond phophoprotein

staining: Proteins were separated on

phosphorylation of sarcomeric

proteins was detected by staining with ProQ Diamond Phosphoprotein gel stain (Thermo Fischer Scientific). 100µg of myofibrils (in calcium rigor) from each sample was used. Transgenic WT LV was used as a standard and densitometric analysis was performed to compare the RLC and TnI phosphorylation levels among different samples.

3.8. The number of observed molecules

To determine the number of actin-phalloidin molecules under observation, the instrument had to be calibrated to determine fluorescence intensity caused by known numbers of molecules of the dye. These numbers were determined by Fluorescence Correlation Spectroscopy (FCS). The autocorrelation function $G(\tau)$ of fluctuations caused by freely diffusing fluorescent molecules entering and leaving the Observational Volume (OV) was constructed. Its value at a delay time 0 is equal to the inverse of the number of molecules contributing to fluctuations, $N = 1/G(\tau=0)$ (Magde et al., 1974; Elson, 1985, 2007). Solutions of the fluorophore in the 1.29 - 77.3 nM range gave six Gs from which the number of fluorophores was determined. The calibration curve, a plot of the number of molecules vs. fluorescence intensity, showed that, on average, 1 molecule of AP contributed 1,250 counts/s. A typical myofibril is shown in **Fig. 2** (top panel). A time course of the orthogonal intensities and polarization of fluorescence of a myofibril is shown in **Fig. 2** (bottom panel). The observed total count was 2,900 counts/s. Therefore in this particular experiment, the observed average number of molecules was 2,900/1,250=2.3. More typically, the count was 4,000 photons/s and the observed average number of molecules was ~3-4. However, it should be emphasized that as long as the number of cross-bridges is mesoscopic (i.e. small), the exact number does not matter, i.e. 3 molecules should give the same result as 30 (Magde et al., 1974; Elson, 1985, 2007). 20-25 half-sarcomeres were sampled. Each measurement lasted 20 s and contained 2 million experimental data points. Data was smoothed by binning by a factor of 1000, so each half-sarcomere produced X=2000 data points. The precision of the measurement of each half-sarcomere is approximately equal to $1/\sqrt{X}=2.2\%$.

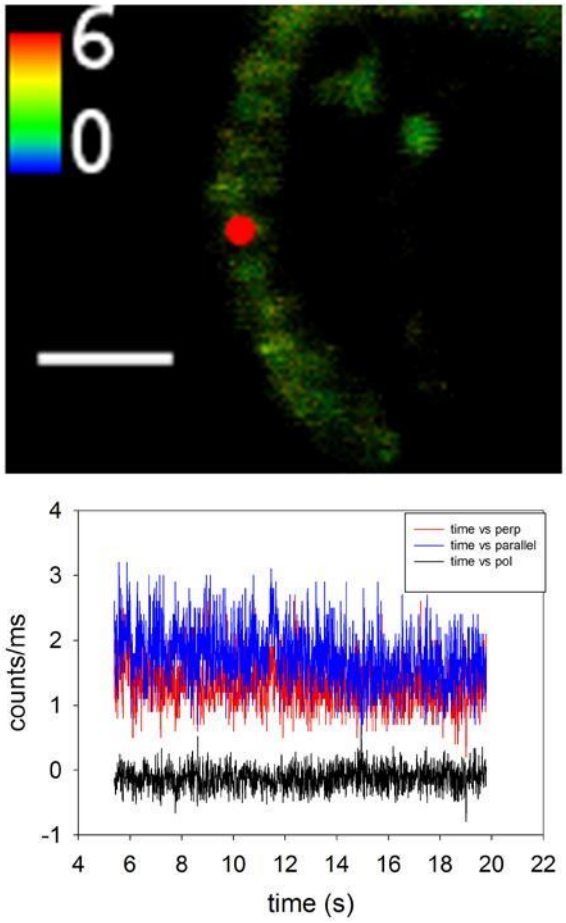

Fig. 2. Imaging myofibrils. Top panel*: A typical lifetime image of a myofibril sparsely labeled with AP (AP:actin=1:1000). Lifetime scale (top left) is in ns. The bar is 2.5 μm. The red circle is a projection of the confocal aperture on the image plane. It indicates the lateral dimensions of the OV. The data was taken only from half-sarcomeres which were oriented vertically (such as the one over which the red circle was placed, and each of its immediate neighbors).* ***Bottom panel****: Raw data from contracting LV-WT muscle. This kind of data was used to estimate number of observed molecules. The first 0-3 sec of data was rejected because of photobleaching (even though it had little effect on polarization of fluorescence because the rate of bleaching for both channels was the same). The polarization of fluorescence signal derived from orthogonal polarization components (red and blue) is in black.*

3.9. Data collection

The myofibrils were placed on the scanning stage of the PicoQuant MT 200 inverse time-resolved

fluorescence instrument coupled to an Olympus IX 71 microscope. Muscles were perfused with rigor, relaxation or contracting solutions as needed. The stage was rotated to align the myofibril under observation vertically in the lab frame of reference. The polarization of the laser was also vertical. The power delivered to each half-sarcomere was adjusted to be within the 1-2 μW range to obtain a similar photon rate for each myofibril (if the power is not equal, the differences between data sets become statistically un-interpretable (Borejdo et al., 2012). Before each experiment, fluorescence of an isotropic solution of a dye with long fluorescence lifetime (such as rhodamine 700 which has 0 anisotropy) was measured to make sure that the parallel and perpendicular channels received equal amount of light. 640 nm laser beam modulated at 20 MHz was focused by an Olympus x60, NA=1.2 water immersion objective on the fluorescent part of a myofibril. A 5 mM contracting solution (containing ATP-regenerating enzymes, see above) was used in experiments carried out during contraction. All experiments were done at room temperature, where ~20-30 myofibrils were examined. The OV (1.7 μm^3) was estimated by measuring the FWHM in the axial and lateral dimensions of an image of a 20 nm fluorescent bead as in ref (Buschmann et al., 2009).

3.10. Statistical analysis

Comparisons between groups were performed using an unpaired Student's t-test (Sigma Plot 11; Systat

Software, Inc., San Jose, CA, USA). The differences were deemed significant when $P<0.05$. SigmaPlot 11was used to compute histograms. Origin v.8.6 (Northampton, MA) was used to compute autocorrelation functions

4. RESULTS

4.1. The effect of mutation is best studied by observing the orientation of actin in the thin filaments

In this work the effect of mutation was studied by observing rotational motion of actin, namely the anisotropy of a probe rigidly attached to an actin monomer. Labeling of actin rather than myosin has two significant advantages: Firstly, the backstroke (re-priming) of XBs which would have been recorded as a change of anisotropy if myosin was labeled, is not recorded. This makes measurements more accurate. Secondly, it is possible to determine the **exact** number of the observed molecules. Labeling actin involves only irrigation of myofibrils with the peptide at room temperature. Addition of a well-defined ratio of labeled phalloidin/unlabeled phalloidin labels only the exact number of actin molecules with a fluorescent probe. In contrast, labeling of myosin involves labeling light chain 1 (LC1) and exchanging it with myofibrillar LC1 under harsh conditions (1/2 hr at 37^{o}C in the presence of trifluoroperazine) (Sweeney, 1995; Ling et al., 1996), which is not well reproducible.

It is possible to infer rotation of cross-bridges from actin measurements because each orientation of actin corresponds to a unique orientation of the myosin head. In a thin filament, seven actin monomers are connected by a tropomyosin double helix. This causes those protomers to act as a cooperative unit (Oosawa et al., 1977; Yanagida and Oosawa, 1978, 1980; Prochniewicz-Nakayama, 1983). The extent of the unit may even stretch beyond 38.5 nm (Hill et al., 1981; Ando, 1989). Most units do not contain labeled actin monomer; its motion remains invisible. But when it does, each interaction with a myosin head results in a change in dipole orientation of the labeled actin. Every transient intermediate step of a XB cycle is associated with a specific anisotropy of the actin filament. This is demonstrated in **Fig. 3.** The figure shows the conventional 4-state model of XB action based on the work of Coureux, Houdusse & Sweeney (Coureux et al., 2004). The cycle begins when ATP binds to myosin, and it dissociates from actin (**Fig. 3C**). The anisotropy of actin is small (0.041); when myosin is not bound to actin, it can rotate nearly free in the myofibrillar space. In **Fig. 3C** an average orientation is represented by the vertical orientation of the transition moment of rhodamine (green arrow). Following hydrolysis of ATP, the myosin head has bound ADP and Pi and binds weakly to actin (**Fig. 3A**).

Fig. 3. 4-state model of XB action. *Labeled actin in is red, myosin XB is blue and the transition dipole of Alexa633 phalloidin is green. T=ATP, D=ADP, P=Pi. XB orientation and anisotropy of actin are related. Weakly and strongly bound myosin has intermediate steady-state anisotropy (SSA) (A) and high (**B**) SSA respectively. Free myosin has low SSA (C), while the free dye has lowest SSA (D).*

Actin rotation is now partially restricted (**Fig. 3A**). Next, myosin releases P and ADP (not necessarily in this order) to bind strongly to actin and execute a power stroke. Actin rotation is now more

restricted and anisotropy is large (SSA=0.171, **Fig. 3B**). Strong binding is terminated by the binding of ATP to the myosin head. (It is a pseudo first order reaction because the concentration of ATP is much larger than the myosin concentration (i.e. [ATP] is constant). The actin dipole is now returned to the original value (**Fig. 3C**). Thus the orientation of the transition dipole of a fluorophore bound to actin reflects binding of the XB.

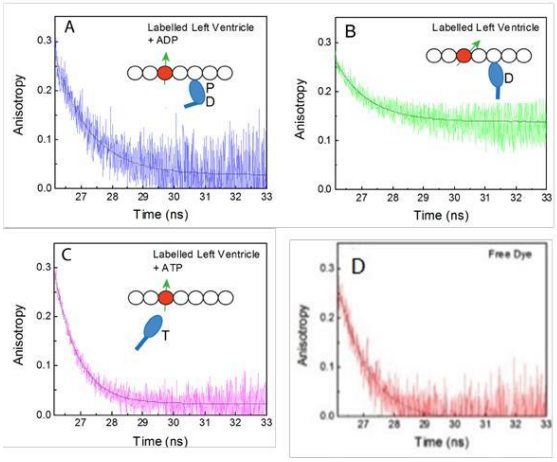

4.2. The effect of mutation on arrangement of actin in thin filaments of LV and RV during contraction

Each half-sarcomere containing 3-4 acto-myosins is sampled 2000 times. It is thus possible to construct a histogram of orientations of this half-sarcomere (plots of orientation vs. probability of this orientation). Full Width at Half Maximum (FWHM) indicates how well actin monomers within thin filaments are ordered. Since the plots are Gaussian curves, they can also be characterized by Standard Deviation [1]. **Fig. 4** shows the representative examples of histograms of contracting mutant and Wild Type (WT) myofibrils.

Fig. 4. Representative examples of histograms. C*lockwise from top left: contracting MUT-LV, MUT-RV, WT- RV and WT-LV. Red lines show fittings to three parameter Gaussians.*

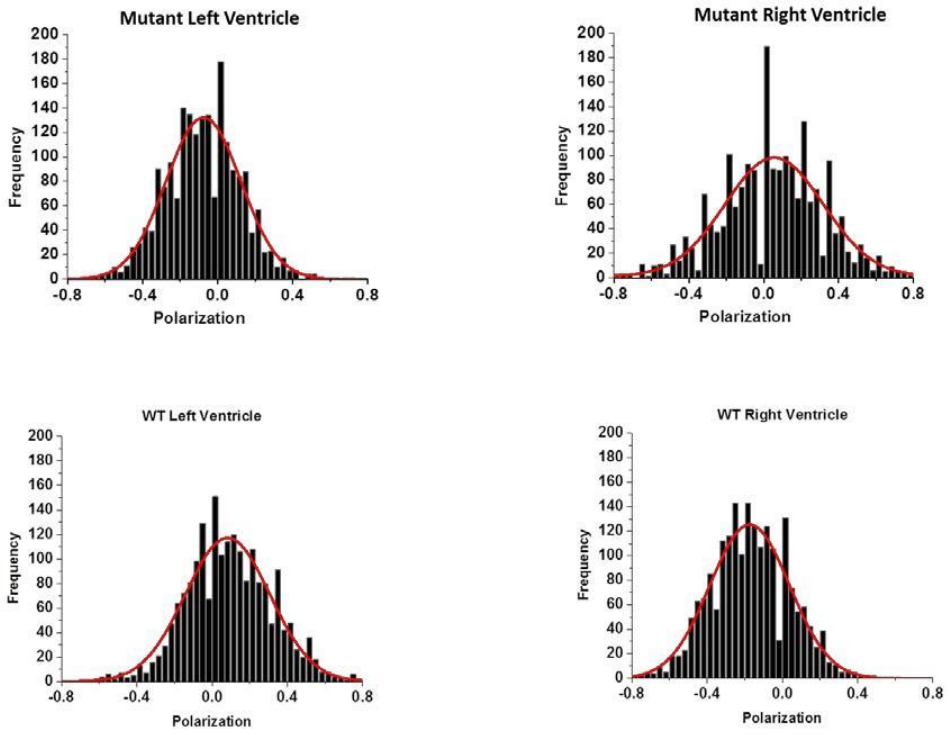

Table 2 shows that FWHM values of mutated LVs were significantly smaller than mutated RVs, suggesting that during contraction XBs of LV assume more ordered configuration.

Contracting ventricles	FWHM	Counts/ms
LV-MUT	0.272±0.055	2.128±0.204
RV-MUT	0.530±0.056	2.038±0.079

Table 2. **Effect of *R21C mutation in TnI on the widths of distribution of actin angles in contracting LV and RV***. *Results of 29 experiments . Errors are SEM*

The difference of -0.258 of FWHM **IS** statistically significant (t = -3.192, P=0.002, with 59 degrees of freedom). The 95 percent confidence interval for the difference of means was from -0.420 to -0.0963. The difference of 0.090 counts/sec is **NOT** statistically significant (t = 0.461, P=0.646 with 58 degrees of freedom). The 95 percent confidence interval for the difference of means was from -0.303 to 0.484. The fact that the difference between the count rate was not statistically significant is an important indicator of the validity of the method. Strong Gaussian signals have systematically small relative errors, while weak signals have large errors. The fact that signals were of the same strength implies that systematic errors do not contribute to the results.

In contrast, when the width of distribution of actin angles in contracting LV and RV wild types was compared, the differences were not statistically significant. The results are summarized in **Table 3**. The difference of 0.016 between the FWHM of WT LV and RV was not statistically significant (t = 0.3360, P=0.7378 with 70 degrees of freedom). The 95 percent confidence interval for the difference of means was from -0.07896 to 0.11096.

Contracting ventricles	FWHM	Counts/ms
LV-WT	0.586±0.189	2.595±0.946
RV-WT	0.570±0.215	3.302±1.497

Table 3. **No effect on the width of *distribution of actin angles in contracting LV and RV wild types***. *Results of 39 experiments from WT LV and 33 experiments from WT RV. Errors are SD.*

4.3. Negative control: The effect of the mutation on the spatial distribution of actin in LV and RV during relaxation

In relaxation, the contact between XBs and thin filaments (at the present ionic strength) is rare. The distribution of angles reflects only thermal fluctuations of actin, and we expect that mutation will make no difference to the FWHM value. **Table 4** shows that indeed there was no difference in FWHM between LV-MUT and RV-MUT.

Relaxation	FWHM	Counts/ms
LV-MUT	0.535±0.059	5.054±0.653
RV-MUT	0.495±0.031	4.872±0.423

Table 4. No effect of *R21C mutation in TnI on the widths of distribution of angles between the left and right ventricles in relaxed muscle*. *24 experiments. Errors are SEM.*

The 0.039 difference between FWHM for LV and RV was **NOT** statistically significant (t = 0.641, P=0.524 with 53 degrees of freedom). The 95 percent confidence interval for difference of means was from -0.0833 to 0.162. The 0.183 difference between counts/s for LV and RV was **NOT** statistically significant (t = 0.245, P=0.808 with 53 degrees of freedom). The 95 percent confidence interval for difference of means was from -1.314 to 1.679.

4.4. Effect of mutation on post-translational modifications

It is known that phosphorylation of TnI modulates calcium sensitivity of thin filaments (Liang et al., 2015). Phosphorylation increases the rate of relaxation and cross bridge kinetics, and reduces calcium affinity of cardiac Troponin C and calcium sensitivity of force generation. Therefore, it became crucial to evaluate the effect of the mutation on cardiac TnI phosphorylation. Differences in RLC phosphorylation were also studied. RLC phosphorylation by cardiac myosin light chain kinase (cMLCK) was also measured because it plays an important regulatory role in cardiac performance. In general, RLC phosphorylation increases calcium sensitivity of myofilament contraction required for normal cardiac performance. It is likely that RLC phosphorylation will be affected in cardiomyopathy (Chang et al., 2015). ProQ Diamond Phosphoprotein gel stain was used to specifically stain the phosphorylated proteins. This stain contains a fluorescent dye, which

specifically binds to the phosphor-proteins non-covalently on polyacrylamide gels. Images were captured to compare the phosphorylation levels in the four different samples. **Fig. 5** shows the SDS PAGE gel stained with ProQ. It should be noted that the differences in the intensities (measured by densitometric analysis) were statistically significant for both TnI and RLC.

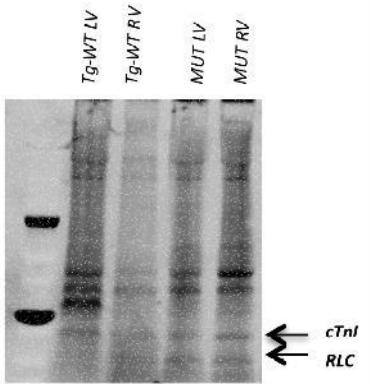

Fig. 5. Effect of phosphorylation of TnI and RLC*. ProQ Diamond Phosphoprotein stained SDS PAGE gel. The five lanes represent the marker, Tg- WT LV, Tg- WT RV, MUT LV and MUT RV respectively. The TnI and RLC phosphorylation bands can be seen at 24,000 Da and 18,000 Da respectively.*

In case of RLC, phosphorylation was increased in WT RV as compared to WT LV ($p<0.01$), while in MUT LV, phosphorylation was increased as compared to MUT RV ($p<0.01$). In general, RLC phosphorylation was decreased in R21C mutant ventricles. It should be noted that the difference in intensities in WT LV and MUT LV was not significant.

TnI phosphorylation levels were significantly decreased in MUT ventricles when compared to their corresponding Wild Types ($P<0.01$) while the difference in TnI phosphorylation in WT LV and WT RV was not significantly different. These differences are represented in **Fig 6.**

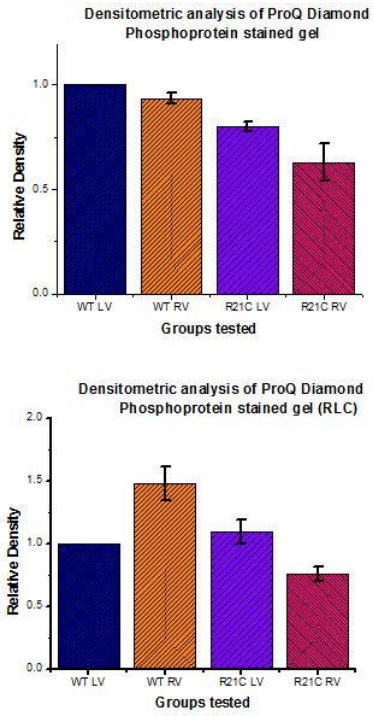

Fig 6. Effect of phosphorylation of TnI and RLC*. Densitometric analysis of ProQ Diamond Phosphoprotein stained gel was performed to detect differences in phosphorylation levels of TnI and RLC in the different groups. WT LV was used as a standard. Top TnI; means and SD relative to WT-LV (from the left): 1, 0.93±0.02, 0.80±0.02, 0.62±0.08; Bottom: RLC; 1, 1.47±0.13, 1.09±0.09, 0.75±0.05*

5. DISCUSSION

In vivo* vs *in vitro* measurements.** Phalloidin imposes higher stiffness on thin filaments (Grazi et al., 2004) without altering its ATPase activity (**Fig. 1, Table 1**), regardless of whether or not EDC was present. Cross-linking allows the measurement of 3-4 molecules during steady-state contraction of a ventricle ***ex-vivo. We think that *in vitro* measurements, which allow detection of single molecules, do not provide a complete picture of molecular events. It has recently been shown (Walcott et al., 2012) that an ensemble of myosin in muscle cannot be viewed as a collection of independent motors. Baker et al. (Baker et al., 2002) showed that *in vitro* an ensemble of myosin moves actin faster than would be predicted from single molecule measurements. Pate and Cooke (Pate and Cooke, 1991) analyzed the Huxley model (Huxley, 1957)} at variable ensemble size, showing that when two myosin molecules work together, each behaves differently than an isolated molecule. Other models reach the same conclusion (Nyitrai and Geeves, 2004). Moreover, molecular crowding is an important factor in *because -vivo* situations. It affects not only the physicochemical properties of cellular environments with a high macromolecular content such as the diffusion coefficients, kinetics and thermodynamic properties of proteins (Minton, 1981; Minton, 1998), but also other processes, such as biochemical activities, structural reorganization of the cytoplasm, cytoplasm fluidity and cellular dormancy (Mourao et al., 2014).

5.1. The effect of mutation on arrangement of actin in thin filaments of LV and RV during contraction.

The width of the spatial distribution of dipole angles of LV mutated ventricles is small in comparison with RV during contraction (**Table 2**). We speculate that the molecular mechanism responsible for $_{for}$this$_{the}$observa$_{right}$ion is the fact that thin filaments in LV and RV feel different external loads: the pressure necessary ventricle to force blood to flow into pulmonary circulation is smaller (mean 15 mm Hg) than the pressure necessary for the left ventricle to force blood to flow into the systemic circulation (mean 100 mm Hg). In spite of this fact, we think that the thin filaments of LV bear lighter loads, because RV wall is thinner than LV. Hence actin protomers in LV are under small tension and are therefore more tightly packed than in RV. This is in line with the fact that RV has higher ATPase activity than LV and with (**Fig. 1**) the results of Liang et al. (Liang et al., 2015) who reported larger tension in isolated RV than LV. We think that the mutation R21C causes conformational change in TnI which result in the cross-linking of overall positively charged TnI to the neighboring overall negatively charged actin protomers (5 & 6 in **Fig. 7A**) in LV-MUT, disrupting the ability of actin to rotate. A conformational change also occurs in RV-MUT but it does not lead to cross-linking because protomers are at an inopportune position (**Fig. 7B).**

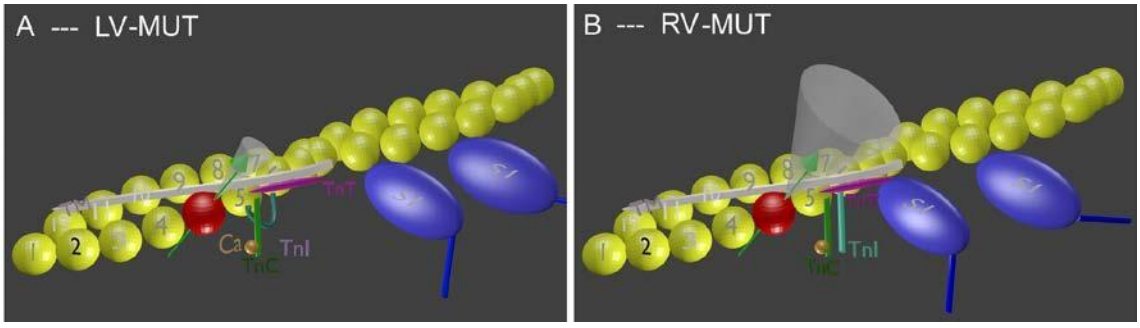

F***ig. 7. The effect of mutation on the cone of angles within which the dipole moment of phalloidin can rotate during contraction***. ***A****: Thin filaments of the LV feel lower tension during contraction. When* Ca^{2+} *(gold sphere)*

binds to TnC (dark green rod) in the presence of MgATP, the disruption of PKA phosphorylation site in TnI (light green) places negatively charged neighboring actin protomers in an opportune distance apart to be cross-linked by positively charged TnI. This stabilizes actin rotation i.e. reduces the range of angles within which actin can rotate (gray cone). ***B****: the effect does not occur in RV, because it experiences larger tension, and actin is not able to cross-link.*

5.2. Macroscopic differences produced by TnI-R21C mutation

The R21C mutation is particularly interesting because it disrupts the protein kinase A (PKA) consensus sequence, preventing phosphorylation of serine-23 and serine-24 and the subsequent modulation of the thin filament function (such as a decrease in Ca^{2+} sensitivity) that occurs in response to β-adrenergic stimulation (Gomes et al., 2005; Wang et al., 2012a). The mutation was strongly associated with SCD in humans (Gomes et al., 2005). Gomes et al. showed that porcine skinned muscle fibers containing the TnI-R21C mutant demonstrated a large increase in Ca^{2+}-sensitivity of force development, and that phosphorylation of these fibers by PKA resulted in a significantly smaller decrease in the Ca^{2+}-sensitivity when compared to WT. However, the mutation did not affect any inhibitory properties of TnI or the maximal ATPase activity (Gomes et al., 2005). These effects were confirmed in experiments performed in the KI mouse model of the R21C mutation which could not be phosphorylated by PKA (Wang et al., 2012a). No changes in the Ca^{2+} sensitivity of force were observed in $R21C^{+/+}$ mice following the treatment of the skinned papillary muscles with exogenous PKA (Wang et al., 2012a). This N-terminal R21C mutation in cardiac TnI has been linked to the malignant phenotype of HCM, but the underlying mechanism is poorly understood. Interestingly, this work reveals phenotypic differences of the R21C action in the left versus right mouse ventricles even though both ventricles express the same isoform of the cardiac TnI. Liang et al showed that the mutation elicited a reduction in the maximal isometric tension in the papillary muscles from left and not right ventricles. No differences in force were noted for WT ventricles (Liang et al., 2015). In addition, they found higher passive tension in the left ventricles of R21C vs. WT mice indicating partial loss of Ca^{2+} regulation at low [Ca^{2+}]. In agreement with (Wang et al., 2012), R21C-KI hearts showed no Ser23/24-cTnI phosphorylation compared to LV or RV of WT mice; however, phosphorylation of the myosin regulatory light chain (RLC) was significantly higher in the RV vs. LV of R21C mice (Liang et al., 2015). ProQ phosphoprotein gel staining performed in this study observed similar results for TnI phosphorylation where the level of phosphorylation was significantly decreased in mutant v/s wild type ventricles. In case of RLC, this work observed that the mutant ventricles exhibited a decrease in the phosphorylation when compared to WT. In particular, MUT RV showed more decline in phosphorylation levels for both RLC and TnI as compared to MUT RV. It must be noted that in recent studies (Chang et al.; 2015), decrease in RLC phosphorylation has been linked to poor cardiac performance. Loss of RLC phosphorylation in conditional cMLCK knock-out mice has been associated with cardiac dilation and loss of cardiac performance. This effect is independent of TnI and myosin binding protein C (MyBPC) and does not affect either of them. This observation is supported by Ishikava et al., who in their study show how the overexpression of MLCK (responsible for phosphorylating RLC) induced sarcomere organization while the downregulation of MLCK caused disturbances in the sarcomere structure. It was also seen that cardiac contractility increased when cardiac MLCK was overexpressed and decreased when the enzyme was downregulated. Such findings suggest that RLC phosphorylation by cardiac MLCK plays a significant role in maintaining sarcomere structure in the heart. Therefore, it was not surprising to detect a decrease in RLC phosphorylation in mutant ventricles.

In conclusion, we observed how the mutation affects both the ventricles differently; right ventricle was affected more adversely compared to the left ventricle. The cross-bridges were better ordered in left ventricle and the phosphorylation levels of RLC and TnI were also higher in left ventricle as compared to the right ventricle. Characterization of RV involvement in FHC is important to elucidate clinical features and assist in development of appropriate treatment methods for cardiac disorders involving RV. It must be mentioned that there are also disadvantages of labeling actin: labeling myosin directly with bifunctional rhodamine is well understood (Bershitsky et al., 1997; Ferenczi et al., 2005) part of a XB which undergoes most prominent rotation - its Regulatory Light Chain - is probed directly, and in contrast to XB labeled with Alexa633 phalloidin, the dipole moment of bifunctional rhodamine in rigor is 100% immobilized by thin filaments.

6. REFERENCES

Alcalai, R., J.G. Seidman, and C.E. Seidman. 2008. Genetic basis of hypertrophic cardiomyopathy: from bench to the clinics. *J Cardiovasc Electrophysiol.* 19(1):104-110.

Ando, T. 1989. Propagation of Acto-S-1 ATPase reaction-coupled conformational change in actin along the filament. *J Biochem (Tokyo).* 105:818-822.

Arad, M., M. Penas-Lado, L. Monserrat, B.J. Maron, M. Sherrid, C.Y. Ho, S. Barr, A. Karim, T.M. Olson, M. Kamisago, J.G. Seidman, and C.E. Seidman. 2005. Gene mutations in apical hypertrophic cardiomyopathy. *Circulation*. 112:2805-2811.

Baker, J.E., C. Brosseau, P.B. Joel, and D.M. Warshaw. 2002. The biochemical kinetics underlying actin movement generated by one and many skeletal muscle myosin molecules. *Biophys J*. 82:2134-2147.

Barman, T., M. Brune, C. Lionne, N. Piroddi, C. Poggesi, R. Stehle, C. Tesi, F. Travers, and M.R. Webb. 1998. ATPase and shortening rates in frog fast skeletal myofibrils by time-resolved measurements of protein-bound and free Pi. *Biophys J.* 74:3120-3130.

Bershitsky, S.Y., A.K. Tsaturyan, O.N. Bershitskaya, G.I. Mashanov, P. Brown, R. Burns, and M.A. Ferenczi. 1997. Muscle force is generated by myosin heads stereospecifically attached to actin. *Nature*. 388:186-190.

Borchert, B., S. Tripathi, A. Francino, F. Navarro-Lopez, and T. Kraft. 2010. The left and right ventricle of a patient with a R723G mutation of the beta-myosin heavy chain and severe hypertrophic cardiomyopathy show no differences in the expression of myosin mRNA. *Cardiol J*. 17:518-522.

Borejdo, J., R. Rich, and K. Midde. 2012. Mesoscopic Analysis of Skeletal Muscle Performance. *In: Biophysical Reviews, J. Garnier, Ed,*. 4:299-231.

Buschmann, V., B. Kramer, and F. Koberlink. 2009. Quantitive FCS: Determination of confocal volume by FCS and bead scabnning with Micro Time 200. *PicoQuant, Application note Quantitative FCS v. 1.1*.

Cadete, V.J., H.B. Lin, J. Sawicka, M. Wozniak, and G. Sawicki. 2012. Proteomic analysis of right and left cardiac ventricles under aerobic conditions and after ischemia/reperfusion. *Proteomics*. 12:2366-2377.

Carlsson, M., E. Heiberg, J. Toger, and H. Arheden. 2012. Quantification of left and right ventricular kinetic energy using four-dimensional intracardiac magnetic resonance imaging flow measurements. *Am J Physiol Heart Circ Physiol*. 302:H893-900.

Chang, A. N., P. K. Battiprolu, P. M. Cowley, G. Chen, R. D. Gerard, J. R. Pinto, J. A. Hill, A. J. Baker, K. E. Kamm, and J. T. Stull. 2015. Constitutive phosphorylation of cardiac myosin regulatory light chain in vivo. *Journal of Biological Chemistry* 290 (17): 10703-16.19

Coureux, P.D., H.L. Sweeney, and A. Houdusse. 2004. Three myosin V structures delineate essential features of chemo-mechanical transduction. *Embo J.* 23:4527-4537.

de la Cruz, M.V., C. Sanchez Gomez, M.M. Arteaga, and C. Arguello. 1977. Experimental study of the development of the truncus and the conus in the chick embryo. *Journal of anatomy*. 123:661-686.

Elson, E.L. 1985. Fluorescence correlataion spectroscopy and photobleaching recovery. *Annu. Rev. Phys. Chem.* 36:379-406.

Elson, E.L. 2007. Introduction to FCS. UNT, Fort Worth. 1-10 pp.

Ferenczi, M.A., S.Y. Bershitsky, N. Koubassova, V. Siththanandan, W.I. Helsby, P. Panine, M. Roessle, T. Narayanan, and A.K. Tsaturyan. 2005. The "roll and lock" mechanism of force generation in muscle. *Structure*. 13:131-141.

Friedberg, M.K., and A.N. Redington. 2014. Right versus left ventricular failure: differences, similarities, and interactions. *Circulation*. 129:1033-1044.

Geeves, M.A., and K.C. Holmes. 2005. The molecular mechanism of muscle contraction. *Adv Protein Chem.* 71:161-193.

Gomes, A.V., K. Harada, and J.D. Potter. 2005. A mutation in the N-terminus of troponin I that is associated with hypertrophic cardiomyopathy affects the Ca(2+)-sensitivity, phosphorylation kinetics and proteolytic susceptibility of troponin. *J Mol Cell Cardiol*. 39:754-765.

Grazi, E., O. Cintio, and G. Trombetta. 2004. On the mechanics of the actin filament: the linear relationship between stiffness and yield strength allows estimation of the yield strength of thin filament in vivo. *J Muscle Res Cell Motil*. 25:103-105.

Herrmann, C., C. Lionne, F. Travers, and T. Barman. 1994. Correlation of ActoS1, myofibrillar, and muscle fiber ATPases. *Biochemistry*. 33:4148-4154.

Hill, T.L., E. Eisenberg, and J.M. Chalovich. 1981. Theoretical models for cooperative steady-state ATPase activity of myosin subfragment-1 on regulated actin. *Biophys J.* 35:99-112.

Hopkins, S.C., C. Sabido-David, U.A. van der Heide, R.E. Ferguson, B.D. Brandmeier, R.E. Dale, J. Kendrick-Jones, J.E. Corrie, D.R. Trentham, M. Irving, and Y.E. Goldman. 2002. Orientation changes of the myosin light chain domain during filament sliding in active and rigor muscle. *J Mol Biol.* 318:1275-1291.

Huxley, A.F. 1957. A hypothesis for the mechanism of contraction of muscle. *Prog. Biophys. Biophys. Chem.* 7:255-318.

Ishikawa, Y., and R. Kurotani. 2008. Cardiac myosin light chain kinase: A new player in the regulation of myosin light chain in the heart. *Circulation Research* 102 (5): 516-8.

Itoya, M., R.T. Mallet, Z.P. Gao, A.G. Williams, Jr., and H.F. Downey. 1996. Stability of high-energy phosphates in right ventricle: myocardial energetics during right coronary hypotension. *Am J Physiol*. 271:H320-328.

Kimura, A., H. Harada, J.E. Park, H. Nishi, M. Satoh, M. Takahashi, S. Hiroi, T. Sasaoka, N. Ohbuchi, T. Nakamura, T. Koyanagi, T.H. Hwang, J.A. Choo, K.S. Chung, A. Hasegawa, R. Nagai, O. Okazaki, H. Nakamura, M. Matsuzaki, T. Sakamoto, H. Toshima, Y. Koga, T. Imaizumi, and T. Sasazuki. 1997. Mutations in the cardiac troponin I gene associated with hypertrophic cardiomyopathy. *Nat Genet*. 16:379-382.

Liang, J., K. Kazmierczak, A.I. Rojas, Y. Wang, and D. Szczesna-Cordary. 2015. The R21C Mutation in Cardiac Troponin I Imposes Differences in Contractile Force Generation between the Left and Right Ventricles of Knock-in Mice. *BioMed Research International*. in press.

Ling, N., C. Shrimpton, J. Sleep, J. Kendrick-Jones, and M. Irving. 1996. Fluorescent probes of the orientation of myosin regulatory light chains in relaxed, rigor, and contracting muscle. *Biophys J*. 70:1836-1846.

Magde, D., E.L. Elson, and W.W. Webb. 1974. Fluorescence correlation spectroscopy. II. An experimental realization. *Biopolymers*. 13:29-61.

Minton, A.P. 1981. Excluded volume as a determinant of macromolecular structure and reactivity. *Biopolymers*. 20:2093-2120.

Minton, A.P. 1998. Molecular crowding: analysis of effects of high concentrations of inert cosolutes on biochemical equilibria and rates in terms of volume exclusion. *Methods Enzymol*. 295:127-149.

Mourao, M.A., J.B. Hakim, and S. Schnell. 2014. Connecting the Dots: The Effects of Macromolecular Crowding on Cell Physiology. *Biophys J*. 107:2761-2766.

Nagwekar, J., D. Duggal, R. Rich, S. Raut, R. Fudala, I. Gryczynski, Z. Gryczynski, and J. Borejdo. 2014. Spatial Distribution of Actin and Mechanical Cycle of Myosin are Different in Right and Left Ventricles of Healthy Mouse Hearts. Biochemistry, in press (Editors Choice). *Biochemistry*. in press (Editors Choice).

Nyitrai, M., and M.A. Geeves. 2004. Adenosine diphosphate and strain sensitivity in myosin motors. *Philos Trans R Soc Lond B Biol Sci*. 359:1867-1877.

Oosawa, F., Y. Maeda, S. Fujime, S. Ishiwata, T. Yanagida, and M. Taniguchi. 1977. Dynamic characteristics of F-actin and thin filaments in vivo and in vitro. *J Mechanochem Cell Motil*. 4:63-78.

Park, I., C. Han, S. Jin, B. Lee, H. Choi, J.T. Kwon, D. Kim, J. Kim, E. Lifirsu, W.J. Park, Z.Y. Park, H. Kim do, and C. Cho. 2011. Myosin regulatory light chains are required to maintain the stability of myosin II and cellular integrity. *Biochem J*. 434:171-180.

Pate, E., and R. Cooke. 1991. Simulation of stochastic processes in motile crossbridge systems. *J. Muscle. Res. Cell Motil.* 12:376-393.

Prochniewicz-Nakayama, E., Yanagida, T., & Oosawa, F. 1983. Studies on conformation of F-actin in muscle fibers in the relaxed state, rigor, and during contraction using fluorescent phalloidin. *J. Cell Biol.* . 97 1663-1667.

Rosenquist, G.C. 1970. Location and movements of cardiogenic cells in the chick embryo: the heart-forming portion of the primitive streak. *Developmental biology*. 22:461-475.

Sabido-David, C., B. Brandmeier, J.S. Craik, J.E. Corrie, D.R. Trentham, and M. Irving. 1998. Steady-state fluorescence polarization studies of the orientation of myosin regulatory light chains in single skeletal muscle fibers using pure isomers of iodoacetamidotetramethylrhodamine. *Biophys J*. 74:3083-3092.

Samarel, A.M. 1989. Regional differences in the in vivo synthesis and degradation of myosin subunits in rabbit ventricular myocardium. *Circ Res*. 64:193-202.

Schwarz, K., S. Singh, D. Dawson, and M.P. Frenneaux. 2013. Right ventricular function in left ventricular disease: pathophysiology and implications. *Heart, lung & circulation*. 22:507-511.

Srivastava, D., T. Thomas, Q. Lin, M.L. Kirby, D. Brown, and E.N. Olson. 1997. Regulation of cardiac mesodermal and neural crest development by the bHLH transcription factor, dHAND. *Nat Genet*. 16:154-160.

Sweeney, H.L. 1995. Function of the N-terminus of the myosin essential light chain of vertebrate striated muscle. *Biophys. J.* 68 112s-119s.

Tsaturyan, A.K., S.Y. Bershitsky, R. Burns, and M.A. Ferenczi. 1999. Structural changes in the actin-myosin cross-bridges associated with force generation induced by temperature jump in permeabilized frog muscle fibers. *Biophys J*. 77:354-372.

Walcott, S., D.M. Warshaw, and E.P. Debold. 2012. Mechanical Coupling between Myosin Molecules Causes Differences between Ensemble and Single-Molecule Measurements. *Biophys J*. 103:501-510.

Wang, Y., J. Pinto, R. Solis, D. Dweck, J. Liang, Z. Diaz-Perez, Y. Ge., J. Walker, and J. Potter. 2012a. Generation and Functional Characterization of Knock-in Mice Harboring the Cardiac Troponin I-R21C Mutation Associated with Hypertrophic Cardiomyopathy. *J Biol Chem.* . 287:2156-2167.

Wang, Y., J.R. Pinto, R.S. Solis, D. Dweck, J. Liang, Z. Diaz-Perez, Y. Ge, J.W. Walker, and J.D. Potter. 2012b. Generation and functional characterization of knock-in mice harboring the cardiac troponin I-R21C mutation associated with hypertrophic cardiomyopathy. *J Biol Chem*. 287:2156-2167.

Wikman-Coffelt, J., C. Fenner, A. Smith, and D.T. Mason. 1975. Comparative analyses of the kinetics and subunits of myosins from canine skeletal muscle and cardiac tissue. *J Biol Chem*. 250:1257-126

Yanagida, T., and F. Oosawa. 1978. Polarized fluorescence from epsilon-ADP incorporated into F-actin in a myosin-free single fiber: conformation of F-actin and changes induced in it by heavy meromyosin. *J Mol Biol.* 126:507-524.

Yanagida, T., and F. Oosawa. 1980. Conformational changes of F-actin-epsilon-ADP in thin filaments in myosin-free muscle fibers induced by Ca2+. *J Mol Biol.* 140:313-320.

CONCLUSION

The long-term goal of this dissertation was to establish an experimental basis to identify and address the issues related to cardiovascular health and its related ailments. The focus of the research has been on comprehending the function of cardiac muscles' characteristics in healthy hearts and their atypical behavior transcending into diseases, with implications far beyond the reach of current medical help to prevent or treat. The objective of the thesis was to elucidate the basic crossbridge cycle in striated muscles, particularly in the ventricles of the heart and the factors that may affect the overall cardiovascular function. An additional investigation into skeletal muscle behavior gave us an edge to have an expanse of knowledge on the working of mammalian muscle system. We addressed these objectives by focusing on four aspects of the study: 1) Decipher the unprecedented distinctness between the left and right ventricles of the healthy hearts that were all along, conceptualized to be identical in the wake of their unnoticed basic functional differences and to gravitate future research into developing treatment modalities specific to the respective ventricular failures than treating them squarely equal. The research began in small/moderate mammalian models like mice and rabbits wherein single live working myofibrils were studied by applying mesoscopic approach to understand the spatiotemporal and kinetic mechanisms of sarcomeric protein – actin. 2) The research was then extended into studying these ventricular differences in human healthy hearts and their functional anomaly in the ventricular tissues of patients that had undergone heart failure. 3) To study profoundly the effects of single point mutations in the sarcomeric proteins that work through affecting the protein phoshorylation sites and disrupt the very finely balanced coordinated performance of these proteins to eventually translate into diseases. 4) To extend the study and investigate the role of phosphorylation of RLC in skeletal muscles.

Disparity in the two ventricles of the heart

This part of the thesis investigates the distinction between the ventricles by studying the fluorophore attached actin myosin interactions and the orientation of cross bridges, kinetic cycle and disproves the prevalent thought of years that LV and RV of hearts are the same. The two ventricular sarcomeric proteins: actin and myosin, originate from their same respective genes (ACTC1 gene for actin and MYH6/7 for heavy chain, MYL2 for regulatory light chains, MYL3 for essential light chains of myosin)[170,171], however, their architecture and implementation in rendering them to work for specific ventricles likely fuel calls for their functional differences.

1. Mammalian model (Mice and Rabbit): The study on understanding the molecular and functional differences in the rodent models was performed using polarization fluorescence with labeled actin molecules in thin filaments. In small rodent models of mouse, the differences in the widths of FWHMs for relaxation and rigor were insignificant in both the ventricles which indicate that in physiological states, the numbers of cross-bridges bound to actin are quite similar. In moderate mammalian models of rabbits, FWHMs of contracting myofibrils were significantly different in the LVs and RVs with LVs greater than RVs. In both the mammalian models, the mean polarization in all the three states of muscle cycle, i.e, contraction, relaxation and rigor were almost similar with their values being higher in RVs than LVs. Their values of kurtosis for rigor were almost alike, with RV greater than LV. The fact that kurtosis of rigor

distributions of RV muscles is high suggests that XBs bind to actin predominantly in a single orientation; i.e., cross-bridges in RVs are better oriented than LVs. During relaxation, not many XBs make contacts with actin filaments. This hence results in a disorder. FWHMs in relaxation in both the models were used as control groups and as stated earlier, show no differences in LVs and RVs.

The results for FWHM suggest that actins in thin filaments of RV are tightly distributed in contracting myofibril which may be because: 1) ventricular wall thickness of RVs is smaller compared to LV which induces 2) increased tension/area ratio compressing the actin monomers ever closer. Greater compression implies restricted movement of actin and also its attached fluorophore. On the contrary, the FWHM of LVs are wider compared to RVs. Possible reason for wider FWHM could be due to the fact that: 1) LVs are higher pressure chambers that supply blood to the entire body and thus the tension on myofibrillar myosins is also greater. 2) Although the ventricular wall thickness is greater in LVs, the absolute tension developed and the resulting stress induced on actin filaments is also greater. Distribution of actins in the thicker ventricular walls may allow actin monomers to develop an exact opposite effect of stretch to the compression effect due to pressure.

The kinetics in mice models show that rate of power stroke (k_2) was significantly higher in LV which emphasizes their higher tension bearing capacities than RVs. However, the rate of dissociation (k_3) was also significantly greater in the LVs which probably mean that XBs spend less time in the tension-generating state. The fact that macroscopic tension was never observed in the myofibrils was possibly because of these opposite effects that set off each other. Unfortunately the kinetics in rabbit models did not fit well and hence could not be included in the study.

2. Human Hearts: Similar set of studies were performed on ventricles of the human hearts that were healthy and the ones that underwent failure. The studies were performed on the protein of the contractile system – actin to analyze the functioning of the heart. Actin molecules were labeled with the dye Alexa-633-Phalloidin that binds rigidly (covalent bond) to the molecules owing to their higher affinity for actin molecules to monitor the mechano and spatiotemporal changes in the cardiac myofibrils.

Ventricular actin labeled with Alexa-633-Phalloidin

This project demonstrates the contractile mechanism in the healthy and failing ventricles of the heart with respect to actin. The model used for the study is a simple k_{PRE} and k_{POST} mechanism depicting the actin orientation during a contractile cycle by a 2-state (Pre and Post power stroke). In the interest of simplicity we ignore small changes between the Myosin (M), M+ATP (MT) and M+ADP (MD), and between anisotropy in the presence of nucleotides. Myosin with ADP binds to actin at the rate k_1 to form AMD. The myosin heads rotate very fast for the population of cross bridges in the pre-power stroke state (k_1) to get detected by the present method. t_{PRE} represents time period with weakly or semi-strongly bound myosin attached ADP to actin molecules in thin filament. This state does not produce tension. t_{PRE} transforms with a rate k_{PRE} to a strongly bound tension generating post-power stroke state AM (actin+myosin) which lasts for a time $t_{POST.}$ AM relaxes with a rate k_{POST} toa short lived bound state before ATP binds myosin and detaches actomyosin bond. This is the AMT state. Thus k_{PRE} represent the lifetime of pre power stroke and

k_{POST} represent the the lifetime of post power stroke states. The rigidity of the bound fluorophore (alexa633Phallooidin) to actin is represented in the form of anisotropy with average values of a_1= 0.240 (dye bound to actin) for the period of time t_1, and a_2= 0.067 (free dye) for a period of time t_2. The higher value of anisotropy is an indication of the immobilized fluorophore on actin molecule.

The k_{PRE} and k_{POST} significantly differed in the ventricles (LV and RV) of non-failing hearts. It was noted that the values for both k_{PRE} and k_{POST} were significantly higher in LV as compared to RV. Larger k_{PRE} in LV implies that the cross-bridges bound weakly or somewhat strongly to actins contribute to smaller t_{PRE}. Since pre-power stroke (non-tension generating) is short, the tension generating state is populated faster and thus leads to an increase in tension generation per myofilament. As the value for k_{PRE} is smaller in RV, it is difficult to deduce the effect of this change on RV. Larger k_{POST} implies smaller t_{POST} and the decrease in tension per myofilament. The widths of the FWHM indicate the orientation of actin bound myosin molecules while the polarization represents the range of angles that the transition dipole of fluorophore assumes with respect to the myofibrillar axis when myosin bind to actins. FWHM of the non-failing LV is larger than in the non-failing RV. Larger FWHMs in LV suggest that XBs have access to a wider choice of actin binding sites which leads to heightened actomyosin complexes built per myofilament and an increase in tension generation per myofilament. The myocytes of LV are thinner and lengthier compared to RVs. Hence, the larger surface area per filament gives ground to the movement of actin monomers thus reduction in the tension on actin filaments as a whole. However, given the ventricular walls of LVs are thicker with more number of myofilaments per cross-sectional area of the myocardium, the tension per filament is magnified on the entire left ventricular wall thus increasing the overall tension in LV. Small FWHM in non-failing RV is also consistent with the fact that pressure and wall thickness are smaller in RV than LV. It is known that RV adapts better to volume overload than pressure overload[172]. However, the stress/area ratio experienced by actin filaments in RV maybe be larger resulting in an increased compression of actin monomers (it may, on occasion, be compensated for by ventricular enlargement - hypertrophy). Greater compression implies that the phalloidin carrying Alexa633 fluorophore is unable to vigorously respond to the thrust exerted by myosin, thus causing actin distribution during contraction of the non-failing RV to be narrower than the LV. Thus it implies that the distribution and packing of actin is narrower in the RVs of non-failing hearts compared to LVs. Since our measurements were carried out on isolated live myofibrils, they suggest the presence of fundamental differences in the function of muscles of both the ventricles.

The results of failing hearts were not surprising. The orientation of actins and kinetic rate constants from five samples of the failing hearts showed no significant differences in the LVs and RVs. Although the patients that underwent heart failure varied in their physiological tests, (one had high Body/Mass Index (#2), one had unusually low End Diastolic Volume and End Systolic Volume (#3) and that one had unusually low Ejection Fraction (#6)), all had similar k_{PRE} and k_{POST}. k_{PRE} of non-failing LVs was larger in comparison with failing LVs. This leads to the increase in LV tension. k_{POST} of non-failing LV was smaller in comparison with failing LV. This also leads to the increase in LV tension. k_{PRE} and k_{POST} of failing RVs were unchanged in comparison with non-failing ones. One of the many reasons to contribute towards a failing heart could be the descend in the ability of the cross-bridges to associate and dissociate efficiently during a cross-bridge cycle which renders the cross-bridges to develop insufficient force and tension in the

myofilament that ultimately renounces its healthy normal function to develop systolic and diastolic dysfunction. When diastolic dysfunction is seen, left ventricular end-diastolic pressure increases out-of-proportion to the volume and induces myocardial stiffness, LV impaired filling, dyspnea and thus heart failure. One third heart failure patients in the USA are known to have heart failure related diastolic dysfunction. As rightly said by Osler, the type of heart failure produced is not only due to the weakening of the heart muscle but is also related to myocardial degeneration called diastolic dysfunction[173]. LV dysfunction appears to be more common in nonischemic cardiomyopathy than in ischemic cardiomyopathy and more closely parallels RV dysfunction[174]. On the other hand, systolic dysfunction in LV pushes the load of pumping the blood on the RVs inducing RV structural and functional impairment in the process.

	Mice		Rabbit		Human	
	LV	RV	LV	RV	LV	RV
Contraction	LV>RV		LV>RV		LV>RV	
FWHM	------	------	Wide 0.439±0.048	Narrow 0.374±0.033	Wide 0.339± 0.027	Narrow 0.318± 0.022
Rate of Power Stroke	K_2 is large 0.159± 0.086	K_2 is small 0.085± 0.035	-----	------	K_{PRE} is large 1.84± 0.75	K_{PRE} is small 1.44± 0.75
Rate of Dissociation	K_3 is large 0.061 ± 0.026	K_3 is small 0.049± 0.008	------	------	K_{POST} is large 0.20± 0.10	K_{POST} is small 0.15± 0.07
Relaxation	LV~RV		LV~RV		LV~RV	
FWHM	0.414± 0.075	0.416 ± 0.266	0.376± 0.051	0.398± 0.040	0.332± 0.021	0.335± 0.030
Rigor	LV>RV		LV~RV		LV>RV	
FWHM	Wide 0.438± 0.069	Narrow 0.339± 0.144	Narrow 0.392± 0.051	Wide 0.401± 0.047	Wide 0.347± 0.035	Narrow 0.305± 0.014

Table 1: Summary of mammalian models exhibiting differences in the LV and RV of hearts.

3. Mutation induced HCM

Rhythmic cycle of heart muscles is contingent upon the makeup of myofibrillar contractile proteins and their smooth working in the muscle. The genes producing these protein compositions have their fair share of misfires which could be either congenital or lifestyle promoted. These altered proteins formed that throw the normal functioning off-board are caused by mutation in genes. The uncertainty in the working of heart

function settles in with addition of these mutations in its functioning proteins. The heart muscles in their attempts to rebalance the abnormal functioning caused due to mutations may undergo hypertrophy. Hypertrophic cardiomyopathy is a heart condition characterized by thickening of the ventricular walls. Every gene mutation related alteration in the protein and their dysfunction can be deciphered through various methods of biochemical assays, biophysical and physiological staining methods. We decipher these mutational changes by biophysical methods. Three hypertrophy causing point mutations were studied in these projects to understand the heart function better.

3.1. A13T Mutation

The project shows FHC mutation induced hypertrophic phenotypes are depicted in the larger widths of FWHMs of 10% mutated (Mut) myofibrils vs wild type (WT). The increase in the widths of FWHMs indicates loss of order of cross-bridges during contraction. The A13T mutated myofibrils (NStd) showed that the widths of the gaussian curves were very large compared to its WT-RLC (Std) and A13T-non-mutated (Std) myofibrils. Even though the differences in kinetics could not be quantified, because of a poor fit to NStd correlation functions, differences at the macroscopic levels were identified. Several experiments performed on the sparsely expressed mutated protein showed decreased Ca^{2+} sensitivity and altered Ca^{2+} binding properties of RLC while some experiments performed also show an increase in force production with severe mid septal and ventricular hypertrophy. The increase in the force production could be a compensatory mechanism of the ventricles in their attempts to normalize the diminished contractile function in the hearts and in the process acquire hypertrophy. The mutation present near the phosphorylation site Ser15 of RLC decreases the ability of RLC to phosphorylate that is reflected as decreased sensitivity to Ca^{2+} ions. Hence, despite lower concentrations of Ca^{2+} and induced altered Ca^{2+} binding properties, A13T mutant produces force significantly higher than the WT muscles which is independent of Ca activated myofibrillar ATPase activity. The polarization fluorescence values (Table.3, Chapter VII) indicate that the values of fluorescence were contributed by both, A13T-non-mutated (Std) and A13T-mutated (NStd) cross-bridges. It was only with the use of the Polarization technique using single molecule detection that 10% mutated myofibrillar contribution towards FHC could be noted. The polarization values ideally can be translated as the angles that transition dipoles of the dye (Rhodamine) assume with respect to the myofibrillar axis.

3.2. K104E Mutation

Understanding the mechanisms how cardiac myosin regulatory light chain (RLC) phosphorylation affects cardiac muscle mechanics is necessary because it is often altered in cardiac diseases. RLC phosphorylation does not change significantly between systolic and diastolic stresses but may alter the cardiac muscle stiffness, pathology and fitness. RLC phosphorylation induces negative charge and thus helps bring myosin heads closer to actin molecules. This enhances XB binding. K104E mutation near the phosphorylation site may alter this very mechanism of XB binding. Our results show that the mutation induced an increase in the rate of power stroke and in particular an increase in the rate of dissociation in the cardiac muscle. This suggests that a mutated ventricle is prone to relaxation abnormalities, ultimately leading to diastolic dysfunction in patients carrying the mutation. Also the degree of order of the XBs were smaller in the Tg-

K10E mutated muscles which indicates that not many XBs interact with actins and thus cannot reach as many actin-binding sites and so the tension developed is low as compared to WT.

3.3. R21C Mutation

We examined Troponin I mutation induced hypertrophic differences in the ventricles of the heart. The study was performed on muscles from the left (LV) and right (RV) ventricles of knock-in mice. This mutation is linked to sudden cardiac deaths (SCD) in many patients. Comparative study performed on the mutation revealed that the mutation affects the two ventricles differently. R21C mutation imposed approximately three-fold decrease in the rate of power stroke and two-fold decrease in the rate of dissociation of the cross-bridges in RV compared to LV. This indicates that the mutated muscles suffered a decrease in the number of force generating cross-bridges resulting in decrease of ventricular tension. As a rescue mechanism, the decrease in power stroke would necessarily lead to a decrease in the rate of dissociation from thin filaments in RV resulting in isometric tension in the mutated muscles due to the inability of XBs to dissociate from thin filaments promptly. The FWHMs of WT-LV were bigger than WT-RV as more numbers of cross-bridges are attached with actin molecules in thin filaments. The normal distributions of XB angles are disrupted with induction of R21C mutation. The widths of FWHM are bigger in MUT-RVs compared to MUT-LVs which imply that more number of force generating cross-bridges present in MUT-RV renders the ventricle to become high ATP consuming unit which was confirmed with the ATPase assay. Similar results were also observed in experiments performed by Liang et.al. Decrease in the number of force producing XBs in MUT-LV compared to WT-LV indicate towards the compromised LV activity in the presence of mutation. The kinetics and relaxation of cardiac muscles is finely regulated by Ca^{2+} ions in the cells. During diastole, phosphorylation of cTnI directly increases the rate of Ca^{2+} dissociation from cTnC and, together with phosphorylated myosin binding protein C (MyBP-C), decreases the Ca^{2+} sensitivity of force production and increases relaxation. Mutations in cTnI alter the calcium sensitivity of cardiac muscle contraction, and result in excitation-contraction uncoupling[175,176]. One of the possible reasons for the induced hypertrophy could be that the R21C mutation disrupts the PKA consensus sequence that curtails PKA-dependent phosphorylation of cTnI that occurs in response to β-adrenergic stimulation in WT mice resulting in faster relaxation and desensitization of myofilaments to calcium[154]. This may lead to hypertrophy[177]. R21C mutation reduced the phosphorylation of cTnI in both mutant LV and RV compared to the WT LV and RV. It is quite unsurprising that the muscles of MUT-LV and MUT-RV show a decrease in k3 (rate of dissociation) which implies that the muscles undergo stiffness and thus are unable to relax. At molecular levels, decrease in force or rate of power stroke may be necessitated with decrease in rate of dissociation as a preventive mechanism. This overproduced working of the muscles induces diastolic dysfunction and thus hypertrophies heart muscle. Most heart attack samples show dephosphorylation of cTnI[178,179] so the study could be further used as diagnostic marker for heart diseases.

4. Phosphorylation in skeletal muscles

S1 head of myosin molecule consists of a subunit called the regulatory or phosphorylatable light chain (P-LC). When muscles are activated, Ca^{2+} binding calmodulin activates MLCK that phosphorylates the light chains. Although phosphorylation of light chains is helpful in modulating skeletal muscle contractions,

phosphorylation is not required for skeletal muscles to contract and a definitive role is not yet known. It has been proposed that phosphorylation may modulate the actomyosin interactions leading to force generation[62]. Often changes in Ca^{2+} sensitivity generated through RLC phosphorylation activated MLCK can affect the functioning of the muscle. Physiologically, RLC phosphorylation induces rapid activation of MLCK by Ca^{2+}-calmodulin and slows its inactivation after relaxation, increases MLCK activity relative to myosin light chain phosphatase (MLCP)[63]. Some studies suggest that RLC phosphorylation may alter the myosin motor function within the myofilaments which increases Ca^{2+} sensitivity of cross-bridges that leads to an increase in force generation in the muscles[62,63,180] and decreasing the rates of decay of force-generating state[141]. Some other studies have shown that RLC phosphorylation has no significant effect on ATPase activity in purified myosins or on maximum velocity of shortening[180]. Our data suggests that phosphorylation of RLC has no effect on the cross-bridge duty cycle and is consistent with the conclusions of Merger et.al. The rate of dissociation represented as k1 in this model, although statistically insignificantly, is however, slightly faster in the phosphorylated than the dephosphorylated muscles while the rates of power stroke and actomyosin binding showed no differences at all. This suggests that the isometric force remain unchanged with RLC phosphorylation at saturated Ca^{2+} concentrations. This may, however, change at low Ca^{2+} concentrations wherein increased phosphorylation may increase force by elevating the number of force generating cross-bridges.

Future Perspectives

The goal of the thesis was to investigate the molecular mechanisms of contraction of striated muscles namely: Cardiac and Skeletal muscles. The central dogma of the projects revolved around elucidating the role of contractile unit in efficient functioning of cardiac/skeletal muscles and to profoundly understand their mechanisms in healthy and diseased states.

The method enables us to study the distribution of orientation of cross-bridges. Single molecule technique could be explored as an alternative inexpensive diagnostic technique for the diseased states. Only a few studies have been performed with this method so far. By focusing on studying fewer cross-bridges, we ensure that a single cross-bridge makes a significant contribution to the signal to enable us to understand the subtle changes in the protein function and behavior. Additionally, this challenging yet rewarding research has helped to make a contribution towards our deeper understanding of the contraction function in muscles in addition to what is already known. The method has the potential to be an alternative and inexpensive diagnostic tool in mutation related studies.

REFERENCES

1. Jose AM. Anatomy and leonardo da vinci. *Yale J Biol Med*. 2001;74(3):185-195.

2. van Leeuwenhoek A. *The select works of anthony van leeuwenhoek: Containing his microscopical discoveries in many of the works of nature.* Vol 1. translator; 1800.

3. Kardel T. Niels stensen's geometrical theory of muscle contraction (1667): A reappraisal. *J Biomech*. 1990;23(10):953-965.

4. Szent-Gyorgyi AG. The early history of the biochemistry of muscle contraction. *J Gen Physiol*. 2004;123(6):631-641. doi: 10.1085/jgp.200409091 [doi].

5. Hill A. The heat of shortening and the dynamic constants of muscle. *Proceedings of the Royal Society of London B: Biological Sciences*. 1938;126(843):136-195.

6. Von Muralt AL, Edsall JT. Studies in the physical chemistry of muscle globulin iv. the anisotropy of myosin and double refraction of flow. *J Biol Chem*. 1930;89(1):351-386.

7. Engelhardt WA, Liubimova MN. Myosin and adenosine triphosphatase (nature, 144, 688, oct. 14, 1939). *Mol Biol (Mosk)*. 1994;28(6):1229-1230.

8. Straub F. Actin, II. *Stud.Inst.Med.Chem.Univ.Szeged*. 1943;3:23-37.

9. Straub FB. Actin. *Stud. Inst. Med. Chem. Univ. Szeged.* 1942;II:3-15.

10. Huxley HE. Electron microscope studies on the structure of natural and synthetic protein filaments from striated muscle. *J Mol Biol*. 1963;7(3):281-IN30.

11. Reggiani C. When fibres go slack and cross bridges are free to run: A brilliant method to study kinetic properties of acto- myosin interaction. *J Physiol (Lond)*. 2007;583(1):5-7.

12. Edman KA. The velocity of unloaded shortening and its relation to sarcomere length and isometric force in vertebrate muscle fibres. *J Physiol*. 1979;291:143-159.

13. Ramsey RW, Street SF. The isometric length- tension diagram of isolated skeletal muscle fibers of the frog. *Journal of Cellular and Comparative Physiology*. 1940;15(1):11-34.

14. Huxley A, Peachey L. The maximum length for contraction in vertebrate striated muscle. *J Physiol (Lond)*. 1961;156(1):150-165.

15. Rack PM, Westbury DR. The effects of length and stimulus rate on tension in the isometric cat soleus muscle. *J Physiol*. 1969;204(2):443-460.

16. Hanson J, Lowy J. The structure of F-actin and of actin filaments isolated from muscle. *J Mol Biol*. 1963;6(1):46IN2-60IN5.

17. Rayment I, Rypniewski WR, Schmidt-Base K, et al. Three-dimensional structure of myosin subfragment-1: A molecular motor. *Science*. 1993;261(5117):50-58.

18. Szent-Györgyi AG. Meromyosins, the subunits of myosin. *Arch. Biochem. Biophys*. 1953;42:305-320.

19. Szent-Gyorgyi AG. The early history of the biochemistry of muscle contraction. *J Gen Physiol*. 2004;123(6):631-641. doi: 10.1085/jgp.200409091 [doi].

20. Craig R, Woodhead JL. Structure and function of myosin filaments. *Curr Opin Struct Biol*. 2006;16(2):204-212.

21. Gordon AM, Homsher E, Regnier M. Regulation of contraction in striated muscle. *Physiol Rev*. 2000;80(2):853-924.

22. Milligan RA. Protein-protein interactions in the rigor actomyosin complex. *Proc Natl Acad Sci U S A*. 1996;93(1):21-26.

23. Rayment I, Holden HM, Whittaker M, et al. Structure of the actin-myosin complex and its implications for muscle contraction. *Science*. 1993;261(5117):58-65.

24. England J, Loughna S. Heavy and light roles: Myosin in the morphogenesis of the heart. *Cellular and Molecular Life Sciences*. 2013;70(7):1221-1239.

25. Burghardt TP, Garamszegi SP, Park S, Ajtai K. Tertiary structural changes in the cleft containing the ATP sensitive tryptophan and reactive thiol are consistent with pivoting of the myosin heavy chain at Gly699. *Biochemistry (N Y)*. 1998;37(22):8035-8047.

26. Cooke R, Holmes KC. The mechanism of muscle contractio. *CRC Crit Rev Biochem*. 1986;21(1):53-118.

27. Diffee GM, Patel JR, Reinach FC, Greaser ML, Moss RL. Altered kinetics of contraction in skeletal muscle fibers containing a mutant myosin regulatory light chain with reduced divalent cation binding. *Biophys J*. 1996;71(1):341-350. doi: S0006-3495(96)79231-7 [pii].

28. Purcell TJ, Naber N, Sutton S, Cooke R, Pate E. EPR spectra and molecular dynamics agree that the nucleotide pocket of myosin V is closed and that it opens on binding actin. *J Mol Biol*. 2011;411(1):16-26.

29. Lo Presti L, Chang F, Martin SG. Myosin vs organize actin cables in fission yeast. *Mol Biol Cell*. 2012;23(23):4579-4591. doi: 10.1091/mbc.E12-07-0499 [doi].

30. Cooper GM. Structure and organization of actin filaments. . 2000.

31. Bork P, Sander C, Valencia A. An ATPase domain common to prokaryotic cell cycle proteins, sugar kinases, actin, and hsp70 heat shock proteins. *Proc Natl Acad Sci U S A*. 1992;89(16):7290-7294.

32. Reisler E. Actin molecular structure and function. *Curr Opin Cell Biol*. 1993;5(1):41-47.

33. Collins JH, Elzinga M. The primary structure of actin from rabbit skeletal muscle. completion and analysis of the amino acid sequence. *J Biol Chem*. 1975;250(15):5915-5920.

34. Dominguez R, Holmes KC. Actin structure and function. *Annu Rev Biophys*. 2011;40:169-186. doi: 10.1146/annurev-biophys-042910-155359 [doi].

35. Milligan RA. Protein-protein interactions in the rigor actomyosin complex. *Proc Natl Acad Sci U S A*. 1996;93(1):21-26.

36. Holmes KC, Popp D, Gebhard W, Kabsch W. Atomic model of the actin filament. *Nature*. 1990;347(6288):44-49. doi: 10.1038/347044a0 [doi].

37. Schmid MF, Sherman MB, Matsudaira P, Chiu W. Structure of the acrosomal bundle. *Nature*. 2004;431(7004):104-107.

38. Egelman EH, Francis N, DeRosier DJ. F-actin is a helix with a random variable twist. *Nature*. 1982;298(5870):131-135.

39. Egelman EH. A tale of two polymers: New insights into helical filaments. *Nature Reviews Molecular Cell Biology*. 2003;4(8):621-631.

40. Egelman EH. The structure of F-actin. *J Muscle Res Cell Motil*. 1985;6(2):129-151.

41. Moore P, Huxley H, DeRosier D. Three-dimensional reconstruction of F-actin, thin filaments and decorated thin filaments. *J Mol Biol*. 1970;50(2):279-292.

42. Begg DA, Rodewald R, Rebhun LI. The visualization of actin filament polarity in thin sections. evidence for the uniform polarity of membrane-associated filaments. *J Cell Biol*. 1978;79(3):846-852.

43. Huxley H. Electron microscope studies of the organisation of the filaments in striated muscle. *Biochim Biophys Acta*. 1953;12(1):387-394.

44. HUXLEY AF, NIEDERGERKE R. Structural changes in muscle during contraction; interference microscopy of living muscle fibres. *Nature*. 1954;173(4412):971-973.

45. Fuchs F, Martyn DA. Length-dependent Ca2 activation in cardiac muscle: Some remaining questions. *Journal of Muscle Research & Cell Motility*. 2005;26(4-5):199-212.

46. Lymn R, Taylor EW. Mechanism of adenosine triphosphate hydrolysis by actomyosin. *Biochemistry (N Y)*. 1971;10(25):4617-4624.

47. Bagshaw CR, Trentham DR. The characterization of myosin-product complexes and of product-release steps during the magnesium ion-dependent adenosine triphosphatase reaction. *Biochem J*. 1974;141(2):331-349.

48. Farah CS, Reinach FC. The troponin complex and regulation of muscle contraction. *FASEB J*. 1995;9(9):755-767.

49. McKillop DF, Geeves MA. Regulation of the interaction between actin and myosin subfragment 1: Evidence for three states of the thin filament. *Biophys J*. 1993;65(2):693-701. doi: S0006-3495(93)81110-X [pii].

50. Xu C, Craig R, Tobacman L, Horowitz R, Lehman W. Tropomyosin positions in regulated thin filaments revealed by cryoelectron microscopy. *Biophys J*. 1999;77(2):985-992.

51. Vibert P, Craig R, Lehman W. Steric-model for activation of muscle thin filaments. *J Mol Biol*. 1997;266(1):8-14.

52. Furch M, Remmel B, Geeves MA, Manstein DJ. Stabilization of the actomyosin complex by negative charges on myosin. *Biochemistry (N Y)*. 2000;39(38):11602-11608.

53. Geeves MA, Holmes KC. Structural mechanism of muscle contraction. *Annu Rev Biochem*. 1999;68(1):687-728.

54. Gollnick PD, Matoba H. The muscle fiber composition of skeletal muscle as a predictor of athletic success. an overview. *Am J Sports Med*. 1984;12(3):212-217.

55. Lieber RL. *Skeletal muscle structure, function, and plasticity*. Lippincott Williams & Wilkins; 2002.

56. Block BA, Imagawa T, Campbell KP, Franzini-Armstrong C. Structural evidence for direct interaction between the molecular components of the transverse tubule/sarcoplasmic reticulum junction in skeletal muscle. *J Cell Biol*. 1988;107(6 Pt 2):2587-2600.

57. Edman KA. The velocity of unloaded shortening and its relation to sarcomere length and isometric force in vertebrate muscle fibres. *J Physiol*. 1979;291:143-159.

58. Melzer W, Herrmann-Frank A, Lüttgau HC. The role of ca 2 ions in excitation-contraction coupling of skeletal muscle fibres. *Biochimica et Biophysica Acta (BBA)-Reviews on Biomembranes*. 1995;1241(1):59-116.

59. Lamb G. Excitation–contraction coupling in skeletal muscle: Comparisons with cardiac muscle. *Clinical and Experimental Pharmacology and Physiology*. 2000;27(3):216-224.

60. Sandow A. Excitation-contraction coupling in skeletal muscle. *Pharmacol Rev*. 1965;17(3):265-320.

61. Tanabe T, Beam KG, Adams BA, Niidome T, Numa S. Regions of the skeletal muscle dihydropyridine receptor critical for excitation–contraction coupling. *Nature*. 1990;346(6284):567-569.

62. Grange RW, Vandenboom R, Houston ME. Physiological significance of myosin phosphorylation in skeletal muscle. *Canadian Journal of Applied Physiology*. 1993;18(3):229-242.

63. Stull JT, Kamm KE, Vandenboom R. Myosin light chain kinase and the role of myosin light chain phosphorylation in skeletal muscle. *Arch Biochem Biophys*. 2011;510(2):120-128.

64. Uyeda TQ, Abramson PD, Spudich JA. The neck region of the myosin motor domain acts as a lever arm to generate movement. *Proc Natl Acad Sci U S A*. 1996;93(9):4459-4464.

65. Lee FA. Hemodynamics of the right ventricle in normal and disease states. *Cardiol Clin*. 1992;10(1):59-67.

66. GOLDSTEIN J. The right ventricle: What's right and what's wrong. *Coron Artery Dis*. 2005;16(1):1-4.

67. Haddad F, Hunt SA, Rosenthal DN, Murphy DJ. Right ventricular function in cardiovascular disease, part I anatomy, physiology, aging, and functional assessment of the right ventricle. *Circulation*. 2008;117(11):1436-1448.

68. Goor DA, Lillehei CW. *Congenital malformations of the heart: Embryology, anatomy, and operative considerations.* Grune & Stratton; 1975.

69. 'Marieb E. *Human anatomy and physiology. 6th Edition, Pearson Benjamin Cummings*. 2004:675-732.

70. 'Martini F. Essentials of anatomy and physiology . *4th Rev Edition, Pearson Benjamin Cummings Publications*. 2007:669-703.

71. 'Vander, A, Sherman, J, and Luciano, D'. Human physiology. *10th Edition. McGraw Hill, New York*. 2005.

72. Ventura-Clapier R, Garnier A, Veksler V. Energy metabolism in heart failure. *J Physiol (Lond)*. 2004;555(1):1-13.

73. Doenst T, Nguyen TD, Abel ED. Cardiac metabolism in heart failure: Implications beyond ATP production. *Circ Res*. 2013;113(6):709-724. doi: 10.1161/CIRCRESAHA.113.300376 [doi].

74. OLSON RE, SCHWARTZ WB. Myocardial metabolism in congestive heart failure. *Medicine*. 1951;30(1):21-42.

75. Sambandam N, Lopaschuk GD, Brownsey RW, Allard MF. Energy metabolism in the hypertrophied heart. *Heart Fail Rev*. 2002;7(2):161-173.

76. Cadete VJ, Lin H, Sawicka J, Wozniak M, Sawicki G. Proteomic analysis of right and left cardiac ventricles under aerobic conditions and after ischemia/reperfusion. *Proteomics*. 2012;12(14):2366-2377.

77. Wei Y, Huang Y, Shen Y, et al. Proteomic analysis reveals significant elevation of heat shock protein 70 in patients with chronic heart failure due to arrhythmogenic right ventricular cardiomyopathy. *Mol Cell Biochem*. 2009;332(1-2):103-111.

78. Wisenbaugh T, Allen P, Cooper G,4th, Holzgrefe H, Beller G, Carabello B. Contractile function, myosin ATPase activity and isozymes in the hypertrophied pig left ventricle after a chronic progressive pressure overload. *Circ Res*. 1983;53(3):332-341.

79. Whitten AE, Jeffries CM, Harris SP, Trewhella J. Cardiac myosin-binding protein C decorates F-actin: Implications for cardiac function. *Proc Natl Acad Sci U S A*. 2008;105(47):18360-18365. doi: 10.1073/pnas.0808903105 [doi].

80. Mun JY, Gulick J, Robbins J, Woodhead J, Lehman W, Craig R. Electron microscopy and 3D reconstruction of F-actin decorated with cardiac myosin-binding protein C (cMyBP-C). *J Mol Biol*. 2011;410(2):214-225.

81. MOORE DH, RUSKA H. Electron microscope study of mammalian cardiac muscle cells. *J Biophys Biochem Cytol*. 1957;3(2):261-268.

82. Lompre AM, Nadal-Ginard B, Mahdavi V. Expression of the cardiac ventricular alpha- and beta-myosin heavy chain genes is developmentally and hormonally regulated. *J Biol Chem*. 1984;259(10):6437-6446.

83. Hoh JF, McGrath PA, Hale PT. Electrophoretic analysis of multiple forms of rat cardiac myosin: Effects of hypophysectomy and thyroxine replacement. *J Mol Cell Cardiol*. 1978;10(11):1053-1076.

84. Palmer JW, Tandler B, Hoppel CL. Biochemical properties of subsarcolemmal and interfibrillar mitochondria isolated from rat cardiac muscle. *J Biol Chem*. 1977;252(23):8731-8739.

85. Fabiato A. Time and calcium dependence of activation and inactivation of calcium-induced release of calcium from the sarcoplasmic reticulum of a skinned canine cardiac purkinje cell. *J Gen Physiol*. 1985;85(2):247-289.

86. Lanner JT, Georgiou DK, Joshi AD, Hamilton SL. Ryanodine receptors: Structure, expression, molecular details, and function in calcium release. *Cold Spring Harb Perspect Biol*. 2010;2(11):a003996. doi: 10.1101/cshperspect.a003996 [doi].

87. Ferrier GR, Howlett SE. Contractions in guinea-pig ventricular myocytes triggered by a calcium-release mechanism separate from na+ and L-currents. *J Physiol*. 1995;484 (Pt 1)(Pt 1):107-122.

88. Zhu J, Ferrier GR. Regulation of a voltage-sensitive release mechanism by ca(2+)-calmodulin-dependent kinase in cardiac myocytes. *Am J Physiol Heart Circ Physiol*. 2000;279(5):H2104-15.

89. Howlett SE, Zhu JQ, Ferrier GR. Contribution of a voltage-sensitive calcium release mechanism to contraction in cardiac ventricular myocytes. *Am J Physiol*. 1998;274(1 Pt 2):H155-70.

90. Bers DM. Cardiac excitation–contraction coupling. *Nature*. 2002;415(6868):198-205.

91. Maier LS, Bers DM. Role of Ca2+/calmodulin-dependent protein kinase (CaMK) in excitation-contraction coupling in the heart. *Cardiovasc Res*. 2007;73(4):631-640. doi: S0008-6363(06)00493-7 [pii].

92. Chapman R. Excitation-contraction coupling in cardiac muscle. *Prog Biophys Mol Biol*. 1980;35:1-52.

93. Lehman W, Craig R, Vibert P. Ca2 -induced tropomyosin movement in limulus thin filaments revealed by three-dimensional reconstruction. . 1994.

94. Balke CW, Goldman L. Excitation contraction coupling in cardiac muscle: Is there a purely voltage-dependent component? *J Gen Physiol*. 2003;121(5):349-352. doi: 10.1085/jgp.200308841 [doi].

95. O'Rourke B. Excitation-contraction coupling and mitochondrial energetics. *Basic Res Cardiol*. 2007;102(5):369-392.

96. Pomeranz B, Macaulay RJ, Caudill MA, et al. Assessment of autonomic function in humans by heart rate spectral analysis. *Am J Physiol*. 1985;248(1 Pt 2):H151-3.

97. Stein PK, Bosner MS, Kleiger RE, Conger BM. Heart rate variability: A measure of cardiac autonomic tone. *Am Heart J*. 1994;127(5):1376-1381.

98. Park I, Han C, Jin S, et al. Myosin regulatory light chains are required to maintain the stability of myosin II and cellular integrity. *Biochem J*. 2011;434(1):171-180. doi: 10.1042/BJ20101473 [doi].

99. Huang W, Liang J, Yuan C, et al. Novel familial dilated cardiomyopathy mutation in MYL2 affects the structure and function of myosin regulatory light chain. *FEBS Journal*. 2015;282(12):2379-2393.

100. Mjaatvedt C, Nakaoka T, Moreno-Rodriguez R, et al. The outflow tract of the heart is recruited from a novel heart-forming field. *Dev Biol*. 2001;238(1):97-109.

101. Buckingham M, Meilhac S, Zaffran S. Building the mammalian heart from two sources of myocardial cells. *Nature Reviews Genetics*. 2005;6(11):826-837.

102. Tam PP, Parameswaran M, Kinder SJ, Weinberger RP. The allocation of epiblast cells to the embryonic heart and other mesodermal lineages: The role of ingression and tissue movement during gastrulation. *Development*. 1997;124(9):1631-1642.

103. Rawles ME. The heart-forming areas of the early chick blastoderm. *Physiol Zool*. 1943;16(1):22-43.

104. Rosenquist GC. Location and movements of cardiogenic cells in the chick embryo: The heart-forming portion of the primitive streak. *Dev Biol*. 1970;22(3):461-475.

105. de la Cruz MV, Sanchez Gomez C, Arteaga MM, Arguello C. Experimental study of the development of the truncus and the conus in the chick embryo. *J Anat*. 1977;123(Pt 3):661-686.

106. Foale R, Nihoyannopoulos P, McKenna W, et al. Echocardiographic measurement of the normal adult right ventricle. *Br Heart J*. 1986;56(1):33-44.

107. Srivastava D, Thomas T, Lin Q, Kirby ML, Brown D, Olson EN. Regulation of cardiac mesodermal and neural crest development by the bHLH transcription factor, dHAND. *Nat Genet*. 1997;16(2):154-160.

108. Romeih S, Kroft LJ, Bokenkamp R, et al. Delayed improvement of right ventricular diastolic function and regression of right ventricular mass after percutaneous pulmonary valve implantation in patients with congenital heart disease. *Am Heart J*. 2009;158(1):40-46.

109. Bruneau BG, Nemer G, Schmitt JP, et al. A murine model of holt-oram syndrome defines roles of the T-box transcription factor Tbx5 in cardiogenesis and disease. *Cell*. 2001;106(6):709-721.

110. Drake JI, Bogaard HJ, Mizuno S, et al. Molecular signature of a right heart failure program in chronic severe pulmonary hypertension. *American journal of respiratory cell and molecular biology*. 2011;45(6):1239-1247.

111. Schwarz K, Singh S, Dawson D, Frenneaux MP. Right ventricular function in left ventricular disease: Pathophysiology and implications. *Heart, Lung and Circulation*. 2013;22(7):507-511.

112. Austin EH. The ventricular myocardial band of torrent-guasp-the controversy: An editorial. . 2007;10(1):87-88.

113. Sallin EA. Fiber orientation and ejection fraction in the human left ventricle. *Biophys J*. 1969;9(7):954-964. doi: S0006-3495(69)86429-5 [pii].

114. Mozaffarian D, Benjamin EJ, Go AS, et al. Heart disease and stroke statistics-2016 update: A report from the american heart association. *Circulation*. 2016;133(4):e38-e360. doi: 10.1161/CIR.0000000000000350 [doi].

115. Barnes S, Gott M, Payne S, et al. Prevalence of symptoms in a community-based sample of heart failure patients. *J Pain Symptom Manage*. 2006;32(3):208-216.

116. Azevedo A, Bettencourt P, Pimenta J, et al. Clinical syndrome suggestive of heart failure is frequently attributable to non-cardiac disorders—population-based study. *European journal of heart failure*. 2007;9(4):391-396.

117. Shaddy RE, Boucek MM, Hsu DT, et al. Carvedilol for children and adolescents with heart failure: A randomized controlled trial. *JAMA*. 2007;298(10):1171-1179.

118. McMurray JJ, Adamopoulos S, Anker SD, et al. ESC guidelines for the diagnosis and treatment of acute and chronic heart failure 2012. *European journal of heart failure*. 2012;14(8):803-869.

119. Williams EH, Kao RL, Morgan HE. Protein degradation and synthesis during recovery from myocardial ischemia. *Am J Physiol*. 1981;240(3):E268-73.

120. Friehs I, Moran AM, Stamm C, et al. Impaired glucose transporter activity in pressure-overload hypertrophy is an early indicator of progression to failure. *Circulation*. 1999;100(19 Suppl):II187-93.

121. Poels EM, da Costa Martins PA, van Empel VP. Adaptive capacity of the right ventricle: Why does it fail? *Am J Physiol Heart Circ Physiol*. 2015;308(8):H803-13. doi: 10.1152/ajpheart.00573.2014 [doi].

122. Vonk-Noordegraaf A, Haddad F, Chin KM, et al. Right heart adaptation to pulmonary arterial hypertension: Physiology and pathobiology. *J Am Coll Cardiol*. 2013;62(25_S).

123. Olivetti G, Abbi R, Quaini F, et al. Apoptosis in the failing human heart. *N Engl J Med*. 1997;336(16):1131-1141.

124. Bing OH. Hypothesis: Apoptosis may be a mechanism for the transition to heart failure with chronic pressure overload. *J Mol Cell Cardiol*. 1994;26(8):943-948.

125. Szczesna D, Ghosh D, Li Q, et al. Familial hypertrophic cardiomyopathy mutations in the regulatory light chains of myosin affect their structure, Ca2+ binding, and phosphorylation. *J Biol Chem*. 2001;276(10):7086-7092. doi: 10.1074/jbc.M009823200 [doi].

126. Szczesna-Cordary D, Guzman G, Ng SS, Zhao J. Familial hypertrophic cardiomyopathy-linked alterations in Ca2+ binding of human cardiac myosin regulatory light chain affect cardiac muscle contraction. *J Biol Chem*. 2004;279(5):3535-3542. doi: 10.1074/jbc.M307092200 [doi].

127. Teekakirikul P, Padera RF, Seidman JG, Seidman CE. Hypertrophic cardiomyopathy: Translating cellular cross talk into therapeutics. *J Cell Biol*. 2012;199(3):417-421. doi: 10.1083/jcb.201207033 [doi].

128. Marsiglia JDC, Pereira AC. Hypertrophic cardiomyopathy: How do mutations lead to disease? *Arq Bras Cardiol*. 2014;102(3):295-304.

129. Kimura A, Harada H, Park J, et al. Mutations in the cardiac troponin I gene associated with hypertrophic cardiomyopathy. *Nat Genet*. 1997;16(4):379-382.

130. Mogensen J, Andersen PS, Steffensen U, et al. Development and application of linkage analysis in genetic diagnosis of familial hypertrophic cardiomyopathy. *J Med Genet*. 2001;38(3):193-198.

131. Watkins H, McKenna WJ, Thierfelder L, et al. Mutations in the genes for cardiac troponin T and α-tropomyosin in hypertrophic cardiomyopathy. *N Engl J Med*. 1995;332(16):1058-1065.

132. Bonne G, Carrier L, Richard P, Hainque B, Schwartz K. Familial hypertrophic cardiomyopathy: From mutations to functional defects. *Circ Res*. 1998;83(6):580-593.

133. Cirino AL, Ho C. Hypertrophic cardiomyopathy overview. In: Pagon RA, Adam MP, Ardinger HH, et al, eds. *GeneReviews(R).* Seattle (WA): University of Washington, Seattle; 1993. NBK1768 [bookaccession].

134. Rayment I, Holden HM, Whittaker M, et al. Structure of the actin-myosin complex and its implications for muscle contraction. *Science*. 1993;261(5117):58-65.

135. Szczesna-Cordary D, Jones M, Moore JR, et al. Myosin regulatory light chain E22K mutation results in decreased cardiac intracellular calcium and force transients. *FASEB J*. 2007;21(14):3974-3985. doi: fj.07-8630com [pii].

136. Robertson SP, Johnson JD, Potter JD. The time-course of Ca2+ exchange with calmodulin, troponin, parvalbumin, and myosin in response to transient increases in Ca2+. *Biophys J*. 1981;34(3):559-569. doi: S0006-3495(81)84868-0 [pii].

137. Kamm KE, Stull JT. Signaling to myosin regulatory light chain in sarcomeres. *J Biol Chem*. 2011;286(12):9941-9947. doi: 10.1074/jbc.R110.198697 [doi].

138. Poetter K, Jiang H, Hassanzadeh S, et al. Mutations in either the essential or regulatory light chains of myosin are associated with a rare myopathy in human heart and skeletal muscle. *Nat Genet*. 1996;13(1):63-69.

139. Hougs L, Havndrup O, Bundgaard H, et al. One third of danish hypertrophic cardiomyopathy patients have mutations in MYH7 rod region. *European Journal of Human Genetics*. 2005;13(2):161-165.

140. Ding P, Huang J, Battiprolu PK, Hill JA, Kamm KE, Stull JT. Cardiac myosin light chain kinase is necessary for myosin regulatory light chain phosphorylation and cardiac performance in vivo. *J Biol Chem*. 2010;285(52):40819-40829. doi: 10.1074/jbc.M110.160499 [doi].

141. Colson BA, Locher MR, Bekyarova T, et al. Differential roles of regulatory light chain and myosin binding protein-C phosphorylations in the modulation of cardiac force development. *J Physiol (Lond)*. 2010;588(6):981-993.

142. Huang W, Liang J, Kazmierczak K, et al. Hypertrophic cardiomyopathy associated Lys104Glu mutation in the myosin regulatory light chain causes diastolic disturbance in mice. *J Mol Cell Cardiol*. 2014;74:318-329.

143. Andersen PS, Havndrup O, Hougs L, et al. Diagnostic yield, interpretation, and clinical utility of mutation screening of sarcomere encoding genes in danish hypertrophic cardiomyopathy patients and relatives. *Hum Mutat*. 2009;30(3):363-370.

144. Huang W, Liang J, Kazmierczak K, et al. Hypertrophic cardiomyopathy associated Lys104Glu mutation in the myosin regulatory light chain causes diastolic disturbance in mice. *J Mol Cell Cardiol*. 2014;74:318-329.

145. Zile MR, Brutsaert DL. New concepts in diastolic dysfunction and diastolic heart failure: Part I: Diagnosis, prognosis, and measurements of diastolic function. *Circulation*. 2002;105(11):1387-1393.

146. Redfield MM, Jacobsen SJ, Burnett Jr JC, Mahoney DW, Bailey KR, Rodeheffer RJ. Burden of systolic and diastolic ventricular dysfunction in the community: Appreciating the scope of the heart failure epidemic. *JAMA*. 2003;289(2):194-202.

147. Gordon AM, Homsher E, Regnier M. Regulation of contraction in striated muscle. *Physiol Rev*. 2000;80(2):853-924.

148. Layland J, Solaro RJ, Shah AM. Regulation of cardiac contractile function by troponin I phosphorylation. *Cardiovasc Res*. 2005;66(1):12-21. doi: S0008-6363(05)00002-7 [pii].

149. Perry S. Troponin I: Inhibitor or facilitator. In: *Muscle physiology and biochemistry*. Springer; 1999:9-32.

150. Kranias E, Solaro R. Phosphorylation of troponin I and phospholamban during catecholamine stimulation of rabbit heart. *Nature*. 1982;298:182-184.

151. Jaquet K, Thieleczek R, Heilmeyer LM. Pattern formation on cardiac troponin I by consecutive phosphorylation and dephosphorylation. *European Journal of Biochemistry*. 1995;231(2):486-490.

152. Gomes AV, Harada K, Potter JD. A mutation in the N-terminus of troponin I that is associated with hypertrophic cardiomyopathy affects the ca 2 -sensitivity, phosphorylation kinetics and proteolytic susceptibility of troponin. *J Mol Cell Cardiol*. 2005;39(5):754-765.

153. Robertson SP, Johnson J, Holroyde M, Kranias E, Potter J, Solaro R. The effect of troponin I phosphorylation on the Ca2 -binding properties of the Ca2 -regulatory site of bovine cardiac troponin. *J Biol Chem*. 1982;257(1):260-263.

154. Liang J, Kazmierczak K, Rojas AI, Wang Y, Szczesna-Cordary D. The R21C mutation in cardiac troponin I imposes differences in contractile force generation between the left and right ventricles of knock-in mice. *BioMed research international*. 2015;2015.

155. Chang AN, Parvatiyar MS, Potter JD. Troponin and cardiomyopathy. *Biochem Biophys Res Commun*. 2008;369(1):74-81.

156. Arad M, Penas-Lado M, Monserrat L, et al. Gene mutations in apical hypertrophic cardiomyopathy. *Circulation*. 2005;112(18):2805-2811. doi: 112/18/2805 [pii].

157. Kennelly PJ, Krebs EG. Consensus sequences as substrate specificity determinants for protein kinases and protein phosphatases. *J Biol Chem*. 1991;266(24):15555-15558.

158. Gomes AV, Harada K, Potter JD. A mutation in the N-terminus of troponin I that is associated with hypertrophic cardiomyopathy affects the ca 2 -sensitivity, phosphorylation kinetics and proteolytic susceptibility of troponin. *J Mol Cell Cardiol*. 2005;39(5):754-765.

159. Biesiadecki BJ, Tachampa K, Yuan C, Jin JP, de Tombe PP, Solaro RJ. Removal of the cardiac troponin I N-terminal extension improves cardiac function in aged mice. *J Biol Chem*. 2010;285(25):19688-19698. doi: 10.1074/jbc.M109.086892 [doi].

160. Despa F, Orgill DP, Lee RC. Molecular crowding effects on protein stability. *Ann N Y Acad Sci*. 2006;1066(1):54-66.

161. Cheung MS, Klimov D, Thirumalai D. Molecular crowding enhances native state stability and refolding rates of globular proteins. *Proc Natl Acad Sci U S A*. 2005;102(13):4753-4758. doi: 0409630102 [pii].

162. Horbett TA. Adsorption of proteins from plasma to a series of hydrophilic-hydrophobic copolymers. II. compositional analysis with the prelabeled protein technique. *J Biomed Mater Res*. 1981;15(5):673-695.

163. Jeffrey GA, Saenger W. Hydration of proteins. In: *Hydrogen bonding in biological structures.* Springer; 1994:459-486.

164. Kuntz ID,Jr, Kauzmann W. Hydration of proteins and polypeptides. *Adv Protein Chem*. 1974;28:239-345.

165. Sugi H, Pollack GH. *Mechanisms of work production and work absorption in muscle.* Vol 453. Springer Science & Business Media; 2012.

166. Lenart TD, Murray JM, Franzini-Armstrong C, Goldman YE. Structure and periodicities of cross-bridges in relaxation, in rigor, and during contractions initiated by photolysis of caged Ca2+. *Biophys J*. 1996;71(5):2289-2306. doi: S0006-3495(96)79464-X [pii].

167. Giuliani A, Di Paola L, Setola R. Proteins as networks: A mesoscopic approach using haemoglobin molecule as case study. *Current Proteomics*. 2009;6(4):235-245.

168. Elson E, Webb W. Concentration correlation spectroscopy: A new biophysical probe based on occupation number fluctuations. *Annu Rev Biophys Bioeng*. 1975;4(1):311-334.

169. Giardini A, Lovato L, Donti A, et al. A pilot study on the effects of carvedilol on right ventricular remodelling and exercise tolerance in patients with systemic right ventricle. *Int J Cardiol*. 2007;114(2):241-246.

170. Posch MG, Waldmuller S, Müller M, et al. Cardiac alpha-myosin (MYH6) is the predominant sarcomeric disease gene for familial atrial septal defects. *PLoS One*. 2011;6(12):e28872.

171. Song W, Dyer E, Stuckey DJ, et al. Molecular mechanism of the E99K mutation in cardiac actin (ACTC gene) that causes apical hypertrophy in man and mouse. *J Biol Chem*. 2011;286(31):27582-27593. doi: 10.1074/jbc.M111.252320 [doi].

172. Davlouros PA, Niwa K, Webb G, Gatzoulis MA. The right ventricle in congenital heart disease. *Heart*. 2006;92 Suppl 1:i27-38. doi: 92/suppl_1/i27 [pii].

173. Osler W. *The principles and practice of medicine: For the use of students and practitioners.* Appleton; 1905.

174. Juilliere Y, Barbier G, Feldmann L, Grentzinger A, Danchin N, Cherrier F. Additional predictive value of both left and right ventricular ejection fractions on long-term survival in idiopathic dilated cardiomyopathy. *Eur Heart J*. 1997;18(2):276-280.

175. Dweck D, Hus N, Potter JD. Challenging current paradigms related to cardiomyopathies. are changes in the Ca2+ sensitivity of myofilaments containing cardiac troponin C mutations (G159D and L29Q) good predictors of the phenotypic outcomes? *J Biol Chem*. 2008;283(48):33119-33128. doi: 10.1074/jbc.M804070200 [doi].

176. Robinson P, Griffiths PJ, Watkins H, Redwood CS. Dilated and hypertrophic cardiomyopathy mutations in troponin and alpha-tropomyosin have opposing effects on the calcium affinity of cardiac thin filaments. *Circ Res*. 2007;101(12):1266-1273. doi: CIRCRESAHA.107.156380 [pii].

177. Wang Y, Pinto JR, Solis RS, et al. Generation and functional characterization of knock-in mice harboring the cardiac troponin I-R21C mutation associated with hypertrophic cardiomyopathy. *J Biol Chem*. 2012;287(3):2156-2167. doi: 10.1074/jbc.M111.294306 [doi].

178. Messer AE, Gallon CE, McKenna WJ, Dos Remedios CG, Marston SB. The use of phosphate-affinity SDS-PAGE to measure the cardiac troponin I phosphorylation site distribution in human heart muscle. *PROTEOMICS-Clinical Applications*. 2009;3(12):1371-1382.

179. Bodor GS, Oakeley AE, Allen PD, Crimmins DL, Ladenson JH, Anderson PA. Troponin I phosphorylation in the normal and failing adult human heart. *Circulation*. 1997;96(5):1495-1500.

180. Sweeney HL, Bowman BF, Stull JT. Myosin light chain phosphorylation in vertebrate striated muscle: Regulation and function. *Am J Physiol*. 1993;264(5 Pt 1):C1085-95.